



TECHNISCHE UNIVERSITÄT MÜNCHEN

Fachgebiet für Biowissenschaftliche Grundlagen
in Kooperation mit der Gemeinsamen Forschungsstelle der Europäischen
Kommission (DG JRC) in Ispra (Italien)

**Physiologically- based toxicokinetic and toxicodynamic modelling of single and
repeated dose toxicity**

Monika Gajewska

Vollständiger Abdruck der von der Fakultät Wissenschaftszentrum Weihenstephan
für Ernährung, Landnutzung und Umwelt der Technischen Universität München zur
Erlangung des akademischen Grades eines

Doktors der Naturwissenschaften

genehmigten Dissertation.

Vorsitzender: Univ.-Prof. Dr. H.-W. Mewes

Prüfer der Dissertation:

1. apl. Univ.-Prof. Dr. K.-W. Schramm
2. Univ.-Prof. Dr. H. Briesen

Die Dissertation wurde am **28.10.2014** bei der Technischen Universität München
eingereicht und durch die Fakultät Wissenschaftszentrum Weihenstephan für
Ernährung, Landnutzung und Umwelt am **02.02.2015** angenommen.

Abstract

To analyse the effects of human exposure to selected chemicals, physiologically-based toxicokinetic (PBTK) and toxicodynamic (PBTD) models for the healthy adult Caucasian population were constructed and parameterised for the following nine case study compounds, which include industrial chemicals and substances found in consumer products and food: coumarin, estragole, hydroquinone, caffeine, ethanol, isopropanol, methyl iodide, styrene and nicotine. Literature quantitative structure-property relationships (QSPRs) for skin permeation, plasma protein binding and blood-to-air partition coefficient were collected and evaluated for these substances. A simple PBTK model structure was first refined in terms of the skin, gastrointestinal and respiratory tracts by introducing sub-compartments to give a better simulation of absorption profiles. Subsequently the PBTK model was applied for the purposes of interspecies (rat-to-human) and route-to-route extrapolations of experimental no-observed adverse effect level (NOAEL) doses, *in vitro*-to-*in vivo* correlations of skin permeation and liver clearance, and the prediction of metabolites in blood and urine. Selected case studies for the route-to-route extrapolations showed that the Area under Curve (AUC) in blood was the parameter indicating the lowest dermal thresholds. Under defined exposure conditions, these thresholds were higher than those corresponding to oral NOAEL values (oral NOAEL doses are protective) for coumarin and ethanol but were lower for hydroquinone, caffeine and isopropanol. The simulated skin permeation of caffeine and coumarin using *in vitro* parameters was found to be lower than the estimated *in vivo* permeation. On average, the liver clearance (calculated as a sum of V_{\max}/K_m ratios of all formed metabolites) *in vitro* was found to be higher than the one optimised from *in vivo* blood data. The application of joint PBTK-TD modelling was illustrated by simulating the effects of nicotine and caffeine on acute heart rate and blood pressure for selected daily exposure scenarios and, in the case of caffeine only, on cell-level changes (HepaRG cell viability). These effects were related to external doses under defined oral and dermal exposure scenarios (for nicotine also following inhalation). A multi-scale modelling approach (PBTK combined with a virtual cell-based assay) revealed almost no effect of caffeine (up to 5.33 mg/kg body weight) on the viability of liver (HepaRG) cells, regardless of the absorption route. Finally, the PBTK model for oral absorption was successfully applied to simulate the concentration–time profiles of ethanol, and its two metabolites, ethyl sulfate and ethyl glucuronide, in blood and urine, following the ingestion of 4 and 8 units of ethanol. In this novel application of PBTK modelling, a Euclidean-based strategy was used to help back extrapolate the time of ethanol consumption.

Table of Contents

1.	Background and the aim of the work	5
2.	Introduction	8
2.1	Toxicokinetic and toxicodynamic (PBTK-TD) modelling	8
2.2	Modelling of exposure routes.....	14
2.2.1	Oral absorption.....	14
2.2.2	Dermal absorption.....	14
2.2.3	Inhalation.....	17
2.3	Metabolism.....	17
2.4	Route-to-route extrapolation	19
2.5	<i>In vitro</i> -to- <i>in vivo</i> extrapolation	21
2.6	Available software for PBTK-TD modelling.....	24
2.7	Literature applications of PBTK/TD models for case study compounds.....	25
2.8	Strengths and limitations of PBTK-TD modelling	27
2.9	Case study compounds.....	30
2.9.1	Coumarin	31
2.9.2	Estragole	33
2.9.3	Hydroquinone	34
2.9.4	Caffeine	35
2.9.5	Ethanol	37
2.9.6	Isopropanol	39
2.9.7	Styrene.....	40
2.9.8	Methyl iodide	42
2.9.9	Nicotine.....	43
2.10	Differences in molecular properties between cosmetic ingredients and drugs	46
3.	Materials and methods	48
3.1	Experimental Data.....	48
3.1.1	Single and repeated toxicokinetics.....	48
3.1.2	Single and repeated toxicodynamics	56
3.1.3	Cell viability.....	57
3.2	PBTK, PBDT and VCBA model structures and equations	58
3.2.1	PBTK model.....	59
3.2.2	PBDT model.....	79
3.2.3	Virtual cell-based assay model.....	81
3.3	Sensitivity Analysis and optimisation.....	85
3.4	Quantitative structure-property relationships (QSPRs).....	91
3.4.1	QSPRs for skin permeation.....	91
3.4.2	Plasma protein binding.....	95

3.4.3	Tissue-to-blood partition coefficients	96
3.4.4	Blood-to-air partition coefficient	97
4.	Results and Discussion.....	98
4.1	Quantitative structure-property relationships (QSPRs).....	98
4.1.1	QSPRs for skin permeation	98
4.1.2	Plasma/ protein binding and blood –to-plasma ratio.....	102
4.1.3	Blood-to-air partition coefficient	102
4.2	Toxicokinetics- modelling refinement of uptake stages in PBTK model	104
4.2.1	Oral and dermal absorption	105
4.2.2	Inhalation.....	121
4.3	<i>In vitro</i> - to- <i>in vivo</i> correlation	129
4.3.1	Skin penetration	129
4.3.2	Liver clearance	143
4.3.3	Cell viability.....	154
4.4	Interspecies extrapolation.....	160
4.5	Route-to-route extrapolation	169
4.5.1	Oral-to-dermal extrapolation.....	171
4.5.2	Oral-to-inhalation extrapolation.....	179
4.5.3	Dermal-to-inhalation extrapolation	182
4.6	Ethanol case studies	185
4.6.1	Simulation of ethanol metabolites in serum and urine following oral administration	185
4.6.2	Effect of different concentrations and vehicles on skin absorption of ethanol	201
4.7	Joint toxicokinetic and toxicodynamic modelling of single and multiple doses.....	205
4.7.1	Nicotine	205
4.7.2	Caffeine	223
5.	Evaluation of uncertainty in input parameters to the PBTK-TD models	233
6.	Conclusions.....	243
	Literature.....	247
APPENDIX 1		

1. Background and the aim of the work

The main goal of this PhD project was to develop and optimise computer-assisted physiologically-based toxicokinetic (PBTK) and dynamic (PBTK) models to predict the biological and toxicological effects of chemicals in humans under single and repeated exposure conditions. The modelling approach was illustrated through its application (to selected chemicals found in consumer products and food, as well as some drugs) in *in vitro* –to- *in vivo*, interspecies and route-to-route extrapolations. With a view to the implementation of the models into open-source tools, the models were programmed in R¹ (the project for statistical computing) for further incorporation into KNIME² workflows. KNIME is a user-friendly graphical workbench for the analysis process such as data access, data transformation, initial investigation, visualization and reporting. It integrates various components for machine learning and data mining through its modular data pipelining concept. A graphical user interface allows assembly of nodes for data preprocessing, for modelling and data analysis and visualization. KNIME is widely used in pharmaceutical research.

The entire work program consisted of five main deliverables: i) set-up, parameterization, calibration and structure refinement of the oral, dermal and inhalation PBTK model for the Caucasian population; ii) its application in oral-to-dermal, oral-to-inhalation and dermal-to-inhalation extrapolations; iii) *in vitro*- to- *in vivo* correlations of liver clearance and skin absorption; iv) prediction of metabolites in blood and urine of selected case-study compounds; v) joint PBTK-TD dose-response modelling of selected acute cardiovascular effects; and vi) link of PBTK model with the virtual cell-based assay (VCBA) model to predict the HepaRG cell viability.

The list of the main activities in the project:

1. Physiologically- based Toxicokinetic (PBTK) modelling: structure refinement of classical literature PBTK models in terms of absorption stages (gastrointestinal tract, skin, respiratory tract) to be applicable for various chemicals for single and repeated dosing.
2. Compilation of literature Quantitative Structure-Property Relationships (QSPRs) for predicting skin absorption parameters, tissue-to-blood partition coefficients, plasma protein binding and blood-to-air partition coefficient.
3. Rat-to-human and route-to-route extrapolation of no -observed adverse effect level (NOAEL) doses for selected chemicals.
4. Application of the PBTK model in predicting blood/plasma and urinary metabolites of ethanol. Sensitivity Analysis, parameters estimation problem and back-extrapolation to the time of alcohol intake.

¹ <http://cran.r-project.org/> (last access: 06.10.2014)

² <http://www.knime.org/> (last access: 06.10.2014)

5. Joint toxicokinetic and toxicodynamic modeling of caffeine and nicotine to predict observable effects on organism level such as heart rate and blood pressure (PBTK-TD modelling) and on cell level (for caffeine only) such as liver cell viability (PBTK-VCBA modelling). Contribution to the risk assessment: analysis of the selected daily exposure scenarios and the development of dose-response modelling: HepaRG cells viability as a function of caffeine external dose. Then, a comparison with HepG2 case.

The following chemicals were studied in this work: coumarin, estragole, hydroquinone, caffeine, ethanol, isopropanol, styrene, methyl iodide and nicotine.

The data gathering/organization strategy is presented in **Figure 1.1**. Information about analysed compounds was placed into separate directories that contained the PBTK and PBDT model (if available) R code for up to 4 exposure routes; sensitivity analysis/optimisation functions, experimental data, compound-specific parameters in excel (csv) files and dosing parameters in a text file. Simulated results were saved as excel tables with appropriate graphics.

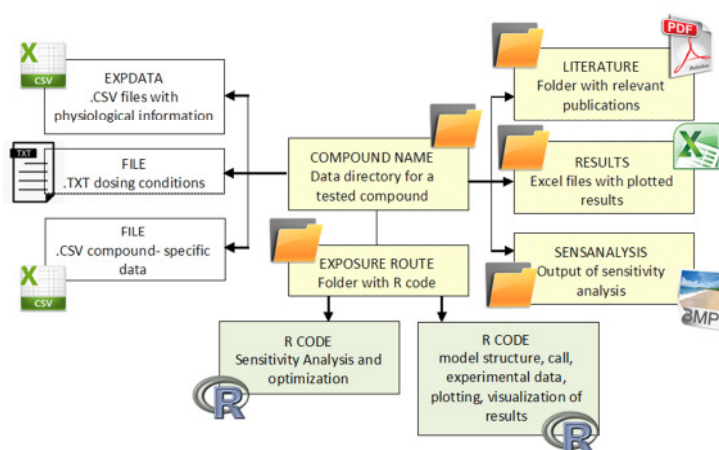


Fig 1.1. Current data organization and storage into a directory folder.

Acknowledgements

M. Gajewska carried out this research project as a grantholder of the European Commission's Joint Research Centre (JRC). The work was partially funded by Cosmetics Europe and by the Seventh Framework Program (FP7/2007-2013) COSMOS³ (Integrated In Silico Models for the Prediction of Human Repeated Dose Toxicity of Cosmetics to Optimise Safety) Project.

The COSMOS project promotes the use of integrated *in-silico* models for the prediction of human repeated dose toxicity of cosmetics to optimise safety and it belongs to Seurat-1⁴ cluster: European research initiative

³ <http://www.cosmostox.eu/home/welcome/> (last access: 06.10.2014)

⁴ <http://www.seurat-1.eu/> (last access: 06.10.2014)

with the long-term goal of achieving “Safety Evaluation Ultimately Replacing Animal Testing” (towards the replacement of in-vivo repeated dose systemic toxicity).

Supervisory team and workplace

The project was carried out in the Systems Toxicology Unit, Institute for Health and Consumer Protection (IHCP), Joint Research Centre (JRC), Ispra, Italy under the following supervision:

- JRC: Dr Andrew Worth and Dr J. M. Zaldívar.
- Technical University of Munich, Center of Life and Food Sciences Weihenstephan: Prof. Karl-Werner Schramm and Prof. Heiko Briesen.
- University of Milano-Bicocca, Dep. for Sciences and Technologies of Environment and Landscape: Dr Chiara Urani.

Scientific advice and support was also provided by Dr Alexandre Péry (INERIS) and by Dr Ioannis Drossinos (Institute for Environment and Sustainability; JRC), and by Dr Julien Burton, Dr Jose Sala Benito, Dr David Asturiol, Dr Alfonso Lostia, Dr Varvara Gouliarmou, Dr Alicia Paini and Dr Jos Bessems (IHCP, JRC).

2. Introduction

2.1 Toxicokinetic and toxicodynamic (PBTK-TD) modelling

The use of alternatives to animal testing is becoming increasingly important in the safety assessment of chemicals, especially for cosmetic ingredients for which there are EU-wide bans on animal testing and on the marketing of animal-tested ingredients. One of the most popular non-animal methods in recent years is a developed computational approach to explore toxic effects in a living organism and to establish an interface between biological different levels of data: cell models, organ/tissue models and organism level models. Their coupling facilitates *in vitro*- to – *in vivo* extrapolation producing an estimated effect close to observed effective external dose values. The first step is to be able to assess the exposure consequences in a body/organ level and move gradually to a molecular level via an effect target site. A PBTK model simulates internal exposure profiles in a body at the tissue/organ/blood level and can be linked to the dynamic modelling of effects in the target organ (e.g. “observed” acute organism responses) or target cell (e.g. cell viability). Therefore, the physiologically -based toxicokinetic (PBTK) (also called biokinetic, or pharmacokinetic) modelling together with toxicodynamics (TD) is being increasingly applied in the human risk assessment of potential toxicants to link exposure to the estimated dose-response relationship.

Toxicokinetics, described by the PBTK model, is the study of the movement of chemicals around the body. It includes absorption (transfer from the site of administration into the systemic circulation), distribution (via the general circulation into and out of the tissues), metabolism (bioconversion of a chemical) and elimination (excretion of a chemical in its unchanged form) – so-called ADME scenario – defined in a mechanistic, meaningful way, if a mechanism is understood and sufficient data are available. This mechanistic aspect is supported by physiological parameters influencing absorption (e.g. absorption rate from the uptaking organ, pH values and transit times through various sections of the GI tract), distribution (e.g. tissue volumes and composition, tissue-to-blood partition), metabolism (e.g. expression levels of various hepatic enzymes and transporters involved with metabolic elimination), and elimination (e.g. glomerular filtration rate and expression levels of transporters in the kidneys involved with renal elimination), which can be explicitly incorporated in the model. Because the models have a mechanistic basis, extrapolation to situations differing from the conditions of the data used to calibrate the model is justifiable. The mechanistic basis allows PBTK models to be used to determine if results from different experimental designs are consistent, and to explore possible mechanisms responsible for unexpected or unusual data. PBTK modeling has been used to great effect for interspecies extrapolation, both among animal models and for predicting human TK based on animal data (Reddy et al., 2013). As an output the PBTK model estimates concentration-time profiles of a parent chemical and its metabolites in all target organs/tissues/group of organs considered following a pre-defined ADME kinetics. The model represents a simplified body structure and consists of compartments with anatomical interpretation (organs/tissues) connected by flowing blood and parameterised by physiological,

anatomical and compound specific data (a variety of parameters must be provided). From the mathematical point of view, a PBTK model can be defined as a set of differential equations (mass balance equations) of a parent compound and its metabolites (ordinary or partial differential equations). Mass differences in all organs relate to the fraction of cardiac output to a specific organ and the fate of the chemical (excretion and metabolic removal) including its partition between organ and blood (or blood and plasma).

Among the most important parameters there are: kinetic rates (absorption, metabolism, excretion) which are typically derived from *in vitro* studies (absorption rates may also be measured *in vivo*), physiological organ weights, regional blood flow distribution mean percent, tissue- to- plasma partition coefficients and other compound-specific properties predicted by quantitative structure-property relationships (QSPRs), physicochemical properties. Volatile compounds require additionally vapour pressure, blood-to-air and water- to- air partition coefficients (Chiu and White, 2006). Not all the model parameters are experimentally measured or calculated and then the availability of *in vivo* data such as organ/tissue concentrations of a chemical is the limiting criterion for the final choice of chemicals in the study. They are used to fill missing data gaps in modelling via optimisation and to validate the model by direct comparison with simulation results (the ideal case is to have more than one set of experimental data that come from different dosing protocols for better verification of model performance). The use of QSPRs is very common especially in cases of dermal absorption parameters (skin permeation and partition coefficients), volatile compounds requiring unmeasured blood-to-air partition coefficient, physicochemical properties such as: molar volume, vapour pressure, water- to- air partition and general tissue-to-plasma partition coefficients that are often unavailable. Other commonly unavailable *in vivo* parameters are protein binding data, metabolism in realistic biological environment, fate of chemical (accumulation, subsequent reactions, effect of vehicle, etc.), bioavailability, blood-to-plasma ratio, etc., however, they are measured *in vitro*. Another option for estimating parameters value is to use data from other species but a proper interspecies extrapolation is necessary.

PBTK models are composed of individual or population average parameters or are based on parameters distributions. To systematically account for parameter variability within populations, a Bayesian approach is commonly developed quantifying the probability of a parameter given the amount of information contained in the measured data (Krauss et al., 2013). The Bayesian approach provides a formal way to incorporate prior knowledge on model parameters together with observed (*in vivo*) data in the modeling process. The analysis starts with the construction of prior probability distributions of the model parameters of interest, usually based on studies available in the literature. These distributions are then evaluated on the basis of their likelihood given observed data to compute posterior distributions of the model parameters. The inter-individual variations are in physiological (organ weights, percentage of body fat, muscle, tissue – blood flow rate, etc.) and ADME parameters (compound-specific parameters such as clearance, absorption rates).

A chemical exists in blood in two forms: bound and unbound. Its actions may be affected by the degree to which it binds to the proteins within blood plasma. The less bound a substance is, the more efficiently it can traverse cell membranes or diffuse (it is the unbound fraction which exhibits pharmacologic effects).

Common blood proteins that drugs bind to are human serum albumin, lipoprotein, glycoprotein, α , β , and γ globulins.

The general PBTK model structure used in this work (**Figure 2.1.1**) has been built based on variety of literature resources and consists of 3 main uptake compartments (GI tract with 6 sub-compartments - based on (Loizou and Spendiff, 2004)-, skin with 4 skin sub-compartments and hair follicles (Bookout Jr. et al., 1997) and lungs with 4 sub-compartments (Peterman and Longtin, 1984) – see details in **Chapter 2.2**), liver, heart, brain, adipose tissue, poorly and highly perfused tissues, kidney, bladder, urine and rest of the body. This structure was chosen to be simple but elaborate enough, applicable and easily modifiable for various organic compounds (lipophilic, volatile, etc.) for single and repeated dosing pattern giving clear and comprehensible results.

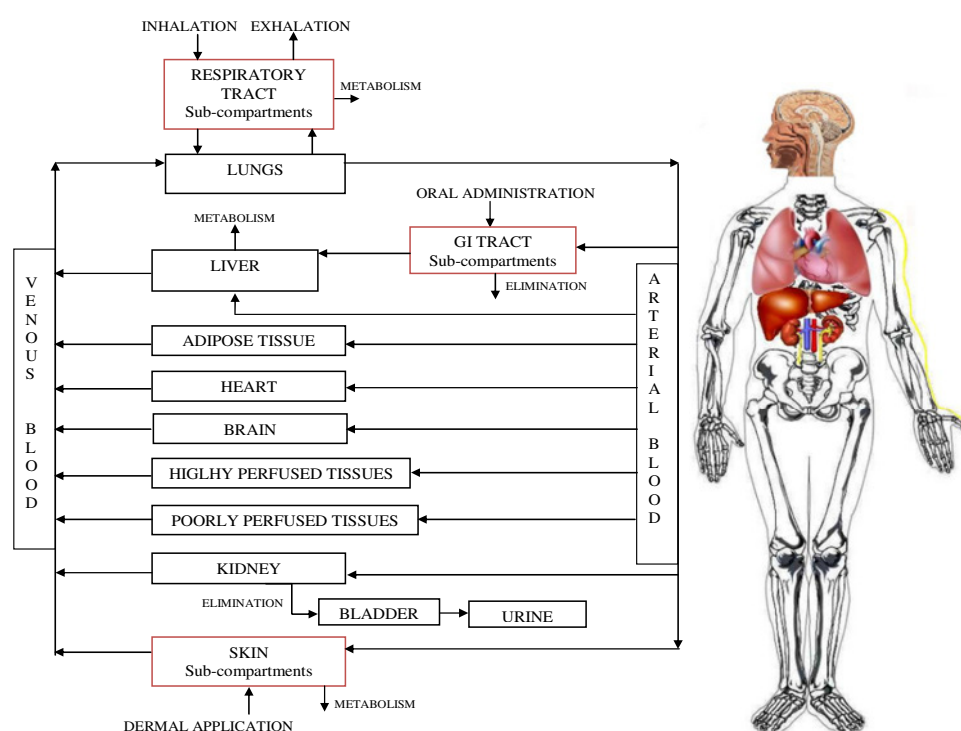


Fig 2.1.1. General structure of the PBTK model.

Toxicokinetic modelling provides as the final output concentration-time profiles of a chemical and its metabolites in all investigated organs/ group of organs/ tissues including toxicokinetic parameters such as: peak concentrations (C_{max}), Area Under Curve (AUC): estimation of a total quantity of substance to which organ is exposed over a simulation time, a compound half-life ($t_{1/2}$), (apparent) volume of distribution (V_d), bioavailability (biov) and total body clearance (CLR_{tot}). If the exposure route is different than intravenous (i.v.) dosing, then the fraction biologically-active or bioavailability (**Equation 2.1.1**) is determined from ratio of the area under the blood/plasma concentration–time curve (AUC) of the parent compound or the percentage dose excreted in urine as the parent compound to the corresponding i.v. results (Renwick, 2005). Bioavailability is important in modelling dose-response effects as it provides a fraction of a chemical that reaches a systemic circulation. Oral bioavailability is calculated from the relation: $bioav.= FaFgFl$, where Fa

– is a fraction that is absorbed from stomach and intestine, F_g – fraction that escapes first pass metabolism in the gut, F_l – fraction that escapes first pass metabolism in the liver.

$$bioav. = \frac{AUC_{route}}{AUC_{i.v.}} \cdot \frac{Dose_{i.v.}}{Dose_{route}} = \frac{\% \text{ in urine as parent compound}}{\% \text{ in urine as parent compound after i.v.}} \quad (2.1.1)$$

Blood or plasma clearance is the most important of all pharmacokinetic parameters. The clearance reflects the overall ability of the body to remove permanently the chemical from the blood/plasma. It can be altered by factors such as enzyme induction/ inhibition, liver disease, kidney disease, inter-individual or inter-species differences in hepatic enzymes or in some cases organ blood flow. Once the chemical is in the blood circulation, the same volume of plasma will be cleared of chemical per minute (i.e. the clearance value) which applies irrespective of the route of delivery of chemical into the circulation. However, the bioavailability will determine the proportion of the dose reaching the general circulation. Therefore, bioavailability has to be taken into account if clearance is calculated from non-intravenous data (Toutain and Bousquet-Melou, 2004):

$$CLR_{tot} = \frac{Dose_{i.v.}}{AUC_{pl,i.v.}} = CLR_{tot} = CLR_{liv} + CLR_{renal} + CLR_{other}; \quad CLR_{tot} = \frac{Dose_{oral} \cdot bioav}{AUC_{oral}} \quad (2.1.2)$$

Total clearance is defined as the ratio of total (body) rate of drug elimination to plasma concentration and is commonly derived from a dose divided by the area under the plasma concentration vs. time curve and composes of a sum of organ clearances. Renal clearance is calculated from the following ratio:

$$CLR_{renal} = \frac{Amount_{urine}}{AUC_{pl}} \quad \text{and the liver clearance is the product of the liver blood flow (} f_{liv} \text{) and the hepatic}$$

extraction ratio E_{hep} – that is the percentage of drug which is irreversibly removed during a single (first) passage. Percentage of first pass metabolism in the liver is calculated from: $FPE = CLR_{tot} / f_{liv} \cdot 100$. Blood clearance can be directly evaluated by measuring blood concentration vs. time profiles or alternatively, plasma concentration vs. time profiles, and transforming the plasma clearance to the blood clearance using the hematocrit value (H) and the blood-to-plasma (RBP) partition ratio (which can be measured *in vitro* or computed using QSPRs and is assumed to be constant). It is applicable under conditions that a rapid equilibrium exists between plasma and red blood cells (Toutain and Bousquet-Melou, 2004) and provides an indication of drug binding to erythrocytes.

$$C_{ven,bl} = \frac{C_{ven,pl}}{RBP} \quad (2.1.3)$$

The overall rate of elimination, as indicated by the terminal half-life (t), is dependent on two physiologically related and independent variables:

$$t_{1/2} = \frac{0.693 \cdot V_d}{CLR_{tot}} \quad (2.1.4)$$

Apparent volume of distribution (V_d) measures the extent to which the compound has left the general circulation in a reversible equilibrium with tissues (sum of AUC in all organs (whole body) /circulating concentration at a time when distribution is complete ($V_d = \text{Dose} / C_{\text{ven,pl}}$; steady state $V_{ss} = \text{MRT} \cdot \text{CLR}_{\text{tot}}$). It is a mathematical term that can be explained as the volume of dilution into which the dose is added to produce the observed change in concentration. The larger the volume of distribution, the greater the dilution of a dose, and the smaller the increase in circulating concentration. Volume of distribution does not necessarily correspond to a true physiologic body fluid or tissue volume—hence it is “apparent” (Gibaldi and Koup, 1981).

Toxicodynamics (TD) refers to a process through which a chemical brings about an effect in a body including time course and its intensity. It relates to the processes and changes that occur in the target tissue, such as acute changes in metabolic bioactivation, heart rate, blood/ pulse pressure, biochemical biomarkers and covalent binding. The interaction occurs at the molecular level, however, the described effect by the model can be often simplified to relating it with organ level concentrations. This is commonly due to lack of in-depth biological information and need for sophisticated model parameters. The simplest TD model consists of 2-3-sub-compartments coupled to the TK model via central system concentration (venous blood/plasma concentration) unless an effect appears in any of the organs considered, in which case it is related to an organ concentration. First a target side is defined (it could be typically either receptor, enzyme, ion channel or carrier molecule) and interaction type (affinity, (partial) agonism, (non-)competitive antagonism) (Ronald, 2011). The PD model relates concentration of a chemical at the target side with resulting effect. In the long run it is possible to study the following relationships: applied dose – internal “effective” concentration – target-site concentration concentration – effect and finally applied dose – effect. The link between the PBTK model blood/plasma concentration and PBTD model provides a basis for integration with dynamics for the prediction of an effect from a given dose – **Figure 2.1.2**. When PK and PD profiles are aligned in time then a direct link is sufficient. A link compartment, that describes a chemical transfer from plasma to biophase (normally) by a first order rate constant, is necessary when PK and PD profiles are not aligned (there is a time-lag between a C_{max} in plasma and maximal PD response) but there is no shift with a dose (Goutelle et al., 2008). Otherwise indirect response model, so called “turn-over” model would be needed.

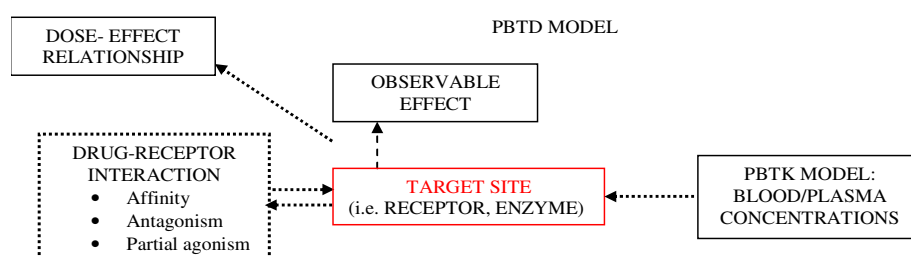


Fig 2.1.2 General structure of the toxicodynamic model.

In most of cases, it is implicitly assumed that the transport of a chemical between plasma and target occurs by passive diffusion. Steady-state drug concentration-effect relationships are described using a hyperbolic function when there is no time shift between PK and PD (i.e., the Hill equation, commonly referred to as direct Emax model):

$$E = E_0 + \frac{E_{\max} \cdot C_{\text{eff}}^y}{C_{\text{eff}}^y + C_{50,\text{eff}}^y} \quad (2.1.5)$$

where y is a Hill factor that accounts for the steepness of the concentration-effect curve - introduced as a deviation from the standard hyperbolic model, E_0 – base- line effect value, C_{eff} – concentration of a chemical at a site of action, E_{\max} - maximal effect (see section 2.2 for more details). In the case of noncompetitive antagonism (eg. tolerance development to an effect) and for $y=1$ **Equation 2.1.6** takes the form (Goutelle et al., 2008) :

$$E(t) = E_0 + \frac{E_{\max} \cdot \left(\frac{C_{\text{eff}}}{C_{50,\text{eff}}} \right)}{\left(1 + \frac{C_{\text{Ant}}}{C_{50,\text{Ant}}} \right) \cdot \left(1 + \frac{C_{\text{eff}}}{C_{50,\text{eff}}} \right)} \quad (2.1.6)$$

This equation represents non-linear and saturable dose-response relationship. The main advantage of this equation is its flexibility and effectiveness in fitting experimental data. The joint PBTK/TD workflow from initial data collections to final dose-effect study is described in **Figure 2.1.3**.

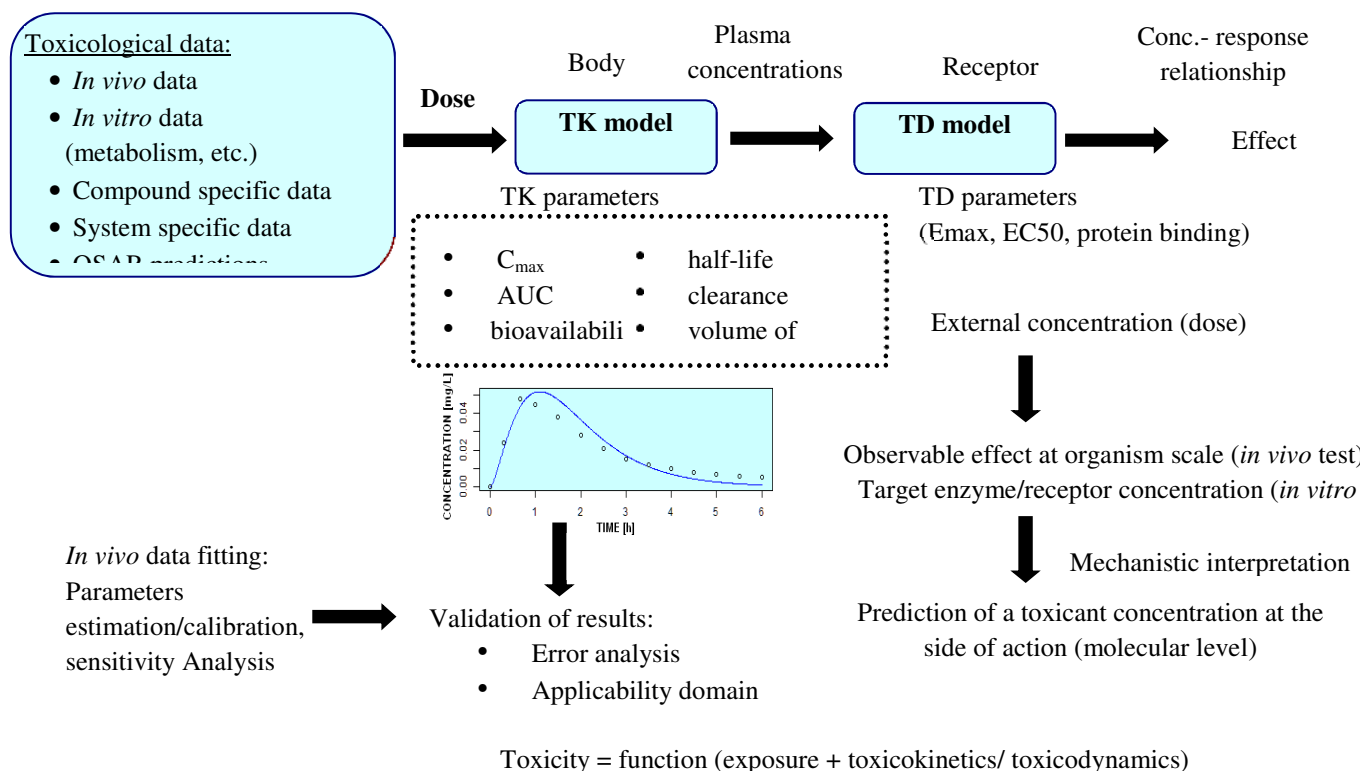


Fig 2.1.3 Joint toxicokinetics and toxicodynamics modeling workflow.

2.2 Modelling of exposure routes

2.2.1 Oral absorption

Oral administration of chemicals occurs normally either via gavage, drinking or dissolution from matrix (use of coated tablets). (Costa and Sousa Lobo, 2001) described modelling of dissolution profiles from various matrices. The disintegration time can be modified for a rapid effect or for sustained release. A water-soluble drug incorporated in a matrix is mainly released by diffusion, while for a low water-soluble drug the self-erosion of the matrix will be the principal release mechanism. Zero order kinetics is used to describe a drug dissolution from pharmaceutical dosage forms that do not disaggregate and release the drug slowly (assuming that area does not change and no equilibrium conditions are obtained)- eg. some transdermal systems, as well as matrix tablets with low soluble drugs, coated forms, etc. First order kinetics is used when the dissolution phenomena of a solid particle in a liquid media implies a surface action - the pharmaceutical dosage forms following this dissolution profile, such as those containing water-soluble drugs in porous matrices, release the drug in a way that is proportional to the amount of drug remaining in its interior. Other, more advanced equations tailored for specific applications have also been proposed (Costa and Sousa Lobo, 2001) and may be used in more advanced PBTK modelling, eg. Higuchi model: $at^{0.5}$, Weibull model: $100(1-\exp(-t/a))^b$. Detailed oral absorption studies are especially important for drugs. Most of them behave in solution as weak acid, base or sometimes both – weak acid and base (Cairns, 2008). The pKa and pKb (logarithms of acid or base dissociation constants) give information about the strengths of acids and bases (ionization power), whereas acidic or basic nature is identified by analyzing functional groups in the molecule. Typical functional groups of acids are: carboxylic group, phenol group or $-SO_2$ group (with electron withdrawing effects). The lower the pKa the stronger the acid. Amines are common bases with $-NH_2$ group in which nitrogen atom has the lone pair of electrons available for reactions with protons. However, this pair may be unavailable in cases of C-N bonds in amides. The higher the pKa, the stronger the base. Basic drugs are normally administered as their water-soluble salts to lower their ionization in the stomach. Free acids and bases when they are unionised tend to dissolve well in non-polar solvents; upon ionization, they become more soluble in eg. water and buffer (polar solvents). Acidic drugs are soluble in organic solvents at low pH and basic drugs at high pH. The absorption of a chemical in the GI tract may be influenced by factors like: its release from the formulation, dissolution, stability in GI environment, permeability through the gut wall, first-pass metabolism on the gut wall (Sinhaa et al., 2012).

2.2.2 Dermal absorption

Dermal absorption can be quantified by estimating permeability (or diffusion) coefficient given experimental conditions and time of skin contact with an investigated substance or fraction of a total applied dose that is absorbed across the skin in a specified time. The latter is not an independent constant value but it is highly

related to an exposure scenario (including application area and applied dose). Normally, permeability or diffusion coefficient are determined as a constant average value (of several measurements) from Fick's first law assuming that the penetrant is applied in moderate concentrations causing no skin damage or its alterations. The coefficients are either measured in *in vitro* experiments or evaluated from *in vivo* data via fitting by toxicokinetic model. In *in vivo* study often very rough approximation is given or insufficient data are collected to estimate maximum absorption rate (Mathes et al., 2014). As shown in some studies, absorption does not always increase linearly with dose. Moreover, it can be affected by vehicle type, physicochemical properties and concentration of a chemical in vehicle, anatomical skin site, degree of hydration (well-hydrated skin is less permeable than relatively dry skin as a result of an increased thickness). Other aspects that increase skin permeation are: low polarity, very acidic or alkaline conditions, size of molecules (large molecules penetrate skin slowly), gender differences (water permeability coefficient in abdominal skin was reported 0.00131 cm/h for men and 0.00093 cm/h for women (Bronaugh, Robert L. Raymond and Congdon, 1983)). As an example, **Figure 2.2.1** shows skin absorption of various chemicals from ethanol and acetone vehicles *in vivo*. We see that, on average, ethanol proves to be a better carrier than acetone. The most commonly applied permeation enhancers include: water, ethanol, propylene glycol, propylene glycol + ethanol 7:3, dimethyl sulfoxide, oleic acid, etc. In the safety assessment of cosmetics, it is important to take into account dermal bioavailability, which is the net result of absorption/penetration as well as local and systemic metabolism.

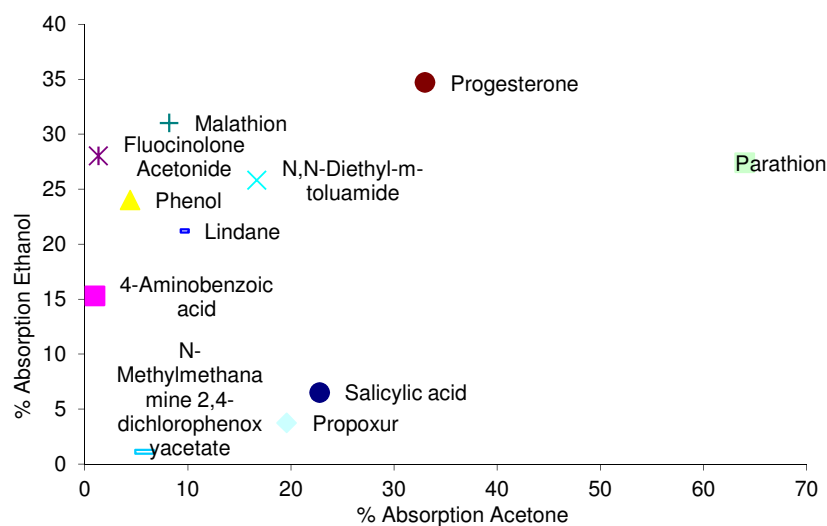


Fig 2.2.1. Skin absorption of various chemicals from ethanol and acetone vehicles. Source: <http://research.ncl.ac.uk/edetox> (last access: 06.10.2014).

Stratum corneum that is heterogeneous external skin layer (the corneocytes, the terminally differentiated keratinocytes, are arranged in pillars forming clusters: 75-80% proteins, 5-15% lipids, 5-10% unidentified elements) efficiently limits the penetration of compounds. However, skin penetration enhancers can trigger structural changes in it like undesired immune systems reactions such as irritation, allergy and inflammation.

Viable epidermis, in turn, includes metabolic systems that drive biochemical processes such as desquamation, creation of extracellular lamellar sheets, programmed cell death, sebum, sweat excretion (Dayan, 2005). To permeate, a compound first partitions in *stratum corneum* then diffuses through it. The major pathway depends on this partition coefficient. Hydrophilic compounds preferably partition into the intercellular domains (like intrafollicular pathway), whereas lipophilic ones may cross the *stratum corneum* through the intracellular way. Most of the molecules, however, used both pathways (Dayan, 2005). In fact, concentrations of a chemical between skin layers and between vehicle and skin surface and between inner skin layer and blood are corrected by partition coefficients. Chemicals sometimes bind to a skin (especially *stratum corneum*) which can be expressed by the Langmuir equation:

$$C_{skn,imb} = \frac{L \cdot b \cdot C_{skn,surf}}{1 + L \cdot C_{skn,surf}} \text{ and } C_{skn,free} = PC_{skn} \cdot C_{skn,surf} \quad (2.2.1)$$

where L is the Langmuir affinity and b is the saturation constant. Based on the fact that total concentration of a chemical ($C_{skn,tot}$) in skin is a sum of its free ($C_{skn,free}$) and immobilised ($C_{skn,imb}$) concentration:

$C_{skn,tot} = C_{skn,free} + C_{skn,imb}$ (Chandrasekaran et al., 1980) we get the following:

$$\frac{\partial C_{skn,tot}}{\partial t} = D_{skn} \cdot \frac{\partial^2 C_{skn,tot}}{\partial x^2} = \frac{\partial C_{skn,free}}{\partial t} + \frac{\partial C_{skn,imm}}{\partial t} \quad (2.2.2)$$

$$\left[1 - \frac{L \cdot b}{PC_{skn} \cdot (1 + L \cdot C_{skn,free} / PC_{skn})^2} \right] \cdot \frac{\partial C_{skn,free}}{\partial t} = D_{skn} \cdot \frac{\partial^2 C_{skn,free}}{\partial x^2} \quad (2.2.3)$$

And additionally, if a chemical reaction, i.e. metabolism (MET_{skn}) takes place in the skin:

$$\left[1 - \frac{L \cdot b}{PC_{skn} \cdot (1 + L \cdot C_{skn,free} / PC_{skn})^2} \right] \cdot \frac{\partial C_{skn,free}}{\partial t} = D_{skn} \cdot \frac{\partial^2 C_{skn,free}}{\partial x^2} - MET_{skn}(C_{skn,free}) \quad (2.2.4)$$

Diffusion coefficient, although assumed constant in the modelling, normally depends on the total concentration of diffusing substance, free and immobile (Crank, 1975) and release of a chemical from vehicle (Kubota and Ishizaki, 1986). Moreover, diffusion coefficient has been shown not constant within the depth of skin. The effects of a penetration enhancer (oleic acid) on the profiles were modelled and the results indicated that, except of the presence of an enhancer, the profiles are little altered by a position-dependent diffusion coefficient (Watkinson et al., 1992).

A wide variety of *in vitro* methods can express key metabolic pathways which can be used for more quantitative determinations of chemical metabolic fate. *In vitro* tests (cultured human skin cells- epidermal keratinocytes) are widely applied as it is possible to maintain the barrier properties of the *stratum corneum* in excised skin. Reconstructed human epidermal models mimic whole skin more closely, although monolayer cultures may also be useful, depending on the expected metabolic fate of the compound of interest (for

example, as predicted by *in silico* methods). An alternative *in vitro* approach, which avoids differences observed between cell lines and epidermis models, is to use enzyme cocktails that mimic whole skin metabolism. With the eventual aim of animal-free risk assessment, it was concluded that a promising approach is to use the experimental data generated by *in vitro* methods (penetration and metabolism) as input variables in PBTK models. These models are also chemistry-based to the extent that key physicochemical and partitioning properties can sometimes be predicted from chemical structure, depending on the availability of relevant and reliable QSPRs (Bronaugh et al., 1982; Russell and Guy, 2009; SCCP, 2006).

2.2.3 Inhalation

Inhalation exposure to volatile chemicals is complicated in terms of modelling and requires a special attention. In literature the exchange of solvent between blood and alveolar air is usually assumed to be very rapid and all exchange occurs in the alveoli and not in other parts of the respiratory tree (Ramsey et al., 1980). The first assumption is plausible, as volatiles are small, non-charged molecules, which easily penetrate the cell membranes. Often a suitable mathematical model is needed to well simulate the function of lungs. (Peterman and Longtin, 1984) used 24 generations of the Weibel model that assume that gases are transported in the lungs via convection and diffusion from one sub-compartment to the other (a mouth, to 12 convection only, 13-22 convection + diffusion, 17-23 diffusion + blood mix). Clearance of gases from the lungs occurs by blood perfusion and the driving force of inhalation and exhalation is the filling and emptying of the alveolar volume which follows a sinusoidal pattern. However, simple few-compartment models taking into account only the uptake of a chemical in the mucous layer of the respiratory tract was proved to give a satisfactory simulating profiles for simple chemicals such as acetone (Kumagai and Matsunaga, 1995). When it comes to aerosols (particle diameter 0.001-10 µm) deposition profile along the respiratory tract needs to be taken into account as these substances are affected by combined forces of diffusion, sedimentation and impaction while moving from nose/mouth to alveolar-interstitial region. For simple gases it is commonly assumed that whole the inhaled dose reaches the alveoli.

2.3 Metabolism

Main metabolizing organs are commonly liver, skin, GI and respiratory tract. Enzymes enhance rates of reactions in the living organism. A typical metabolism pathway is the oxidation of a parent compound (phase I oxidation) followed by conjugation of the oxidised intermediate with highly polar molecules such as glucose, sulfate, methionine, cysteine or glutathione (phase II conjugation). The key enzymes for the first phase are the isoforms of the cytochrome P450 (CYP) family. The major human CYP isoforms involved in the metabolism are: CYP1A2, CYP2A6, CYP2D6, CYP2E1, CYP3A4 (responsible for the majority of xenobiotic metabolism). Other non-CYP enzymes are eg. alcohol and aldehyde dehydrogenase (ADH/ALDH), flavin-containing monooxygenase, monoamine oxidases, hydrolic enzymes

(carboxylesterases, paraoxonases, cholinesterases, sulfotransferase and carbonyl reductase. The phase II enzymes include UDP-dependent glucuronosyl transferase, phenol sulfotransferase, estrogen sulfotransferase, etc. (Li, 2001). The metabolism of a given substance is associated with: metabolic stability (fast metabolism means low stability that requires multiple or continuous dosing over time to reach sustained or high plasma concentrations that are important for therapeutic effects), drug-drug interactions (inhibition or induction of metabolism), toxicity issues (a compound becomes toxic due to metabolic activation).

The enzymatic activity is described by kinetic equations. If it is a first order rate then the rate of catalysis rises linearly as substrate concentration increases (normally it is assumed for metabolites formed at low concentrations). However, most common case is when initially the rate of catalysis rises linearly with substrate concentration but then it begins to level off and approach a maximum at higher substrate concentrations. This behaviour is described by the Michaelis-Menten kinetics. **Figure 2.3.1** shows the relationship between an initial reaction velocity and a substrate concentration in an enzyme. Michaelis-Menten kinetics shows that the maximal velocity (V_{max}) is approached asymptotically and the Michaelis constant (K_m) is the substrate concentration yielding a velocity of $V_{max}/2$. The extent of product formed as a function of time for a series of substrate concentrations first increases with time and then eventually a time is reached when there is *no net change* in the concentration of substrate and product. The enzyme is still actively converting substrate into product but the reaction equilibrium has been attained. At very low substrate concentration, when substrate concentration is much less than K_m , the rate is directly proportional to the substrate concentration. At high substrate concentration, when its concentration is much greater than K_m , $V = V_{max}$; that is, the rate is maximal, independent of its concentration.

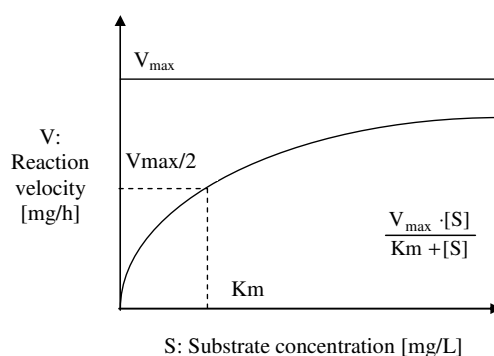


Fig 2.3.1 Michaelis-Menten kinetics.

The K_m value for an enzyme depends on the substrate type and on environmental conditions such as pH, temperature, and ionic strength⁵. Modifying the equation to describe the organ concentration (C_{org}) of a given chemical corrected by its partition in an organ (PC_{org}):

⁵ <http://www.ncbi.nlm.nih.gov/books/NBK22430/> (last access: 06.10.2014)

$$\frac{V_{\max} \cdot \frac{C_{\text{org}}}{PC_{\text{org}}}}{Km + \frac{C_{\text{org}}}{PC_{\text{org}}}} \quad (2.3.1)$$

Michaelis-Menten equation is a special type of Hill equation: V_{\max} is a dynamic effect while Km is a static or steady-state effect. Under conditions $C_{\text{org}} \ll Km$: $CLR_{\text{int}} = \frac{V_{\max}}{Km}$. CLR_{int} is the intrinsic clearance that is a measure of enzyme activity independent of other physiological factors such as the liver blood flow or drug binding in the blood. It is a proportionality factor between rate of metabolism and the drug substrate concentration at the enzyme site. Due to lack of possibility to show the differences in activity of the enzymes constant enzyme concentration and the same activity of the enzymes in different people are assumed. This is a normal and quite widely accepted assumption in this field when it comes to the use of deterministic PBTK modelling approaches for risk assessment purposes. Obviously, clear reference has to be indicated to the source of the V_{\max} value if this information is available in literature. We do not assume it is a constant, but we use one value from a relevant reference as best estimate for deterministic PBTK modelling. However, if this value cannot be referenced for *in vivo* case then it is fitted from *in vivo* group blood/plasma or any other organ concentrations. As starting values, normally *in vitro* measured parameters scaled up to the liver level, are used (Houston et al., 2012). Notwithstanding, there are many factors that contribute to inter-individual differences in total activity of specific enzymes and drug metabolism rates that are dependent on this. The maximum total activity of biotransformation enzymes is dependent for example on genetic polymorphisms, prior (enzyme induction) or concomitant (enzyme stabilisation and reversible or irreversible inhibition) exposure to drugs and environmental chemicals, presence or depletion of cofactors, dietary factors, diseased states, epigenetic factors and endogenous hormonal factors, which change with age and differ between male and female subjects (Venkatakrisnan et al., 2000).

2.4 Route-to-route extrapolation

Human can be exposed to chemicals via several routes; when dealing with food ingredients and consumer products, such as cosmetics, we need to carefully consider three routes of exposure: oral, dermal, and inhalation. The exposure to a specific compound depends on the mode/application /usage of the product and the physical and chemical characteristics of the substance. To predict safety level of human exposure we are usually relying on animal studies which are carried out mainly by oral route, since it is the main route of exposure to a wide range of chemicals and also the practical experimental considerations associated with the long duration of chronic toxicity studies. In particular, health risks that may result from consumer exposure to chemicals are assessed by comparing daily oral, dermal and inhalation exposure levels to Points of Departure usually derived from animal toxicity studies, typically no-observed-adverse-effect-levels (NOAELs) or benchmark doses (BMDs- the dose that is expected to result in pre-specified level of effect). Often, due to a lack of toxicity data for one or more routes, there is a need for route-to-route extrapolation

(RtR). However, RtR extrapolation is not easy to apply, being associated with considerable uncertainties, including the difficulty of accounting for the occurrence of local effects, the rate of absorption and possible metabolism during absorption (first pass metabolism). Several factors need to be considered in applying this extrapolation, such as the variability in the experimental data, intra- and inter-species variation, the nature and severity of the effect, and the sensitivity of the human (sub-) population (ECHA, 2012). Therefore route-to-route extrapolation may be considered for systemic effects when reliable data on ADME are available, rather than carrying out an additional animal study using a second route. For example, it may be possible to carry out an assessment of systemic effects via inhalation exposure based on the results of an oral toxicity study. Recent studies have focused on the development of computational models to support extrapolations such as RtR. In particular, PBTK models can be used to simulate animal and human concentration-time profiles of a parent chemical and its (relevant) metabolites in the blood and other organs following a specific exposure scenario and external dose. Once sufficiently evaluated using (an) experimental data set(s), they can be useful in extrapolating internal dose metrics between species and routes of exposure. It is important to realise that a PBTK model has an applicability domain – it is calibrated for a specific exposure scenario (exposure conditions and dose ranges) and should not be used to predict internal doses following significantly different exposure scenarios (e.g. formulation concentration, applied vehicle, frequency of exposure). The use of PBTK modelling for RtR extrapolation is based on comparisons of simulated internal blood or organ concentrations which are typically characterised by a peak value (C_{max}) and area under curve (AUC) after inhalation, oral or dermal absorption of the same absolute external dose (Chiu and White, 2006; Mielke et al., 2011). In this way, experimentally determined safe limits such as the oral no-observed-adverse-effect-level (NOAEL) dose can be translated to a dermal or inhalation threshold via toxicokinetic modelling. Differences in the absorption step (under given exposure conditions) result in differences in the internal dose and consequently different biological or toxic effects. Since human experimental data are generally lacking, there is often a need to scale from animal results. The common conversion of drug doses to a human equivalent dose (HED – **Equation 2.4.1**) is based on body weight and body surface area (Reagan-Shaw et al., 2008). The K_m factor that stands for a body weight [kg] divided by body surface area (BSA) [m^2] is used to convert the mg/kg dose used in a study to mg/m^2 dose and the ratio between animal and human K_m values is an extrapolation factor.

However, this does not take explicitly into account all of the differences in absorption, metabolism and excretion between species. A PBTK model, in contrast, provides a quantitative evaluation of the underlying biological processes, and is therefore a more reliable, systems biology driven approach to interspecies extrapolation (Kenyon, 2012).

$$HED \left[\frac{mg}{kgBW} \right] = NOAEL_{ANIMAL} \cdot \frac{K_{mANIMAL}}{K_{mHUMAN}} \quad (2.4.1)$$

Major factors that may result in variations in toxicity between routes include (Pepelko and Withey, 1985):

- Difference in absorption efficiency (uptake rate in time is different) that additionally changes in time for prolonged or repeated exposure (i.e. absorption saturation may occur- usually skin).
- Dosing conditions are normally differently expressed (inhalation: atmospheric concentration of chemicals to which humans are exposed in ppm per time interval, oral: total absolute amount of a chemical, dermal: concentration of a chemical in vehicle sol. applied onto the skin over a given time period) – which may result in different total amounts of chemical reaching circulation.
- Difference in systemic effects and occurrence of critical toxicological effects at the portal of entry
- First-pass effects resulting in inactivation or activation of the chemical agent before it reaches the target organ.
- Variations in temporal patterns of target organ concentrations.

(Pepelko and Withey, 1985) additionally reported the equivalent dosing measures for exposures via oral, dermal and inhalation routes:

$$\begin{aligned}
 D_{inhal.} &= \frac{\text{inh. rate [L/min]} \cdot \text{exposure conc. [mg/L]} \cdot \text{exposure time [min]} \cdot f}{\text{BW [kg]}} \approx \\
 D_{derm.} &= \frac{\text{Amt. applied per area [mg/cm}^2\text{]} \cdot \text{exposed area [cm}^2\text{]} \cdot f}{\text{BW [kg]}} \approx \\
 D_{oral} &= \frac{\text{Intake dose [mg]} \cdot f}{\text{BW [kg]}}
 \end{aligned}
 \tag{2.4.2}$$

2.5 *In vitro*-to- *in vivo* extrapolation

In vitro experiments are mostly carried out to determine: i) the molecular basis of a chemical's biological activity, including its mechanism(s) of toxic action, prediction of biological reactivity on the basis of a compound's physicochemical properties, such as structure, molecular size, reactive groups, plasma protein binding (by means of equilibrium dialysis) and the blood/plasma ratio, ii) solubility of substances in intestinal fluids, intestinal permeability of substances (Caco-2 cell system- human colon adenocarcinoma), skin permeability and partition coefficients, metabolic turnover (metabolic clearance rate of substances), microsomal binding and identification of metabolites.

The use of *in vitro* alternatives to replace *in vivo* toxicity studies exploits the use of, for example, human cell lines such as HepG2, HepaRG, and freshly isolated hepatocytes, liver slices, liver microsomes, recombinant enzymes. Liver microsomes (no transporters, greater potential for unspecified binding, short life time) are prepared by the homogenization of a liver and are good for measuring phase I metabolism only (as phase II metabolites are absent) and metabolic inhibition. They are removed from pieces of endoplasmic reticulum. Intact hepatocytes are freshly isolated from the liver. Cryopreserved hepatocytes represent the ideal system for screening of metabolic stability. The advantage of hepatocytes lies in the intact cellular structure and full complement of drug-metabolising enzymes, including both phase I and II. They are also commonly used in analysing drug-drug interactions (inhibition and induction) and the compound toxicity (cell viability) (Li,

2001). Activity of drug-metabolising enzymes in hepatocyte cultures studies have often been advocated to provide better predictions as compared with microsomes. But their isolation is elaborate procedure and the cells have limited life time. In addition hepatocytes have scarce availability and high interindividual variability. More recently, recombinant CYP systems have gained more widespread interest for their ability to predict both inter-individual variability of drug clearance within the population and potential drug–drug interactions (Buck and C.E., 2007).

HepaRG (cryopreserved) are terminally differentiated hepatic cells derived from human (15-year old male) hepatic progenitor cell line that retains many features of primary hepatocytes. HepaRG offer reproducible results, metabolically complete (enzymes, nuclear receptors, drug transporters) and scalable system, long-term stability of relevant enzymes activity, lack of donor variability, more economical and convenient alternative to hepatocytes. HepaRG cells are commonly used for *in vitro* determinations of acute/ chronic toxicity, mitochondrial damage, metabolite-dependent toxicity and genotoxicity. HepG2 (derived from a liver tumour of a female suffering from hepatocellular carcinoma) are another substitute candidate for primary hepatocytes but used mostly in toxicogenomic applications (they are able to activate mutagens, carcinogens) due to lower expression of phase I and II biotransformation enzymes (Jennen et al., 2010).

Results obtained from *in vitro* studies are often not directly applicable to the *in vivo* situation. One of the most obvious differences between the situation *in vitro* and *in vivo* is the absence of processes regarding absorption, distribution, metabolism and excretion that govern the exposure of the target tissue of the organism *in vivo*. The concentrations to which *in vitro* systems are exposed may not correspond to the actual situation at the target tissue after *in vivo* exposure (Blaauboer, 2001).

In vivo experiments involve animals and humans. Different approaches of interspecies scaling of results are used. The most common one is, for the case of clearance, to use a simple body weight (BW) relationship: human CL = animal CL \cdot (human BW/ animal BW)^{0.75} (Bungay et al., 2011). Such straightforward extrapolations are possible only when a toxicodynamic response caused by a substances is situated in the blood (Lavé et al., 2007).

There is a mutual interest of interacting between experimentation and modelling. Modeling of *in vitro* systems can help verify which parameters in the system are important for control and modification for better accuracy of results of PBTK model. It is also the only way to obtain some quantitative and extrapolable results from the *in vitro* tests. However, information on free concentration outside and inside cells and partition coefficients is needed. TK model can help design of *in vitro* systems by predicting expected range of concentrations at target organ level for applied dose.

Despite considerable progress in the development of these *in silico* approaches, there is still a need to develop practical tools for risk assessors, who increasingly need to rely on *in vitro* -to- *in vivo* extrapolations of chemical toxicity in order to carry out animal-free safety assessments. Recent work performed by

(Broeders, 2013) has illustrated several approaches to perform IVIVE or quantitative *In vitro* -to- *In vivo* extrapolation (QIVIVE). Uncertainties in the extrapolation from *in vitro* concentrations to *in vivo* human exposure conditions, including the influence of differences between species and exposure routes, can be taken into account by using the toxicokinetic and toxicodynamic computational models of a specific compound after oral, inhalation, or dermal exposure.

In vitro -to- *in vivo* correlation (IVIVC) has been defined by some authors to be a linear relationship between *in vitro* experimental results (eg. dissolution profiles of drugs) and *in vivo* experimental results (absorption rate) (Cardot and Beyssac, 2013). But in most cases it refers to extrapolating measurable *in vitro* effects to *in vivo* exposure scenarios and cellular *in vitro* responses to toxic responses *in vivo* (Blaauboer, 2010). In order to do it, we must first create a model representing well *in vitro* scenario and the model simulating *in vivo* effects and evaluate differences in predicting the same quantity. For example, *in vivo* -to- *in vitro* correlation (percentage of total absorption of chemical in the receptor fluid in terms of applied dose) ratio in assessing percutaneous skin absorption has been proposed by (Lehman et al., 2011). The authors used harmonised and non-harmonised dataset of 92 compounds including 30 organic ones. IVIV was found to be 0.96 for the harmonised data indicating higher absorption *in vivo*.

The prediction of *in vivo* liver clearance from *in vitro* kinetic parameters of metabolism, using a variety of systems including primary isolated or cryopreserved hepatocytes, hepatic microsomes and recombinantly expressed enzymes, requires *in vitro*- *in vivo* scaling (Barter et al., 2007; Pelkonen and Turpeinen, 2007). The clearance data obtained from *in vitro* studies are typically expressed as a function of microsomal protein concentration or on a per million hepatocyte basis, and thus needs to be scaled to reflect *in vivo* clearance rate - CLR (L/h/kg BW). For microsomes the *in vivo* scaling is calculated according to the enzyme content of the microsomal system (i.e., amount microsomal protein per gram of liver), and for hepatocytes, the scaling factor is determined by the hepatocyte content of the whole organ (i.e., number of cells per gram of liver). The obtained CLR_{int} values can then be easily scaled on a per kilogram body weight basis using the species-specific amount of liver (gram) per kilogram body-weight. This scaling however does not always well represent *in vivo* metabolism and additional parameters calibration with respect to *in vivo* blood concentration is often necessary. **Table 2.5.1** shows the most common scaling factors grouped together according to (Pelkonen and Turpeinen, 2007). Once the scaling is done (intrinsic clearance determined in vitro is scaled to *in vivo* total clearance), commonly the resulting clearance value is adjusted for liver clearance using liver blood flow (f_{liv}). There are two models to do so: well-stirred model (WSM) and parallel tube model (PTM) (Hallifax et al., 2010).

Table 2.5.1. Scaling factors for *in vitro*-to-*in vivo* extrapolation of liver metabolism

Type of system	Units of the measured rate	Multiplication factor
Liver slices	$\frac{pmol}{min \cdot mg_{total\ protein}}$	$HomPPGL = \frac{mg_{total\ protein}}{g_{liv}}$ Mg of homogenate protein per gram liver

Hepatocytes	$\frac{pmol}{min \cdot 10^6 cells}$	$HPGL = \frac{10^6 cells}{g_{liv}}$ Number of hepatocytes per gram liver
Liver microsomes	$\frac{pmol}{min \cdot mg_{protein}}$	$MPPGL = \frac{mg_{protein}}{g_{liv}}$ Mg of microsomal protein per gram liver
Recombinantly expressed enzymes	$\frac{pmol}{min \cdot pmol CYP_{isoform}}$	$MPPGL = \frac{mg_{protein}}{g_{liv}}$ and $CYP_{isoform} = \frac{pmol}{mg_{protein}}$ CYP content per mg of microsomal protein
Scaled total clearance from in vitro systems (CLR _{IVIVE}) to liver clearance (CLR _{liv})		
Model 1. WSM $CLR_{liv} = \frac{CLR_{IVIVE} \cdot f_{liv}}{CLR_{IVIVE} + f_{liv}}$ Model 2. PTM $CLR_{liv} = f_{liv} - f_{liv} \cdot \exp\left(-\frac{CLR_{IVIVE}}{f_{liv}}\right)$		

Cell-level toxicodynamics is described by the Virtual Cell-Based Assay (VCBA); this model simulates processes in an *in vitro* system, especially the fate of a chemical within the well, taking into account partitioning with protein, lipids, and plastic binding (Zaldívar et al., 2011, 2010). The model also features a growth model, which takes into account the cell growth phases (G1, S, G2, M phases). An additional feature takes into account the partitioning of compounds within the cell, and a toxicity model. The latter part of the model is based on two parameters: the no-effect concentration (NEC) and the killing rate (kt), which are linked to experimental cell viability. The main property simulated is the intracellular concentration of a specific chemical in the cell, and its effect (cell viability) to associate an *in vitro* effect (cell viability). In order to link this effect with a specific external dose, it is necessary to join a PBTK model with the VCBA: the cell growth and division model, the cell partitioning model, and the toxicity and effects model (which are elements of the VCBA model). The integration of these models, so called multi-scale modelling, allows *in vitro* – to – *in vivo* extrapolation to be performed. As mentioned before, the main objective of a multi-scale modelling is to study the methodology- based feasibility of overcoming the problems associated with the gaps between scales (i.e. cell and organ levels). This will allow to explore the continuum toxic effects and to establish an interface between different levels in terms of data and results transferability. The joint PBTK-VCBA models describe the relationship between the tissue dose, early chemical-tissue interactions, and resulting toxic effect(s); thus it can be used to predict the toxicologically effective target organ dose. The HepaRG and HepG2 cell lines are a good candidate for these studies (Zanelli et al., 2012).

2.6 Available software for PBTK-TD modelling

The Simcyp Simulator includes the Advanced Dissolution Absorption and Metabolism (ADAM) multi-compartmental GI tract (stomach, 7 small intestine parts and one colon) within which a substance exists in unreleased, undissolved, dissolved or degraded states (under fasting or fed conditions). Simcyp offers the

possibility to extrapolate results to different human populations based on a body condition (healthy, diseased, obese, slim, etc.), age (adults, children, and elderly), race (Caucasian, Asian populations, etc.). *In vitro*- to- *in vivo* extrapolations are possible, eg. in predicting drug-drug interactions by utilizing a relationship between *in vivo* inhibitor concentration at the active site and the inhibition constant determined *in vitro*. SimCyp not only simulate mean results but also the extremes in the population by applying Monte Carlo approach (Lavé et al., 2007). GastroPlus distributed by Simulations Plus uses the Advanced Compartmental Absorption Transit (ACAT) mechanistic absorption model. It includes a drug release simulation from the formulation (for immediate or controlled release), solubility (aqueous solubility-pH relationship, solubility factor – the ratio of ionised to unionised forms), dissolution (Weibull function), / precipitation rate (when a drug concentration exceeds its solubility), chemical stability, permeability, carrier mediated influx/ efflux and gut wall metabolism. Gastroplus contains an elaborate library with human and pre-clinical species physiologies. PK-Sim distributed by Bayer Technology Services consists of GI tract of 12 segments. Each compartment is sub-divided into vascular (plasma, red blood cells) and extravascular (cellular, interstitial) fractions. Multiple drug interactions are allowed and different virtual patient types. PBTK modelling in pre-clinical species and humans can simulate physiological variability in response. An additional feature of PK-Sim is its combinations with MoBi software which enables constructure of completely new PBTK model or modification of existing structures (Kostewicz et al., 2014). General modelling software such as Matlab, R or Berkley- Madonna provide a programming language for the model code, numerical solutions for differential equations that define the modelled system and basic graphical representation of results. These modelling software types offer much flexibility to the developers when compared to commercial software that contains a model library and allow for a specified structure of models only (being however more user friendly) (Khalil and Läer, 2011).

2.7 Literature applications of PBTK/TD models for case study compounds

Physiologically-based kinetic models can contribute to clinical research on drug development, including evaluation of efficacy and safety of active ingredients, enhancement of information during the development process, identify factors that contribute to drug response variability, dose requirements, time intervals between the dose injection and response, intensity and duration of effect, time-lag of absorption to systemic circulation, sensitivity of parameters to pharmacological effect. As mentioned before PBTK models are mainly applied in inter-or extrapolating between: i) dosing levels: e.g. from the high concentrations typically used in laboratory experiments to lower ones typically found in the environment; ii) exposure duration: e.g., from continuous to discontinuous, or single to multiple exposures; iii) routes of administration: e.g., from oral exposure to dermal or inhalation; iv) species: e.g., transpositions from rodents to human, prior to giving a drug for the first time to subjects of a clinical trial, or when experiments on humans are deemed unethical, such as when the compound is toxic without therapeutic benefit; v) individuals: e.g., from males to females, from adults to children, between populations; vi) from *in vitro*- to- *in vivo*. Other PBTK model applications

include: designing *in vitro*, *in vivo* experiments, determination of absorption rates, clearance, partition coefficients, etc., investigation of local effects-such as metabolism or bioaccumulation. **Table 2.7.1** lists the literature applications of PBTK models for the selected nine compounds.

Table 2.7.1 Review of literature applications of PBTK models for selected compounds

Compound	PBPK model for oral absorption	PBPK model for dermal absorption	PBPK model for inhalation	Application of the model
Coumarin	(Mielke et al., 2011; Rietjens et al., 2008; Ritschel et al., 1977)	(Mielke et al., 2011)	-	Oral-to-dermal extrapolation of the TDI oral dose, cross species dosimetry
Caffeine	(Ginsberg et al., 2004)	(Liu et al., 2011)	-	Development of predictive model and differences in modelling between neonates and adults; modelling of hair follicles impact on overall skin absorption
Hydroquinone	(Corley et al., 2000)	(Poet et al., 2010)	-	Estimation of concentration of toxic metabolite using rat oral NOEL dose and worst-case human dermal exposure to hydroquinone – determination of a margin of safety
Ethanol	(Loizou and Spendiff, 2004; MacDonald et al., 2002; Umulis et al., 2005)	(Webster and Gabler, 2008)	-	To predict ethanol and acetaldehyde blood/serum concentrations
Isopropanol	(Clewell Iii et al., 2001; Gentry et al., 2002)			Route-to-route and cross species dosimetry Reference dose and concentration metrics calculated for the developmental endpoints
Estragole	(Punt et al., 2009; Rietjens et al., 2010)	-	-	Interspecies extrapolation
Styrene	-	-	(Csanady et al., 1994; Jonsson and Johanson, 2002; Nakayama et al., 2005; Ramsey and Andersen, 1984; Sarangapani et al., 2002; Tornero-Velez and Rappaport, 2001)	Prediction of inhaled styrene in blood, investigation of metabolites
Methyl iodide	-	-	-	(Sweeney et al., 2009): Analysis of chemical specific

			rate parameters
Nicotine	(Teeguarden et al., 2013)	-	(Teeguarden et al., 2013) Simulating nicotine and its metabolite concentration-time profiles in blood

Toxicodynamic models when coupled to biokinetics are used to: derive dose-response relationships, simulate intensity of effect and its changes in time, predict acute effects (eg. blood pressure, heart rate) rather than chronic changes, indicate a bioavailable concentration of a chemical at a site of action that produces maximal effect. **Table 2.7.2** lists the literature applications of PBTK-TD models for selected compounds.

Table 2.7.2 Review of literature applications of PBTK-TD models for selected compounds

Compound	PBTK + toxicodynamics	Toxicodynamic endpoint
Coumarin	-	-
Caffeine	(Shi, 1993) (Hartley et al. 2000), (Denaro et al. 1990) (Acheson et al. 1980) (Damirchi et al. 2009) (Robertson et al. 1981)	Mean arterial pressure Systolic/ diastolic pressure Metabolic rate Heart rate Plasma renin activity
Hydroquinone	-	-
Ethanol	(MacDonald et al., 2002)	Central nervous system toxicity
Isopropanol	-	-
Estragole	-	-
Styrene	-	-
Methyl iodide	-	-
Nicotine	(Porchet et al., 1988; Teeguarden et al., 2013) (Fattinger et al. 1997) (Mundel and Jones, 2006)	Heart rate Diastolic, systolic blood pressure, plasma epinephrine

2.8 Strengths and limitations of PBTK-TD modelling

PBTK models differ from classical PK models in that they include physiological information about the living organism in specific organ/tissue compartments involved in exposure, toxicity, biotransformation and clearance processes that are connected by blood flow. Incorporation of physiologically meaningful parameters allows for interspecies extrapolation by altering the physiological parameters appropriately. Mechanistically- based PBTK models offer the following advantages over empirically based phenomenological models in risk assessment applications:

- In principle, it is permissible to extrapolate the predictions of mechanistic models beyond a validated range, whereas only interpolation within a validated range is strictly permissible for empirical

models (PBPK model versus compartmental approach) eg. PBTK model can extrapolate from fasted to fed state to investigate food effects.

- They are more suited to perform interspecies and route-to-route extrapolations than are empirical models. Since the former models describe the physical processes underlying the observed phenomena, the models can be iteratively refined to describe the underlying processes in greater detail as additional data becomes available and modifications to the model are necessitated (Roy and Georgopoulos, 1997). Empirical models require prior *in vivo* measure of concentration-time profiles to define the model parameters. The models are flexible in terms of their structures: if information about fate of chemicals in particular organs is not available, to reduce determination of a number of uncertain parameters in the model so called lumping of parameters is commonly employed to reduce the dimensionality and complexity of whole body model placing tissues that show similar kinetics together to form fewer compartments (e. highly or poorly perfused tissues). Despite the complexity and data-rich nature of the models, they proved to be reliable in predicting plasma profiles.
- PBTK-TD models are commonly used in pre-clinical research of drugs to estimate efficacious human dose and to design and help clinical trials become confirmatory (Khalil and Läer, 2011). The models can bridge between a pharmacology of different populations, reduce unnecessary animal testing and save time and resources used for testing by exploring “what if” scenarios to determine the most likely cause of altered pharmacokinetics and help in guiding clinical trials by suggesting a dose or dose range or optimal sampling times (Khalil and Läer, 2011). The models can identify and prioritise compounds for *in vivo* studies.

Limitations are mainly in the following aspects:

- Comprehensive data about the physiological, biochemical, and physicochemical processes are required to build a PBTK model. They are not available from only one source, which may lead to some confusion and to a problem in establishing a reliable source of accurate and consistent information. Often PBTK models describe well only some processes but others are partly or poorly characterised, as information gaps may exist (Khalil and Laer, 2011). Building of PBTK model requires measured chemical concentrations in numerous organs and tissues. It is difficult to build robust predictive models when blood/plasma concentrations are available only.
- The model often fails to optimally describe the pharmacokinetic behavior of some drugs in a population due to lack of variability in simulated ADME processes between different subjects. Therefore, it is important to emphasise the applicability domain of the model and the quality of simulations (Khalil and Laer, 2011).
- The models are subject to parameters estimation problems, uncertainty, variability and prediction errors. Poor quality modeling and simulations practices could lead to a biased model or overestimation of the predictive power of the model (Khalil and Laer, 2011).

- Model parameters calibrated for a specific exposure scenario and group of people may not be extrapolable for other conditions especially for single vs repeated dosing, different type of vehicles, concentration of chemical, etc.
- The PBTK models are built on a lumped different tissue compartments (like the interstitial and cellular sub-compartment), and they assume a quasi-equilibrium between the concentrations in the compartments ("steady state assumption") and model parameters are in most cases assumed constant in time.

Advantages and limitations of literature models and lack of models for case-study substances are described in **Table 2.8.1**.

Table 2.8.1. Pros and cons of PBTK modelling for selected substances in literature

Compound	Advantages	Main limitations
Coumarin	<ul style="list-style-type: none"> - Simple PBPK modelling, up to 11 single compartments - Kinetics of toxic metabolite included - oral-to-dermal and interspecies extrapolations performed - <i>in vitro</i>- to- <i>in vivo</i> scaling of liver metabolism - simulated liver and blood concentrations 	<ul style="list-style-type: none"> - Assumed first order rate of absorption for both oral (straight to the liver) and dermal administrations (straight to the blood) - PBPK model for dermal absorption was not validated on <i>in vivo</i> data - Single dosing conditions only
Caffeine	<ul style="list-style-type: none"> - A basic five-compartment flow-limited model - The model takes into account metabolism differences between neonates and adults - Kinetics of metabolites included - <i>in vitro</i>- to- <i>in vivo</i> scaling of liver metabolism 	<ul style="list-style-type: none"> - Skin model consisted of <i>stratum corneum</i> and hair follicles as sub-compartments only attached to the overall body compartment, first order rate absorption rather than diffusion were used - Single dosing conditions only - No RtR extrapolation
Hydroquinone	<ul style="list-style-type: none"> - Simple PBPK modelling, up to 9 single compartments - Kinetics of metabolites included - oral-to-dermal and interspecies extrapolation performed - <i>in vitro</i>- to- <i>in vivo</i> scaling of liver metabolism - Blood and urine concentrations simulated - Hydroquinone binding to plasma considered 	<ul style="list-style-type: none"> - Assumed first order rate of absorption for oral administration and dermal permeability coefficient for the first order rate absorption from the skin - No partition between skin and vehicle was taken into account - Single dosing conditions only
Ethanol	<ul style="list-style-type: none"> - Simple and more refined models with sub-compartments in GI tract available - Good performance of proposed model structure in predicting ethanol and its main metabolite concentrations in blood - Simulated brain concentrations - <i>in vitro</i>- to- <i>in vivo</i> scaling of liver 	<ul style="list-style-type: none"> - No inhalation modelled - No detailed structure of PBPK model for dermal absorption - ADME profiles of only main metabolite modelled - No RtR and interspecies extrapolations - Single dosing conditions only

	metabolism	
Isopropanol	<ul style="list-style-type: none"> - Sub-compartments in respiratory and GI tract better reflect absorption profiles - Kinetics of metabolite included - Interspecies extrapolation - Simulated concentrations in arterial and venous blood, exhaled air and urine 	<ul style="list-style-type: none"> - Skin absorption was not predicted - No RtR extrapolation - Single dosing conditions only
Estragole	<ul style="list-style-type: none"> - Simple 9-compartment PBPK model (no sub-compartments) - Kinetics of metabolites considered - <i>in vitro</i>- to- <i>in vivo</i> scaling of liver metabolism - simulated liver and blood concentrations - interspecies extrapolation 	<ul style="list-style-type: none"> - No dermal PBPK model available - Oral PBPK model not validated on <i>in vivo</i> data (lack of data) – only data for metabolites available - Metabolism rates measured <i>in vitro</i> - No information about oral absorption rates - No RtR extrapolation - Single dosing conditions only
Styrene	<ul style="list-style-type: none"> - Probabilistic approach of PBPK modelling (Bayesian population approach) - Refined description of lungs - Simulated blood and exhaled air concentrations - interspecies extrapolation - <i>in vitro</i>- to- <i>in vivo</i> scaling of liver metabolism 	<ul style="list-style-type: none"> - No dermal and oral modelling - No RtR extrapolation - Single dosing conditions only
Methyl iodide	<ul style="list-style-type: none"> - Interspecies comparison of ADME parameters 	<ul style="list-style-type: none"> - No PBPK model predictive performance showed for any of exposure routes except for i.v. dose (lack of <i>in vivo</i> data) - No RtR extrapolation
Nicotine	<ul style="list-style-type: none"> - Relatively simple models, no sub-compartments - Repeated exposure was considered for i.v. injection and inhalation - Simulated concentrations in venous/ arterial blood, brains 	<ul style="list-style-type: none"> - Dermal absorption was not modelled - Most of the PBPK models were validated on i.v. data - No RtR extrapolation - No simulated repeated exposure for oral and dermal routes

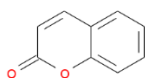
2.9 Case study compounds

This section provides general information about occurrence, physicochemical properties, health risks, human exposure and metabolism/elimination of 9 case study compounds (cosmetic, food ingredients and industrial chemicals) used as the subject of the thesis: coumarin, estragole, hydroquinone, caffeine, ethanol, isopropanol, styrene, methyl iodide and nicotine (**Table 2.9.1**).

Table 2.9.1 Case- study compounds used in this work for single and repeated exposure

Compound name	PBTK: oral	PBTK: dermal	PBTK: inhalation	PBTK-PBTD	VCBA
Coumarin	single	single	-	-	-
Estragole	single	-	-	-	-
Hydroquinone	single	single	-	-	-
Caffeine	single	single	-	single	single
	repeated			repeated	repeated
Ethanol	single	single	single	-	-
Isopropanol	single	single	single	-	-
Styrene	-	-	single	-	-
Methyl iodide	-	single		-	-
Nicotine	single	single	single	Single	-
	repeated	repeated	repeated	Repeated	

2.9.1 Coumarin



Coumarin (CAS: 91-64-5) is used as a fragrance and is a natural ingredient of several herbs, beverages, tobacco and spices. Oral intake of coumarin is mostly related to consumption of cinnamon-containing foods or cinnamon as a spice. Dermal exposure can occur since synthetic coumarin is added as a fragrance ingredient to perfumes, skin gels, lotions and deodorants as a masking agent. The maximum daily human exposure to coumarin from dietary sources for a 60- kg- consumer has been estimated to be 0.02 mg/kg/day (Lake, 1999). From fragrance use in cosmetic products, dermal coumarin exposure has been estimated to be 0.04 mg/kg/day (The Metabolomics Innovation Centre, 2013). The total daily human exposure from dietary sources together with fragrance use in cosmetic products is thus 0.06 mg/kg/day (Lake, 1999). Physicochemical properties of coumarin are provided in **Table 2.9.2**. Coumarin shows hepatotoxic and carcinogenic properties mainly in rodents, and can also trigger allergic reactions and dermatitis. The European Food Safety Authority derived a TDI of 0 to 0.1 mg coumarin/kg body weight based on a NOAEL of 10 mg coumarin/kg BW/day observed for liver toxicity in a two year dog study (EFSA, 2004). In rats, no-effect levels for hepatotoxic effects ranged from 50-130 mg/kg BW/day (EFSA, 2004). However, (Carlton et al., 1996) shows that survival of Sprague-Dawley rats was decreased at 333 ppm (\approx 16 mg/kg BW/day). Therefore, in this study, the rat LOAEL of 16 mg/kg BW/day (Carlton et al., 1996) was taken as the most relevant external Point of Departure (POD) to simulate an internal human exposure.

As illustrated in **Figure 2.9.1**, coumarin is extensively metabolised by the liver to various polar products including 3-, 4- and 7-hydroxycoumarins (3-HC, 4-HC and 7-HC) 6,7-dihydroxycoumarin (6,7-DiHC), o-coumaric acid (o-CA), o-hydroxyphenyl-acetaldehyde (o-HPA), o-hydroxyphenylethanol (o-HPE), o-hydroxyphenylacetic acid (o-HPAA) and o-hydroxyphenylpropionic acid (o-HPPA) and to product(s) that bind covalently to microsomal proteins (van Iersel et al., 1994). In humans, it appears that coumarin is extensively metabolised to 7-hydroxycoumarin (7-HC), and in a smaller amount to 3-hydroxycoumarin (3-

HC), while in the rat and mouse the major route of metabolism is by a 3,4-epoxidation pathway resulting in the formation of coumarin 3,4 -epoxide which is rearranged to a toxic metabolite, o-hydroxyphenylacetaldehyde (o-HPA) which is detoxified to o-hydroxyphenylacetic acid (o-HPAA) and o-hydroxyphenylethanol (o-HPE) (Rietjens et al., 2008).

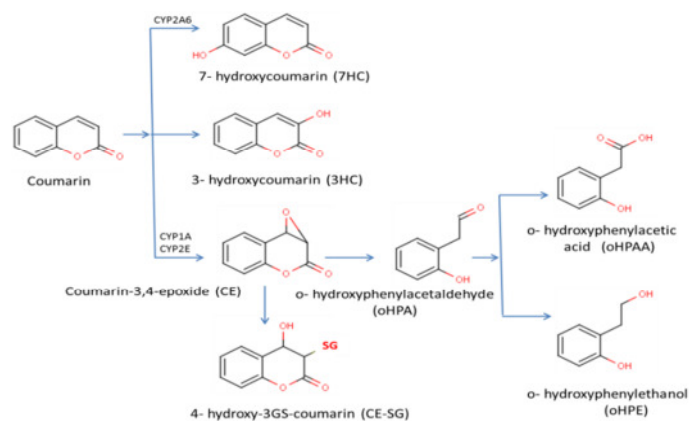


Fig 2.9.1: Major metabolic pathways for coumarin in rat and human liver (Rietjens et al., 2008).

The construction of simple physiologically-based predictive models incorporating the metabolic pathways of coumarin has already been described in the literature (Mielke et al., 2011; Rietjens et al., 2008; Ritschel et al., 1977). In those studies, the RtR extrapolation of a single tolerable daily intake (TDI) dose of coumarin (0.1 mg/kg BW; see above) was carried out by comparing the AUC and C_{max} of coumarin in blood and liver. The dermal AUC of blood was found to be higher (Mielke et al., 2011) than the oral one in this study.

Table 2.9.2. Physicochemical properties of coumarin

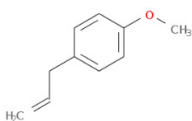
Physicochemical properties	Value	Reference
MW - molecular weight	146.14	
MV - molar volume	117.1	
HBA - hydrogen bond acceptors	2	
HBD- hydrogen bond donors	0	(1)
Hb - number of hydrogens	6	
cb - the number of carbons not involved in a C= O bond	8	
MR - molecular refractivity	39.8	
Mpt - melting point	71	
pKa	6.5	assumed
$\log P_{oct}$ - octanol-water partition coefficient	1.39	
fu (free fraction of drug in plasma)	0.5	(2)
RBP	0.99	(3)

(1) ChemSpider: <http://www.chemspider.com/> (last access: 06.10.2014)

(2) EDETOX database: <http://edetox.ncl.ac.uk/chemicals.aspx?id=97> (last access: 06.10.2014)

(3) ADMET Predictor computer software available from <https://www.simulations-plus.com/> (last access: 06.10.2014)

2.9.2 Estragole



Estragole (CAS: 140-67-0) occurs naturally in many culinary herbs, including anise, star anise, basil, bay, tarragon, fennel, and marjoram. Widespread human exposure to estragole occurs through the consumption of these herbs and through the use of the oils derived from them as flavors and fragrances in numerous foods, cosmetics, and other consumer products. Estragole is a constituent of turpentine oil, and indoor air exposure may result from the use of turpentine oil in furniture and other wood treatments. Physicochemical properties of estragole are provided in **Table 2.9.3**. The compound is metabolised by the liver to 1'-hydroxyestragole and several epoxide compounds (**Figure 2.9.2**). 1'-Hydroxyestragole is further conjugated with sulfate to form a sulfuric acid ester compound that readily binds to DNA and is responsible for most, if not all, of estragole's hepatocellular carcinogenicity in mice. The ultimate carcinogenic metabolite is unstable and degrades in aqueous environment to a reactive carbocation that is capable of forming DNA adducts. Metabolism of estragole through this pathway appears to be quantitatively consistent among humans and rodents. However, species differences in metabolism and metabolic activation can also occur, eg. male rats are more efficient in sulfonation of 1'-hydroxyestragole than humans. In addition, dose-dependent effects in metabolism of estragole have been revealed in both rats and mice exposed to different oral doses of estragole. In these species the relative extent of O-demethylation decreased with increasing doses accompanied by a relative increase in excretion of 1'-hydroxyestragole glucuronide in the urine (Punt et al., 2009).

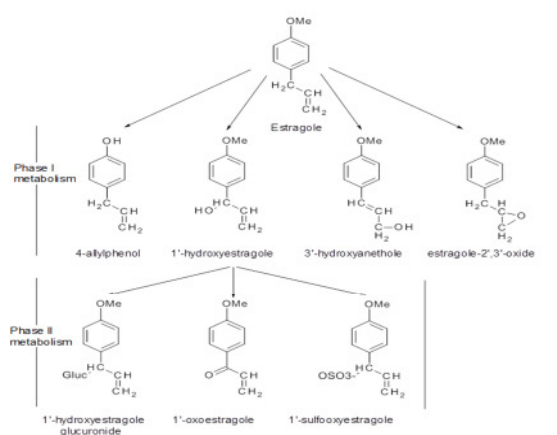


Fig 2.9.2. Metabolic pathways of estragole in liver (Punt et al., 2009).

Table 2.9.3. Physicochemical properties of estragole

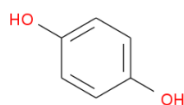
Physicochemical properties	Value	Reference
MW - molecular weight	148.2	

MV - molar volume	157.9	
HBA - hydrogen bond acceptors	1	
HBD- hydrogen bond donors	0	(1)
Mpt - melting point	272	
Hb - number of hydrogens	12	
cb - the number of carbons not involved in a C= O bond	10	
MR - molecular refractivity	46.8	
pKa	not available	
logP _{oct} - octanol-water partition coefficient	3.13	(Punt et al., 2009)
fu (free fraction of drug in plasma)	0.37	
RBP	0.91	(2)

(1) ChemSpider: <http://www.chemspider.com/> (last access: 06.10.2014)

(2) ADMET Predictor computer software available from <https://www.simulations-plus.com/> (last access: 06.10.2014)

2.9.3 Hydroquinone



Hydroquinone (CAS: 123-31-9) is used as a skin whitening agent in creams to reduce the colour of the skin, in oxidative hair dyes, and in artificial nail (manicure) preparations. Physicochemical properties of hydroquinone are provided in **Table 2.9.4**. Repeated oral dosing caused tremors and reduced activity (≥ 64 mg/kg), reduced body weight gain (≥ 200 mg/kg BW), convulsions (≥ 400 mg/kg BW), and nephropathy in F-344 rats (≥ 100 mg/kg BW). An overall rat NOAEL (for all effects) of 20 mg/kg BW/day was derived (OECD SIDS, 1996; Poet et al., 2010). Metabolism to reactive intermediates in the liver is involved in the renal toxicity and exacerbation of chronic progressive nephropathy associated with hydroquinone ingestion. The formation of benzoquinone is the first critical step toward the formation of toxic metabolites (**Figure 2.9.3**). Following oral administration, the majority of metabolites are conjugates of glucuronic (up to 67%) and sulphuric (up to 33%) acids (Corley et al., 2000; McGregor, 2007; Poet et al., 2010). Skin enzymes responsible for metabolism of hydroquinone are reported to have activities ranging from $<1\%$ up to 25% of the activity in the liver (Poet et al., 2010). PBTK model for hydroquinone has been already used in the literature to compare human internal dose metrics following oral and dermal exposures of estimated glutathione conjugates at the applied NOAEL dose (human equivalent concentration) (Corley et al., 2000; McGregor, 2007; Poet et al., 2010).

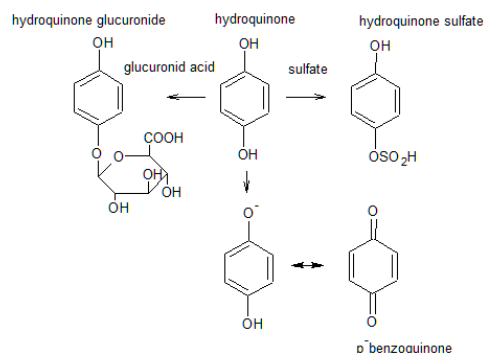


Fig 2.9.3. Metabolism of hydroquinone in liver (McGregor, 2007).

Table 2.9.4. Physicochemical properties of hydroquinone

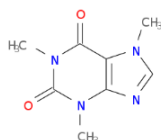
Physicochemical properties	Value	Reference
MW - molecular weight	110.1	
MV - molar volume	86.3	
HBA - hydrogen bond acceptors	2	(1)
HBD- hydrogen bond donors	2	
Mpt - melting point	173.5	
Hb - number of hydrogens	6	
cb - the number of carbons not involved in a C= O bond	6	
MR - molecular refractivity	30.0	
pKa	10.9	(2)
logP _{oct} - octanol-water partition coefficient	0.59	
fu (free fraction of drug in plasma)	0.97 (irreversible) 0.42 (reversible)	(Corley et al., 2000)
RBP	0.15	(3)

(1) ChemSpider: <http://www.chemspider.com/> (last access: 06.10.2014)

(2) EDETOX database: <http://edetox.ncl.ac.uk/chemicals.aspx?id=97> (last access: 06.10.2014)

(3) ADMET Predictor computer software available from <https://www.simulations-plus.com/> (last access: 06.10.2014)

2.9.4 Caffeine



Caffeine (CAS: 58-08-2) is found in varying quantities in the seeds, leaves, and fruit of some plants. It is used in many creams and lotions since it is believed to slow down the photoaging process of the skin and to absorb ultraviolet radiation thereby preventing the development of tumours after skin exposure to sunlight. It is also used as an active compound in anti-cellulite products as it is argued to prevent excessive accumulation

of fat in cells. This alkaloid has potent antioxidant properties. It supposedly increases the microcirculation of blood in the skin and also stimulates the growth of hair through inhibition of the 5- α -reductase activity (Herman and Herman, 2012). Physicochemical properties of caffeine are provided in **Table 2.9.5**.

Caffeine is rapidly absorbed from the gastrointestinal (GI) tract, and is almost completely metabolised in the liver. The amount of unchanged caffeine excreted in urine was found very small, typically 0.5-3.5% of the administered dose (Newton et al., 1981). The main route of metabolism in humans (70-80%) is via N-3 demethylation to paraxanthine (**Figure 2.9.4**). This reaction is carried out by CYP1A2 in the liver. Experiments with human liver microsomes estimate that 1-N-demethylation to theobromine accounts for approximately 8% of caffeine metabolism with 7-N-demethylation to theophylline also around 8%. The remaining 15% of caffeine undergoes C-8 hydroxylation to form 1,3,7-trimethyluric acid (OECD SIDS, 2002a) (not shown in figure). The metabolism and toxicokinetics of caffeine, and the use of this information in PBTK modelling, have been described in previous studies (Csajka et al., 2005; Ginsberg et al., 2004; Lelo et al., 1986; Zandvliet et al., 2005).

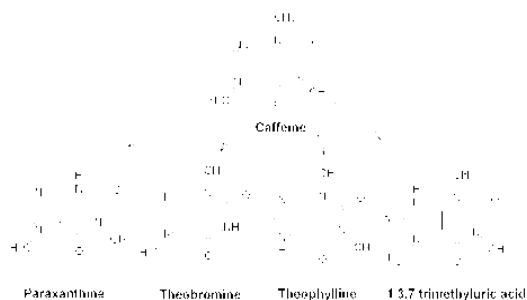


Fig 2.9.4: Major metabolic pathways for caffeine⁶.

Recent animal studies have demonstrated that depending on the method of administration and species, NOAELs can vary quite largely. A number of references were considered, such as the OECD SIDS report (OECD SIDS, 2002b). Amongst others the following NOAEL indications were found: a developmental NOAEL in rodents of approximately 30 mg/kg BW/day, a teratogenic NOAEL of 100 mg/kg BW/day, a reproductive NOAEL of 80–120 mg/kg BW/day, a NOAEL for offspring <12.5 mg/kg BW/d and a NOAEL for fetotoxicity of 10 mg/kg BW/day. As the purpose of this study is not to scrutinise existing information for the most relevant NOAEL, we have arbitrarily chosen a rat NOAEL of 10 mg/kg BW/day (Brent et al., 2011; OECD SIDS, 2002b). As far as the authors of this report are aware, no clarity exists as to the MOA of the adverse effects observed or the substance responsible for the effect that the various NOAELs are based on, be it caffeine, (a) metabolite(s), or a combination of parent compound and metabolites.

Table 2.9.5. Physicochemical properties of caffeine

Physicochemical properties	Value	Reference
MW – molecular weight	194.2	

⁶ <http://udel.edu/~danikoll/metabolism.html> (last access: 06.10.2014)

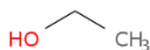
MV – molar volume	133.4	
HBA – hydrogen bond acceptors	6	(1)
HBD- hydrogen bond donors	0	
Mpt – melting point	238	
Hb – number of hydrogens	9	
cb - the number of carbons not involved in a C= O bond	6	
MR – molecular refractivity	50.4	
pKa	10.4	
logP _{oct} – octanol-water partition coefficient	-0.07	(2)
fu (free fraction of drug in plasma)	0.65	(Yamazaki and Kanaoka, 2004)
RBP	0.35	(3)

(1) ChemSpider: <http://www.chemspider.com/> (last access: 06.10.2014)

(2) EDETOX database: <http://edetox.ncl.ac.uk/chemicals.aspx?id=97> (last access: 06.10.2014)

(3) ADMET Predictor computer software available from <https://www.simulations-plus.com/> (last access: 06.10.2014)

2.9.5 Ethanol



In addition to its industrial applications, ethanol (CAS: 64-17-5) has widespread use as a solvent, preservative or an intermediate in personal care products and pharmaceuticals including scents, flavorings, cough treatments, antibiotics, vaccines, tablets, vitamins and many others. However, it is best known as the psychoactive ingredient commonly used in a variety of alcoholic beverages. Physicochemical properties of ethanol are in **Table 2.9.6**. High NOAEL dose (1.73 g/kg BW/day) was determined in subchronic rat studies for the endpoints in renal tubular epithelial hyperplasia in males (ECHA, 2014a). LOAEL dose was identified to be 3.16 g/kg BW/ day.

The excretion of ethanol from the human body is very rapid and the detection time in saliva, breath or blood is typically limited to 12 hours and a few hours longer in urine, depending on the amount of alcohol ingested (Helander et al., 1996; Ramchandani et al., 2001; Wurst et al., 2000). This makes ethanol detection difficult in situations in which it is important to know if there has been recent alcohol intake and particularly also the time since ethanol was consumed. This is the case in forensic investigations such as drunk driving claims, proof of drinking by courts, clinical analysis to document abstinence in treatment programmes and for random alcohol testing in workplaces and schools. Furthermore, in anti-doping control programmes, the detection of ethanol could be useful since there is evidence that excessive alcohol consumption may cause false-positive detection for testosterone abuse by influencing the urinary testosterone/epitestosterone ratio (Große et al., 2009; Sarkola and Eriksson, 2003). Following alcohol intake, most (>90-95 %) of the ethanol is metabolised in the liver by alcohol dehydrogenase to acetaldehyde and then to acetic acid by aldehyde

dehydrogenase (Ramchandani et al., 2001; Wurst et al., 2000). Ethyl glucuronide (EtG) and ethyl sulfate (EtS), two minor metabolites of ethanol (about <0.1% of ethanol ingested is excreted in this way), can be detected for longer than ethanol itself and their presence in urine provides a strong indication of recent drinking (Helander and Beck, 2005; Seidl et al., 2001; Wurst and Metzger, 2002; Wurst et al., 2006, 2003a, 2003b, 2000) – **Figure 2.9.5**. Hence, these metabolites are used as valuable biomarkers of alcohol intake and they can extend the time window for detection of recent alcohol drinking. Many analytical methods, mainly using mass spectrometry, have been developed to analyse EtG and EtS in several biological matrices (e.g. serum, urine, hair) (Bicker et al., 2006; Dresen et al., 2004; Favretto et al., 2010; Politi et al., 2005). (Lostia et al., 2013) published the results of a drinking experiment designed to obtain a more accurate and comprehensive description of EtG and EtS concentration-time profiles in biological matrices. Furthermore, some controlled drinking experiments, using human volunteers, were designed to investigate the kinetics of ethyl glucuronide and ethyl sulfate in urine and serum as a means to evaluate their possible use to calculate the time of alcohol consumption (Halter et al., 2008; Høiset et al., 2010). Using the experimental data from these drinking experiments, two simple computer-based models have been developed to simulate the kinetics of EtG and EtS in blood (Droenner et al., 2002; Schmitt et al., 2010). Physiologically-based toxicokinetic modelling of ethanol and acetaldehyde (following single oral administration of alcohol) is described in literature by (Loizou and Spendiff, 2004; Pastino and Conolly, 2000; Umulis et al., 2005), whereas experimental results on human subjects by (Jones et al., 1990, 1988; Wilkinson et al., 1977a, 1977b). *In vivo* dermal absorption of ethanol has also been investigated with emphasis on influence of different ethanol concentrations on overall absorption by (Kramer et al., 2007).

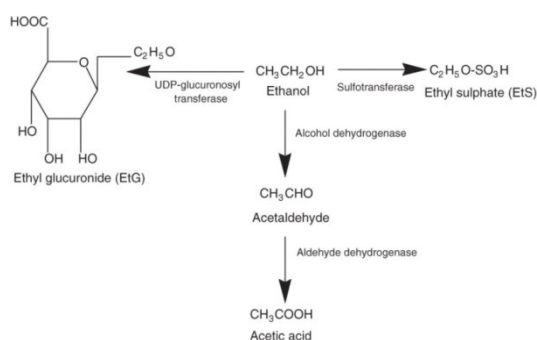


Fig 2.9.5. Ethanol metabolism in liver.

Table 2.9.6. Physicochemical properties of ethanol

Physicochemical properties	Value	Reference
MW - molecular weight	46.07	
MV - molar volume	59.1	
HBA - hydrogen bond acceptors	1	
HBD- hydrogen bond donors	1	(1)
Mpt - melting point	-114.1	
Hb - number of hydrogens	6	

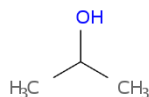
cb - the number of carbons not involved in a C= O bond	2	
MR - molecular refractivity	12.9	
pKa	15.9	
VP- vapour pressure [Pa]	7910	(2)
logP _{oct} - octanol-water partition coefficient	-0.31	
fu (free fraction of drug in plasma)	1	
RBP	1	(3)

(1) ChemSpider: <http://www.chemspider.com/> (last access: 06.10.2014)

(2) EDETOX database: <http://edetox.ncl.ac.uk/chemicals.aspx?id=97> (last access: 06.10.2014)

(3) ADMET Predictor computer software available from <https://www.simulations-plus.com/> (last access: 06.10.2014)

2.9.6 Isopropanol



Isopropanol (CAS: 67-63-0) is a colorless liquid alcohol found in many consumer products. Most consumers will be familiar with isopropanol in the form of rubbing alcohol for disinfection of wounds. It is also used as a solvent in a number of consumer and industrial products including antifreeze, lotions, car care products, and cosmetics. Physicochemical properties of isopropanol are given in **Table 2.9.7**. Exposure to low levels of isopropanol is not expected to be hazardous. Subchronic rat experiments (with liver as target organ) were carried out to determine NOAEL (2mg/kg BW/day) and LOAEL (20mg/kg BW/day) doses (FDA, 1968). Commercially available hand rubs include ethanol and isopropyl alcohol. Isopropyl alcohol appears to be more toxic than ethanol, but less so than methanol. . Toxicity usually occurs after ingestion (the fatal oral dose in adult humans has been reported to be 240 mL) but also toxicity after inhalation and dermal absorption. Symptoms and signs of isopropyl alcohol intoxication include headache, dizziness, incoordination, hypoglycaemia, abdominal pain, nausea, vomiting, respiratory depression, hypotension, and coma. Apart from the acute toxicity noted above, animal studies suggest that exposure to isopropyl alcohol is a low potential hazard to human health.. 20 to 50% of an absorbed isopropanol dose is excreted unchanged. Most isopropyl alcohol is oxidised in the liver by alcohol dehydrogenase to acetone, which is probably further metabolised to acetate, formate, and finally carbon dioxide (**Figure 2.9.6**). Acetone may contribute to the CNS depression seen in isopropanol poisoning⁷.

⁷ <http://www.inchem.org/> (last access: 06.10.2014)

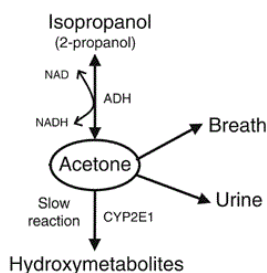


Fig 2.9.6. Metabolism of isopropanol to acetone in liver⁸.

Table 2.9.7. Physicochemical properties of isopropanol

Physicochemical properties	Value	Reference
MW - molecular weight	60.1	
MV - molar volume	75.9	
HBA - hydrogen bond acceptors	1	(1)
HBD- hydrogen bond donors	1	
Mpt - melting point	-89.16	
Hb - number of hydrogens	7	
cb - the number of carbons not involved in a C= O bond	2	
MR - molecular refractivity	17.4	
VP- vapour pressure [Pa]	6050	
pKa	17.1	(4)
logP _{oct} - octanol-water partition coefficient	0.03	(OECD SIDS, n.d.)
fu (free fraction of drug in plasma)	1	(3)
RBP	1	

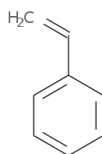
(1) ChemSpider: <http://www.chemspider.com/> (last access: 06.10.2014)

(2) EDETOX database: <http://edetox.ncl.ac.uk/chemicals.aspx?id=97> (last access: 06.10.2014)

(3) ADMET Predictor computer software available from <https://www.simulations-plus.com/> (last access: 06.10.2014)

(4) http://chemweb.unp.ac.za/chemistry/Physical_Data/pKa_values.htm (last access: 06.10.2014)

2.9.7 Styrene



⁸ <http://www.proteinpower.com/drmike/important-information/low-carbers-beware-the-breathalyzer/> (last access: 06.10.2014)

Styrene (CAS: 100-42-5) is primarily a synthetic chemical. It is also known as vinylbenzene, ethenylbenzene, cinnamene, or phenylethylene. It's a colorless liquid that evaporates easily and has a sweet smell. Styrene is used predominately in the production of polystyrene plastics and resins. Styrene is also used as an intermediate in the synthesis of materials used for ion exchange resins and to produce copolymers. Low levels of styrene also occur naturally in a variety of foods such as fruits, vegetables, nuts, beverages, and meats. Physicochemical properties of styrene are provided in **Table 2.9.8**.

Exposure to styrene is most likely to occur from breathing indoor air that is contaminated with styrene vapors from building materials, tobacco smoke, and use of copying machines. Exposure may also occur by breathing automobile exhaust. People who work where styrene is used or manufactured are likely to be exposed to it by breathing workplace air. Breathing styrene is most likely to affect the nervous system. Styrene is low in acute and chronic toxicity (Ramsey and Andersen, 1984). The majority of the absorbed material (about 90%) in man is metabolised in the liver by oxidation of the vinyl side group to styrene oxide. Styrene oxide is the active metabolite. The resulting major metabolites which are excreted are mandelic acid (60-80%) and phenylglyoxylic acid (about 30%) – **Figure 2.9.7**. Only very small quantities of hippuric acid are produced. The main metabolites, mandelic acid and phenylglyoxylic acid, are excreted in the urine. Hippuric acid and 4-vinylphenol are minor metabolites of styrene. About 1 to 2% of a dose is exhaled unchanged. Breath styrene concentrations represent about 25% of the corresponding air styrene concentration during constant exposure. (Csanady et al., 1994) developed a PBTK model for styrene and its metabolite (styrene-7,8-oxide).

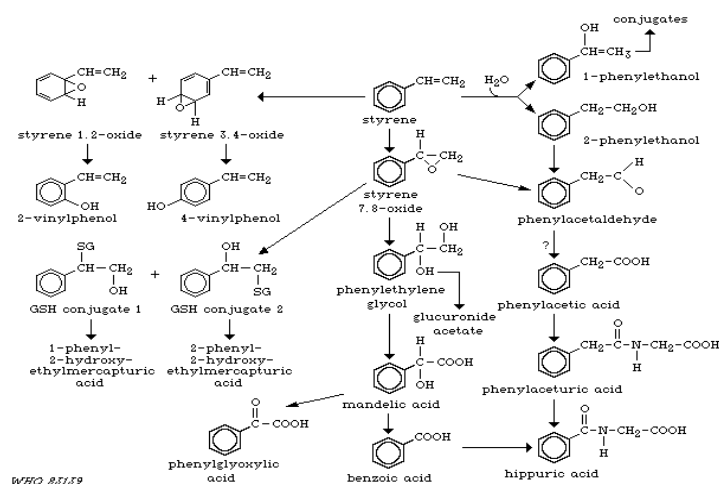


Fig 2.9.7. Metabolic pathways of styrene⁹.

Table 2.9.8. Physicochemical properties of styrene

Physicochemical properties	Value	Reference
MW - molecular weight	104.15	

⁹ <http://www.inchem.org/documents/ehc/ehc/ehc26.htm> (last access: 06.10.2014)

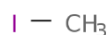
MV - molar volume	115.4	
HBA - hydrogen bond acceptors	0	(1)
HBD- hydrogen bond donors	0	
Mpt - melting point	-48.3	
Hb - number of hydrogens	8	
cb - the number of carbons not involved in a C= O bond	8	
MR - molecular refractivity	37.2	
pKa	-	
VP- vapour pressure [Pa]	853	(2)
logP _{oct} - octanol-water partition coefficient	2.95	
fu (free fraction of drug in plasma)	0.68	
RBP	1.22	(3)

(1) ChemSpider: <http://www.chemspider.com/> (last access: 06.10.2014)

(2) EDETOX database: <http://edetox.ncl.ac.uk/chemicals.aspx?id=97> (last access: 06.10.2014)

(3) ADMET Predictor computer software available from <https://www.simulations-plus.com/> (last access: 06.10.2014)

2.9.8 Methyl iodide



Methyl iodide (CAS: 74-88-4) or iodomethane has similar structure to methane with replacement of one hydrogen atom by an atom of iodine. It has been used as methylating agent, laboratory reagent or pesticide as iodomethane is a new agricultural active ingredient. The compound is used also as an intermediate in the manufacture of some pharmaceuticals, in methylation processes, and in the field of microscopy. Physicochemical properties of iodomethane are provided in **Table 2.9.9**. People may be exposed to low levels of iodomethane in air from agricultural uses due to volatilization following application. Specifically, fumigants can off-gas into air and be transported off-site by meteorological processes. Agricultural field workers may be exposed to iodomethane during or after the application process. However, there are no reported human exposure incident reports related to agricultural uses (Mileson et al., 2009).

Many recent studies indicated neurotoxic as well as fetal toxic effects in laboratory animals. There are 11 cases of acute methyl iodide exposure in the medical literature. The human exposure to methyl iodide occurs through routes like dermal, inhalation, and oral ingestion. Acute exposures to methyl iodide have frequently occurred in the workplace. Predominantly neuropsychiatric symptoms of acute exposure to monohalomethanes consist of headache, nausea, vomiting, drowsiness, dizziness, giddiness, diarrhea, confusion, ataxia, slurred speech, paralysis, convulsions, delirium, coma, and death (Parkar and Mayanil, 2012). One case of suicidal parenteral exposure has been reported (Robertz-Vaupel et al., 1991). The primary target organs in cases of severe poisoning are lungs, liver, kidney, and brain. Animal studies have shown methyl iodide to be a potential carcinogen and teratogen. More information about toxicity of this compound

is provided in (Buckell, 1950; Nair and Chatterjee, 2010; Parkar and Mayanil, 2012). Dermal rat NOAEL dose is 30 mg/kg BW/day (ECHA, 2014b) based on secondary histopathological effects and organ weight changes; several secondary effects attributed to the severe skin irritation including changes in hematology, clinical chemistry and urinalysis.

Metabolism of methyl iodide occurs in the liver, kidney, skin and nasal respiratory/ olfactory epithelium where its glutathione conjugation was measured (Sweeney et al., 2009).

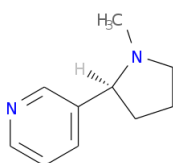
Table 2.9.9. Physicochemical properties of iodomethane

Physicochemical properties	Value	Reference
MW - molecular weight	141.95	
MV - molar volume	63.9	
HBA - hydrogen bond acceptors	0	
HBD- hydrogen bond donors	0	
Mpt - melting point	-95.17	(1)
Hb - number of hydrogens	3	
cb - the number of carbons not involved in a C= O bond	1	
MR - molecular refractivity	19.7	
pKa	5 (assumed)	
logP _{oct} - octanol-water partition coefficient	0.17	
fu (free fraction of drug in plasma)	1	(2)
RBP	1.77	

(1) ChemSpider: <http://www.chemspider.com/> (last access: 06.10.2014)

(2) ADMET Predictor computer software available from <https://www.simulations-plus.com/> (last access: 06.10.2014)

2.9.9 Nicotine



Nicotine (CAS: 54-11-5), a commonly used stimulant (a tertiary amine composed of a pyridine and a pyrrolidine ring), has been investigated extensively in previous years, both in terms of *in vivo* and *in vitro* effects on human body. Physicochemical properties of nicotine are presented in **Table 2.9.10**. Nicotine NOAEL and LOAEL doses (based on rat studies) are 1.25 and 2.5 mg/kg BW/ day respectively (for short and intermediate health risks such as episodic oral, dermal, and inhalation toxicity endpoints (EPA, 2008).

This psychoactive substance is known to increase heart rate, affect the nervous system and influence other biological processes including behavioral effects and metabolic responses (Grundy et al., 1981). Nicotine is

an addictive drug and its consistent use is likely to result in the development of tolerance to (and dependence on) its actions. Cigarette smoking as a delivery mechanism is inherently more likely to produce addiction. There is therefore interest in the development of nicotine replacement therapies based on alternative exposure routes (e.g. coated tablets, chewing gum, nasal spray, inhalator, microtablets and transdermal patches). Human exposure to nicotine may occur via all three routes: inhalation, oral and dermal absorption. Cigarettes vary in their nicotine content: the tobacco from the bidi cigarettes has on average 21.2 mg/g of nicotine compared to the tobacco from filtered and unfiltered commercial cigarettes containing 16.3 mg/g and 13.5 mg/g of nicotine respectively (Malson et al., 2001). To estimate a daily nicotine consumption (Benowitz et al., 1982) reported that smoking of usual, low-, and high- nicotine commercial cigarettes deliver 1.2mg, 0.4 mg and 2.5 mg of nicotine respectively. Transdermal patches normally contain from 5 to 30 mg nicotine and are applied over 24 hours (de Landoni, 1991). *In vivo* experiments showed that less than 100% of the nicotine absolute dose in a patch reaches systemic circulation. The amount of nicotine absorbed has been reported to be between 65-90% of the total dermal dose (Bannon et al., 1989; Gupta et al., 1993). This absorption was found independent of a dose and the undelivered amount is believed to be lost either by evaporation or possible skin metabolism.

(Papathanasiou et al., 2013) recently studied the effect of nicotine smoking on heart rate at rest and during exercise in 298 young adults. The authors concluded that smokers had significantly higher resting heart rate values than non-smokers but the reverse was observed during exercise. The maximal values achieved during exercise were around 191-193 bpm (smokers) and 198-199 bpm (non-smokers). There are many literature studies and reviews describing in detail the absorption, distribution, metabolism and excretion (ADME) processes of nicotine (Benowitz, 1990; Hukkanen et al., 2005).

Nicotine is a water and lipid soluble drug which, in the free base form, is readily absorbed via respiratory tissues, skin, and the gastrointestinal tract. Inhaled nicotine enters the blood almost as rapidly as after rapid intravenous injection (de Landoni, 1991). Nicotine readily reaches organs and tissues and undergoes extensive metabolism mainly in liver (nicotine bioavailability = 30-40 %). Plasma protein binding was reported to be only around 5% (Yamazaki and Kanaoka, 2004). Nicotine undergoes liver metabolism by cytochrome P450 enzymes (mostly CYP2A6, and also by CYP2B6). A major metabolite is cotinine (ca. 80% of nicotine conversion). Other metabolites include nicotine *N'*-oxide, nornicotine, nicotine isomethonium ion, 2-hydroxynicotine and nicotine glucuronide (**Figure 2.9.8**). Renal clearance accounts for 2-35% of total nicotine clearance (Tutka et al., 2005). Additionally, there are observed differences in plasma concentrations between smokers and nonsmokers suggesting differences in total clearance rates, with non-smokers showing faster clearance than smokers (Tutka et al., 2005; Yun et al., 2008). The apparent volume of distribution of nicotine was determined in one clinical study to be 2.0 L/kg in smokers and 3.0 L/kg in nonsmokers (Ellenhorn, 1988).

Nicotine toxicity facts are well-outlined in literature (Brcic Karaconji, 2005). In 2004, The Committee on Updating of Occupational Exposure Limits agreed on the no- observed adverse effect level (NOAEL) of 0.5

mg/m³ based in a two-year inhalation rat study as a starting point in deriving a health-based recommended occupational exposure limit.

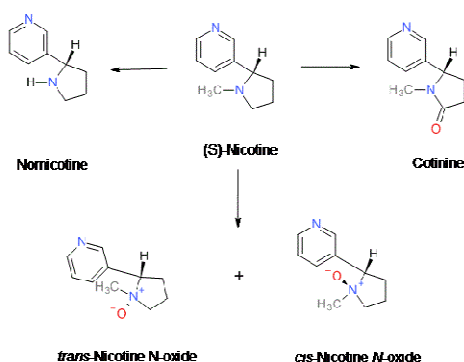


Fig 2.9.8. Human liver metabolism pathways of nicotine¹⁰.

Nicotine has a rapid onset of action therefore is a good candidate to model observable acute effects. Toxicodynamics of nicotine is very complex and reflect the influence of tolerance development to actions of this stimulant on the dose-response relationship. Therefore, the effect-side part of the model should be described by means of noncompetitive antagonist receptor model to account for a “force” driving tolerance that acts to reduce drug effect. Nicotine use can have different effects on the body such as: decreases the appetite, increases activity of intestines, increases heart rate and blood pressure, and stimulates memory and alertness. There are also symptoms of nicotine withdrawal within 2 – 3 hours after the use of tobacco especially among heavy smokers and these include: an intense craving for nicotine, anxiety, depression, headaches, increased appetite and problems concentrating.

There are already presented various PBTK-TD models for nicotine in literature (Green et al., 1999; Porchet et al., 1988; Robinson et al., 1992; Teeguarden et al., 2013). They all present relatively simple but satisfactory representation of nicotine ADME process following three exposure routes.

Table 2.9.10. Physicochemical properties of nicotine

Physicochemical properties	Value	Reference
logP _{oct} – octanol-water partition coefficient	1.17	
MW – molecular weight	162.2	
MV – molar volume	157.18	
HBA – hydrogen bond acceptors	2	
HBD- hydrogen bond donors	0	(1)
Mpt – melting point	57.34	
Hb – number of hydrogens	11	
cb - the number of carbons not involved in a C= O bond	10	
MR – molecular refractivity	49.26	
pH	8.8	(Hukkanen et al., 2005)

¹⁰ <http://quantum.esu.edu/~scady/damra/Page5.htm> (last access: 06.10.2014)

pKa	8	(Benowitz, 1990)
VP- vapour pressure [Pa]	3.1 (EDETOX - 3)	(1)
fu (free fraction of drug in plasma)	0.038	(Yamazaki and Kanaoka, 2004)
RBP	0.95	(2)
logP _{oct} - octanol-water partition coefficient	1.2	(3)
	1.17	(3)

(1) ChemSpider: <http://www.chemspider.com/> (last access: 06.10.2014)

(2) ADMET Predictor computer software available from <https://www.simulations-plus.com/> (last access: 06.10.2014)

(3) EDETOX database: <http://edetox.ncl.ac.uk/chemicals.aspx?id=97> (last access: 06.10.2014)

2.10 Differences in molecular properties between cosmetic ingredients and drugs

A set of 207 drugs taken from (Wetmore et al., 2012) is compared in terms of molecular property diversities (**Figures 2.10.1-2**) with a set of 40 cosmetics ingredients: coumarin, hydroquinone, caffeine, ethanol, isopropanol, estragole, lindane, ethylene glycol, propylene glycol, glycerine, salicylic acid, sodium lauryl sulfate, ammonia, aqua, ascorbic acid, benzophenone-2, benzophenone-3, benzophenone-4, benzyl alcohol, benzyl alcohol, benzyl benzoate, benzyl salicylate, butane, butyloctanol, butylparaben, cetearyl alcohol, cetyl alcohol, cinnamyl alcohol, citric acid, citronellol, dilinoleic acid, lactic acid, limonene, linalool, palmitic acid, panthenol, phenoxyethanol, propane, propylparaben. Principal component analysis clearly visualises differences between these sets and may serve as an indicator that QSPRs developed on drug properties may not be applicable for cosmetic ingredients.

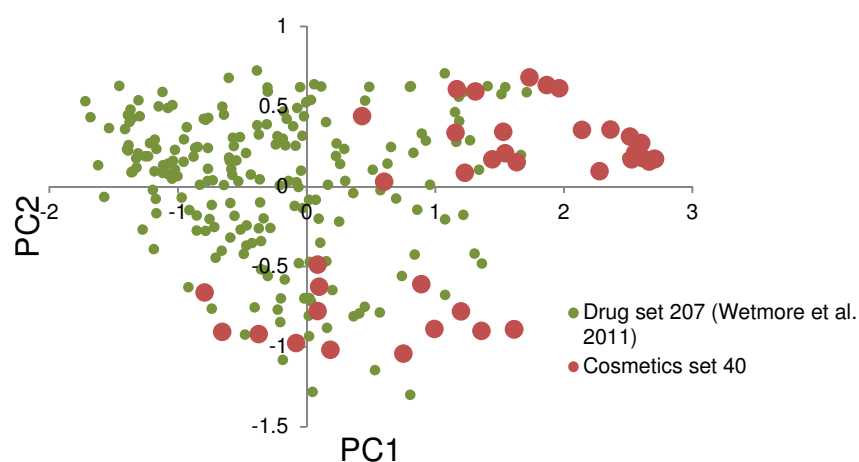


Fig 2.10.1. Structural space of drugs versus cosmetics.

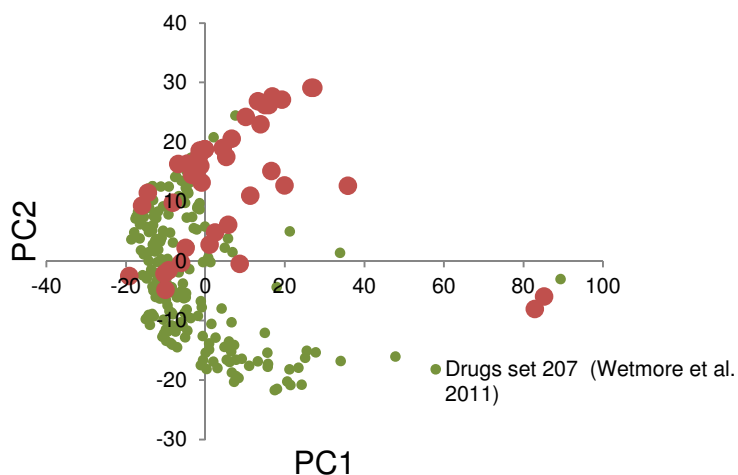


Fig 2.10.2. Molecular properties diversity of drugs versus cosmetics.

Atom pair fingerprints (all possible pairs of atoms within a defined radius were counted and fingerprinted – topological rather structural approach) and 12 simple physicochemical properties ($\log P_{\text{oct}}$, atomic polarizabilities, bond polarizabilities, aromatic atoms count, aromatic bonds, HBA, HBD, rotatable bonds count, topological polar surface, MW, no. of heavy atoms) were calculated by RDkit¹¹ in KNIME. Percentage of variance for the structural plot was 54% and for the physicochemical properties 91%.

¹¹ <http://www.rdkit.org/docs/Overview.html> (last access: 06.10.2014)

3. Materials and methods

In the first part of this chapter all the experimental (*in vivo*, *in vitro*) data used for the calibration, validation and application of the models (PBTK, PBDT, VCBA) are listed. Most of these data come from the available literature. In the second part, the model structures (PBTK, PBDT and VCBA) and equations are defined, followed by the functions used for sensitivity analysis and optimisation, and a compilation of the QSPRs for skin absorption, plasma protein binding, air-to-blood and blood-to-tissue partition coefficients.

3.1 Experimental Data

3.1.1 Single and repeated toxicokinetics

a) Coumarin

In vivo (literature)

- Oral (0.857 mg/kg BW) administration data of coumarin dissolved in propylene glycol to (i) four healthy subjects – individual blood concentrations of coumarin were published (Ritschel et al., 1979) and (ii) six healthy volunteers: 4 males, 2 females – mean blood concentrations were used to calibrate the oral PBTK model (Ritschel et al., 1977).
- *In vivo* dermal absorption was studied by (Ford et al., 2001) on three male subjects. 6 h-exposure to 0.02 mg/cm² of coumarin in 1 mL of 70% aq. ethanol was measured on the back-site 100 cm² of skin area with 30 min of alcohol evaporation and then occlusion. Individual plasma concentrations of coumarin were published.

In vitro (literature)

- Percutaneous absorption of coumarin was measured across the human scalp and abdominal skin (skin area = 0.636 cm²) by (Ritschel et al., 1989). A coumarin solution of 5.5 mCi/mmol in phosphate buffer (pH 7.4) was applied to the *stratum corneum*. Amount of coumarin permeated in time over skin area, was published and used to calibrate *in vitro* parameters of the PBTK model.
- Coumarin metabolism to 7-HC, o-HPA, 3-HC (first pass) and o-HPA metabolism to o-HPAA and o-HPE (second pass) were studied in human liver microsomes by (Born et al., 2000; Rietjens et al., 2008; Vassallo et al., 2004). Coumarin concentrations ranging from 0 to 4000 µM were added to microsomal incubations as 1% (v/v) from a 100 times concentrated stock solution in dimethyl sulfoxide (DMSO). The apparent V_{max} and K_m values were determined for 2-4 different donors. Microsomal yield of 35 mg/g liver was used to scale *in vitro* results to the liver level.

b) Estragole

In vivo (literature)

Three male and four female subjects drank 500 mL of a fennel tea made from freshly broken fruits within 10 min. One female volunteer drank in separate trials another 1000 and 250 mL of the fennel tea, respectively, with intervals of at least 2 months between the tests. The urinary excretion of metabolites was investigated. Concentration (average) of 1'-hydroxyestragole (the main estragole metabolite) in human blood plasma were provided at different times after the consumption of fennel tea containing 3.5 mg (68 µg/kg BW) of estragole (Zeller et al., 2009).

In vitro (literature)

Mixed gender human liver microsomal preparations were incubated with estragole in the presence of nicotinamide adenine dinucleotide phosphate (NADPH) to determine the kinetic constants for the formation of phase I metabolites of estragole. These incubations were carried out for 10 min at a substrate concentration that ranged from 10 to 400 µM of estragole. Under these conditions the formation of the different estragole metabolites was linear with time and microsomal protein concentration. Additional incubations were carried out to determine the kinetic constants for glucuronidation of 1'-hydroxyestragole at substrate concentrations that ranged from 50 to 2000 µM of 1'-hydroxyestragole (Punt et al., 2009). Microsomal protein yield used in this work was 32 mg/g liver.

c) Hydroquinone

In vivo (literature)

- For calibration of the oral PBTK model, single exposure results from one healthy adult male Caucasian were available (Corley et al., 2000). He ingested 275 mg of hydroquinone (by ingestion of 27.5 g of the dose solution through a drinking straw) followed by two rinses of 50 ml water. Free and protein-bound hydroquinone concentrations in the blood were provided (however total amount was considered in the calibration of the model) together with cumulative amounts of hydroquinone eliminated as glucuronide, sulfate and glutathione conjugates in the urine.
- For calibration of the dermal exposure model, 2.5 mg of hydroquinone in 0.125 g of cream was applied to the forehead and left forearm (25 cm²) of 6 volunteers. The dosed skin site was washed 8h after dosing. Plasma radioactivities of hydroquinone were provided as group mean results taken contralateral (opposite arm) to dosing place (Wester et al., 1998). Urine concentrations were measured after topical application of hydroquinone to forehead site.

In vitro (literature)

Isolated hepatocytes were used to determine metabolic rate constants for the conversion of hydroquinone to HQ-SG (glutathione conjugates), HQ- Gluc (glucuronide) on other later-phase hydroquinone conjugates.

Cryopreserved hepatocytes prepared from six different donors were incubated with 45, 227, or 2270 μM of hydroquinone (Poet et al., 2004). The estimated yield of isolated hepatocytes was $5.02 \cdot 10^7$ cells/g liver.

d) Caffeine

In vivo (literature)

- Five different single absorption oral studies in humans were selected for the PBTK model calibration and validation. For calibration, plasma concentrations were taken from (Lelo et al., 1986) and from (Newton et al., 1981). In the former study, one non-smoking male volunteer ingested 270 mg of caffeine in a gelatin capsule whereas in the latter study one male subject ingested a gelatin capsule containing 300 mg of caffeine (single dose administration studies). For model validation, plasma concentrations were taken from the oral study by (Csajka et al., 2005) where in addition to a gelatin capsule, caffeine was applied as a commercial dietary supplement. In the first part of the study, 8 subjects received a single oral dose -2 capsules of a commercial dietary supplement, Metabolift, labelled to contain 200 mg caffeine and in the second part, a single oral dose of 200 mg of caffeine sulphate was administered alone to 16 subjects. Validation of the model for repeated caffeine absorption was based on the experimental design of (Denaro et al., 1991). Nine healthy non-smokers, habitual coffee consumers, were given 6 cups of coffee per day (4.2 and 12 mg/kg BW). Mean plasma concentrations of caffeine measured over 24 h during low and high caffeine consumption were published. Finally, single and repeated effects of 8 mg/kg BW of caffeine (in a gelatin capsule) were investigated in six healthy subjects (Acheson et al., 1980). Individual plasma caffeine concentrations were provided.
- To calibrate the model for dermal exposure, the experiment of (Otberg et al., 2008) was used, in which caffeine in an ethanol/propylene glycol vehicle was administered to 6 male volunteers by applying the liquid onto a chest area of 25 cm^2 for 24 h. In contrast to other dermal absorption studies, the additional impact of hair follicles on the overall absorption process was considered.

In vitro data for skin permeation

To calibrate the PBTK model for *in vitro* permeation of caffeine the following studies were used:

Literature:

- Permeation of caffeine in oil/water (O/W) and a water/oil/water (W/O/W) emulsions consisting of hydrophilic and oil phases in defined ratios was studied by (Doucet et al., 1998). A 1% caffeine solution in 260 mg/cm^2 was applied on 1 cm^2 of abdominal biopsies. The amount of caffeine permeated per cm^2 was measured over 24 h.
- 4 mg/mL of caffeine in ethanol/water solution (ethanol to water ratio 1:1 [v/v]) was applied on 1.5 cm^2 of full thickness breast and abdominal skin from surgical waste (Wilkinson et al., 2006). The cumulative amount of caffeine in receptor fluid over 24 h was reported.

- High (15 mg/mL) and low (320 µg/mL) caffeine solutions in acetone were pipetted onto a skin area of 3.14 cm² (human abdominal skin) (Treffel et al., 1993) under normal pressure. Mean fluxes and permeated amounts over 24 h were published. At 24 h high caffeine solution led to permeated amount of 0.009421 mg/cm² and low solution to 0.001631 mg/cm².
- 25.82 mg/mL of caffeine in water were applied to 1 cm² of excised human upper leg skin. The diffusion experiment was performed over 24 h- period with sampling every 2 h up to 12 h and at 24 h. Diffusion and partition coefficients in stratum corneum were measured together with permeation coefficient and permeated amount of caffeine through epidermis were published (Dias et al., 1999).

Provided by Cosmetics Europe:

Cosmetics Europe provided their experimental results in terms of the diffusion coefficient in *stratum corneum* and the *stratum corneum*/vehicle partition coefficient following permeation of 10 mg/mL of caffeine in ethanol/propylene glycol/water through human frozen cadaver skin (1.5 cm², the skin was thawed and pieces were cut from the main skin piece) and following permeation of 1 % caffeine solution in ethanol/propylene glycol/water through human abdominal skin.

In vitro data for liver metabolism (literature):

The biotransformation of caffeine was studied *in vitro* using human cytochrome P-450 isoenzymes (CYPs) expressed in human B-lymphoblastoid cell lines, namely CYP1A1, 1A2, 2A6, 2B6, 2D6-Val, 2E1 and 3A4, and microsomal epoxide hydroxylase (EH). In addition, CYP2D6-Met was also studied, in which a valine in the wild type (CYP2D6-Val) had been replaced by a methionine due to a G to A mutation in position 112. A 0.05-2 mmol/L solution of caffeine in sodium phosphate buffer pH= 7.4 was applied (Ha et al., 1996).

e) Ethanol

In vivo (literature)

- For calibration of the ethanol oral absorption model, blood ethanol concentrations were taken from two drinking experiments performed by (Wilkinson et al., 1977a, 1977b), under fasting conditions: i) eight healthy adult white male volunteers received 15, 30, 45 and 60 mL of 95% ethanol in orange juice (total volume of each dose was 150 mL); ii) a single adult male volunteer was given 30 mL of 95% alcohol in a total volume of 180 mL (made up with orange juice).
- Acetaldehyde concentrations used to optimise reverse metabolism rates of ethanol to acetaldehyde were taken from (Jones et al., 1988) where 10 healthy male volunteers ingested 0.25 g/kg BW of ethanol. Individual blood concentrations were provided.
- For calibration and validation of the skin exposure model, the study of (Kramer et al., 2007) was used. 12 volunteers applied three hand-rubs containing 95%, 85% and 55% ethanol. For hygienic hand disinfection, 4 mL were applied 20 times for 30s, with a 1 minute break between applications.

For surgical hand disinfection, 20 mL of each hand rub was applied to hands and arms up to the level of the elbow 10 times for 3 minutes, with a break of 5 minutes between applications. Blood concentrations of ethanol and acetaldehyde were determined as the group average results.

- For calibration of the ethanol inhalation model, 5 healthy adult men were exposed to 1000 ppm of ethanol over 6 h. Exposure was carried out in a dynamic controlled-environment exposure chamber measuring 18.1 m³ with the fresh air and ethanol inflow conditions as specified in (Nadeau et al., 2003). Mean ethanol concentrations in blood and expired air were published.

In vivo (provided by King's College London)

For validation and further model refinement of oral absorption, serum concentrations of ethanol and serum and urinary concentrations of ethyl glucuronide (EtG) and ethyl sulfate (EtS) were taken from the drinking study of (Lostia et al., 2013). In the latter study, eighteen healthy volunteers (9:9 male: female, non-Asian, 18–35 years old and with a body weight between 50 and 80 kg) participated in two separate controlled drinking experiments, with at least 1 week interval in-between, and provided blood and urine samples. For each drinking experiment, volunteers abstained from alcohol during the 3 days before the study (based on self-reporting and confirmed by analysis of EtG and EtS in urine), and for 3 days after alcohol administration. In the first experiment, 4 units of alcohol (corresponding to a mean value of 0.76 g of ethanol/kg of body weight, calculated by the Widmark equation; Widmark factors used: 0.68 for males and 0.55 for females) were administered, while in the second one, 8 units of alcohol (corresponding to a mean value of 1.53 g/kg) were administered. Ethanol was consumed at lunch time (12 a.m.) over a total period of 60 min (for 4 units, volunteers had to drink 100 mL of alcoholic drink every 15 min, while for 8 units they drank 125 mL every 15 min). Urine samples were collected after alcohol administration every hour for the first 7 h and then after 10, 24, 48 and 72h. For each sample, the entire urine volume was collected and measured. Blood samples of 15 ml were collected every hour for the first 6 h and then after 24 and 48 h. After collection, the serum fraction was isolated and used for the analysis. The following analytes were measured: EtG and EtS in serum and urine, ethanol in serum and urinary creatinine. The analysis was performed by the Drug Control Centre (King's College, London), which is accredited to ISO 17025 and by the World Anti-Doping Agency for drug testing analysis, using validated methods developed in house. Individual serum, urine (ethanol in serum, EtG and EtS in serum and urine), and urinary creatinine concentrations were provided for this work.

f) Isopropanol

In vivo (literature)

- To calibrate the oral absorption model, the experiment of (Monaghan et al., 1995) was used in which 3 healthy male subjects ingested 0.6 ml/kg 70% isopropanol in 240 ml water over a 5 min-period. Mean venous blood concentrations of isopropanol and its metabolite were published (Clewell

Iii et al., 2001; Monaghan et al., 1995). For validation, the study conducted by (Lacouture et al., 1989) was taken in which 3 male subjects ingested 0.4 ml/kg 70% IPA in 210 ml apple juice over 10 min. In a similar manner to the previous work, mean venous blood concentrations of isopropanol and its metabolite were provided (Clewell Iii et al., 2001; Lacouture et al., 1989).

- To model isopropanol inhalation, experimental data from (Kumagai et al., 1999) were taken. In their work, respiratory uptake in humans was investigated in 4 healthy male volunteers who inhaled concentrations of 50, 100, or 200 ppm acetone or isopropanol at rest for 10 min. The subjects inhaled the vapours through a mouthpiece equipped with a valve to isolate exhaled air, and samples of exhaled air were collected 1 min prior to exposure, during the 10 min of exposure, and for 5 min following exposure. Exhaled air concentrations were reported for the average concentration over an exhalation period (mean of three exposure groups) as well as for the concentration at the end of an exhalation.
- The dermal absorption PBTK model was calibrated with respect to study of (Turner et al., 2004) in which 3 mL of isopropyl alcohol-containing hand rub (52.6 % w/w) was applied to the hands every 10 min over 4 h. 10 healthy adults participated in the experiment. Blood concentrations of isopropanol after 4 h were published separately for males and females.

g) Styrene

In vivo (literature)

To calibrate the PBTK model for inhalation of styrene, experimental data were taken from: (i) (Ramsey and Young, 1978) in which human volunteers (2 male subjects with an average body weight of 83.1 kg) were exposed to 80 ppm of styrene for 6 h – average blood concentrations were used; ii) (Wigaeus et al., 1984) in which six male subjects (average body weight = 69 kg) were exposed to 293 mg/m³ of styrene for 2 h. The mean concentration of styrene in arterial blood was published. To validate the inhalation PBTK model, data on 4 male volunteers inhaled styrene vapors (50 ppm) for 2 h (during 50-W workload) were used (Johanson et al., 2000). Individual venous blood concentrations were presented.

h) Methyl iodide

In vivo (literature)

- A 19-year-old patient intending to commit a suicide gave himself an i.v. injection of about 14 g of methyl iodide. Three serum concentrations after ca. 3 h were provided, and then after 0,2,4,8 and 28 h after hemoperfusion (Robertz-Vaupel et al., 1991).
- 4 volunteers inhaled methyl-iodide labelled with iodine-132. In the first experiment, the compound was administered over 5 min using special apparatus and in the second inspired as a single deep breath (held for about 45 s). About 150 µg of stable methyl iodide was used in each preparation.

Urinary concentrations and 2 concentration-time points of iodine-132 in blood in individual subjects were published (Morgan et al., 1967; Morgan and Morgan, 1967).

i) Nicotine

In vivo (literature)

- To calibrate the liver metabolic rates for conversion of nicotine to cotinine, intravenous experimental data were used (Porchet et al., 1988). In this study, 8 healthy subjects (all habitual smokers), in a state of rest, were given two i.v. administrations of nicotine (2.5 µg of nicotine per kg body weight for 30 min) at intervals of 1, 2 and 3.5 h. For validation, blood data from 9 subjects following intravenous injection of nicotine (ca. 0.7 µg per kg body weight for 180 min) were chosen (Fattinger et al., 1997).
- For calibration of the oral PBTK model, single and repeated doses (8 times, once every 1.5 h) of nicotine with the Straw (4, 8, 12 mg) were administered in a group of 24 smokers (D'Orlando and Fox, 2004). Mean plasma concentrations were calculated from individual nicotine levels presented in the paper. For validation, nicotine-containing capsules (6 and 15 mg) were administered as a single dose to 12 subjects, nonsmokers (Green et al., 1999).
- To calibrate the dermal PBTK model, a nicotine patch (NicolanTM) study was used (Bannon et al., 1989). Nicotine was applied in patches at various doses (15, 30 and 60 mg) on the skin of healthy human volunteers (all smokers) for 24 h as single doses and 30 mg applied in repetitive way once every 24 h up to the 7th day. Mean plasma nicotine concentrations were published. To validate the model, single and multiple applications of a nicotine transdermal system (NTS) were investigated on 13 healthy adult male smokers (1.5 mg/h of nicotine released over 24 h) (Gupta et al., 1993). Mean plasma nicotine concentrations were presented.
- To calibrate the inhalation PBTK model, a study describing the smoking of 0.4, 1.2, 2.5 mg-containing cigarettes (30 per day) by 12 healthy volunteers (all smokers) was chosen (Benowitz et al., 1982). Mean blood nicotine concentrations were published. For validation, data were taken from (Hansson et al., 1994) which investigated the inhalation of 0-64 mg/mL of nicotine in 24 healthy non-smoking subjects.

Table 3.1 provides a summary of all *in vivo* and *in vitro* data resources used in this work.

Table 3.1. Summary of experimental data sources for toxicokinetic modelling.

Compound	<i>in vitro</i> data	<i>in vivo</i> data
Coumarin	Skin permeation: (Ritschel et al., 1977)	Oral data: Single: (Ritschel et al., 1979, 1977) Dermal data: Single: (Ford et al., 2001)
	Liver metabolism: (Born et al., 2000; Rietjens et al., 2008;	

	Vassallo et al., 2004)	
Estragole	Metabolic rates in liver microsomes: (Punt et al., 2009)	Oral data: (Zeller et al., 2009)
Hydroquinone	Liver metabolism: Isolated hepatocytes (Poet et al., 2004)	Oral data: (Corley et al., 2000) Dermal data: (Wester et al., 1998)
Caffeine	Skin permeation: Cosmetics Europe JRC (Mennecozi et al., 2011) and (Doucet et al., 1998; Treffel et al., 1993) (Wilkinson et al., 2006) Liver metabolism: (Ha et al., 1996)	Oral data: Single: gelatin capsule (Lelo et al., 1986) Single: commercial dietary supplement (Csajka et al., 2005) Single: gelatin capsule (Newton et al., 1981) Single: beverage (Robertson et al., 1981) Single and repeated: gelatin capsule (Acheson et al., 1980) Repeated: coffee (Denaro et al., 1991) Dermal data : Single: Caffeine in 30%ethanol/70% propylene glycol (Otberg et al., 2008)
Ethanol	-	Oral data: (Jones et al., 1988; Wilkinson et al., 1977a, 1977b) (Lostia et al., 2013) + King's College Dermal data: (Kramer et al., 2007) Inhalation: (Nadeau et al., 2003)
Isopropanol	-	Inhalation data: (Kumagai et al., 1999) (Clewel Iii et al., 2001) Oral data: (Clewel Iii et al., 2001; Lacouture et al., 1989; Monaghan et al., 1995) Dermal data: (Turner et al., 2004)
Methyl Iodide	-	Inhalation data: (Morgan et al., 1967; Morgan and Morgan, 1967) i.v. data (Robertz-Vaupel et al., 1991)
Styrene	-	Inhalation data: (Johanson et al., 2000; Ramsey and Young, 1978; Wigaeus et al., 1984)
Nicotine	-	IV infusion: Repeated (Porchet et al., 1988) Oral data: Nicotine capsules: single (Green et al., 1999) Nicotine with the straw: single and repeated (D'Orlando and Fox, 2004) Dermal data: Nicotine patch: single and repeated (Bannon et al., 1989) Nicotine patch: single and repeated (Gupta et al., 1993) Via straw: Inhalation: repeated (Teegarden et al., 2013)

3.1.2 Single and repeated toxicodynamics

a) Nicotine (literature)

A toxicodynamic model of heart rate was developed using data published by (Porchet et al., 1988) and was validated using experimental results of (Fattinger et al., 1997). In both cases, heart rate responses to intravenous nicotine were measured at rest. In the second study, systolic and diastolic blood pressure responses were used to calibrate the PBTD model in terms of the acute effect on blood pressure. In addition, the study of (Sofuoglu et al., 2012) was used to further validate heart rate and blood pressure simulations. In this work, 107 non-treatment-seeking smokers were given intravenous injections of 0.7 $\mu\text{g}/\text{BW}$ for 5 min followed by an injection of 1 $\mu\text{g}/\text{BW}$ 30min later (also for 5 min). Measurements of blood pressure following single IV doses were taken from (Fattinger et al., 1997), and following double IV injections from (Sofuoglu et al., 2012).

To simulate the effect of nicotine on heart rate during exercise, a study was chosen in which the effects of nicotine (7 mg transdermal nicotine patch) were measured on cycling endurance. The study was carried out on twelve healthy males (Mündel and Jones, 2006).

b) Caffeine (literature)

The toxicodynamic model of heart rate (sigmoid model) was parameterised using experimental data based on prolonged exercise of lean 6 subjects. The increase of heart rate was measured during treadmill exercise, following intake of 5 mg/kg BW of caffeine in gelatin capsules (Damirchi et al., 2009).

The toxicodynamic model of mean arterial blood pressure was calibrated using experimental data based on 8 subjects at rest. Eight healthy men drank a decaffeinated coffee to which 4 mg/kg BW of caffeine had been added; mean arterial pressure (MAP) results were published (Shi, 1993).

To validate the models, the following studies were used:

- (Daniels et al., 1998) measured heart rate and blood pressure at rest and during dynamic leg exercise (10 trained cyclists received 6 mg/kg BW of caffeine in gelatin capsule) Mean recordings were provided.
- (Mousavi et al., 2011) investigated mean heart rates and blood pressures were published at rest and during exercise after administration on 5 mg/kg BW caffeine in gelatin capsule.
- (Ping et al., 2010) published heart rate recordings were provided after absorption of 7 mg/kg BW of caffeine by nine male Malaysian runners during exercise conditions.

- (Robertson et al., 1981) study was used to calculate MAP values from mean systolic and diastolic pressure results following administration of 250 mg of caffeine in a beverage at rest by 18 healthy subjects.
- (Karatzis et al., 2005) investigated MAP changes after consumption on 80 mg of caffeine in a coffee. The experiment was carried out on 16 healthy volunteers. Mean central systolic and diastolic pressure results were published.
- From (Denaro et al., 1991) experiment MAP values calculated from published systolic and diastolic pressure changes after repeated dosing of caffeine (4.2 and 12 mg/kg BW).

Table 3.2 provides a summary of all heart rate and blood pressure experimental data resources used in this work.

Table 3.2. Summary of experimental data sources for toxicodynamic modelling

Compound	Cardiovascular effect	References
Nicotine		(Fattinger et al., 1997; Mündel and Jones, 2006; Porchet et al., 1988; Sofuoglu et al., 2012)
Caffeine	Blood pressure Heart rate	(Damirchi et al., 2009; Daniels et al., 1998; Denaro et al., 1991; Karatzis et al., 2005; Mousavi et al., 2011; Ping et al., 2010; Shi, 1993; Sung et al., 1990)

3.1.3 Cell viability

HepaRG cells: *In vitro* data were generated in-house at the JRC

Caffeine was purchased from Fluka. TMRE, Toto 3, and Hoechst 33342 were purchased from Invitrogen. A cryopreserved human cell line HepaRG was obtained from INSERM's laboratory U522. The methodology was based on (Mennecozzi et al., 2011). To develop the *in silico* virtual cell-based assay (VCBA) model, and to carry out the *in vitro-in vivo* extrapolation study in this thesis, an in house experiment on HepaRG exposed to different concentrations of caffeine was carried out and viability was assessed at several time points 24, 48, 72, and 96 h.

In vitro studies at the JRC were performed according to (Mennecozzi et al., 2011). HepaRG cells were seeded at a density of 2.6×10^4 cells/cm² in a growth medium composed of Williams E medium supplemented with 10% FCS, 100 units/mL penicillin, 100 µg/mL streptomycin, 5 µg/mL insulin, 2 mM glutamine and 5×10^{-5} M hydrocortisone hemisuccinate. Further culturing was carried out for 2 more weeks with the same medium supplemented with 2% DMSO in a 75 cm² culture flask. The medium was renewed every 2 to 3 days. After differentiation, HepaRG cells were detached by gentle trypsinization, and then seeded at a density of $4-5 \times 10^4$ /well in 96 well microtiter plates (BD Biosciences) to allow the selection of hepatocyte-like populations. The cells were used for testing within one week after plate seeding. Caffeine

was solubilised in 100% DMSO and then diluted in culture medium with 5% HyClone Fetalclone III serum to obtain a final concentration of DMSO of 0.1%. Eleven concentrations of caffeine, ranging from 0 to 75 mM (24 h- exposure, single exposure) or 0 to 9.1 mM for the repeat exposure (at several time points 24 h, 48, 72, and 96 h) were tested, using 5 or 3 wells for each concentration (technical replicates), respectively. After 24 h of exposure, treated HepaRG cells were stained with tetramethylrhodamine (TMRE), Toto 3, and Hoechst 33342 for 30 minutes. This assay was performed five times (biological replicates) for a single exposure and once for repeated exposure. Viability was assessed with a high-content analysis (HCA) approach using Cellomics ArrayScan vTi (Thermo Scientific, Pittsburgh, PA, USA). A 10x objective was used to collect 10 image fields per well for two fluorescence channels with the XF93 filter set. Cell count analysis was performed using the Target Activation Bioapplication v.4 from Cellomics Scan Software.

HepG2 cells (literature)

Viability in HepG2 was assessed using colorimetric MTT assay. *In vitro* data generated by a JRC partner in the context of the EU FP6 project ACuteTox were used (Clothier et al., 2013). The concentration-response curves (0-75 mM) were generated by using the MTT assay data.

In brief, HepG2 cells were cultured in 96-well plates. After 24 h treatment with chemicals, cells were incubated with the MTT solution. The formazan (yellow reduced to purple in living cells) formed in the cells was solubilised in DMSO and measured colorimetrically. The amount of formazan produced was then quantified using a simple colorimetric assay. The results were obtained using a multi-well scanning spectrophotometer (ELISA reader). Cytotoxicity was expressed as the Inhibitory Concentration (IC₅₀) of a chemical resulting in an X% reduction of the cell number/viability, as compared to the untreated control. This assay was performed in triplicate (biological triplicates).

In order to validate the *in silico* models, additional cytotoxicity data were sought from internet sources, using the following searching engines: google scholar, web of science, and pub med. Only one article describing the long-term cytotoxicity testing of caffeine on HepG2 cells could have been found (Scheers et al., 2001) which was therefore used as the source of validation data. The cells were treated twice a week with the same concentration of a test compound: 0.058, 0.173 or 4.67 mM of caffeine.

3.2 PBTK, PBTB and VCBA model structures and equations

List of symbols

V_{org} – volume of organ/tissue

A_{org} – amount of a chemical in organ/tissue [mg]

C_{org} – concentration of a chemical in organ/tissue [mg/L]

f_{crd} – cardiac output
 f_{org} – regional blood flow rates
 PC_{org} – tissue-to- blood partition coefficients
 $PC_{\text{blood,air}}$ – blood/air partition coefficient
 Dt – drinking rate [L/h]
 $Diss$ – dissolution from a coated matrix [L/h]
 ka_{stm} – absorption rate into stomach tissue [1/h]
 $k_{\text{min}}, k_{\text{max}}$ – kinetic constants of stomach emptying rate of a chemical to small intestine [1/h]
 ka_{SI} – absorption rate from small intestine lumen [1/h]
 $flow_{\text{LI}}$ –flow rate from small intestine into large intestine [L/h]
 ka_{LI} – absorption rate from large intestine lumen [1/h]
 kel_{LI} – elimination rate in large intestine lumen [1/h]
 CLR – renal clearance rate [L/h]
 V_{max} – the maximum rate metabolic rate at maximum (saturating) concentration of a chemical [mg/h]
 Km – chemical concentration at which the reaction rate is half of the maximal [mg/L]
 $Kmet$ – first order rate of formation of metabolites [L/h]
 $R_{\text{formCreat}}$ – formation rate of creatinine[mg/h]
 Rem_{blid} – bladder emptying rate [1/h]
 f_{crd} – cardiac output [L/h]
 f_{org} – regional blood flow rates [L/h]
 RBP – blood-to-plasma concentration ratio
 L_{ve} – thickness of viable epidermis [cm]
 L_{sc} – thickness of *stratum corneum* [cm]
 ka_{form} – intake rate of chemical from formulation by *stratum corneum* [mL/h]
 ka_{HF} – intake rate of a chemical from formulation by hair follicles [mL/h]
 PC_{SC} – partition coefficient *stratum corneum*/ solvent
 PC_{SCVE} – partition coefficient *stratum corneum*/ viable epidermis
 PC_{HF} – partition coefficient hair follicle /solvent
 $Area$ – application Area on skin [cm²]
 D_{SC} – diffusion coefficient in *stratum corneum* [cm²/h]
 D_{VE} – diffusion coefficient in viable epidermis [cm²/h]
 D_{HF} – diffusion coefficient in coefficient in hair follicles [cm²/h]
 ALV – alveolar ventilation [L/h]
 RR – Respiratory rate [1/h]

3.2.1 PBTK model

Three structurally different PBTK models were constructed in order to select one that best simulates ADME processes in humans. They are represented as a set of nonlinear differential equations with clearance rates (either liver or kidney) being dependent on a chemical concentration within a given organ/tissue and its

tissue-to-blood partition. To distinguish between the models, different names are given (PBTK1-3). The schematic representation of the main organs considered (**Figure 3.2.1**) applies to all the three models and the differences between them are in the GI tract, respiratory tract and skin compartments only, as explained below:

- The GI tract and the skin, in PBTK1_orl and PBTK 1_skn, respectively, are described by a single compartment with a first order rate of absorption, as described in the literature for coumarin and hydroquinone (Mielke et al., 2011; Poet et al., 2010; Rietjens et al., 2008). Whereas for inhalation, in PBTK1_inh – the respiratory tract is described by 3 compartments (Kumagai and Matsunaga, 1995).
- PBTK2_skn is applied for dermal absorption only. It consists of the surface compartment and two skin compartments with unidimensional diffusion (Fick's second law) across a single skin layer (*stratum corneum* and viable epidermis are grouped together) into the dermis and there are no hair follicles.
- PBTK3 is the refined PBTK model with various sub-compartments in the GI tract (PBTK3_orl), in the skin (PBTK3_skn) and in the respiratory tract (PBTK3_inh). Depending on the exposure route, multiple sub-compartments are added: GI tract with 6 sub-compartments (for oral exposure only), skin with the surface compartment and 4 skin sub-compartments (for dermal exposure only) and respiratory tract with 24 Weibel's generations (for inhalation only). The sub-compartments serve to account for the complexity of the absorption process (especially the time-lag in absorption). In the GI tract, three different administration types are considered: gavage, drinking rate, and dissolution from matrix. A first order rate of absorption from stomach, small and large intestine and stomach emptying rate are included according to (Loizou and Spendiff, 2004). The skin is divided into the *stratum corneum*, viable epidermis and dermis with blood mix. Unidimensional diffusion describes the transport in fine skin and hair follicles according to Fick's second law with specified initial and boundary conditions. The diffusion coefficient is different for the *stratum corneum*, viable epidermis and hair follicles. Diffusion via hair follicles is considered for caffeine only. In the respiratory tract, there is a mouth/nose compartment, 1-13 generations for convection only, 14-17 generations for convection and diffusion, 18-24 generations for convection and diffusion with blood mixing. See details below.

The general structure of the refined PBTK model is presented in **Figure 3.2.1**.

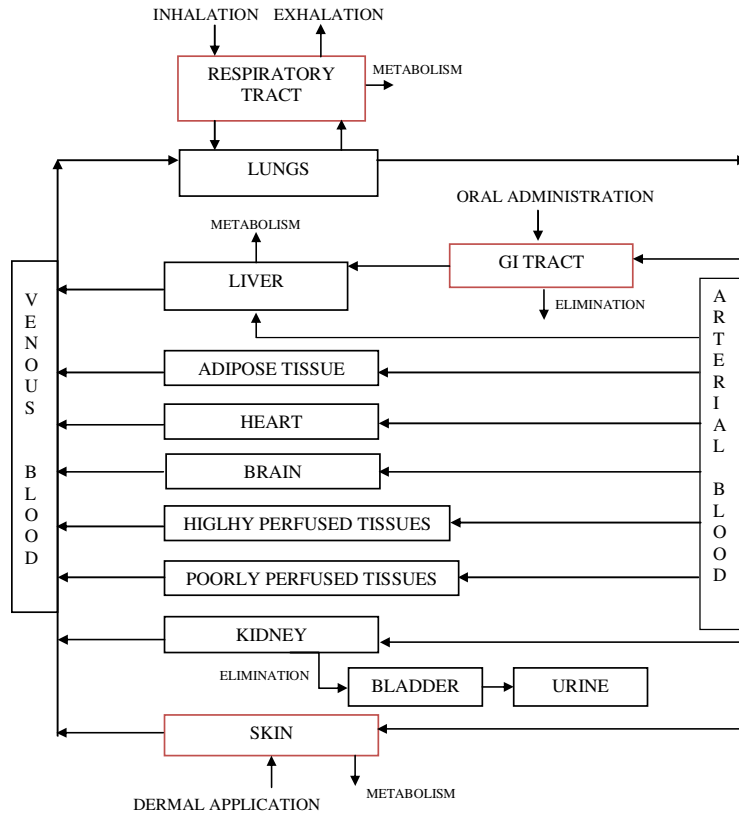


Fig 3.2.1 General structure of the refined PBTK model.

Unless metabolism or any side reaction are considered in any of the following organs: **adipose tissue, highly perfused tissues (brain - brn, heart-hrt, rest of body -rb.), poorly perfused tissues (muscle – msl, skeleton – skl, skin – skn), rest of body (rb)**, then the mass balance equations can be simply assumed to take the following form:

$$\frac{dA_{org}}{dt} = f_{org} \cdot \left(C_{art} - \frac{C_{org}}{PC_{org}} \right), \quad A_{org}(t=0) = 0, \quad C_{art} = \frac{C_{art}}{V_{art}}, \quad C_{org} = \frac{A_{org}}{V_{org}} \quad (3.2.1)$$

where: org = organ name (adp, hpt (brn, hrt), ppt, rb)

Kidney and urinary system:

The urinary system is modelled with the kidney as a single compartment linked to the bladder, which in turn, is connected to the urine compartment. Urine is normalised to the urinary creatinine concentration to adjust for a variation in urine flow rate between individuals (correction factor). The implicit assumption is that creatinine formation and excretion is constant over time for a given individual. A separate creatinine compartment is added. The level of creatinine is an indicator of the concentration of the urine. The higher the creatinine value, the more concentrated the urine specimen is. The lower the creatinine value, the more dilute the urine specimen is. The creatinine level fluctuates based on fluid intake.

$$\frac{dA_{kid}}{dt} = f_{kid} \cdot \left(C_{art} - \frac{C_{kid}}{PC_{kid}} \right) - CLR \cdot \frac{C_{kid}}{PC_{kid}} \quad (3.2.2)$$

Bladder, creatinine and urine composition:

$$\frac{dA_{bld}}{dt} = CLR \cdot \frac{C_{kid}}{PC_{kid}} - Re m_{bld} \cdot A_{bld} \quad (3.2.3)$$

$$\frac{dA_{Creat}}{dt} = R_{form} - CLR_{Creat} \cdot A_{Creat} \quad (3.2.4)$$

$$urine = \frac{Re m_{bld} \cdot A_{bld}}{CLR_{Creat} \cdot A_{Creat}} \quad (3.2.5)$$

Liver – without zonation:

$$\frac{dA_{liv}}{dt} = Fl_{GIT} + FORM_{liv} + f_{liv} \cdot \left(C_{art} - \frac{C_{liv}}{PC_{liv}} \right) - MET_{liv}, \quad A_{liv}(t=0) = 0, \quad C_{liv} = \frac{A_{liv}}{V_{liv}} \quad (3.2.6)$$

For a parent compound:

$$GI \text{ tract with sub-compartments: } Fl_{GIT} = fra \cdot f_{git} \cdot \frac{C_{stm}}{PC_{git}} + frb \cdot f_{git} \cdot \frac{C_{st}}{PC_{git}} + frc \cdot f_{git} \cdot \frac{C_{LI}}{PC_{git}}$$

$$FORM_{liv} = 0 \text{ (rate of formation of a given metabolite)}$$

$$MET_{liv} = \text{includes all the metabolism equations}$$

Liver – with zonation (and metabolism in the third zone):

$$\text{Zone 1: } \frac{dA_{liv,1}}{dt} = Fl_{GIT} + f_{liv} \cdot \left(C_{art} - \frac{C_{liv,1}}{PC_{liv}} \right) \quad (3.2.7)$$

$$\text{Zone 2: } \frac{dA_{liv,2}}{dt} = f_{liv} \cdot \left(\frac{C_{liv,1}}{PC_{liv}} - \frac{C_{liv,2}}{PC_{liv}} \right) \quad (3.2.8)$$

$$\text{Zone 3: } \frac{dA_{liv,3}}{dt} = f_{liv} \cdot \left(\frac{C_{liv,2}}{PC_{liv}} - \frac{C_{liv,3}}{PC_{liv}} \right) - MET_{liv} \quad (3.2.9)$$

Venous blood:

$$\frac{dA_{ven}}{dt} = f_{liv} \cdot \frac{C_{liv}}{PC_{liv}} + f_{ppt} \cdot \frac{C_{ppt}}{PC_{ppt}} + f_{hpt} \cdot \frac{C_{hpt}}{PC_{hpt}} + f_{adp} \cdot \frac{C_{adp}}{PC_{adp}} + f_{kid} \cdot \frac{C_{kid}}{PC_{kid}} + Fl_{skn} - f_{crd} \cdot C_{ven}, \quad A_{ven}(t=0) = 0, \quad C_{ven} = \frac{A_{ven}}{V_{ven}} \quad (3.2.10)$$

Where:

$$f_{hpt} \cdot \frac{C_{hpt}}{PC_{hpt}} = f_{brn} \cdot \frac{C_{brn}}{PC_{brn}} + f_{hrt} \cdot \frac{C_{hrt}}{PC_{hrt}} + f_{rb} \cdot \frac{C_{rb}}{PC_{rb}}$$

$$f_{ppt} \cdot \frac{C_{ppt}}{PC_{ppt}} = f_{msl} \cdot \frac{C_{msl}}{PC_{msl}} + f_{skt} \cdot \frac{C_{skt}}{PC_{skt}} + f_{skn} \cdot \frac{C_{skn}}{PC_{skn}}$$

For dermal absorption only:

Skin with sub-compartments (PBTK3_skn): $Fl_{skn} = \frac{3}{4} \cdot f_{skn} \cdot \frac{C_{skn}}{PC_{skn}} + \frac{1}{4} \cdot f_{skn} \cdot \frac{C_{sknhf}}{PC_{skn}}$

PBTK2_skn: $Fl_{skn} = f_{skn} \cdot \frac{C_{skn}}{PC_{skn}}$

Plasma quantification: $C_{ven,PL} = \frac{A_{ven}}{RBP / (0.55 \cdot V_{ven})}$ (3.2.11)

I assumed that plasma accounts for 55% of the human blood's composition according to (Ghafourian and Amin, 2013).

Arterial blood and lungs in the case of non-volatile compounds and no inhalation:

$$\frac{dA_{lng}}{dt} = f_{lng} \cdot \left(C_{ven} - \frac{C_{lng}}{PC_{lng}} \right); \quad A_{lng}(t=0) = 0; \quad C_{lng} = \frac{A_{lng}}{V_{lng}} \quad (3.2.12)$$

$$\frac{dA_{art}}{dt} = f_{crd} \cdot \left(\frac{C_{lng}}{PC_{lng}} - C_{art} \right); \quad A_{art}(t=0) = 0 \quad (3.2.13)$$

Arterial blood and lungs in the case of volatile compounds and no inhalation:

If a substance is volatile, a correction factor in the form of the blood/air partition coefficient needs to be incorporated in the lungs and arterial blood mass balances:

$$\frac{dA_{lng}}{dt} = f_{lng} \cdot \left(C_{ven} - PC_{blood,air} \cdot \frac{C_{lng}}{PC_{lng}} \right); \quad A_{lng}(t=0) = 0; \quad C_{lng} = \frac{A_{lng}}{V_{lng}} \quad (3.2.14)$$

$$\frac{dA_{art}}{dt} = f_{crd} \cdot \left(PC_{blood,air} \cdot \frac{C_{lng}}{PC_{lng}} - C_{art} \right); \quad A_{art}(t=0) = 0 \quad (3.2.15)$$

a) Oral absorption

In case of PBTK1_orl there is only one compartment describing the GI tract with a first order rate absorption constant (k_{GI} [1/h]) and a first order rate elimination constant (kel_{GI} [1/h]):

GI tract:

$$\frac{dA_{GI}}{dt} = -ka_{GI} \cdot A_{sGI} - kel_{GI} \cdot A_{GI} \quad (3.2.16)$$

PBTK3_orl comprises the following sub-compartments in the GI tract: stomach content and absorbed quantity, small (duodenum, jejunum, ileum) and large intestine (caecum, colon) content and their absorbed quantities- presented in **Figure 3.2.2**. In total, GI tract consists of 6 sub-compartments with a first order rate absorption from the content to the tissue/wall part. Special attention has been paid to the rate of emptying from stomach to intestines:

Stomach content:

$$\frac{dA_{stm,cont}}{dt} = D_{rt} - ka_{stm} \cdot C_{stm,cont} - kGIT \cdot A_{stm,cont} \quad (3.2.17)$$

$$\text{with: } C_{stm,cont} = \frac{A_{stm,cont}}{V_{stm}}, \quad kGIT = \frac{k_{max}}{(1+k_{min} \cdot C_{stm})}$$

and:

- administration via drinking: $D_{rt} = D_r \cdot C_{dose}$ and $C_{dose} = \frac{Dose}{V_{drink}}$, $A_{stm,cont}(t=0) = 0$
- administration via gavage: $D_{rt} = 0$ and $A_{stm,cont}(t=0) = Dose$
- administration by a coated tablet:

$$D_{rt} = \frac{dA_{stm,cont,diss}}{dt} = -Diss \cdot A_{stm,cont,diss} \text{ and } A_{stm,cont,diss}(t=0) = dose, A_{stm,cont}(t=0) = 0$$

Absorbed quantity from the stomach:

$$\frac{dA_{stm}}{dt} = ka_{stm} \cdot C_{stm,cont} + fra \cdot f_{git} \cdot \left(C_{art} - \frac{C_{stm}}{PC_{git}} \right), \quad A_{stm}(t=0) = 0, \quad C_{art} = \frac{A_{art}}{V_{art}}, \quad C_{stm} = \frac{A_{stm}}{V_{stm}} \quad (3.2.18)$$

Small Intestine lumen and absorbed quantity:

$$\frac{dA_{sl,lumen}}{dt} = kGIT \cdot A_{stm,cont} - (ka_{sl} + flow_{LI}) \cdot C_{sl,lumen}, \quad A_{sl,lumen}(t=0) = 0, \quad C_{sl,lumen} = \frac{A_{sl,lumen}}{\left(\frac{3}{4} \cdot V_{int} \right)} \quad (3.2.19)$$

$$\frac{dA_{sl}}{dt} = ka_{sl} \cdot C_{sl,lumen} + frb \cdot f_{git} \cdot \left(C_{art} - \frac{C_{sl}}{PC_{git}} \right), \quad A_{sl}(t=0) = 0, \quad C_{sl} = \frac{A_{sl}}{\left(\frac{3}{4} \cdot V_{int} \right)} \quad (3.2.20)$$

Large Intestine lumen and absorbed quantity:

$$\frac{dA_{LI,lumen}}{dt} = flow_{LI} \cdot C_{SI,lumen} - (kel_{LI} + ka_{LI}) \cdot C_{LI,lumen}, \quad A_{LI,lumen}(t=0) = 0, \quad C_{LI,lumen} = \frac{A_{LI,lumen}}{\left(\frac{1}{4} \cdot V_{int}\right)} \quad (3.2.21)$$

$$\frac{dA_{LI}}{dt} = ka_{LI} \cdot C_{LI,lumen} + frc \cdot f_{git} \cdot \left(C_{art} - \frac{C_{LI}}{PC_{git}}\right), \quad A_{LI}(t=0) = 0, \quad C_{LI} = \frac{A_{LI}}{\left(\frac{1}{4} \cdot V_{int}\right)} \quad (3.2.22)$$

It is assumed that 75% of gut blood flow goes to small intestine and 25% to large intestine.

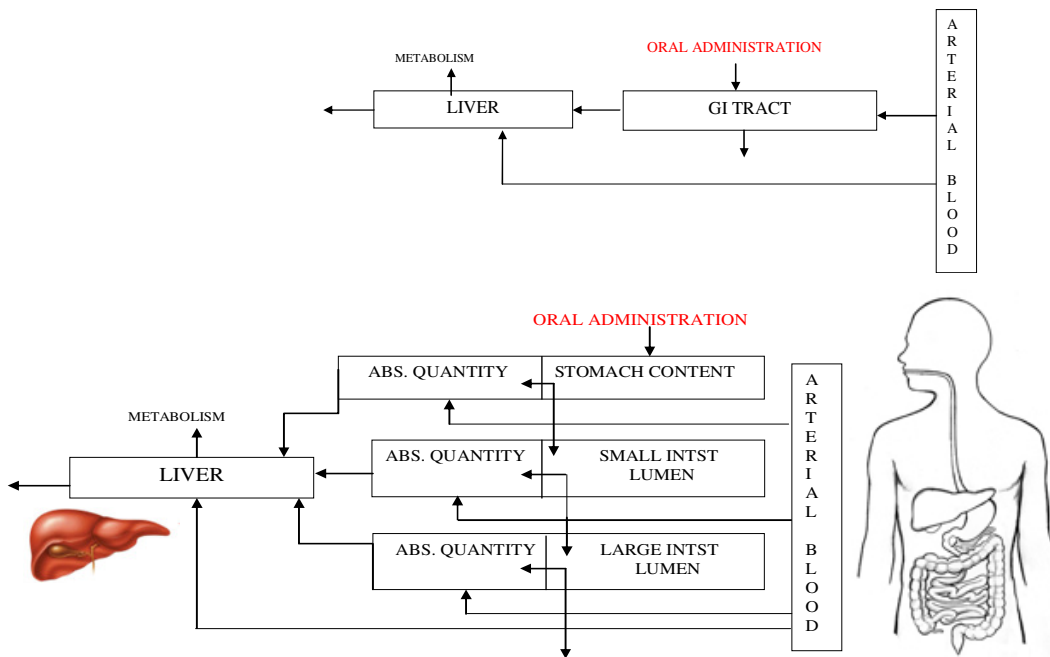


Fig 3.2.2 GI tract divided into sub-compartments in PBTk1_orl (top) and PBTk3_orl (bottom).

b) Dermal absorption

PBTk1: Skin: 1 compartment with first order rate of absorption (ka_{skn} [mL/h]):

$$\text{if } (t > t_{lag}) \quad \frac{dA_{skn}}{dt} = -ka_{skn} \cdot C_{skn} \quad \text{else} \quad \frac{dA_{skn}}{dt} = 0, \quad C_{skn} = \frac{A_{skn}}{V_{skn}}, \quad V_{skn} = Area \cdot L \quad (3.2.23)$$

where: t_{lag} is the time lag of absorption in the skin, Area is the application area [cm²], L- skin thickness [cm].

The absorbed amount is directed straight to the venous blood (added to mass balance equation).

PBTK2: Skin: 2 compartments: one with Fickian diffusion (E = *stratum corneum* + *viable epidermis*) and one with blood mixing.

$$\frac{dC_{E,j}}{dt} \approx -\frac{q_{E,j+1} - 2 \cdot q_{E,j} + q_{E,j-1}}{\left(\frac{L_E}{N}\right)} - \frac{BioC_{E,j}}{V_{E,j}}; j = 1 : N \quad C_{E,j} = \frac{A_{E,j}}{V_{E,j}} \quad (3.2.24)$$

where:

$$q_{E,j} = -D_{E,j} \cdot \frac{C_{E,j+1} - 2 \cdot C_{E,j} + C_{E,j-1}}{\left(\frac{L_E}{N}\right)}; j = 1 : N$$

If skin metabolism occurs, it is assumed to follow Michaelis-Menten kinetics:

$$BioC_{E,j} = \frac{V_{max,j} \cdot C_{E,j}}{K_m + C_{E,j}} \quad \text{otherwise} \quad BioC_{E,j} = 0$$

Initial and boundary conditions:

$$C_E(t = 0) |_{0 \leq y \leq L_E} = 0$$

$$\frac{dC_E}{dt}(t > 0) |_{x=0} = ka_{form} \cdot C_{form}$$

$$C_E(t > 0) |_{y=L_E} = PC_{skn} \cdot C_{skn}$$

$$C_E(t > 0) |_{x=0} = PC_E \cdot C_{form}$$

Where: PC_{skn} is the skin-to-blood partition coefficient and PC_E represents the partitioning between E and vehicle, D_E is the diffusion coefficient in E compartment [cm^2/h], L_E is the thickness of E [cm] and ka_{form} – uptake of chemical from formulation by the skin [mL/h].

Dermis and mixing with the blood:

$$\frac{dA_{skn}}{dt} = f_{skn} \cdot \left(C_{art} - \frac{C_{skn}}{PC_{skn}} \right) + q_{E,j=N} \cdot Area \quad A_{skn}(t=0) = 0 \quad (3.2.25)$$

PBTK3_skn: Skin: skin surface, *stratum corneum*, viable epidermis, dermis with blood and hair follicles.

Parallel diffusional transport via fine skin and hair follicles is added to compensate for highly heterogeneous skin composition and different permeation profiles at different sites. The following uptake phenomena are additionally considered: first order rate of intake and zero order rate of evaporation from the skin surface, possible metabolism in viable epidermis and binding in *stratum corneum*. In most cases, the role of hair follicles is limited to a minimum.

Sub-compartments in skin: skin surface, *stratum corneum*, viable epidermis, hair follicles.

Modelling assumptions:

- A tested compound is applied in a pure solvent (vehicle) onto the skin to account for a simple formulation (i.e. in ethanol, acetone) only. No mixture effects (possible interactions between formulation constituents) are considered.
- Diffusion coefficients are different for *stratum corneum*, viable epidermis and hair follicles but constant (in time) throughout the absorption process.

Given the complex structure and functionality of the skin, several assumptions are taken to simplify the overall transport kinetics:

- Fick's first law relates the diffusive flux to the concentration gradient under the assumption of steady state conditions. There is no convection of a chemical in the direction of the diffusion (unidimensional transport).
- To account for its heterogeneous structure, *stratum corneum* and epidermis are further divided into a number of sub-layers with properties of well-mixed (homogeneous) media of constant volume. However, the physiological condition of the skin is neglected.
- The *stratum corneum* is the rate-limiting part of the skin and its full thickness contributes to the diffusion barrier
- The skin is not altered by the penetrant or vehicle regardless of concentration. Possible interactions between the penetrant and vehicle are not considered. No active diffusion (diffusion with chemical reaction) and no carrier effects occur.
- There are no size-limiting pores to affect the absorption
- Attainment of equilibrium between skin layers and between its outermost layer and vehicle is rapid (PCs are constant).

The diffusion coefficient, here assumed constant, is in reality affected by several factors including:

- The skin structure, thickness and condition
- Applied vehicle that evidently affects a percentage of absorbed dose and value of the penetrant diffusion coefficient (it could be a function of solvent concentration and distance within the skin) (Crank, 1975). Solubility of penetrant in vehicle is also important.
- High concentrations of penetrant and vehicle (especially at alkaline or acidic pH) affects the skin condition, thereby affecting the diffusion coefficient which may change in time
- The early non-steady state uptake is greater from evaporating vehicle.

Skin surface:

$$\frac{dC_{form}}{dt} = DepRate - AbsRate - EvapRate \quad C_{form} = \frac{A_{form}}{V_{0,appliedForm}} \quad (3.2.26)$$

If the deposition rate is instantaneous, $DepRate=0$, otherwise, an exposure scenario describing the application (frequency, contact duration) is given.

$$or (t \leq t_{appl}) AbsRate = -(ka_{form} \cdot C_{form} + ka_{hf} \cdot C_{form}) \text{ and } for (t > t_{appl}) AbsRate = 0 \quad (3.3.27)$$

Where: t_{appl} is the application time of a formulation on the skin.

The evaporation of a solute (EvapRate) is calculated for volatile substances as (Tibaldi et al., 2011):

$$EvapRate = \frac{-k_{evp}}{TL} \quad (3.2.28)$$

For a vehicle (solvent) this evaporation is quantified in terms of decrease of the applied solution volume in time rather than mass of the solvent:

$$\frac{dV_{appliedForm}}{dt} = -\frac{k_{evp} \cdot Area}{1000 \cdot \sigma_{form}} \quad V_{appliedForm}(t=0) = V_{0,appliedForm} \quad (3.2.29)$$

$$\text{where: } k_{evp} = \frac{\beta \cdot MW \cdot V_p}{R \cdot T \cdot 10} \left[\frac{mg}{h \cdot cm^2} \right] \quad \beta = \frac{0.01 \cdot v_{air}^{0.96} \cdot D_g^{0.19}}{\nu^{0.15} \cdot X^{0.04}}$$

where β is the mass transfer coefficient in the vapour phase ($m \cdot h^{-1}$), MW the molecular weight, V_p the vapour pressure of the liquid at skin temperature [Pa], R the gas constant in $J \cdot mol^{-1} \cdot K^{-1}$, T the skin temperature (assumed to be 303 K), v_{air} the velocity of air (in the workplace it ranges from 0.3-0.6 $m \cdot s^{-1}$), D_g the diffusivity of the liquid in the gas phase (range: 0.03 to 0.06 $m^2 \cdot h^{-1}$), ν the kinematic viscosity of air (value of 0.054 $m^2 \cdot h^{-1}$ as used by (Tibaldi et al., 2011)), X the length of the evaporation area in the direction of air stream, TL a thickness of applied substance layer [cm], $Area$ the application area [cm^2] and δ_{form} the density of solvent [$g \cdot cm^{-3}$].

Stratum Corneum (SC):

Stratum corneum represents terminally differentiated keratinocytes (composed of water, proteins, lipids) – corneocytes. Passive diffusion is modelled according to Fick's second law of unidimensional diffusion with initial and boundary conditions (t_{appl} is the duration time of the application, once it is over- the remaining formulation is wiped off from skin surface). The diffusion coefficient is assumed to be constant throughout the process:

$$\frac{dC_{SC,i}}{dt} \approx -\frac{q_{SC,i+1} - 2 \cdot q_{SC,i} + q_{SC,i-1}}{\left(\frac{L_{SC}}{N}\right)}; i = 1 : N \quad C_{SC,i} = \frac{A_{SC,i}}{V_{SC,i}} \quad (3.2.30)$$

$$q_{SC,i} = -D_{SC,i} \cdot \frac{C_{SC,i+1} - 2 \cdot C_{SC,i} + C_{SC,i-1}}{\left(\frac{L_{SC}}{N}\right)}; i = 1 : N$$

where:

Initial and boundary conditions:

$$C_{SC}(t=0)|_{0 \leq x \leq L_{SC}} = 0$$

$$\frac{dC_{SC}}{dt}(t > 0)|_{x=0} = k_{a,form} \cdot C_{form}$$

$$D_{SC} \cdot \frac{dC_{SC}}{dx}(t > t_{appl})|_{x=0} = 0$$

$$C_{SC}(t > 0)|_{x=0} = PC_{SC} \cdot C_{form}$$

$$C_{SC}(t > 0)|_{x=L_{SC}} = PC_{SCVE} \cdot C_{VE}$$

The *stratum corneum* is assumed to have a homogenous structure, even though in reality it consists of two layers, *stratum disjunctum* and *stratum compactum* (Anissimov and Roberts, 2004).

Viable Epidermis (VE):

Epidermis is composed of keratinocytes, melanocytes, receptor cells such as Merkel cells (chemo-, photo-, thermos-, mechano- receptors), Langerhans cells (antibody generator in case of bacterial infection). Passive diffusion with constant diffusion coefficient takes also place in viable epidermis (diffusion with reaction if metabolism occurs):

$$\frac{dC_{VE,j}}{dt} \approx -\frac{q_{VE,j+1} - 2 \cdot q_{VE,j} + q_{VE,j-1}}{\left(\frac{L_{VE}}{M}\right)} - \frac{BioC_{VE,j}}{V_{VE,j}}; j=1:M \quad C_{VE,j} = \frac{A_{VE,j}}{V_{VE,j}} \quad (3.2.31)$$

Where:

$$q_{VE,j} = -D_{VE,j} \cdot \frac{C_{VE,j+1} - 2 \cdot C_{VE,j} + C_{VE,j-1}}{\left(\frac{L_{VE}}{M}\right)}; j=1:M \quad \text{and} \quad BioC_{VE,j} = \frac{V_{max,j} \cdot C_{VE,j}}{K_{m,j} + C_{VE,j}}$$

Initial and boundary conditions:

$$C_{VE}(t=0)|_{0 \leq y \leq L_{VE}} = 0$$

$$C_{VE}(t > 0)|_{y=0} = \frac{C_{SC,i=N}}{PC_{SCVE}}$$

$$D_{SC} \frac{dC_{SC}}{dx} \Big|_{x=L_{SC}} = D_{VE} \cdot \frac{dC_{VE}}{dy} \Big|_{y=0}$$

$$C_{VE}(t > 0)|_{y=L_{VE}} = PC_{skn} \cdot C_{skn}$$

The model simulations were run for N=M=10 layers.

The partial differential equations for stratum corneum and viable epidermis (diffusion with metabolism if occurs) are solved by means of the method of lines approach.

Dermis and mixing with the blood:

$$\frac{dA_{skn}}{dt} = \frac{3}{4} \cdot f_{skn} \cdot \left(C_{art} - \frac{C_{skn}}{PC_{skn}} \right) + q_{VE,j=M} \cdot (1-nf) \cdot Area \quad A_{skn}(t=0) = 0 \quad C_{skn} = \frac{A_{skn}}{10^{-3} \cdot \frac{2}{3} \cdot Vde} \quad (3.2.32)$$

where: nf is a fraction of skin covered by hair follicles and sweat glands.

Hair follicles & sweat glands (HF) compartment (Bookout Jr. et al., 1997):

$$\frac{dC_{hf,i}}{dt} \approx -\frac{q_{hf,i+1} - 2 \cdot q_{hf,i} + q_{hf,i-1}}{\left(\frac{L_{hf}}{K}\right)}; i=1:K \quad L_{hf} = \frac{388}{560} \cdot L \quad (3.2.33)$$

$$q_{hf,i} = -D_{hf,i} \cdot \frac{C_{hf,i+1} - 2 \cdot C_{hf,i} + C_{hf,i-1}}{\left(\frac{L_{hf}}{K}\right)}; i=1:K$$

The initial and boundary conditions:

$$C_{hf}(t=0)|_{0 \leq x \leq L_{hf}} = 0$$

$$\frac{dC_{hf}}{dt}(t > 0)|_{x=0} = ka_{hf} \cdot C_{form}$$

$$D_{hf} \cdot \frac{dC_{hf}}{dx}(t > t_{appl})|_{x=0} = 0$$

$$C_{hf}(t > 0)|_{x=0} = PC_{hf} \cdot C_{form}$$

$$C_{hf}(t > 0)|_{x=L_{hf}} = PC_{skn} \cdot C_{sknhf}$$

No metabolism in hair follicles was considered due to lack of this information in literature.

Mixing with the blood:

$$\frac{dA_{sknhf}}{dt} = \frac{1}{4} \cdot f_{skn} \cdot \left(C_{art} - \frac{C_{sknhf}}{PC_{skn}} \right) + q_{hf,i=k} \cdot nf \cdot Area \quad A_{sknhf}(t=0) = 0 \quad C_{sknhf} = \frac{A_{sknhf}}{10^{-3} \cdot \frac{1}{3} \cdot Vde} \quad (3.2.34)$$

It is assumed that 75% of skin blood flow goes to the fine skin (epidermis) and 25% to hair follicles, sweat glands. Dermis compartment mixes the blood flowing from epidermis and follicles.

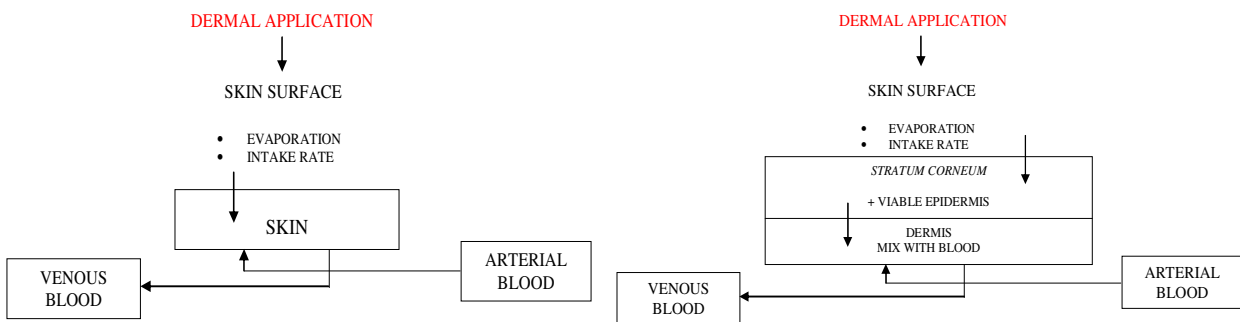


Fig 3.2.3. Skin compartment in PBTK1_skn (left), PBTK2_skn (right).

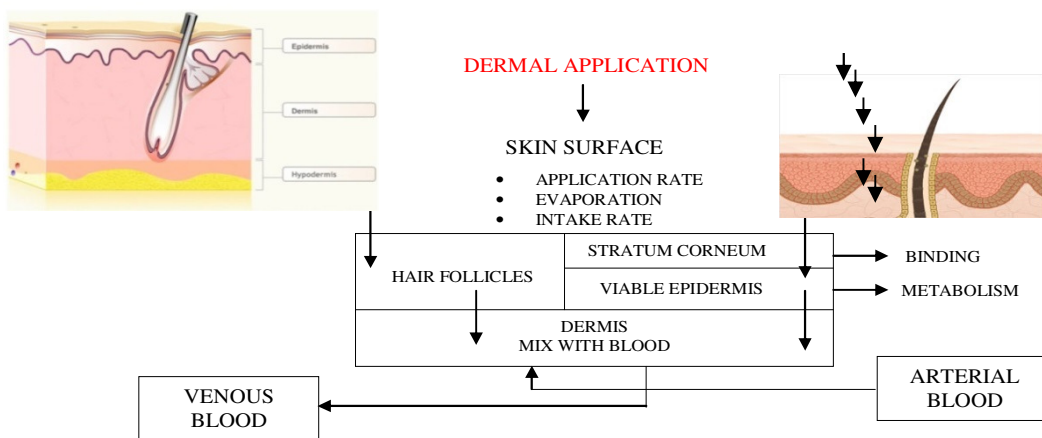


Fig 3.2.4. Skin divided into sub-compartments in PBTK3_skn.

c) Inhalation

The PBTK1_inh model accounts for inhalation consists of 3 compartments according to (Kumagai and Matsunaga, 1995):

Inhaled air tract:

$$\frac{dA_{INH}}{dt} = ALV \cdot \frac{C_{exp}}{PC_{waterair}} + 2 \cdot RR \cdot C_{EXH} - ALV \cdot \frac{C_{INH}}{PC_{waterair}} - 2 \cdot RR \cdot C_{INH}; \quad A_{INH}(t=0)=0; \quad C_{INH} = \frac{A_{INH}}{VAT} \quad (3.2.35)$$

Exhaled air:

$$\frac{dA_{EXH}}{dt} = ALV \cdot \frac{C_{ing}}{PC_{waterair}} + 2 \cdot RR \cdot C_{INH} - ALV \cdot \frac{C_{EXH}}{PC_{waterair}} - 2 \cdot RR \cdot C_{EXH}; \quad A_{EXH}(t=0)=0; \quad C_{EXH} = \frac{A_{EXH}}{VAT} \quad (3.2.36)$$

Lungs:

$$\frac{dA_{ing}}{dt} = f_{ing} \cdot \left(C_{ven} - PC_{Blood,air} \cdot \frac{C_{ing}}{PC_{ing}} \right) + ALV \cdot \frac{C_{INH}}{PC_{waterair}} - \frac{ALV}{PC_{waterair}} \cdot \frac{C_{ing}}{PC_{ing}}; \quad A_{ing}(t=0)=0; \quad C_{ing} = \frac{A_{ing}}{V_{ing}} \quad (3.2.37)$$

Where:

VAT – is the mucous volume of inhaled/exhaled air [L]

RR – is the respiratory rate [1/h]

ALV – is the alveolar rate [L/h] ((tidal volume-dead space) · RR) – volume of gas per time that reaches alveoli.

PC_{water,air} – is the water/air partition coefficient

PBTK3_inh: for more complex substances, metal particles, nanoparticles and aerosols (these substances were not illustrated in this thesis- styrene, isopropanol and ethanol were used instead) there is a multi-compartment lungs model that is more commonly applied (Peterman and Longtin, 1984). In this model, the respiratory tract consists of the flow-in compartment (mouth/nose), 24 generations of the Weibel model (Peterman and Longtin, 1984; Weibel, 1979) and arterial blood mass balance (**Figure 3.2.5**). The entire numerical procedure is described in (Peterman and Longtin, 1984). Here the airways and lung compartment are additionally coupled with all the remaining compartments of PBTK model. The compartments that describe inhalation/exhalation processes are defined as follows:

- a mouth/nose compartment : A_{mouth}
- 1-13 generations for convection only (NC=13) : A_{conv} [1–13]
- 14-17 generations for convection and diffusion (ND=4): A_{diff} [1–4]
- 18-24 generations for convection and diffusion with blood mixing (NDB=7): A_{diffb} [1–7]

- arterial blood: A_{art}

The respiratory tract consists of 3 main compartments (24 Weibel generations): convection and diffusion segments and mix with blood (with metabolism that may occur at any stage) (**Figure 3.2.6**). This dynamic lungs model is more suitable for reactive substances, drugs and nanoparticles. For simple compounds this refinement is not necessary but it allows for a better control of the inhalation/exhalation process. A sinusoidal breathing pattern is incorporated in the model with time frame in seconds (higher computational burden than other exposure types). The model, additionally, consists of blood/air partition coefficient, Ostwald solubility in lungs and rate of dissolved gas removed from lungs due to blood perfusion on overall model prediction performance. The last three parameters need to be optimised for a given chemical with respect to available *in vivo* blood concentrations.

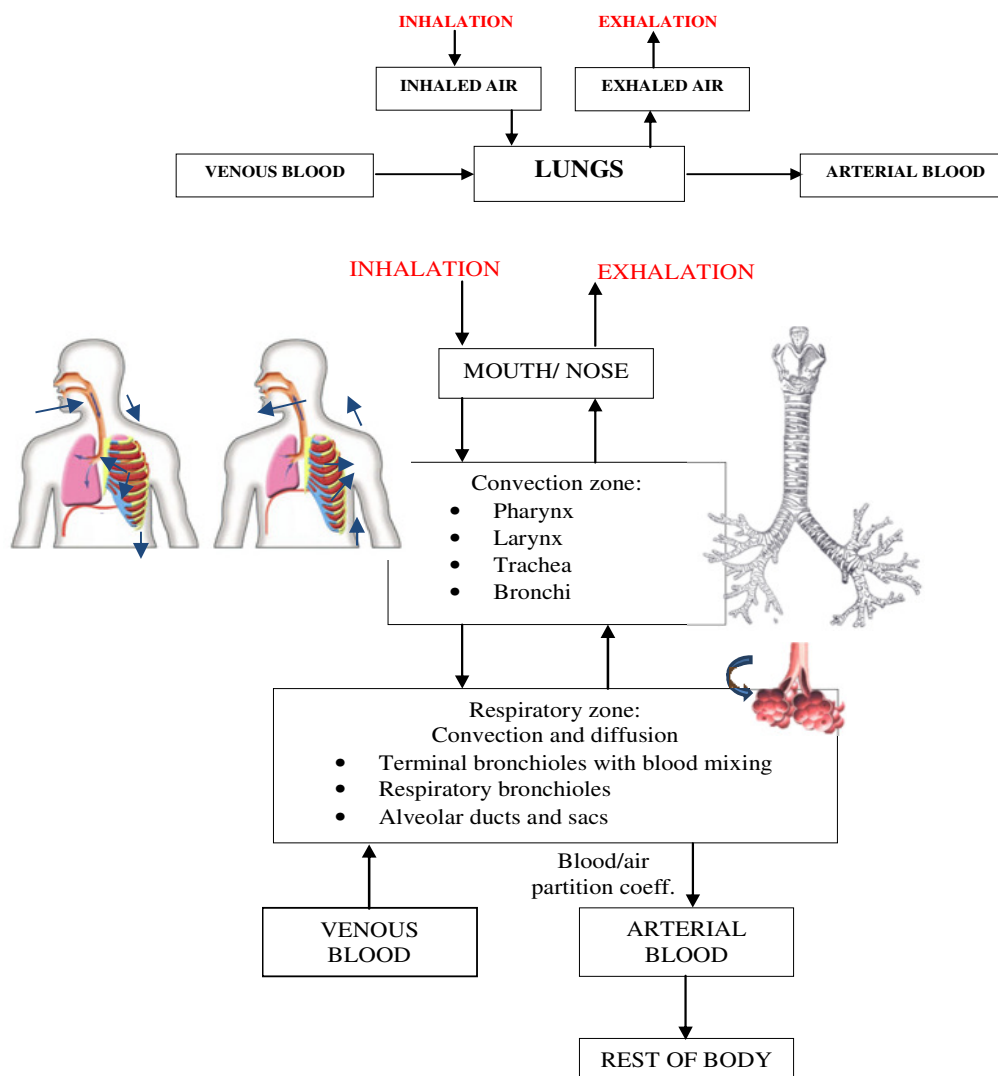


Fig 3.2.5. Respiratory tract: Simple structure (above), complex structure divided into 24 generations (based on Weibel, 1963) (below).

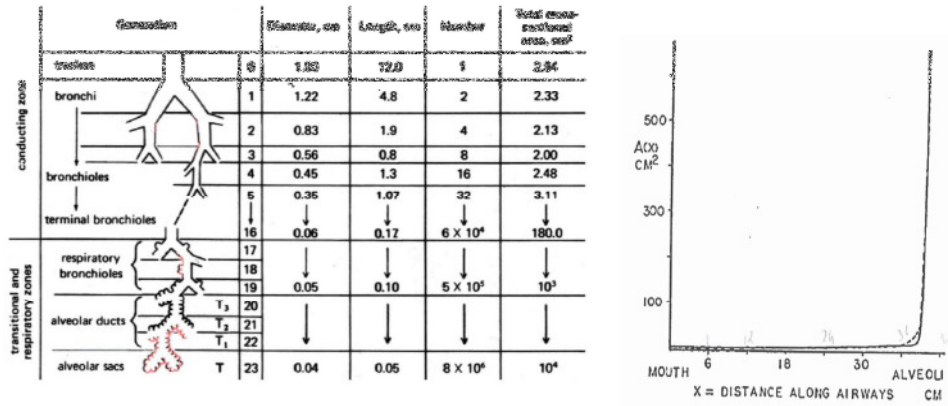


Fig 3.2.6 Airway tree organised into zones (convection and respiratory zones and their physiological properties) (Weibel, 1979).

The total cross-sectional area increases through 24 generations from 2.54 cm² up to 10⁴ cm². For the last 12 generations this increase can be described by means of the following function:

$$Area(x) = \frac{50}{40.2 - x} \quad \text{with } x = n \cdot 16 \quad \text{where } n = 13 : 24 \quad (3.2.38)$$

$AreaVec = Area(x = n \cdot 1.66)$ is the vector of a length 12 (ND + NDB + 1)

$AreaDiff[0] = AreaVec[1]$; $AreaDiff = AreaVec[2:5]$; $AreaDiffB = AreaVec[6:12]$

Table 3.2.1. Airways system specific data

Quantity used in the model and its characteristics	Value	Abbreviation used in the model
Total number of alveoli	3·10 ⁸	NalvTot
There is an assumption that the number of alveoli per generation increases uniformly in the last 7 generations (by 4/5·NalvTot/28)		
The previous 14-17 generations consist of 1/5 of total No. of alveoli		
Alveolar surface area [cm ²]	1420000	AreaALV
Distance between generations [cm]	0.05	deltax
Capillary surface area [cm ²]	1250000	AreaCAP
The volume of airways [cm ³] in the generations 1-24 is calculated by multiplying Total cross-sectional area of a given segment by its length (Figure 3.2.6)		Genvol[1:24]
The rate of dissolved gas removed from the lungs due to blood perfusion [mL/s] – roughly estimated	35	r
Volume of mouth [mL]	20	V _{mouth}

Mouth/ Nose compartment:

$$\begin{aligned} \text{Inhalation:} \quad & \text{if } (t \leq t_{\text{exp}}) \rightarrow \frac{dA_{\text{mouth}}}{dt} = Q_m \cdot \left(C_{\text{exp}} - \frac{A_{\text{mouth}}}{V_{\text{mouth}}} \right) = \frac{dA_{\text{conv}}}{dt} [0] \\ & \text{if } (t > t_{\text{exp}}) \rightarrow \frac{dA_{\text{mouth}}}{dt} = Q_m \cdot \left(- \frac{A_{\text{mouth}}}{V_{\text{mouth}}} \right) = \frac{dA_{\text{conv}}}{dt} [0] \end{aligned}$$

(3.2.39)

$$\text{Exhalation: } \frac{dA_{mouth}}{dt} = Q_m \cdot \left(\frac{A_{conv}[1]}{V_{conv}[1]} - \frac{A_{mouth}}{V_{mouth}} \right) = \frac{dA_{conv}}{dt} [0] \quad (3.2.40)$$

where:

t_{exp} – the time of exposure to a chemical

Q_m [mL/s] is the total flow rate of a gas into mouth applied for 1-16 generations. A sinusoidal breathing pattern is assumed with the breathing period of $p=4s$. The sign of the resulting flow rate value reflects whether inhalation or exhalation takes place.

$$Q_m = q_0 \cdot \sin\left(\frac{2\pi}{p}\right) \text{ with } \int_0^p \left(q_0 \cdot \sin\left(\frac{2\pi}{p}\right) \right) dt = 500 \rightarrow q_0 = \frac{500\pi}{p} \quad (3.2.41)$$

In the alveolated region (generations 17-24) the flow rate is slightly modified by:

$$Q_m[17-24] = Q_m \cdot \left(1 - \frac{1}{\frac{4}{5} \cdot \text{NalvTot}} \cdot \sum_{i=17}^{i=24} \text{Nalv}_i \right) = Q_{mi} \quad (3.2.42)$$

The vector with volume values per generation is divided accordingly:

$$\begin{aligned} V_{conv}[1:NC] &= \text{GenVol}[1:NC] & V_{conv}[0] &= V_{mouth} \\ V_{diff}[1:ND] &= \text{GenVol}[(NC+1):(NC+ND)] & \text{with: } V_{diff}[0] &= V_{conv}[NC] \\ V_{diffb}[1:NDB] &= \text{GenVol}[(1+NC+ND):(NC+ND+NDB)] & V_{diffb}[0] &= V_{diff}[ND] \end{aligned}$$

Convection compartment:

For: $nc = 1:13$, $k = nc-1$ and $i = nc+1$

$$\text{Inhalation: } \frac{dA_{conv}}{dt}[nc] = Q_m \cdot \left(\frac{A_{conv}[k]}{V_{conv}[k]} - \frac{A_{conv}[nc]}{V_{conv}[nc]} \right) \quad (3.2.43)$$

$$\text{Exhalation: } \frac{dA_{conv}}{dt}[nc] = Q_m \cdot \left(\frac{A_{conv}[i]}{V_{conv}[i]} - \frac{A_{conv}[nc]}{V_{conv}[nc]} \right) \quad (3.2.44)$$

Convection and diffusion compartment:

For: $nd=1:4$, $k=nd-1$, $i=nd+1$

Inhalation:

$$\frac{dA_{diff}}{dt}[nd] = Q_m \cdot \left(\frac{A_{diff}[k]}{V_{diff}[k]} - \frac{A_{diff}[nd]}{V_{diff}[nd]} \right) - \frac{D_i \cdot \text{AreaDiff}[nd]}{\text{deltax}} \cdot \left(\frac{A_{diff}[nd]}{V_{diff}[nd]} - \frac{A_{diff}[i]}{V_{diff}[i]} \right) - \frac{D_i \cdot \text{AreaDiff}[k]}{\text{deltax}} \cdot \left(\frac{A_{diff}[nd]}{V_{diff}[nd]} - \frac{A_{diff}[k]}{V_{diff}[k]} \right) \quad (3.2.45)$$

Exhalation:

$$\frac{dA_{diff}}{dt}[nd] = Q_m \cdot \left(\frac{A_{diff}[i]}{V_{diff}[i]} - \frac{A_{diff}[nd]}{V_{diff}[nd]} \right) - \frac{D_l \cdot AreaDiff[nd]}{deltax} \cdot \left(\frac{A_{diff}[nd]}{V_{diff}[nd]} - \frac{A_{diff}[i]}{V_{diff}[i]} \right) - \frac{D_l \cdot AreaDiff[k]}{deltax} \cdot \left(\frac{A_{diff}[nd]}{V_{diff}[nd]} - \frac{A_{diff}[k]}{V_{diff}[k]} \right) \quad (3.2.46)$$

Convection and diffusion compartment with blood mixing:

For: ndb=1:7, k=ndb-1, i=ndb+1

Inhalation:

$$\begin{aligned} \frac{dA_{diffb}}{dt}[ndb] = & Q_{mi} \cdot \frac{A_{diffb}[k]}{V_{diffb}[k]} - Q_{mi} \cdot \frac{A_{diffb}[ndb]}{V_{diffb}[ndb]} - \frac{D_{cn,lng} \cdot AreaDiffB[ndb]}{deltax} \cdot \left(\frac{A_{diffb}[ndb]}{V_{diffb}[ndb]} - \frac{A_{diffb}[i]}{V_{diffb}[i]} \right) \\ & - \frac{D_{cn,lng} \cdot AreaDiffB[k]}{deltax} \cdot \left(\frac{A_{diffb}[ndb]}{V_{diffb}[ndb]} - \frac{A_{diffb}[k]}{V_{diffb}[k]} \right) - r \cdot \left(\lambda_{cn} \cdot \frac{A_{diffb}[ndb]}{V_{diffb}[ndb]} - \frac{A_{ven}}{PC_{blood/air} \cdot V_{ven} \cdot 1000} \right) \end{aligned} \quad (3.2.47)$$

For ndb=7 :

$$\frac{dA_{diffb}}{dt}[7] = Q_{mi} \cdot \frac{A_{diffb}[7]}{V_{diffb}[7]} - \frac{D_{cn,lng} \cdot AreaDiffB[7]}{deltax} \cdot \left(\frac{A_{diffb}[7]}{V_{diffb}[7]} - \frac{A_{diffb}[6]}{V_{diffb}[6]} \right) - r \cdot \left(\lambda_{cn} \cdot \frac{A_{diffb}[7]}{V_{diffb}[7]} - \frac{A_{ven}}{PC_{blood/air} \cdot V_{ven} \cdot 1000} \right) \quad (3.2.48)$$

Exhalation:

$$\begin{aligned} \frac{dA_{diffb}}{dt}[ndb] = & Q_{mi} \cdot \frac{A_{diffb}[i]}{V_{diffb}[i]} - Q_{mi} \cdot \frac{A_{diffb}[ndb]}{V_{diffb}[ndb]} - \frac{D_{cn,lng} \cdot AreaDiffB[ndb]}{deltax} \cdot \left(\frac{A_{diffb}[ndb]}{V_{diffb}[ndb]} - \frac{A_{diffb}[i]}{V_{diffb}[i]} \right) \\ & - \frac{D_{cn,lng} \cdot AreaDiffB[k]}{deltax} \cdot \left(\frac{A_{diffb}[ndb]}{V_{diffb}[ndb]} - \frac{A_{diffb}[k]}{V_{diffb}[k]} \right) - r \cdot \left(\lambda_{cn} \cdot \frac{A_{diffb}[ndb]}{V_{diffb}[ndb]} - \frac{A_{ven}}{PC_{blood/air} \cdot V_{ven} \cdot 1000} \right) \end{aligned} \quad (3.2.49)$$

For MB=7

$$\frac{dA_{diffb}}{dt}[7] = -Q_{mi} \cdot \frac{A_{diffb}[7]}{V_{diffb}[7]} - \frac{D_{cn,lng} \cdot AreaDiffB[7]}{deltax} \cdot \left(\frac{A_{diffb}[7]}{V_{diffb}[7]} - \frac{A_{diffb}[7]}{V_{diffb}[7]} \right) - r \cdot \left(\lambda_{cn} \cdot \frac{A_{diffb}[7]}{V_{diffb}[7]} - \frac{A_{ven}}{PC_{blood/air} \cdot V_{ven} \cdot 1000} \right) \quad (3.2.50)$$

where

$D_{cn,lng}$ – diffusion coefficient of a compound in lungs (assumed constant).

λ_{cn} – Ostwald solubility coefficient of a compound in lungs (blood-to-gas partition coefficient representing solubility of a gas in blood).

r- rate of gas removed from lungs due to blood perfusion (estimated to be 2.1 L/min (Peterman and Longtin, 1984))

Additional assumptions: diffusion across walls of respiratory tract is neglected. Metabolism in lungs is considered only in a very limited extent due to lack of this information for the investigated substances in literature.

Arterial blood:

$$\text{Inhalation: } \frac{dA_{art}}{dt} = f_{-crd} \cdot \left(\frac{PC_{blood/air} \cdot r \cdot \lambda \cdot \sum_{i=1}^{i=MB} \frac{A_{diffb}[i]}{V_{diffb}[i]}}{V_{lg}} - \frac{A_{cart}}{V_{art}} \right) \quad (3.2.51)$$

$$\text{Exhalation: } \frac{dA_{art}}{dt} = f_{-crd} \cdot \left(-\frac{A_{art}}{V_{art}} \right) \quad (3.2.52)$$

PBTK model simulations can provide some useful toxicokinetic parameters like: maximum concentration of a chemical in an organ (C_{max}), total amount of chemical to which an organ is exposed to (Area under curve AUC), bioavailability, volume of distribution and total clearance. Additionally, as mentioned before, plasma protein binding and blood- to- plasma concentration ratio may be roughly estimated by ADMET predictor if measured values are not available.

The entire PBTK modelling process is based on the following assumptions:

- a) Tissues are homogeneous with respect to the concentration of a chemical. Transport between blood and tissue is assumed to be perfusion-rate limited. Upon entry with blood circulation, the chemical distributes freely and instantly across the membranes without diffusion barriers (transport barriers between free molecules of chemical in blood and tissue are negligible and equilibrium between free and bound fractions in blood and tissue is instantaneous).
- b) This is a well-stirred model with no concentration gradient within a tissue/organ compartment.
- c) Inter-individual differences in metabolism and excretion are not explicitly considered. To partially account for such variations, the metabolic rates are corrected by the subject's body weight.
- d) Investigated substances do not alter physiological properties such as cardiac output (they are assumed compound independent).

To compare the performance of the models PBTK1, PBTK2 and PBTK3, the coefficient of determination (R^2), mean squared error (MSE) and Akaike's Information Criterion (AIC) (Kletting and Glatting, 2009) were used. For model discrimination, AIC penalises models with a large number of parameters when having the same agreement in terms of mean squared error. The model with the lowest algebraic AIC therefore indicates the best agreement with experimental data while minimizing the risk of over fitting. In addition, a corrected AIC (AICc) was applied to adjust for a small number of data points (Kletting and Glatting, 2009).

$$R^2 = 1 - \frac{\sum (y - x)^2}{\sum (y - \text{mean}(y))^2} \quad (3.2.53)$$

where: x – predicted results, y-observed data.

$$AICc = n \cdot \log(MSE) + 2 \cdot k + \frac{2 \cdot k \cdot (k + 1)}{n - k - 1} \quad (3.2.54)$$

where: n – number of observations, k- number of parameters in the model, MSE – mean squared error

The model parameters come from the scientific literature and available online databases (i.e. the PK/DB database for pharmacokinetic properties¹², TOXNET: toxicology data network¹³, EDETOX database¹⁴) and chemistry-based prediction software (ADMET Predictor¹⁵, QSAR toolbox¹⁶).

The mathematical equations were programmed in R by combining functionalities of the following R packages: deSolve, PK, FME, rgenoud and AICcmodavg¹⁷. Ordinary differential equations (ODEs) were solved by the method *lsoda* available in the deSolve package, which switches automatically between stiff and non-stiff methods. The method of lines was used to solve PDEs.

Physiological parameters for the healthy adult Caucasian population

All physiological parameters for a reference man and woman from the healthy adult Caucasian population that are independent of the administered substance and constitute a constant part of the model equations are given in **Table 3.2.2**. The values were taken from the study of (Brown et al., 1997) except for adipose tissue that was calculated by using the equation taken from (Deurenberg et al., 1998): $\frac{1.29 \cdot BMI + 0.2 \cdot Age - 8}{100}$ for a man and $\frac{1.29 \cdot BMI + 0.2 \cdot Age - 19.4}{100}$ for a woman (BMI: Body Mass Index = BW/ (height)²) and skin as a fraction

of body weight that was calculated according to: $\frac{BSA[m^2] \cdot L[m] \cdot \delta_{skin} \left[\frac{g}{m^3} \right]}{BW[g]}$, where δ_{skin} is the skin density assumed equal to 1.4 g/m³ (Brown et al., 1997). In addition, alveolar ventilation rate was calculated as a function of a body weight: $BW \cdot (0.7 \cdot 0.332 \cdot BW^{0.74})$ (Kumagai and Matsunaga, 1995).

¹² <http://miro.ifsc.usp.br/pkdb/> (last access: 06.10.2014)

¹³ <http://toxnet.nlm.nih.gov/> (last access: 06.10.2014)

¹⁴ <http://edetox.ncl.ac.uk/> (last access: 06.10.2014)

¹⁵ <http://www.simulations-plus.com/Products.aspx?pID=13> (last access: 06.10.2014)

¹⁶ <http://www.qsartoolbox.org/> (last access: 06.10.2014)

¹⁷ available from The Comprehensive R Archive Network website: <http://cran.r-project.org/> (last access: 06.10.2014)

Table 3.2.2. Physiological parameters used in the model for a reference man and woman.

Organ weight fractions (organ weight as fraction of total body weight)	Reference woman	Reference man
Average Body Weight (BW) [kg]	64	75
Age	25	25
Liver	0.026	0.026
Adipose tissue	Variable (see text)	Variable (see text)
Lungs	0.0105	0.012
Brain	0.02	0.02
Heart	0.0044	0.0044
Kidney	0.0044	0.0044
GI tract:	0.0265	0.025
Stomach:	0.00337	0.00318
Small Intestine:	0.0146	0.0138
Large Intestine:	0.0085	0.0080
Poorly perfused tissues	0.44	0.52
Skin	Variable (see text)	Variable (see text)
Blood	0.065	0.072
Venous blood	0.04875	0.054
Rest of body	Variable ca. 0.13	Variable Ca. 0.16
Regional blood flow rates (fraction of cardiac output)		
Total cardiac output [L/h]	$15 \cdot BW^{0.74}$	$15 \cdot BW^{0.74}$
Liver	0.25	0.24
Adipose tissue	0.055	0.04
Lungs	0.025	0.025
Brain	0.114	0.114
Heart	0.04	0.04
Skin	0.05	0.05
Kidney	0.19	0.2
Poorly perfused tissues	0.135	0.16
GI tract	0.14	0.13
Fractions for stomach, small intestine and large intestine		
Rest of body	ca. 0.001	ca. 0.001
Skin thickness L [cm]	0.204	0.2906
Stratum corneum thickness L_{SC} [cm]	0.0018	0.0017
Viable Epidermis thickness L_{VE} [cm]	0.0032	0.0047
Alveolar ventilation ALV [L/h]	Variable (see text)	Variable (see text)

Respiratory rate RR [1/h]	820	840
Volume of mucous layer of inhaled/exhaled air over 1 h VAT [L]	0.4	0.5

3.2.2 PBTD model

The physiologically-based toxicodynamic (PBTD) model is represented by two compartments (including tolerance that acts against the modelled effect). The general structure is presented in **Figure 3.2.7**. In the analysed cases of heart rate and blood pressure it is a venous blood concentration corrected by plasma protein binding (f_u) that is directly linked to an effect (it is only the unbound fraction of a chemical in blood that causes an effect). In this work only direct Emax model is considered (under assumption there is no time-lag between PK and PD profiles and no shift with a dose).

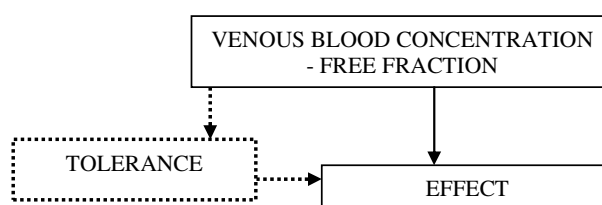


Fig 3.2.7 Effect compartment - toxicodynamics.

Tolerance (hypothetical noncompetitive antagonist) mass balance:

Antagonist formation and elimination rates are assumed constant and dependent on the venous blood concentration of a stimulant.

$$\frac{dA_{Ant}}{dt} = k_{a,Ant} \cdot (f_u \cdot C_{ven}) - k_{el,Ant} \cdot C_{Ant} \quad (3.2.55)$$

Where:

C_{Ant} is the antagonist concentration [mg/L]

C_{ven} is the venous blood concentration of a chemical causing effect [mg/L]

$k_{a,Ant}$ and $k_{el,Ant}$ – are formation and elimination rates [L/h] of the antagonist

f_u - free fraction of chemical

a) Heart rate

The PBTD model is a modification of a previously published nicotine effect model (sigmoid direct Emax model) in which a “tolerance” compartment represents a hypothetical noncompetitive antagonist (Porchet et

al., 1988). The modification, introduced for better fit, includes addition of an exponential term (y) in the considered concentrations to modify the hyperbolic form of the original model (**Equations 3.2.56 and 3.2.57**). However, this modification is necessary only in case of ongoing exercise. This assumption comes from the fitting results of the sigmoid model with respect to nicotine data showing an effect on the heart rate during a cycling exercise (Mündel and Jones, 2006). However, further experiments are necessary to confirm this assumption as this study has been additionally performed on non-smokers, so there are variety of factors that could be responsible for a need of adding this exponential term. As in the paper of (Porchet et al., 1988), to avoid identifiability problems, I further assumed that the chemical concentration in blood (C_{ven}) is always much less than concentration needed to produce half of the maximal effect ($C_{ven,50}$), i.e. $C_{ven} \lll C_{ven,50}$.

Modified sigmoid model with hypothetical noncompetitive antagonist:

$$E = E_0 + \frac{\frac{E_{max}}{C_{ven,50}^y} \cdot C_{ven}^y}{\left(1 + \frac{C_{Ant}^y}{C_{Ant,50}^y}\right) \cdot \left(1 + \frac{C_{ven}^y}{C_{ven,50}^y}\right)} \rightarrow E = E_0 + \frac{\frac{E_{max}}{C_{ven,50}^y} \cdot C_{ven}^y}{1 + \frac{C_{Ant}^y}{C_{Ant,50}^y}} \rightarrow E = E_0 + \frac{S \cdot C_{ven}^y}{1 + \frac{C_{Ant}^y}{C_{Ant,50}^y}} \quad (3.2.56)$$

$$E = E_0 + \frac{S \cdot (fu \cdot C_{ven})^y}{1 + \left(\frac{C_{Ant}}{C_{Ant,50}}\right)^y} \quad (3.2.57)$$

Where:

E is the effect on heart rate

E_0 is base-line effect

E_{max} is the maximal effect

$C_{ven,50}$ is the venous blood concentration of a chemical causing 50% of the maximal effect [mg/L]

S- is equal to the ratio of E_{max} (maximal effect) / C_{50} (concentration of a chemical causing half of the effect)

$C_{Ant,50}$ – the concentration of non-competitive antagonist (tolerance) attainable for a steady-state chemical concentration

y - exponential term introduced as a deviation from the standard hyperbolic model

b) Blood pressure

A sigmoid model with hypothetical noncompetitive antagonist is used to model a chemically induced blood pressure increase according to (Shi, 1993):

$$E = E_0 + \frac{S \cdot (fu \cdot C_{ven})}{1 + \left(\frac{C_{Ant}}{C_{Ant,50}} \right)} \quad (3.2.58)$$

3.2.3 Virtual cell-based assay model

The Virtual cell-based assay (VCBA) model describes and predicts what is happening in an in vitro system, especially the fate of a chemical within the well, taking into account partitioning with protein, lipids, and plastic binding (Comenges, J.-M.Z Wambaugh and Judson, 2012; Zaldívar et al., 2011, 2010). The model integrates:

- a. *Fate and transport model* that calculates the time-dependent chemical concentration in the medium as well as in the headspace (**Figure 3.2.8**). It takes into consideration a series of processes including evaporation, partitioning of chemicals from the dissolved phase to serum proteins and lipids, adsorption onto the plastic, and also degradation and metabolism.
- b. *Cell growth and division model* that is based on a four stage based approach (Gérard and Goldbeter, 2009), with each stage corresponding to one of the four cell cycle phases: G1, S, G2 and M (Zaldívar et al., 2010). In the stage-based type of modelling the matrix A, called the Leslie matrix, describes the transformation of a population from time t to time t+1.
- c. *Cell partitioning model* that was built on the assumption that once the chemical is taken up by the cell, a partitioning occurs between three compartments: one aqueous fraction and two non-aqueous fractions corresponding to structural components (proteins) and energy resources (lipids).
- d. *Toxicity and effects model* which takes into account the direct effects of a chemical concentration, C, on cell dynamics (survival/mortality) expressed by using the killing rate, k_t , and the no effect concentration, NEC (Billoir et al., 2007; Lopes et al., 2005) - **Equation 3.2.59**. The main property simulated is the real intracellular concentration of a specific chemical affecting the cell, and its effect (cell viability).

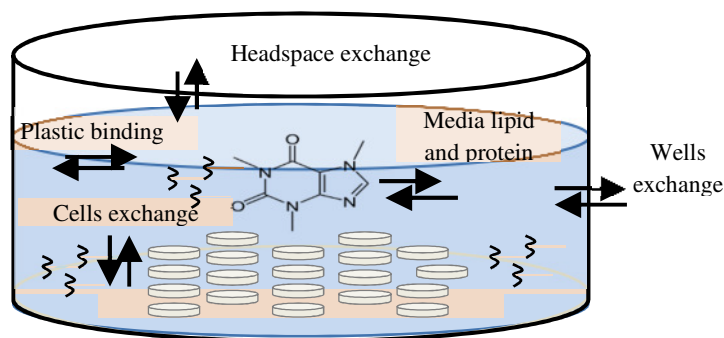


Fig 3.2.8 Overview of the process included in the fate and transport model.

The direct effect of a chemical concentration within a cell (C_b) on its survival is expressed as follows:

$$z_i = \begin{cases} z_i - k_t (C_b - NEC) & \text{if } C_b > NEC \text{ and } t > t_0 \\ z_i & \end{cases} \quad (3.2.59)$$

The link between the PBTk and VCBA models

The PBTk model calculates the internal concentration of a chemical at the organ level in the human body following a specified exposure scenario. The simulated liver concentrations of the chemical in time are assumed to be a concentration outside the hepatic cells (HepaRG). Using mass balance equations, the concentration of the chemical inside the cells is calculated from (part of) the VCBA model (Zaldivar et al., 2012). The cell model consists of 3 compartments (lipid, protein and aqueous). The interchange of the chemical through the cell membrane occurs via diffusion and then the chemical is distributed into the 3 compartments of the cell by its partitioning. In the present work the chemical was assumed to be taken up by passive diffusion. However it is important to highlight that the cell membrane also allows other mechanisms of uptake, such as receptor mediated transport. When the chemical enters into the cell a toxicokinetic process occurs which is governed by two parameters: No- Effect Concentration (NEC) and killing rate (k_t) (**Figure 3.2.9**). These parameters are calculated and optimised to predicted cell viability via the VCBA model using the *in vitro* experimental results.

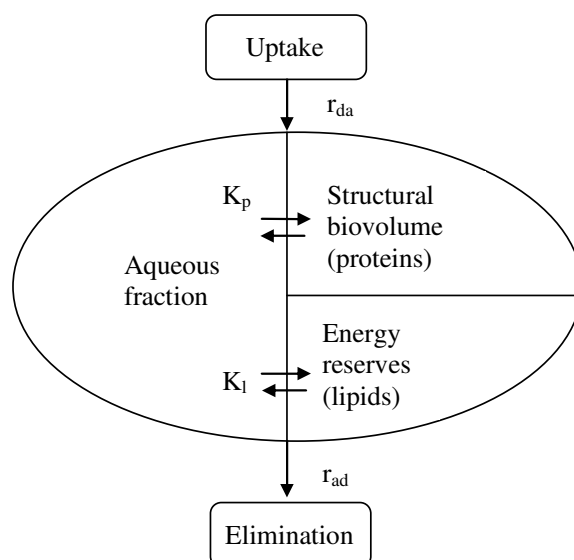


Fig 3.2.9. Representation of the cell partitioning model. Once a chemical is up taken in the cell it partitions between 3 compartments and is then eliminated (by excretion from the cell).

The total number of moles of a compound in the cell is the sum of them in the different compartments:

$$n_{tot} = n_{aq} + n_p + n_L = (V_{aq} \cdot C_{aq} + V_p \cdot C_p + V_L \cdot C_L) \quad (3.2.60)$$

Where: the V_i^s refer to the compartment volumes and the C_i^s refer to the compartments concentration [mol.L⁻¹]. Also the total number of moles of a chemical can be expressed as:

$$n_{tot} = W \cdot C_b / MW \quad (3.2.61)$$

where W is the cell weight [g], MW is the molecular weight of the chemical [g mol⁻¹] and C_b is the chemical concentration in the cell [g/g_{cell}]. The chemical is assumed to be in equilibrium between the different compartments with fixed value partition coefficients: $K_p = C_p / C_{aq}$ and $K_L = C_L / C_{aq}$.

The time evolution of this substance in the cell can be calculated by a simple mass balance, assuming that the uptake and elimination rates r_{ad} and r_{da} [L/m²/h⁻¹] are proportional to the surface area of the cell (passive diffusion) and the transfer occurs through the aqueous compartment only as:

$$\frac{dn_{tot}}{dt} = V^{2/3} \cdot k' \cdot (r_{da} \cdot C_{diss} - r_{ad} \cdot C_{aq}) \quad (3.2.62)$$

where C_{diss} and C_{aq} refer to the chemical concentration (mol.L⁻¹) ($C_{diss} = C_{liv} / MW / 1000$) outside of the cell (given by the PBTK model) and in the aqueous compartment of the cell [mol.L⁻¹], respectively; k' and V are constant and the volume of the cell as defined in (Zaldívar et al., 2011, 2010). Applying the product rule of derivation to **Equation 3.2.61** we get:

$$\frac{dn_{tot}}{dt} = \frac{1}{MW} \cdot \left(W \frac{dC_b}{dt} + C_b \frac{dW}{dt} \right) \quad (3.2.63)$$

by rearranging the terms we obtain:

$$\frac{dC_b}{dt} = \frac{MW \cdot V^{2/3}}{W} \cdot (r_{da} \cdot C_{diss} - r_{ad} \cdot C_{aq}) - \frac{C_b}{W} \cdot \frac{dW}{dt} \quad (3.2.64)$$

the latest term represents the dilution due to growth of the cell, which in the case of HepaRG can be neglected (HepaRG do not proliferate).

Since the concentration in the aqueous fraction C_{aq} is not a value that is measured, then we have to convert in terms of C_b using the partitioning approach. The cell wet weight, W , can also be expressed as a function of the volumes of the different compartments:

$$W = \rho \cdot V = \rho \cdot (V_{aq} + V_P + V_L) \quad (3.2.65)$$

On the other hand:

$$V_P = W_P / \rho_P ; V_L = W_L / \rho_L ; V_{aq} = W_{aq} / \rho_{aq} \quad (3.2.66)$$

where W_P , W_L and W_{aq} are the masses of proteins, lipids and aqueous compartments in the cells and ρ_P , ρ_L and ρ_{aq} their densities.

To find the correlation between C_{aq} and C_b we have to combine n_{tot} in **Equations 3.2.60-61**, the partition coefficients and **Equation 3.2.66**, then we have:

$$C_{aq} = \frac{C_b}{MW \cdot \left(\frac{f_{aq}}{\rho_{aq}} + \frac{f_L}{\rho_L} K_L + \frac{f_P}{\rho_P} K_P \right)} \quad (3.2.67)$$

where f_i refer to the mass fraction of each compartment (aqueous, lipid, proteins) in the cell. Replacing this equation into **Equation 3.2.63** and rearranging we obtain:

$$\frac{dC_b}{dt} = \left(\frac{MW \cdot V^{2/3}}{W} r_{da} \right) C_{diss} - \left[\frac{V^{2/3}}{W \left(\frac{f_{aq}}{\rho_{aq}} + \frac{f_L}{\rho_L} K_L + \frac{f_P}{\rho_P} K_P \right)} r_{ad} \right] C_b - \left(\frac{1}{W} \frac{dW}{dt} \right) C_b \quad (3.2.68)$$

The last term can be neglected in the case of HepaRG cells. The **Equation 3.2.68** gives the concentration inside of the cell from outside concentration, chemical concentration in the liver obtained from the PBTK model.

The direct effects of a chemical concentration, C , on survival may be expressed by:

$$\frac{dn}{dt} = -kt \cdot (C_b - NEC) \cdot n \quad (3.2.69)$$

where n is the number of cells, kt is the killing rate and NEC is the No Effect Concentration. C_b is the same term in **Equation 3.2.68**. The **Equation 3.2.69** is appropriate in the case of HepaRG cells since the cell cycle has only one step. In this way the joint PBTK-VCBA modelling (PBTK model: liver compartment + VCBA: **Equations: 3.2.68-69**) can predict, in the long run, the liver cell viability –dose relationship.

3.3 Sensitivity Analysis and optimisation

To perform sensitivity analysis and optimisation, the FME R package¹⁸ was used. This contains functions for model calibration, sensitivity and identifiability of parameters, Monte Carlo analysis of nonlinear models and a Markov-chain based method to estimate parameter confidence intervals. The package co-works with the deSolve R package¹⁹ that contains functions for solving initial value problems of systems of first-order ordinary differential equations (ODE), partial differential equations (PDE), differential algebraic equations (DAE), and delay differential equations. The package offers routines designed for solving ODEs resulting from 1-D, 2-D and 3-D partial differential equations (PDE) that have been converted to ODEs by numerical differencing.

Three main problems are considered: i) identifying the most sensitive parameters with respect to model output; ii) finding the best fit of a parameter with respect to observed data; iii) showing that the parameters are identifiable.

Model calibration is necessary to determine missing parameters or improve their values in order to improve the model fit to experimental data. As the model equations are generally nonlinear, parameter estimation constitutes a non-linear optimisation problem, where the objective is to find parameter values that minimise a measure of badness of fit, usually a least squares function, or a weighted sum of squared residuals.

Identifiability analysis deals with the problem of uniqueness of the parameter values after fitting a model to a set of observations. A model is said to be “identifiable” if it is theoretically possible to determine the true value of the model’s underlying parameter after obtaining an infinite number of observations from it. If the model is not qualitatively identifiable, then several or infinitely many parameter sets generate identical predictions of the observed quantities (Vajda et al., 1989).

In addition, it is also important to provide an estimate of the parameter uncertainty, and to quantify the effects of that uncertainty on other, unobserved, variables. The latter is necessary to evaluate the robustness of model-based predictions in the light of uncertain parameters.

¹⁸ <http://cran.r-project.org/web/packages/FME/index.html> (last access: 06.10.2014)

¹⁹ <http://cran.r-project.org/web/packages/deSolve/index.html> (last access: 06.10.2014)

a) Global Sensitivity Analysis

The aim of global sensitivity analysis is to determine the effect of a set of specified parameters with their pre-defined ranges on a defined output variable. The parameter values are drawn according to a predefined distribution, the model is re-run with each of possible parameter combinations calculating the values of the selected output variables at each output interval. In this way we can indicate which state variable in the systems is most prone to changes when modifying parameter values in a pre-defined range and how big this change is. We can consider all state variables (organ concentrations) and all the parameters in a vector required for the model simulations.

```
sensRange (func, parms = NULL, sensvar = NULL, dist = "unif",  
           parInput = NULL, parRange = NULL, parMean = NULL,  
           parCovar = NULL, map = 1, num = 100, ...) 20
```

The function includes the following parameters:

- func: function that includes the model structure and a call for integration in time
- parms: vector of parameters
- dist: the distribution according to which the parameters should be generated, one of "unif" (uniformly random samples), "norm", (normally distributed random samples), "latin" (latin hypercube distribution), "grid" (parameters arranged on a grid). if "norm" is chosen, the mean value of each parameter "parMean" and the parameter's variance-covariance matrix "parCovar" must be specified. In this study, the used latin hypercube distribution (stratified random sampling without replacement) was used.
- sensvar: the output variables for which the sensitivity needs to be estimated.
- num: the number of times the model has to be run.
- parRange: the range (min, max) of the sensitivity parameters as a matrix with one row for each parameter, and two columns with the minimum (1st) and maximum (2nd) value. The rownames should be parameter names.
- map: the column number with independent variable, by default = 1.
- parCovar: only when dist is "norm": the parameter's variance-covariance matrix.

Summary of the function gives out a data frame with mean, sd, min, max and quantiles for sensitive variable at each time point. The sensRange method only represents the distribution of the model response variables as a function of the parameter values.

²⁰ <http://127.0.0.1:17422/library/FME/html/sensRange.html> (last access: 06.10.2014)

b) Local Sensitivity Analysis

The aim of local sensitivity analysis is to find out which parameters affect the changes of a given state variable at most (univariate sensitivity). We normally study one or two state variables (like blood and liver concentrations) and a set of parameters.

In local sensitivity analysis all parameters are evaluated individually in a very small region close to their nominal value (Brun et al., 2001; Omlin et al., 2001a, 2001b; Soetaert and Petzoldt, 2010; Soetaert, 2010).

```
sensFun (func, parms, sensvar = NULL, senspar = names(parms),
        varscale = NULL, parscale = NULL, tiny = 1·10-8, map = 1, ...)21
```

The function includes the following parameters:

- func: function that includes the model structure and a call for integration in time
- parms: vector of parameters
- sensvar: the output variables for which the sensitivity needs to be estimated.
- parscale: vector with the scaling (weighing) factors for sensitivity parameters, NULL indicates that the parameter value is used. I used a parameter value divided by the average of simulated outputs was used as a scaling factor (SF).
- tiny: the perturbation, or numerical difference: The sensitivity functions are estimated numerically therefore each parameter value θ_j is perturbed as $\max(\text{tiny}, \theta_j) \cdot (1 + \text{tiny})$ where $\text{tiny} = 1 \cdot 10^{-8}$.

The function outputs a data frame with the following columns: time points, local variable name, sensitivities of all the parameters. The summary function provides a table with parameter names in rows and columns containing: parameter value, scaling factor, L1, L2, Mean, Min, Max of the sensitivity functions, N and output variable name.

$$\dot{x} = f(x, u, \theta) \quad y = g(x, \theta) \quad S_{ij} = \left(\frac{\theta_{j0}}{SF} \right) \frac{\partial y_i}{\partial \theta_j} \Big|_{\theta = \theta_0} \quad (3.3.1)$$

$$L1 = \frac{\sum |S_{ij}|}{N} \quad L2 = \sqrt{\frac{\sum (S_{ij}^2)}{N}} \quad (3.3.2)$$

Where:

y- vector of function outputs for a specific variable (organ/serum concentration)

x- vector of state variables (considered organs/serum concentrations)

θ - vector of parameters (θ_0 - parameter estimate)

u- vector of inputs (initial conditions)

²¹ <http://127.0.0.1:24190/library/FME/html/sensFun.html> (last access: 06.10.2014)

N- number of time points (with a time step of 0.1)

The sensitivity of the model output to the parameter values in a set of so-called sensitivity functions is estimated. When applied in conjunction with observed data, for each data point, the derivative of the corresponding modelled value with respect to the selected parameters is calculated. The higher the absolute sensitivity value, the more important is the parameter. The normalised, dimensionless sensitivities of model output to parameters are in a sensitivity matrix whose ij-th element S_{ij} is given by **Equation 3.3.1**.

The two summary values (L1 and L2) showed in **Equation 3.3.2** are used as selection criteria to rank the most sensitive parameters. Afterwards, the highly ranked ones are checked for parameter identifiability with respect to the same experimental data using a collinearity value (**Equation 3.3.3**).

$$\gamma = \frac{1}{\sqrt{\min \left(EV \left[\hat{S}^T \cdot \hat{S} \right] \right)}} \quad (3.3.3)$$

\hat{S} – refers to inputs of equation 3.3.1

EV- estimates the eigenvalue

As a rule of thumb, a collinearity value (γ) less than about 20 means "identifiable" (in general, when the collinearity index exceeds 20, the linear dependence is assumed to be critical. The procedure is explained in (Brun et al., 2001; Omlin et al., 2001a)). The collinearity is a measure of approximate linear dependence between sets of parameters. The higher its value, the more the parameters are related. In this context, "related" means that several parameter combinations may produce similar values of the output variables.

`collin (sensfun, parset = NULL, N = NULL, which = NULL)`²²

- sensFun: model sensitivity functions as estimated by SensFun
- parset: selected parameter combination (a vector of parameters names) or if NULL or combinations are considered unless specified by N.
- N: the number of parameters in the set; if NULL then all combinations will be tried. Ignored if parset is not NULL. I tried all the combinations of investigated parameters.

c) Fitting the model to experimental data

The selected sensitive parameters in this thesis were optimised according to the Levenberg-Marquardt algorithm for nonlinear data fitting (Moré, 1978). Experimental data are saved in a matrix with a first column

²² <http://127.0.0.1:24190/library/FME/html/collin.html> (last access: 06.10.2014)

with time points and a second column with measured endpoint values having a name that is equivalent to the name of the variable it refers to in the simulated output of the model.

An objective function is required that returns a model cost: for a given a solution of a model and set of observed data, the function estimates the residuals, the variable, and the model cost (sum of squared residuals).

```
modCost (model, obs, x = "time", y = NULL, err = NULL,
weight = "none", scaleVar = FALSE, cost = NULL, ...) 23
```

- model: the model integrated in time output as a data frame
- obs : the observed data in matrix format
- x,y: the names of the independent and dependent variables
- err: the name of the column with the *error* estimates, used to weigh the residuals.
- weight: only if err=NULL: how to weigh the residuals, one of "none", "std", "mean".
- cost: if not NULL, the output of a previous call to modCost; in this case, the new output will combine both

The model cost is calculated according to:

$$ModelCost = \sum_{n=1}^{n=N} \frac{VarCost_n}{Var_SC_n} \quad (3.3.4)$$

Where:

Var_SCn is a variable scaling factor

the *variable costs*, i.e. the sum of squared weight residuals per variable:

$$VarCost_n = \sum_{i=1}^{i=J} (Res_i)^2 \quad (3.3.5)$$

J is the total number of time points and n is a variable number.

The weighted *residuals*, one for each data point:

$$Res_i = \frac{y_i - x_i}{err_i} = (y_i - x_i) \cdot weight_i \quad (3.3.6)$$

Where:

y, x - are simulated and observed data at each time point i.

Grouping it together:

- for the group data

²³ <http://127.0.0.1:24190/library/FME/html/modCost.html> (last access: 06.10.2014)

$$ModelCost = \sum_{n=1}^{n=N} \sum_{i=1}^{i=J} \left(\left(y_{n,i} - \frac{1}{M} \sum_{m=1}^{m=M} x_{n,i,m} \right) \cdot weight_i \right)^2 \quad (3.3.7)$$

Where M is a number of subjects in a group

- for the individual data

$$ModelCost = \sum_{n=1}^{n=N} \sum_{i=1}^{i=J} \left((y_{n,i} - x_{n,i}) \cdot weight_i \right)^2 \quad (3.3.8)$$

Model cost is further directed to the modFit function that locates the minimum:

```
modFit (f, p, ..., lower = -Inf, upper = Inf, method = c("Marq", "Port", "Newton",
"Nelder-Mead", "BFGS", "CG", "L-BFGS-B", "SANN",
"Pseudo"), jac = NULL,...)24
```

- f: a function to be minimised, with first argument the vector of parameters over which minimization is to take place. It should return either a vector of *residuals* (of model versus data) or an element of class *modCost* (as returned by a call to modCost).
- p: initial values for the parameters to be optimised over.
- Lower, upper: lower and upper bounds on the parameters; if unbounded set equal to -Inf/ Inf
- method: The method to be used, one of "Marq", "Port", "Newton", "Nelder-Mead", "BFGS", "CG", "L-BFGS-B", "SANN", "Pseudo".
- jac: A function that calculates the Jacobian; it should be called as jac(x, ...) and return the matrix with derivatives of the model residuals as a function of the parameters. Supplying the Jacobian can substantially improve performance; see last example

The output of this function includes the best set of parameters found, the sum of squared residuals, evaluated for the best set of parameters, a symmetric matrix giving an estimate of the Hessian at the solution found, the result of the last f evaluation; that is, the residuals, etc..

d) Monte Carlo analysis of nonlinear models

Finally, Monte Carlo simulations were used to confirm the choice of the most sensitive parameters. These simulations quantify the impact of variability and uncertainty in parameters distributions separately by drawing parameter values according to some predefined distribution (normally distributed random samples), running the model with each of these parameter combinations, and calculating the values of the selected output variables at each output interval.

²⁴ <http://127.0.0.1:24190/library/FME/html/modFit.html> (last access: 06.10.2014)

```

modCRL (func, parms = NULL, sensvar = NULL, dist = "unif",
        parRange = NULL, parMean = NULL, parCovar = NULL,
        num = 100, ...) 25

```

The function includes the parameters:

- func: an R-function that has as first argument parms and that returns a vector with variables whose sensitivity should be estimated
- parms: parameters passed to func; should be either a vector, or a list with named elements.
- sensvar: the output variables for which the sensitivity needs to be estimated. Either NULL, the default=all output variables, or a vector with output variable names (which should be present in the vector returned by func), or a vector with indices to output variables as present in the output vector returned by func.
- dist: the distribution according to which the parameters should be generated, one of "unif" (uniformly random samples), "norm", (normally distributed random samples), "latin" (latin hypercube distribution), "grid" (parameters arranged on a grid).
- parRange: the range (min, max) of the sensitivity parameters, a matrix or (preferred) a data.frame with one row for each parameter, and two columns with the minimum (1st) and maximum (2nd) value. The rownames of parRange should be parameter names that are known in argument parms.
- parMean: only when dist is "norm": the mean value of each parameter.
- parCovar: only when dist is "norm": the parameter's variance-covariance matrix
- num: the number of times the model has to be run.

In this work the effect of parameters variability within a provided range on maximum concentration of an investigated compound or AUC in the liver and blood or were investigated.

3.4 Quantitative structure-property relationships (QSPRs)

3.4.1 QSPRs for skin permeation

Most QSPRs for skin penetration available in literature are based on *in vitro* experiments in which the substance in an aqueous solvent or phosphate buffer was applied on the skin (applicability domain: $18 < MW < 750$, $-2.3 < \log P_{\text{oct}} < 5.5$). These QSPR equations include: 20 QSPRs for the overall skin permeability coefficient (K_p), 9 for the *stratum corneum* permeability coefficient, 5 for the viable epidermis permeability

²⁵ <http://127.0.0.1:24190/library/FME/html/modCRL.html> (last access: 06.10.2014)

coefficient ($K_{p_{VE}}$), 10 for the *stratum corneum*/water partition coefficient (PC_{SC}), 6 for the *stratum corneum*/viable epidermis partition coefficient ($PC_{SC_{VE}}$) and 7 for the maximal flux through the skin (J_{max}). Optimal properties of substances to be well-predicted by QSPRs are: $MW < 500$, $1 < \log P_{oct} < 3$ and water sol. > 0.1 mg/mL. Prediction performance of all the equations is evaluated with respect to available experimental data of investigated substances. The criterion for selecting the QSPRs from literature based on easily implementable descriptors such as physicochemical properties.

The list of all QSPR equations studied is presented in **Tables 3.4.1-3.4.6**.

Table 3.4.1. QSPR models for overall skin permeability coefficient - K_p

No.	Unit	Model	Reference
1	cm h ⁻¹	If $150 > MW$ & $\log P_{oct} < 0.5$ $\log K_p = -3$ If $150 > MW$ & $\log P_{oct} > 3$ $\log K_p = -0.5$ If $150 > MW$ & $\log P_{oct} \leq 3$ & $\log P_{oct} \geq 0.5$ $\log K_p = \log P_{oct} - 3.5$ If $150 > MW$ & $\log P_{oct} < 0.5$ $\log K_p = -5$ If $150 < MW$ & $\log P_{oct} > 3.5$ $\log K_p = -1.5$ If $150 < MW$ & $\log P_{oct} \leq 3.5$ & $\log P_{oct} \geq 0.5$ $\log K_p = \log P_{oct} - 5.5$	(Geinoz et al., 2004)
2	cm s ⁻¹	$\log K_p = 0.72 \cdot \log P_{oct} - 0.0059 \cdot MW - 6.36$	(Geinoz et al., 2004), (Potts and Guy, 1992)
3	cm s ⁻¹	$\log K_p = 0.8 \cdot \log P_{oct} + 0.0108 \cdot MW - 5.91$	(Geinoz et al., 2004)
4	cm s ⁻¹	$\log K_p = 0.93 \cdot \log P_{oct} + 0.013 \cdot MW - 5.67$	(Geinoz et al., 2004)
5	cm s ⁻¹	If $-1.38 \leq \log P_{oct} \leq 1.96$ $\log K_p = 0.79 \cdot \log P_{oct} - 0.0371 \cdot MR - 5.82$ If $1.53 \leq \log P_{oct} \leq 2.97$ $\log K_p = 1.05 \cdot \log P_{oct} - 0.0259 \cdot MR - 6.8$ If $2.5 \leq \log P_{oct} \leq 5.49$ $\log K_p = 0.95 \cdot \log P_{oct} - 0.037 \cdot MR - 0.107 \cdot HBA - 6.48$	(Geinoz et al., 2004; Magee, 1998)
6	cm s ⁻¹	$\log K_p = 0.773 \cdot \log P_{oct} - 0.0103 \cdot MW - 5.89$	(Geinoz et al., 2004), (Cronin et al., 1999)
7	cm h ⁻¹	$\log K_p = -1.36 \cdot (3.54 \cdot HBD - 0.37) - 3.39$	(Geinoz et al., 2004), (Tayar et al., 1991)
8	cm h ⁻¹	$\log K_p = -0.07 \cdot (\log P_{oct})^2 + 0.84 \cdot \log P_{oct} - 0.27 \cdot Hb - 1.84 \cdot \log MW + 0.8337$	(G Lian et al., 2008), (Lien and Gao, 1995)
9	cm s ⁻¹	$\log K_p = -2.47 - 0.191 - 5.67 \cdot Hb - 0.0853 \cdot cb$	(Pugh et al., 2000)
10	cm s ⁻¹	$\log K_p = 0.820 \cdot \log P_{oct} - 0.0093 \cdot MV - 5.91 - 0.004 \cdot Mpt$	(Geinoz et al., 2004), (Barratt, 1995)
11	cm s ⁻¹	$\log K_p = 0.830 \cdot \log P_{oct} - 0.0119 \cdot MV - 5.87$	(Geinoz et al., 2004)
12	cm h ⁻¹	$\log K_p = 0.688 \cdot \log P_{oct} + 0.181 \cdot \sqrt{MW} - 1.526$	(Wilschut et al., 1995), (Frasch, 2002), (Pugh et al., 1996)
13	cm h ⁻¹	$K_p = \frac{K_{lip}}{1 + K_{lip} \cdot \frac{\sqrt{MW}}{2.6}}$ $\log K_{lip} = -2.32 + 0.574 \cdot \log P_{oct} - 0.005 \cdot MW$	(Frasch, 2002), (Cleek and Bunge, 1993)
14	cm h ⁻¹	$K_p = MW^{-2.404} \cdot \left[-5 \cdot 10^{-6} + \frac{0.0025}{-0.089 + 0.393 \cdot \sqrt{P_{oct}}} \right]$	(Frasch, 2002), (McKone and Howd, 1992)

15	cm h ⁻¹	$K_p = \left[\frac{1}{K_{lip} + K_{pol}} + \frac{1}{K_{aq}} \right]^{-1}$ $\log K_{lip} = -1.286 + 0.620 \cdot \log P_{oct} - 0.159 \cdot \sqrt{MW}$ $K_{pol} = \frac{1 \cdot 10^{-10}}{\sqrt{MW}} K_{aq} = \frac{2.5}{\sqrt{MW}}$	(Frasch, 2002), (Wilschut et al., 1995)
16	cm h ⁻¹	$\log K_p = 0.74 \cdot \log P_{oct} - 0.0091 \cdot MW - 2.39$	(Moss and Cronin, 2002)
17	cm h ⁻¹	$(18 \leq MW \leq 584.6 \ \& \ -3.70 \leq \log P_{oct} \leq 5.49)$ $K_{pSC-intercellular} = 10^{-2.59 + 7.318 \cdot 10^{-1} \cdot \log P_{oct} - 6.832 \cdot 10^{-3} \cdot MW}$ $K_{pSC-transcellular} = \frac{4.3 \cdot 10^{-2}}{MW^{1.361}}$ $K_p = K_{pSC-intercellular} + K_{pSC-transcellular}$	(ten Berge, 2009), (ten Berg, 2014)
18	cm s ⁻¹	$\log K_p = 0.44 \cdot R_2 - 0.49 \cdot \pi_2^H - 1.48 \cdot \sum \alpha_2^H - 3.44 \cdot \sum \beta_2^H + 1.94 \cdot V_x - 5.13$	(Geinoz et al., 2004), (Abraham and Martins, 2004), (G Lian et al., 2008)
19	cm s ⁻¹	$K_p = 5.6 \cdot 10^{-6} P_{oct} 0.7 \exp(-0.46r^2) = 5.6 \cdot 10^{-6} P_{oct} 0.7 \exp\left(-0.1662 MW^{\frac{2}{3}}\right)$	(G Lian et al., 2008), (Mitrageotri, 2002)
20	cm h ⁻¹	$\log K_p = 0.71 \cdot \log P_{oct} - 0.0061 \cdot MW - 2.72$	(Stoick et al., 2007)

Table 3.4.2. QSPR models for permeability coefficient in *stratum corneum* – K_{pSC}

No.	Unit	Model	Reference
1	cm h ⁻¹	$\log K_{pSC} = \log \left(\frac{10^{-0.096 \cdot (\log P_{oct})^2 + 1.027 \cdot \log P_{oct} - 0.201 \cdot \text{HBD} - 2.633 \cdot \log MW + 5.597}}{1000} \right)$	(Pouillot et al., 2008), (Polak et al., 2012), (Lien and Gao, 1995)
2	cm h ⁻¹	$\log K_{pSC} = 0.4814 \cdot \log P_{oct} + 0.1434 \cdot MW^{0.5} - 1.551$	(Pouillot et al., 2008), (Polak et al., 2012)
3	cm h ⁻¹	$\log K_{pSC} = \log \left(\frac{10^{0.372 \cdot \log P_{oct} - 0.351 \cdot \text{HBD} + 1.396}}{1000} \right)$	(Polak et al., 2012), (Lien and Gao, 1995)
4	cm h ⁻¹	$\log K_{pSC} = \log \left(\frac{(10^{0.285 \cdot \log P_{oct} - 0.674 \cdot \text{HBD} - 6.81})}{0.0018} \right)$	(Yamaguchi et al., 2008)
5	cm h ⁻¹	$\log K_{pSC} = 0.006 \cdot MW - 2.8$	(Krüse et al., 2007)
6	cm h ⁻¹	$\log K_{pSC} = -0.004475 \cdot MW + 0.5752 \cdot \log P_{oct} - 2.64368$	(Polak et al., 2012)
7	cm h ⁻¹	$\log K_{pSC} = 0.616 \cdot \log P_{oct} - 0.01014 \cdot MW - 0.812$	(Bogen and Keating, 2000)
8	cm h ⁻¹	<p>If $18 \leq MW \leq 584.6 \ \& \ -3.70 \leq \log P_{oct} \leq 5.49$</p> $K_{pSC-intercellular} = 10^{-2.59 + 7.318 \cdot 10^{-1} \cdot \log P_{oct} - 6.832 \cdot 10^{-3} \cdot MW}$ $K_{pSC-transcellular} = \frac{4.3 \cdot 10^{-2}}{MW^{1.361}}$ $K_{pSC} = K_{pSC-intercellular} + K_{pSC-transcellular}$	(ten Berge, 2009), (ten Berg, 2014)
9	cm h ⁻¹	$\log K_{pSC} = 0.71 \cdot \log P_{oct} - 0.0061 \cdot MW - 2.72$	(Stoick et al., 2007)

Table 3.4.3 QSPR models for partition coefficient: *Stratum corneum*/ viable epidermis- $PC_{SC/VE}$

No.	Model	Reference
1	$PC_{SC/VE} = 1$	(Chinery and Gleason, 1993)
2	$PC_{SC/VE} = \frac{P_{oct}}{5}$	(Polak et al., 2012), (McCarley and Bunge, 2001)
3	$PC_{SC/VE} = 12.6 \cdot P_{oct}^{0.36}$	(McCarley and Bunge, 2001)
4	$PC_{SC/VE} = 0.46 \cdot P_{oct}^{0.48}$	(Tojo, 1987)
5	$PC_{SC/VE} = \frac{(1-f_{SC}) + f_{SC} \cdot P_{oct}}{(1-f_{VE}) + f_{VE} \cdot P_{oct}}$ fsc = 3 - 6%, fve = 2 - 2.5%	(McCarley and Bunge, 2001)
6	$PC_{SC/VE} = (12.36 \cdot P_{oct}^{0.36}) - 1$	(Polak et al., 2012)

Table 3.4.4. QSPR models for partition coefficient *stratum corneum*/ water – PC_{SC}

No.	Model	Reference
1	$\log(PC_{SC}) = 0.74 \cdot \log P_{oct}$	(McCarley and Bunge, 2001), (Polak et al., 2012)
2	$\log(PC_{SC}) = \log(0.7201 \cdot P_{oct}^{0.4298})$	(ten Berge, 2009)
3	$\log(PC_{SC}) = 1.2771 + 0.1208 \cdot P_{oct}$	(McCarley and Bunge, 2001)
4	$\log(1/PC_{SC}) = 0.078 \cdot (\log P_{oct})^2 + 0.868 \cdot \log P_{oct} - 2.04$	(Hui et al., 1995), (Polak et al., 2012)
5	$1/PC_{SC} = 0.43 \cdot P_{oct}^{0.81}$	(Nitsche and Kasting GB, 2007)
6	$PC_{SC} = \phi_{prot} \cdot 7.52 \cdot P_{oct}^{0.31} + \phi_{lip} \cdot 0.9 \cdot P_{oct}^{0.69} + \phi_{water}$ where θ are protein, lipid and water volume fractions in <i>stratum corneum</i>	(Wang et al., 2010)
7	$\log(PC_{SC}) = 0.59 \cdot \log P_{oct} - 0.024$	(Roberts et al., 1995)
8	$\log(PC_{SC}) = 0.514 \cdot \log P_{oct} + 0.104$	(Roberts et al., 1996), (Polak et al., 2012)
9	$\log(PC_{SC}) = 0.418 \cdot \log P_{oct} - 0.439$	(Yamashita and Hashida, 2003), (Polak et al., 2012)
10	$PC_{SC} = 0.95 \cdot P_{oct}^{0.59}$	(Wang et al., 2010)

Table 3.4.5. QSPR models for permeability coefficient viable epidermis- water - K_{pVE}

No.	Unit	Model	Reference
1	cm h ⁻¹	$\log K_{pVE} = \log \left(\frac{(10^{0.0715 \cdot \log P_{oct}^2 + 0.142 \cdot \log P_{oct} - 2.63})}{0.0032} \right)$	(Yamaguchi et al., 2008)
2	cm h ⁻¹	$\log K_{pVE} = \log \left(\frac{2.6}{MW^{0.5}} \right)$	(McCarley and Bunge, 2001)
3	cm h ⁻¹	$\log K_{pVE} = -3.15 + \log P_{oct} - 0.00695 \cdot MW$	(McCarley and Bunge, 2001)
4	cm h ⁻¹	$\log K_{pVE} = -0.006 \cdot MW + 0.74 \cdot \log P_{oct} - 2.8$	(Cleek and Bunge, 1993)
5	cm h ⁻¹	$\log K_{pVE} = \log \left(\frac{0.02556 / MW^{0.5}}{0.0032} \right)$	(Krüse et al., 2007)

Table 3.4.6. List of models to estimate the maximal flux through the skin J_{max}

No.	Unit	Model	Reference
1	$\frac{\text{mol cm}^2}{\text{h}^2}$	$J_{max} = MW \cdot 1000 \cdot 10^{-3.90 - 0.019MW - \log(1 + 10^{1.7 + \log P_{oct} - 0.019MW})} \cdot \sqrt{MW}$	(Magnusson et al., 2004)

2	$\frac{\text{mg cm}^{-2}}{\text{h}^{-1}}$	$J_{\max} = \frac{10^{-2.1+1.7 \log P_{\text{oct}} - 21.6 \log(10^{\log P_{\text{oct}} - 4} + 1)}}{1000}$	(Zhang et al., 2009)
3	$\frac{\text{mg cm}^{-2}}{\text{h}^{-1}}$	$J_{\max} = \frac{\text{AppID} (10^{-0.6 \text{VEH} - 0.0140 \text{MR} - 0.157 \text{HBA} - 0.29 \text{HBD} - 1.40})}{1000}$	(Geinoz et al., 2004), (Hostynek and Magee, 1997)
4	$\frac{\text{mg cm}^{-2}}{\text{h}^{-1}}$	$J_{\max} = \frac{10^{0.147 \log P_{\text{oct}} - 0.0132 \text{MR} - 0.285 \text{HBD} + 0.276 \text{OCCL} + 0.113}}{1000}$	(Hostynek and Magee, 1997)
5	$\frac{\text{mg cm}^{-2}}{\text{h}^{-1}}$	$J_{\max} = \frac{(10^{0.767 \log K_p + 1.23})}{1000}$	(Hostynek and Magee, 1997)
6	$\frac{\text{mg cm}^{-2}}{\text{h}^{-1}}$	$J_{\max} = \frac{(10^{0.458 \log P_{\text{oct}} - 0.0201 \text{MR} - 0.563})}{1000}$	(Hostynek and Magee, 1997)
7	$\frac{\text{mg cm}^{-2}}{\text{h}^{-1}}$	$J_{\max} = \frac{(10^{-0.0218 \text{MR} + 1.13})}{1000}$	(Hostynek and Magee, 1997)

Where:

$\log P_{\text{oct}}$ - octanol-water partition coefficient

MW - molecular weight

MV - molar volume

HBA – number of hydrogen bond acceptors

HBD- number of hydrogen bond donors

Mpt - melting point

Hb - number of hydrogens

cb - the number of carbons not involved in a C= O bond

alpha - H-bond donor acidity

MR - molecular refractivity

VEH – vehicle type

(for acetone VEH=1 and for ethanol VEH=2)

OCCL = 1 open, 2 protected, 3 occluded

AppID = Applied dose [mg/cm^3]

3.4.2 Plasma protein binding

The existing literature QSPR models for plasma protein (f_b - bound fraction to proteins) binding are listed in **Table 3.4.7**

Table 3.4.7. List of QSPRs models to estimate plasma protein binding (f_b)

No.	Unit	Model	Reference
1	-	$f_b = \frac{0.3804 \cdot \exp(\text{LogD}_{\text{pH}8}) + 0.1046}{0.3804 \cdot \exp(\text{logD}_{\text{pH}8}) + 1.1046}$	
2	-	$f_b = \frac{0.5391 \cdot \exp(\text{LogD}_{\text{pH}7.4}) + 0.1074}{0.5391 \cdot \exp(\text{logD}_{\text{pH}7.4}) + 1.1074}$	(Yamazaki and Kanaoka, 2004)
3	-	$f_b = \frac{0.5578 \cdot \exp(\text{LogD}_{\text{pH}7.4}) + 0.0188}{0.5578 \cdot \exp(\text{logD}_{\text{pH}7.4}) + 1.0188}$	
4	-	$f_b = \frac{0.7936 \cdot \exp(\text{LogP}_{\text{oct}}) + 0.2239}{0.7936 \cdot \exp(\text{LogP}_{\text{oct}}) + 1.2239}$	

Where: $\log D$ (water/n-octanol distribution coefficient) at specified pH = $\log ([S]_{\text{ionised, oct}} + [S]_{\text{unionised, oct}}) / ([S]_{\text{ionised, water}} + [S]_{\text{unionised, water}})$; whereas $\log P_{\text{oct}} = \log ([S]_{\text{unionised, oct}}) / ([S]_{\text{unionised, water}})$.

3.4.3 Tissue-to-blood partition coefficients

Schmitt method (Schmitt, 2008) was used to calculate tissue-to-plasma partition coefficients whenever these values could not be taken from the literature. The model calculates steady-state tissue: plasma partition coefficients based on the composition of the tissues in terms of water, neutral lipids, neutral and acidic phospholipids and proteins using the lipophilicity, the binding to phospholipid membranes, the pKa and the unbound fraction in blood plasma as compound specific parameters. The calculations are dependent on the following parameters: molecular weight (MW), pKa, LogP_{oct} and fu (fraction bound to proteins), logMA (membrane affinity), logHSA (Human Serum Albumin) and specifying whether a compound is neutral, acid or base. The general equation is as follows:

$$PC_{org} = \left(\frac{F_{int}}{f_u^{int}} + \frac{F_{cell}}{f_u^{cell}} \right) \cdot f_u^{pl} \quad (3.4.1)$$

Where: F_{int} and F_{cell} are the volume fractions of interstitial and cellular space and f_u^{int} , f_u^{cell} and f_u^p are the unbound fractions in interstitium (surrounding of the cells), cellular space and plasma.

$$\frac{1}{f_u^{pl}} = K_p^{pl} = \frac{1}{F_p^{pl}} \cdot \left(\frac{1}{f_u^{pl}} - F_W^{pl} \right) \quad (3.4.2)$$

$$\frac{1}{f_u^{int}} = K_{int}^{pl} = F_w^{int} + F_p^{int} \cdot K_p^{pl} = F_w^{int} + \frac{F_p^{int}}{F_p^{pl}} \cdot \left(\frac{1}{f_u^{pl}} - F_W^{pl} \right) = \left(0.935 + \frac{0.0252}{0.068} \cdot \left(\frac{1}{f_u^{pl}} - 0.935 \right) \right) \cdot f_u^{pl} \quad (3.4.3)$$

$$\frac{1}{f_u^{cell}} = K_{cell}^{pl} = F_w + K_{n_L} \cdot F_{n_L} + K_{n_PL} \cdot F_{n_PL} + K_{a_PL} \cdot F_{a_PL} + K_p \cdot F_p \quad (3.4.4)$$

Where:

F- volume fractions, n_L neutral lipids, n_PL neutral phospholipids, a_PL acidic phospholipids

With the following:

$$K_{n_PL} = MA \text{ (measured property: PC between phosphatidylcholine and water at pH = 7.4)}$$

$$K_p = 0.163 + 0.0221 \cdot K_{n_PL}$$

If compound is neutral:

$$K_{n_L} = 0.47$$

$$K_{a_PL} = K_{n_PL}$$

If compound is an acid: $K_{n_L} = 0.47$

$$K_{a_PL} = K_{n_PL} + \left[\frac{1}{1 + 10^{pH-pKa}} + 20 \cdot \left(1 - \frac{1}{1 + 10^{pH-pKa}} \right) \right]$$

If compound is a base:

$$K_{n_L} = P_{oct} \cdot \left[\frac{1}{1 + 10^{1-2 \cdot (pH-pKa)}} + 0.001 \cdot \left(1 - \frac{1}{1 + 10^{1-2 \cdot (pH-pKa)}} \right) \right]$$

$$K_{a_PL} = K_{n_PL} + \left[\frac{1}{1 + 10^{pKa-pH}} + 0.05 \cdot \left(1 - \frac{1}{1 + 10^{pKa-pH}} \right) \right]$$

Tissue compositions used in the equations are in **Table 3.4.8**.

Table 3.4.8. Tissue compositions and properties (Schmitt, 2008)

Tissue	pH	F _{cell}	F _{int}	F _w	F _{n,L}	F _{n,PL}	F _{a,PL}	F _p
Adipose	7.1	0.86	0.14	0.03	0.92	5.82·10 ⁻⁰⁶	1.46·10 ⁻⁰⁶	0.058
Bone	7	0.90	0.10	0.26	0.02	0.0003	0.0001	0.211
Brain	7.1	1.00	0.00	0.79	0.04	0.0315	0.008	0.079
Gut	7	0.90	0.10	0.78	0.05	0.006	0.0012	0.147
Heart	7.1	0.86	0.14	0.70	0.05	0.025	0.005	0.185
Kidneys	7.22	0.78	0.22	0.73	0.02	0.029	0.006	0.214
Liver	7.23	0.82	0.18	0.68	0.02	0.0334	0.006	0.212
Lung	6.6	0.50	0.50	0.74	0.02	0.007	0.002	0.108
Muscle	6.81	0.88	0.12	0.76	0.01	0.003	0.0006	0.195
Pankreas	7	-	-	0.00	0.00	0	0	0
Skin	7	0.69	0.31	0.47	0.13	0.0012	0.0004	0.413
Spleen	7	0.79	0.21	0.75	0.01	0.007	0.002	0.229
Stomach	7	-	-	0.00	0.00	0	0	0
Testis	7	0.90	0.10	0.78	0.00	0.029	0.006	0.133
Red Blood Cells	7.2	1.00	-	0.63	0.00	3.66·10 ⁻⁰⁵	8.39·10 ⁻⁰⁵	0.325

3.4.4 Blood-to-air partition coefficient

Short list of available QSPRs equations for calculating blood –to- air partition coefficient (PC_{blood,air}) is provided in **Table 3.4.9**.

Table 3.4.9. List of models to estimate blood/air partition coefficient

No.	Unit	Model	Reference
1	-	$LogPC_{blood,air} = 4.35 - 0.778 \cdot Log(VP)$	
2	-	$LogPC_{blood,air} = 4 - 0.687 \cdot Log(VP)$	(Buist et al., 2012)
3	-	$LogPC_{blood,air} = 6.25 - 0.922 \cdot Log(VP) - 0.586 \cdot LogP_{oct}$	
4	-	$LogPC_{blood,air} = 6.10 - 0.922 \cdot Log(VP) - 0.566 \cdot LogP_{oct}$	
5	-	$LogPC_{blood,air} = 6.96 - 1.04 \cdot Log(VP) - 0.533 \cdot LogP_{oct} - 0.00495 \cdot MW$	
6	-	$LogPC_{blood,air} = 6.65 - 0.982 \cdot Log(VP) - 0.528 \cdot LogP_{oct} - 0.00364 \cdot MW$	

4. Results and Discussion

4.1 Quantitative structure-property relationships (QSPRs)

4.1.1 QSPRs for skin permeation

Table 4.1.1 shows all calculated median QSPR values for the nine case study compounds. Estimated skin permeability coefficients can be compared to the experimental *in vitro* or *in vivo* values provided in brackets. The equation number (eq) with the closest prediction to experimental result is also given. **Figures 4.1.1-4.1.3** present the predictions for overall skin, *stratum corneum* and viable epidermis permeability coefficients with available experimental values marked by a red line.

Table 4.1.1. Median skin permeability coefficients of cosmetics and other chemicals (experimental values are in brackets)

Substance	K _p [cm/h]	K _{pSC} [cm/h]	K _{pVE} [cm/h]	PC _{SC}	PC _{SC/VE}	J _{max} [mg/cm ² /h]	Ref.
Coumarin	0.0023 (<i>in vitro</i> : 0.0091, 0.0125)	0.0032	0.215	4.530	1.828	4.67·10 ⁻³ (<i>in vitro</i> : 1.622·10 ⁻³)	(Ritschel et al., 1989)
Hydroquinone	0.001 (estimated <i>in vivo</i> : 1.49·10 ⁻⁵)	0.003 (<i>in vitro</i> : 9.33·10 ⁻⁶)	0.248	2.118	0.941	1.270·10 ⁻⁴	(Barber et al., 1995; Poet et al., 2010)
Caffeine	0.0001 (<i>in vitro</i> : 2.1-7.2·10 ⁻⁴ ; 19.22·10 ⁻⁶ 29.49·10 ⁻⁶ (<i>in vivo</i> : 1.59·10 ⁻⁴)	3.2·10 ⁻⁴ (<i>in vitro</i> : 0.0016)	0.187 (the closest eq 4: 9.616·10 ⁻⁵) (<i>in vitro</i> : 2.23- 2.58·10 ⁻⁴)	0.876 (<i>in vitro</i> : 5.88, 2.7, 1.79, 0.65, 0.41)	0.6	2.467·10 ⁻⁵ (the closest eq 7: 1.076·10 ⁻³) (<i>in vitro</i> : 1.75·10 ⁻³ , 2.24·10 ⁻³)	(Chambin- Remoussenard et al., 1993, 1982; Dias et al., 1999; Doucet et al., 1998; Treffel et al., 1993; van de Sandt et al., 2004), Cosmetics Europe, (Wilkinson et al., 2006), (Cole and Heard, 2007), (Bronaugh and Franz, 1986),(Southwell et al., 1984), (Kroes et al., 2007)
Ethanol	0.0001 (<i>in vitro</i> : 3.17·10 ⁻⁴ ;	0.006	0.383	0.622 (<i>in vitro</i> :	0.2	1.086·10 ⁻⁴	(Scott et al., 1991); (Wang et al., 2010);

	8.1·10 ⁻⁴ , 9.9·10 ⁻⁴)			0.5-0.74, 0.95)			(Abraham and Martins, 2004); (G Lian et al., 2008)
Isopropanol	0.00153 (<i>in vitro</i> : 0.00119- propanol)	0.008	0.335	1.343 (<i>in vitro</i> : 0.21 propan-1- ol value)	0.778	1.464·10 ⁻⁴	(Abraham and Martins, 2004); (G Lian et al., 2008)
Estragole	0.035975	0.0397	0.2136	4.1624	2.360	1.285·10 ⁻³	-
Nicotine	9.7·10 ⁻⁴ <i>in vitro</i> : 0.0103, 0.0033; 0.0104, 0.0189)	0.002	0.2041	4.649	1.518	7.196·10 ⁻⁴ (the closest eq 1: 1.677·10 ⁻²) (<i>in vitro</i> : 1.13·10 ⁻²)	(Degim et al., 1998; Qvist et al., 2000); (G Lian et al., 2008); (Kroes et al., 2007)
Styrene	0.071	0.039	0.2548	3.5963	2.340	2.085·10 ⁻³	-
Iodomethane	0.004	0.004	0.2182	6.2732	2.028	2.496·10 ⁻³	-

The predicted values were in the following ranges: i) for logK_p: from -8.83 (eq. 8) for caffeine to -3.13 cm/s (eq. 9) for iodomethane; ii) for logK_{pSC}: -5.24 (eq. 4) for hydroquinone to 0.48 cm/h (eq. 2) for caffeine; and iii) for logK_{pVE}: from -4.6 (eq. 3) for caffeine to 0.07 cm/h (eq 5) for ethanol.

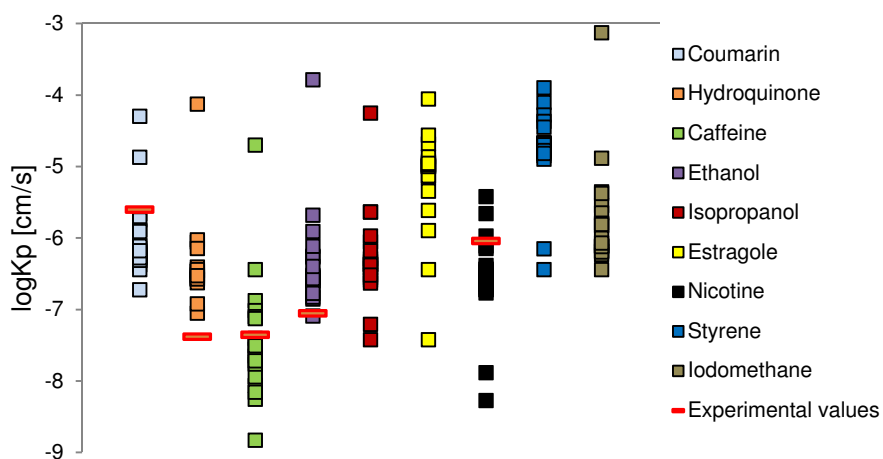


Fig 4.1.1. Skin/water permeability coefficient for nine case study compounds.

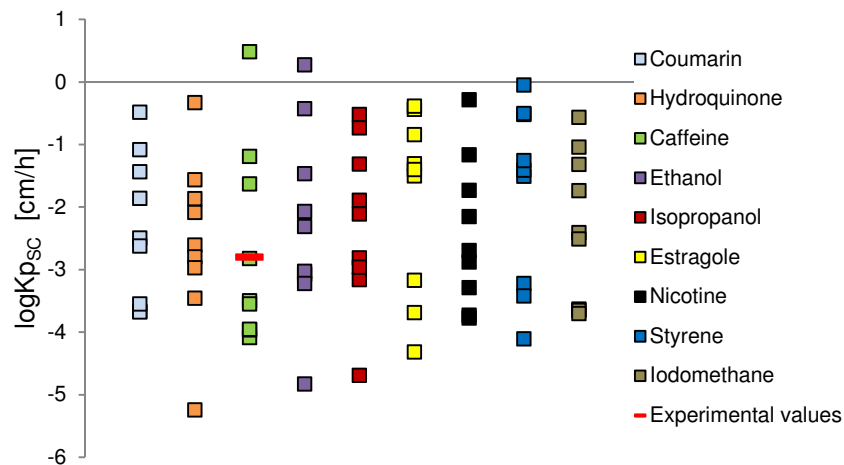


Fig 4.1.2. *Stratum corneum*/water permeability coefficient for selected compounds.

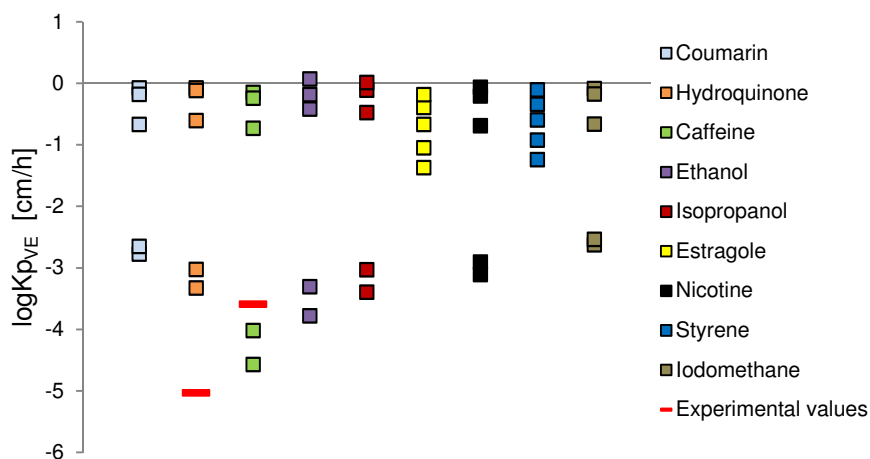


Fig 4.1.3. Viable epidermis/water permeability coefficient for selected compounds.

The estimated partition coefficients between *stratum corneum* and water and between *stratum corneum* and viable epidermis are shown in **Figures 4.1.4-5**. The estimated ranges of the coefficients were as follows: i) for PC_{SC} : from 0.3 (eq 9) for ethanol up to an extreme case of 32 (eq 4) for hydroquinone; ii) for PC_{SCVE} : from 0.03 (eq 7) for coumarin up to 19 (eq 3) for estragole. There was one prediction above 20 for styrene (178 – eq. 2) but I considered this as an outlier and eliminated from the results.

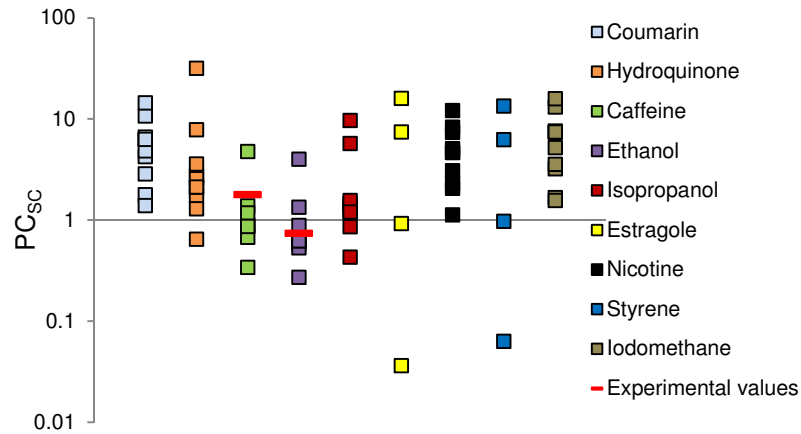


Fig 4.1.4. *Stratum corneum*/water partition coefficient for nine case study compounds.

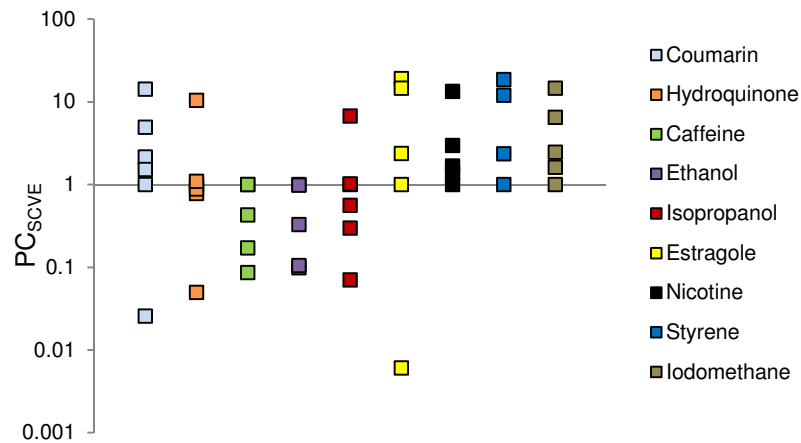


Fig 4.1.5. *Stratum corneum*/viable epidermis coefficient for nine case study compounds.

Figure 4.1.6 shows the calculated maximal flux for the substances with a range from $1.56 \cdot 10^{-7}$ (eq 5) for nicotine to $0.75 \text{ mg/cm}^2/\text{h}$ (eq 1) for ethanol.

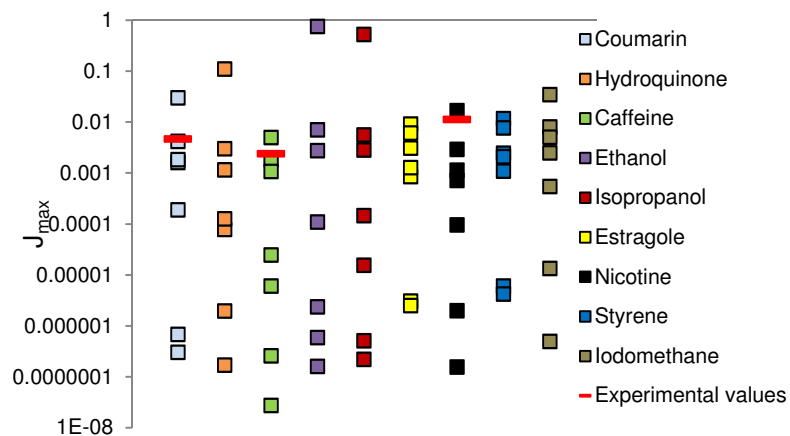


Fig 4.1.6. Maximal flux for nine case study compounds.

4.1.2 Plasma/ protein binding and blood –to-plasma concentration ratio

The experimental and predicted plasma protein binding and blood-to-plasma concentration ratio for all case study compounds are given in **Table 4.1.2**. The ADMET-predicted and PBTK model-optimised results are presented. The available literature QSPR models for plasma protein binding are listed in **Table 3.4.7** but could not be used as they require logD (water/n-octanol distribution coefficient) at specified pH values that were difficult to calculate. Only equation 4 was used giving the following results in terms of bound fractions to plasma: coumarin: 0.77, estragole: 0.95, hydroquinone: 0.62, caffeine: 0.49, ethanol: 0.45, isopropanol: 0.51, styrene: 0.94, MEI: 0.54 and nicotine: 0.74. Out of these predictions only hydroquinone and caffeine were close to the experimental values.

Table 4.1.2. Calculated and experimental plasma partitioning coefficients

Substance	Experimental value: Human blood plasma binding (fb)	Experimental value: Blood-to-plasma concentration ratio	ADMET(1) predictor: Human blood plasma binding (fraction of free drug in human blood plasma- fu)	ADMET(1) predictor: Blood-to-plasma concentration ratio	PBTK model optimised Blood-to-plasma concentration ratio	Literature ref.
Coumarin	< 0.4	-	0.4952	0.99	0.25	(Piller and Schmitt, 1977)
Hydroquinone	0.6	-	0.1616	1.77	0.15	(Corley et al., 2000)
Caffeine	0.35	-	0.5132	1.01	0.28-0.35	(Yamazaki and Kanaoka, 2004)
Ethanol	-	-	1	1.8	1	-
Isopropanol	-	-	1	1.66	1	-
Estragole	-	-	0.3683	0.91	-	-
Nicotine	0.05	-	0.62	1.2	-	(Yamazaki and Kanaoka, 2004)
Styrene	-	-	0.6815	1.22	-	-
Iodomethane	-	-	1	1.77	-	-

(1) ADMET predictor commercial software:

<http://www.simulations-plus.com/Products.aspx?grpID=1&cID=11&pID=13> (last access: 06.10.2014)

4.1.3 Blood-to-air partition coefficient

Blood-to-air partition coefficient predictions together with experimental values (if available) are in **Table 4.1.3** for ethanol, isopropanol, styrene and nicotine. The predicted values were found close to the experimental ones for these compounds.

Table 4.1.3. Experimental versus calculated values are discussed for ethanol, isopropanol and styrene.

Compound	VP [Pa]	Experimental value	QSPR calculated value $PC_{\text{blood,air}}$	Reference
Ethanol	7910	1352.5	1479.108	(Meulenberg and Vijverberg, 2000)
Isopropanol	6050	848	831.7638	(Clewel III et al., 2001)
Styrene	853	48	53.703	(Csanady et al., 1994)
Nicotine	0.038	-	55335.01	-

Discussion

Quantitative structure–property relationships (QSPRs) relate variations in the investigated property of a series of compounds to variations in their physicochemical and/or structural properties. They are widely used as parameter estimates for filling missing experimental data for properties such as skin absorption (Guoping Lian et al., 2008), partitioning between different phases in biological systems (DeJongh et al., 1997; Schmitt, 2008), plasma protein binding (Yamazaki and Kanaoka, 2004), and blood-to-air partition coefficient (Katritzky et al., 2006). QSPRs are useful in predicting behavior of novel compounds and providing insights into mechanisms of activity (Katritzky et al., 2006). They are particularly useful as fast screens in risk assessment processes.

The octanol-water partition coefficient has been shown to be an important parameter for modelling lipophilicity (Flynn, 1990). The log of the octanol-water partition coefficient ($\log P_{\text{oct}}$) is a convenient way of expressing whether a molecule is hydrophilic or lipophilic and appears in most of the QSPR equations. Other parameters include molecular size (molecular weight or volume), aqueous solubility (melting point), volatility (vapour pressure), etc.

In this study I used literature QSPR equations for 9 case study compounds and the calculations were compared with available *in vitro/ in vivo* experimental results. Skin absorption studies are particularly relevant in risk assessments of chemicals that have potential to permeate the skin and cause local or systemic effects. However, existing QSPRs for skin penetration have been limited by the lack of available experimental data. Overall skin and *stratum corneum* permeation coefficients were best estimated by the QSPRs given the fact that the range of predictions was the smallest as compared to the other properties investigated. Estimations were close to experimental values for coumarin, caffeine, ethanol, isopropanol and nicotine. Only hydroquinone predictions were a bit higher than measured values: overall skin permeability and viable epidermis permeability coefficients were 100 times higher than *in vitro* values). This may arise from the fact that the most of the available QSPRs are designed to predict the permeability coefficient, K_p , of a pure organic chemical in an aqueous solvent whereas literature experiments were often performed using vehicles other than water. In the case of hydroquinone, phosphate buffer was used (Barber et al., 1995). Other factors that affect these differences are: concentration of a chemical in solvent, application conditions, and skin type. Higher variations in predictions were observed for partition coefficients, especially for hydroquinone PC_{SC} : 0.64-32 and for estragole and styrene PC_{SCVE} : 0.006-19; whereas smaller variations

were found for ethanol P_{SC} : 0.27- 4 and for caffeine: P_{SCVE} : 0.09-1. The highest, variation in estimated values was found for maximal flux (the highest range for ethanol: $1.59 \cdot 10^{-07}$ - 0.76 and smallest for caffeine: $2.58 \cdot 10^{-07}$ -0.005 mg/cm²/h).

Plasma protein binding is especially important for modelling of toxicodynamic effects of substances (especially drugs). It is the reversible association of a drug with the proteins of the plasma due to hydrophobic and electrostatic interactions such as van der Waals and hydrogen bonding. The bound drug exists in equilibrium with the free drug. This reversible interaction can greatly influence the toxicokinetic properties such as the volume of distribution, clearance and elimination and as a result the toxicodynamic response because only the unbound (f_u) chemical is able to pass across cell membranes (Ghafourian and Amin, 2013). Existing QSPR models were either developed based on linear regression of complex descriptors (e.g. van der Waals surface area or fraction of base ionised at pH 7.4) or non-linear data mining methods. Moreover, the training set was always composed of drugs for which experiments were carried out (Yamazaki and Kanaoka, 2004) therefore other chemicals such as food, cosmetic ingredients or industrial solvents may fall outside the applicability domain. The only simple equation 4 showed a good performance for hydroquinone and caffeine but poor for nicotine when compared to experimental values. For other substances no experimental values were available for verification.

Literature QSPRs for human and rat blood-to- air partition coefficient base on three parameters only (VP, $\log P_{oct}$ and MW) and were concluded robust and reliable models (Katritzky et al., 2006). These equations work well in case of ethanol, isopropanol and styrene giving satisfactory predictions. Absorption of volatile substances (usually inhalation) is a function of the blood solubility of a vapour indicated by the blood-to-air partition coefficient that further affects the circulation of a chemical in the body. The more soluble the substance is in blood compared to in air, the more it binds to plasma proteins in the blood and the higher the blood-to-air partition coefficient.

4.2 Toxicokinetics- modelling refinement of uptake stages in PBTK model

In this section I analyse the difference in using various PBTK model structures in predicting ADME profiles (concentration-time profiles) of selected chemicals in blood or plasma. I emphasise the importance of using sub-compartments in the absorption stage (GI tract, skin and respiratory tract) that help obtain a better match of *in vivo* blood and plasma data, especially the time of peak concentration. This is because of slower simulation of absorption phase and therefore slower distribution of a compound to the liver – the main metabolizing organ. In this way, there is no need to specify a time-lag variable (like in the simplest model with a one-absorption compartment only) that accounts for the delay between the administration of a chemical and its appearance in blood. For this purpose three different PBTK model structures (PBTK1-3) that differ in uptake compartments are introduced (all other compartments, and distribution and elimination parameters are identical for all the model structures).

For oral and dermal absorption I use four case study compounds: coumarin, hydroquinone, caffeine and isopropanol. For inhalation I selected three compounds: styrene, ethanol and isopropanol. The selection was based on the availability of *in vivo* data for the Caucasian population in the literature. In most cases, only single dose administration was carried out, except for caffeine, where repeated oral exposure data were also available in the public literature.

Three statistical criteria, the coefficient of determination (R^2), mean squared error (MSE) and Akaike's Information Criterion (AIC) (Kletting and Glatting, 2009), were used to evaluate the simulation performance of the model in terms of blood/plasma concentrations of the parent compound.

4.2.1 Oral and dermal absorption

The tissue-to-blood partition coefficients for the four substances used in all the model structures are given in **Table 4.2.1**, oral and dermal absorption parameters for the PBTK3 are in **Table 4.2.2** and for the PBTK1-2 in **Table 4.2.3**. These parameters, for the PBTK3, include literature and optimised values. The literature values comprise: stomach emptying rates, some of the absorption rates (diffusion coefficient in *stratum corneum* for caffeine, small intestine absorption rate for hydroquinone, etc.) and tissue-to-blood partition coefficients for hydroquinone and isopropanol. QSPRs were used to calculate median predicted values of diffusion coefficients and partition coefficients between *stratum corneum* and viable epidermis. The following parameters were optimised with respect to available blood/plasma concentrations:

- coumarin: oral data: stomach absorption rate ($k_{a_{\text{stm}}}$), small intestine absorption rate ($k_{a_{\text{SI}}}$), dermal data: diffusion coefficient in *stratum corneum* (D_{SC}), partition coefficient *stratum corneum* /vehicle (PC_{SC}), coumarin intake rate from the formulation ($k_{a_{\text{form}}}$) (see **Chapter 4.3.1**).
- hydroquinone: oral data: stomach ($k_{a_{\text{stm}}}$) and small intestine absorption rates ($k_{a_{\text{SI}}}$); dermal data: diffusion coefficient in *stratum corneum* (D_{SC}), partition coefficient *stratum corneum* /vehicle (PC_{SC}), hydroquinone intake rate from the formulation ($k_{a_{\text{form}}}$).
- caffeine: oral data: dissolution rate from a tablet (Diss), stomach absorption rate ($k_{a_{\text{stm}}}$), small intestine absorption rate ($k_{a_{\text{SI}}}$), ratio between blood and plasma (RBP); dermal data: diffusion coefficient in hair follicles (D_{HF}), intake rate of caffeine by the skin ($k_{a_{\text{form}}}$) and by hair follicles ($k_{a_{\text{HF}}}$). Due to lack of experimental and alternative QSPRs predictions partition coefficient between hair follicles and vehicle was assumed to be equal to 1 (see **Chapter 4.3.1**).

- Isopropanol: oral data: absorption rate from stomach and small intestine; dermal data: diffusion coefficients in *stratum corneum* (D_{SC}) and viable epidermis (D_{VE}) and isopropanol intake rate from the formulation (k_{form}).

Table 4.2.1. Tissue-to-blood partition coefficients used for all the model structures

Parameter	coumarin	hydroquinone	caffeine	isopropanol
Tissue- to- blood partition coefficients				
PC_{liv}	2.38 (1)	0.8(2)	4.25 (1)	1.16 (3)
PC_{ppt}	0.355 (1)	0.8 (2)	0.995 (1)	1.3 (3)
PC_{brn}	2.09 (1)	0.8 (2)	4.79 (opt.1) (1)	1.33 (3)
PC_{skn}	0.68 (1)	0.8 (2)	1.29 (opt.1) (1)	1.3 (3)
PC_{lng}	0.51 (1)	0.68 (2)	1.23 (1)	1.25 (3)
PC_{kid}	2.08 (1)	0.71(2)	3.76 (1)	1.25 (3)
PC_{git}	0.62 (1)	0.67(2)	1.49 (1)	1.25 (3)
PC_{adp}	1.24 (1)	0.8 (2)	0.68 (1)	0.32 (3)
PC_{hrt}	1.63 (1)	0.8 (2)	3.69 (1)	1.25 (3)

(1) calculated according to (Schmitt, 2008); (2) (Corley et al., 2000); (3) (Clewell Iii et al., 2001).

Table 4.2.2 Oral and dermal absorption parameters for PBTK3

Parameter	coumarin	hydroquinone	caffeine	isopropanol
Kinetic parameters				
Diss [1/h]	-	-	3.2	-
Dt [L/h]	-	4 (3)	-	2.88 (8)
				1.26 (9)
ka_{stm} [1/h]	1.8	0.1	0.2	4.7
ka_{st} [1/h]	0.1	3	1.5	10
ka_{LI} [1/h]	0.01 (assumed)	0.01(assumed)	0.01(assumed)	0.01(assumed)
k_{max} [1/h]	8.16 (2)	8.16 (2)	8.16 (2)	8.16 (2)
k_{min} [1/h]	0.005 (2)	0.005 (2)	0.005 (2)	0.005 (2)
kel_{LI} [1/h]	0.06 (6)	0.1 (5)	0.1	0.1
D_{SC} [cm ² /h]	$2.5 \cdot 10^{-06}$	$4 \cdot 10^{-08}$	$1.4 \cdot 10^{-07}$ (4)	$3 \cdot 10^{-07}$
D_{VE} [cm ² /h]	$9 \cdot 10^{-05}$ (1)	$8 \cdot 10^{-06}$ (1)	$1.5 \cdot 10^{-05}$ (1)	$5.20 \cdot 10^{-05}$
D_{HF} [cm ² /h]	-	-	$1.243 \cdot 10^{-05}$	-
ka_{form} [mL/h]	0.22	0.038	0.2	0.12
ka_{HF} [mL/h]	-	-	0.153	-
PC_{SC}	1.65	1	2.5 (9)	1.343 (1)
PC_{SCVE}	1.829 (1)	0.8 (1)	0.6 (1)	0.778 (1)
PC_{HF}	-	-	1	-
RBP	0.25(7)	0.15(8)	0.28 (dermal, assumed)	1 (7)
			0.35	
% of hair follicles in skin (nf)	-	-	20	-

(1) estimated by QSPRs (2) (Loizou and Spendiff, 2004) (3) (Corley et al., 2000)

(4) (Hansen et al., 2008) (5) (OECD SIDS, 1996)

(6) (Ford et al., 2001) (7) predicted by ADMET Predictor (<https://www.simulations-plus.com/>)

(8) (Monaghan et al., 1995); (9) (Lacouture et al., 1989)

Table 4.2.3 Oral and dermal absorption parameters for PBTK1-2

Parameter	coumarin	hydroquinone	caffeine	isopropanol
Kinetic parameters				
ka_{GI} [1/h]	1.5	1.75 (2)	1.8	2.88 (3)
				1.26 (4)
kel_{GI} [1/h]	3.5	-	-	-

t _{lag} [min]	20 (dermal)	20 (2) 30 (oral)	40 (oral)	10 (oral)
k _{a,skn} [mL/h]	2	0.002	0.02	0.8
bioav.	0.6	1	1	1
D _E [cm ² /h]	(<i>in vitro</i>) 5.824·10 ⁻⁰⁵ (5)	6.976·10 ⁻⁰⁶ (1)	(<i>in vivo</i>) 1.018·10 ⁻⁰⁶ (5)	3·10 ⁻⁰⁴
PC _E	10	11	50	1.343
k _{form} [ml/h]	0.9	0.05	0.5	0.4

(1) estimated by QSPRs ; (2) (Corley et al., 2000); (3) (Monaghan et al., 1995); (4) (Lacouture et al., 1989); (5) see Chapter 4.1.1- **Table 4.1.1**

a) Coumarin

- Oral absorption

Coumarin oral exposure data for 4 individuals (0.857 mg/kg BW of coumarin via gavage (Ritschel et al., 1979) were used. Simulated and experimental concentration-time points in blood are shown in **Figure 4.2.1** –left for PBTK1_orl and right for PBTK3_orl. Measured AUC values in blood were compared with simulated values in **Table 4.2.4**.

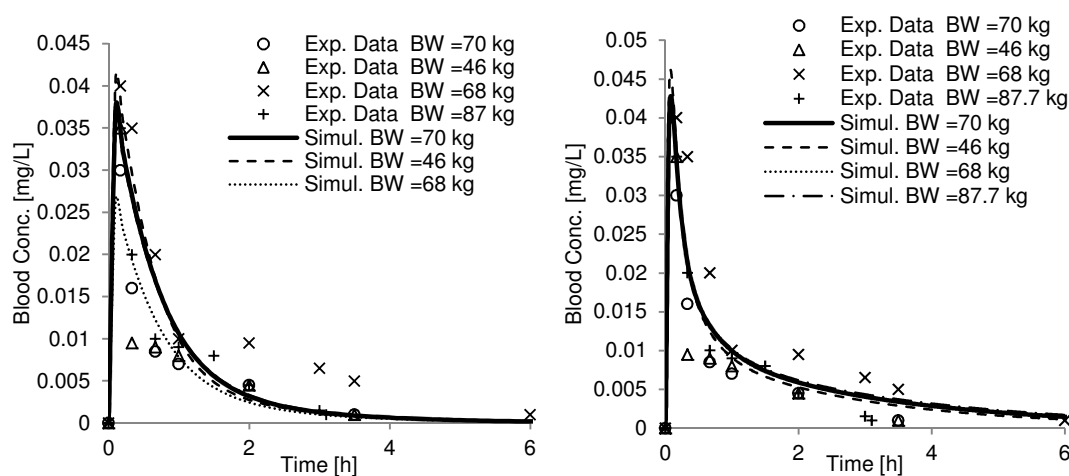


Fig 4.2.1. Simulations of coumarin blood concentrations following oral administration for 4 volunteers (PBTK1_orl –left, PBTK3_orl - right). Experimental data from: (Ritschel et al., 1977)

Table 4.2.4 AUC in blood following oral absorption of coumarin

AUC blood [mg·h/L]	BW= 70 kg	BW= 46 kg	BW= 68 kg	BW= 87.7 kg
PBTK1_orl	0.031	0.0315	0.023	0.031
PBTK3_orl	0.032	0.029	0.025	0.034
(Ritschel et al., 1979)	0.017	0.017	0.042	0.016

Although both model structures appear to be quite satisfactory (see statistics in the discussion section), the PBTK3_orl simulations slightly better represent *in vivo* data in terms of calculated AUC of coumarin in blood when compared to experimental results.

- Dermal absorption

For dermal absorption, the (Ford et al., 2001) experiment carried out on 3 subjects was used. Ca. 0.02 mg/cm² of coumarin in 70% ethanol was applied on 100 cm² back skin area. Simulated and experimental plasma concentrations of coumarin are shown in **Figure 4.2.2** for 3 different model structures.

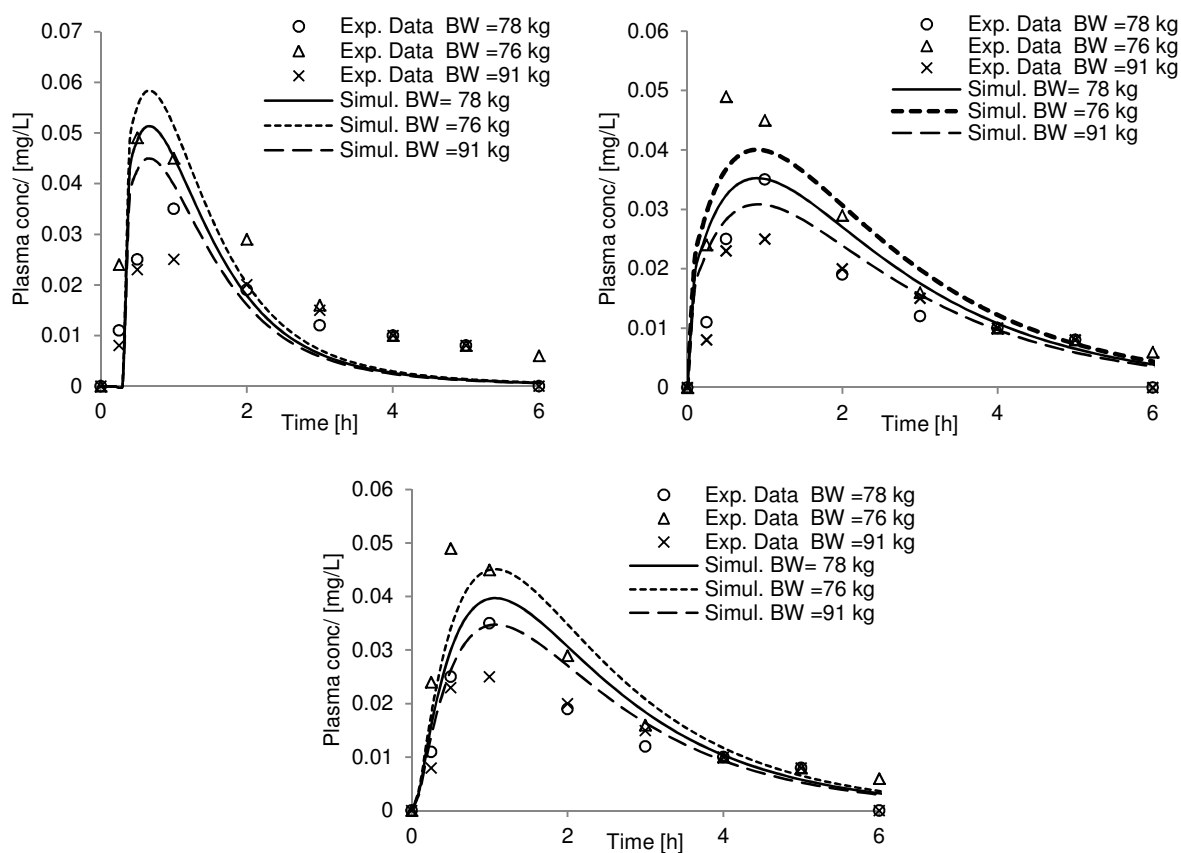


Fig 4.2.2. Simulations of coumarin plasma concentrations following dermal absorption for 3 volunteers (PBTK1_skn – upper left, PBTK2_skn- upper right, PBTK3_skn- bottom). Experimental data from: (Ford et al., 2001).

The first model structure (PBTK1_skn) simulated a rapid absorption after a 20 min- time-lag. This produced a sharp peak concentration and fast elimination as compared to *in vivo* results. PBTK2_skn smoothed the profile showing better representation of experimental data. PBTK3_skn further slowed down the absorption phase to better match the time of peak concentrations. (Ford et al., 2001) reported total percent of coumarin absorbed by the three subjects to be ca. 60% for an ethanol vehicle. I compared these values with simulations

(Table 4.2.5). However, since models do not account for inter-individual differences in skin structure and biology, the same absorption profiles were simulated regardless of body weight and gender characteristics. PBTK3 and PBTK1 gave results closer to experimental ones.

Table 4.2.5. Simulated percentage of dose absorbed

%Abs.	BW= 78 kg	BW= 76 kg	BW= 91 kg
PBTK1_skn		60.00	
PBTK2_skn		80.594	
PBTK3_skn		54.308	
(Ford et al., 2001)	54.5	62.4	67.1

b) Hydroquinone

- Oral absorption

In case of hydroquinone, oral data for only one volunteer were available (Corley et al., 2000) who ingested 275mg of hydroquinone. Blood concentrations of hydroquinone are shown in Figure 4.2.3.

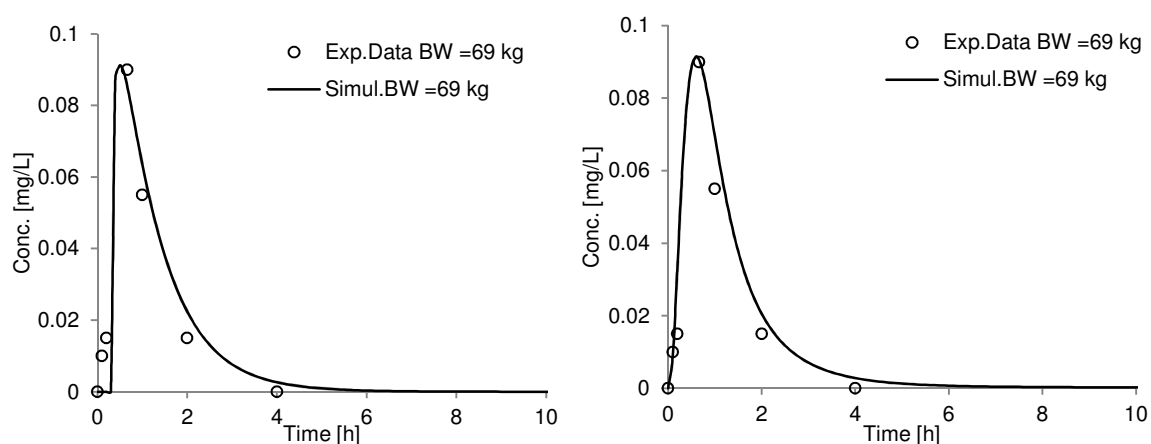


Fig 4.2.3. Simulations of hydroquinone blood concentrations after oral administration for 1 subject (PBTK1_orl –left, PBTK3_orl - right). Experimental data from: (Corley et al., 2000).

For PBTK1_orl I used 20 min of time lag which gave a good match for the elimination phase but data for the absorption phase up to the peak concentrations were not properly predicted. PBTK3_orl compensated for this mismatch giving a better representation of both absorption and elimination phases. The AUC in blood was calculated to be 0.114 mg.h/L by PBTK1_orl and slightly higher 0.128 mg/L/h by PBTK3_orl. However, no experimental value was provided for comparison.

- Dermal absorption

A dermal absorption experiment carried out on 4 human volunteers with mean plasma concentrations was published (Wester et al., 1998). All the simulations were done for an "average" male BW= 69 kg, which matches the majority of participants in the study (**Figure 4.2.4**).

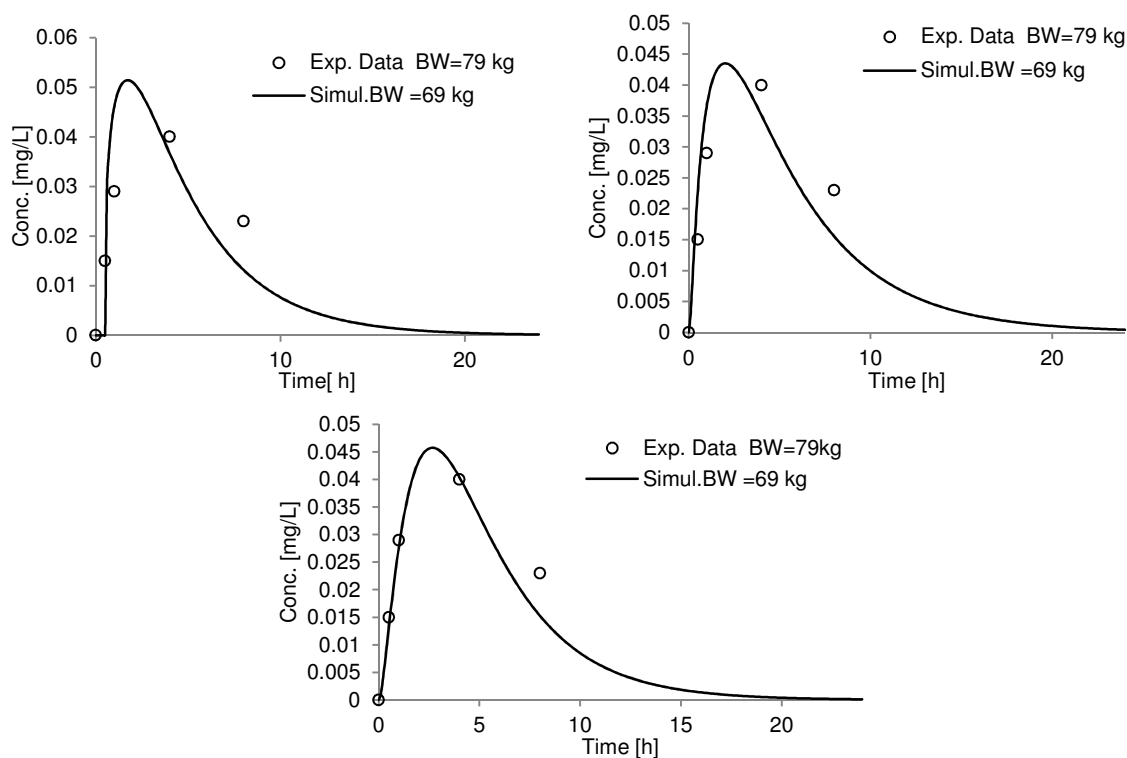


Fig 4.2.4. Simulations of plasma concentrations of hydroquinone following dermal absorption for the "mean" volunteer (PBTK1_skn – upper left, PBTK2_skn- upper right, PBTK3_skn- bottom). Experimental data from: (Wester et al., 1998).

PBTK2_skn and PBTK3_skn accounted for skin metabolism (with rates $V_{max}=0.05$ mg/h, $K_m=4$ mg/L). The metabolism rates were calculated to account for no more than 1% of administered dose. I assumed this value based on (Poet et al., 2010) who indicated that the major enzymes associated with hydroquinone metabolism are present in the skin with activities ranging from 1-25% of the activity in the liver. This metabolism is neglected in PBTK1_skn. Based on **Figure 4.6** it can be seen that all the models simulated quite good results, with PBTK3_skn only slightly better. (Wester et al., 1998) reported total percentage of hydroquinone absorbed and flux through the skin (**Table 4.2.6**). All the models overestimated total absorption and in terms of median flux results, PBTK2_skn and PBTK3_skn were closer to measurements.

Table 4.2.6. Simulated percentage of dose absorbed and flux

Av. man (BW= 69 kg)	%Abs.	Flux [$\text{mg}/\text{cm}^2/\text{h}$]
PBTK1_skn	100	0.0268 (max) 0.001 (median)

PBTK2_skn	85.51	0.016 (max) 0.0013 (median)
PBTK3_skn	82.34	0.0153 (max.) 0.0009 (median) $1 \cdot 10^{-03}$ (forearm)
(Wester et al., 1998)	45.3 (forehead)	Bioav. = 0.08 $1.9 \cdot 10^{-03}$ (forehead) Bioav. = 0.4530

For comparison, the percentage of dose absorbed *in vitro* in the receptor fluid was reported to be 34%; the *in vitro* flux was $2.8 \cdot 10^{-03}$ mg/cm²/h because the dose per cm² was double the *in vivo* dose (Wester et al., 1998).

c) Caffeine

- Oral absorption

As there are many experimental data available in the literature for single oral absorption of caffeine (either pure caffeine or its mixture), several studies were used here for comparison purposes. The PBTK model performance was checked for pure caffeine and its mixture. In most of the oral studies pure caffeine was ingested in the form of a gelatin capsule followed by water. Four different studies were used. In the first experiment (Lelo et al., 1986) mean plasma concentrations were provided for 6 male volunteers, therefore, as before a "mean" male candidate was constructed weighing 83 kg (based on the majority of weights) - **Figure 4.2.5**. The free mean fraction of caffeine in plasma was reported to be 0.68. In the second study (Newton et al., 1981), again a caffeine capsule was used (6 male/female volunteers – mean plasma concentration published) – **Figure 4.2.6**. In the third study (Csajka et al., 2005), in addition to a gelatin capsule, caffeine was applied in a mixture – as a commercial dietary supplement (herbal formulation). Plasma concentration results were provided for all the participating volunteers but I chose their mean values for the analysis (in the first part of the study, 8 subjects received a single oral dose -2 capsules of a commercial dietary supplement - Metabolift - labelled to contain 200 mg caffeine and in the second part, a single oral dose of 200 mg of caffeine sulphate was administered to 16 subjects) - **Figure 4.2.7**. Finally, in the fourth study (Acheson et al., 1980) a caffeine capsule was given in a much higher dose, which challenges the applicability of the model absorption parameters calibrated for doses two times lower (experiment carried out for 6 male/female volunteers – mean plasma concentration provided) - **Figure 4.2.8**. In addition to these five single dose studies, one experiment with repeated dosing was analysed (Denaro et al., 1991). Nine healthy non-smokers, habitual coffee consumers, were given 6 cups of coffee per day (4.2 and 12 mg/kg BW). Mean plasma concentrations of caffeine measured over 24 h during low and high caffeine consumption were published.

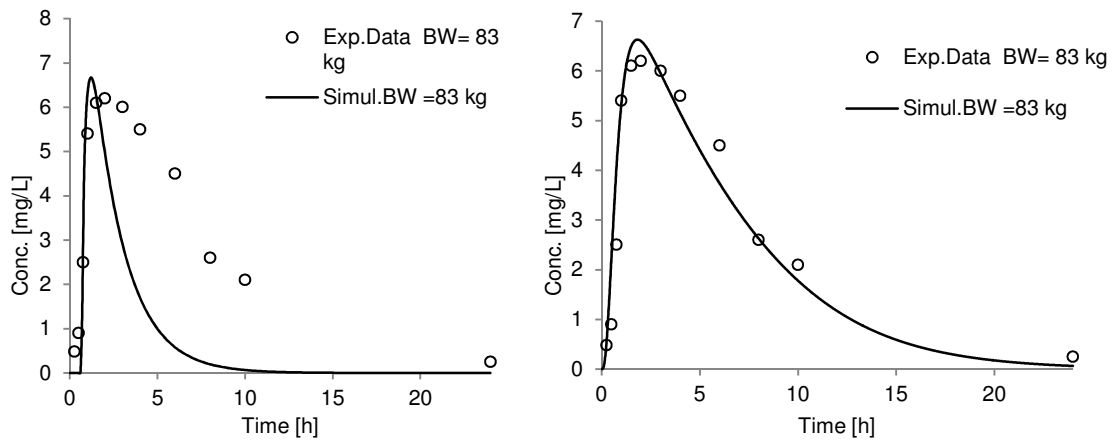


Fig 4.2.5. Simulations of caffeine plasma concentrations following oral absorption (PBTK1_orl –left, PBTK3_orl- right). Experimental data from: (Lelo et al., 1986).

(Newton et al., 1981) reported a total body clearance of caffeine for the doses 50-750 mg to be between 0.045- 0.0672 L/h/BW. The mean body clearance value for 300mg of caffeine given orally to 5 subjects on three separate occasions was found to be ca. 0.0954 L/h/kg BW. The percentage of unchanged caffeine eliminated in urine over 48 was 0.0426 (1.1% of dose- 300mg) - 0.1302 [L/h] (3.5% of dose- 50mg) as a mean results of 5 subjects with an average body weight of 69kg. The bioavailability of caffeine was found to be 0.92 for 300mg, 0.91 at 500mg and 1.06 at 750mg. In all the simulations I used a liver clearance of 0.120 L/h/kg BW (see also **Chapter 4.3.2**) which is the median result of PBTK3_orl model calibrations with respect to experimental data of (Lelo et al., 1986; Newton et al., 1981).

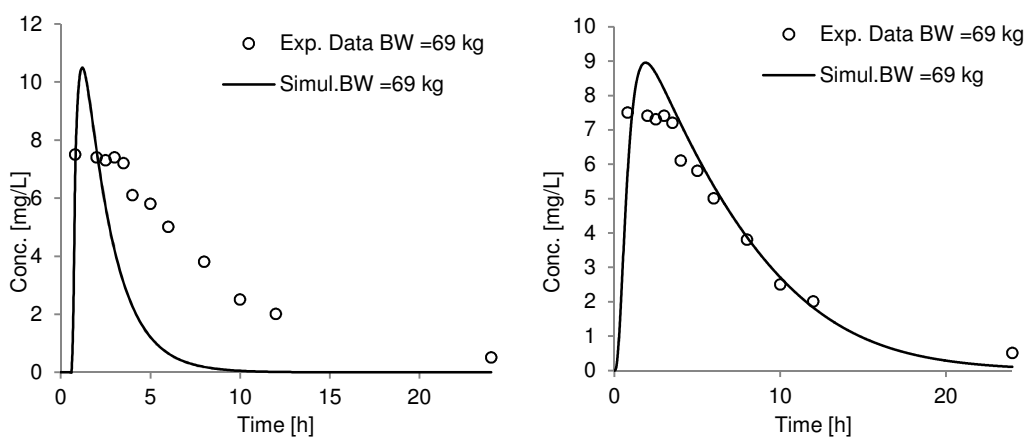


Fig 4.2.6. Simulations of caffeine plasma concentrations following oral absorption (PBTK1_orl –left, PBTK3_orl- right). Experimental data from: (Newton et al., 1981).

As the PBTK models did not give good simulation results for a mixture and higher caffeine dose, the caffeine liver clearance rate parameters were re-calibrated with respect to these experimental data. Other parameters remained unchanged (see adjusted values in **Figures 4.2.7-4.2.8**). In the study of (Csajka et al., 2005) I lowered the liver clearance rate to investigate if slower clearance would produce a better fit of experimental data as clearly elimination phase was much slower than simulated. In this experiment a lag time of 16.7 min was reported and the population mean estimate of $CL=4.98$ L/h (average BW= 69 kg). In the simulations I initially used 8.28 L/h (0.120 L/h/kg BW) that was further re-calibrated to 5 L/h. This, however, improved the fit only slightly.

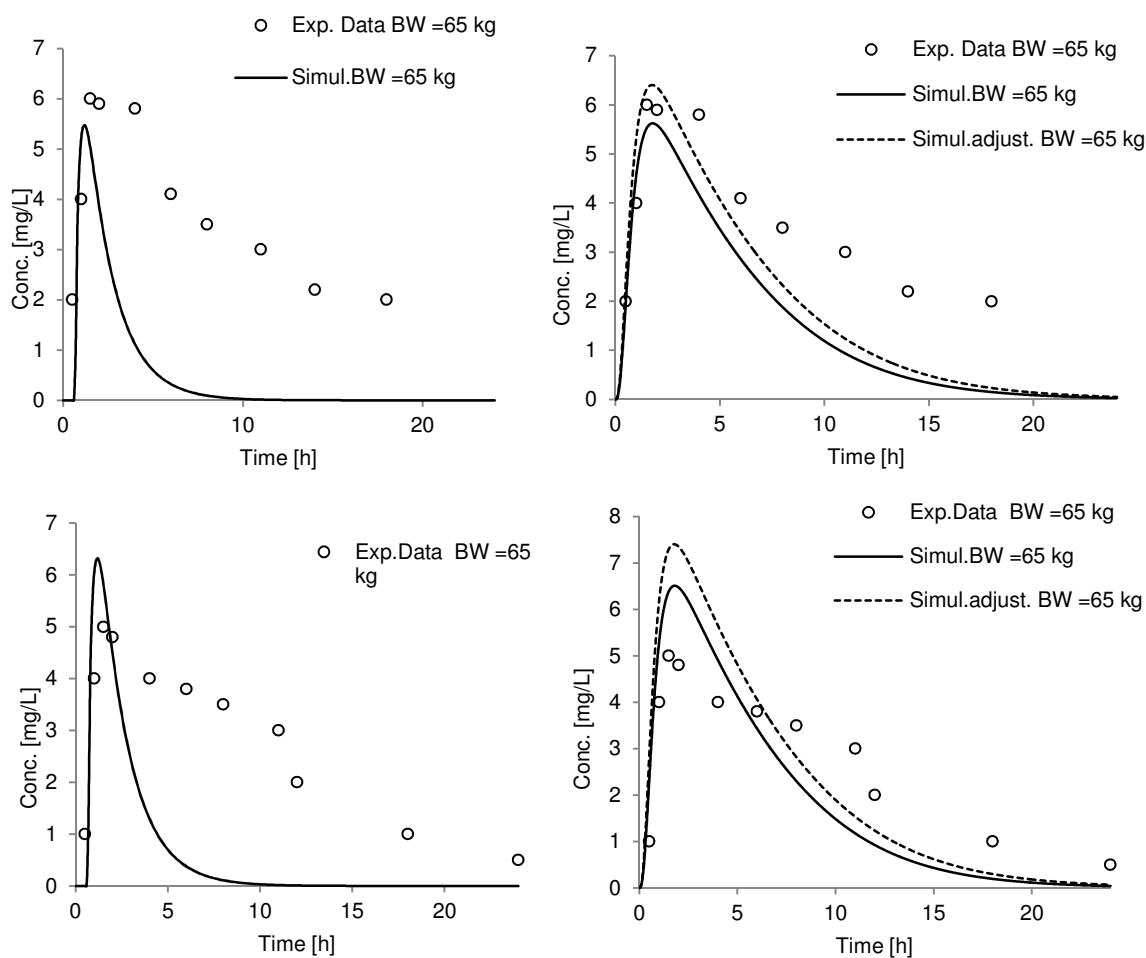


Fig 4.2.7. Simulations of caffeine plasma concentrations following oral absorption (PBTK1_orl –left, PBTK3_orl- right) . Experimental data from: (Csajka et al., 2005).

In contrast, experimental results of (Acheson et al., 1980) suggested a higher liver clearance than 0.120 L/h/kg BW. Optimisation indicated 0.3 L/h/kg BW (almost 3 times higher clearance) to be the most appropriate solution – see **Figure 4.2.8**.

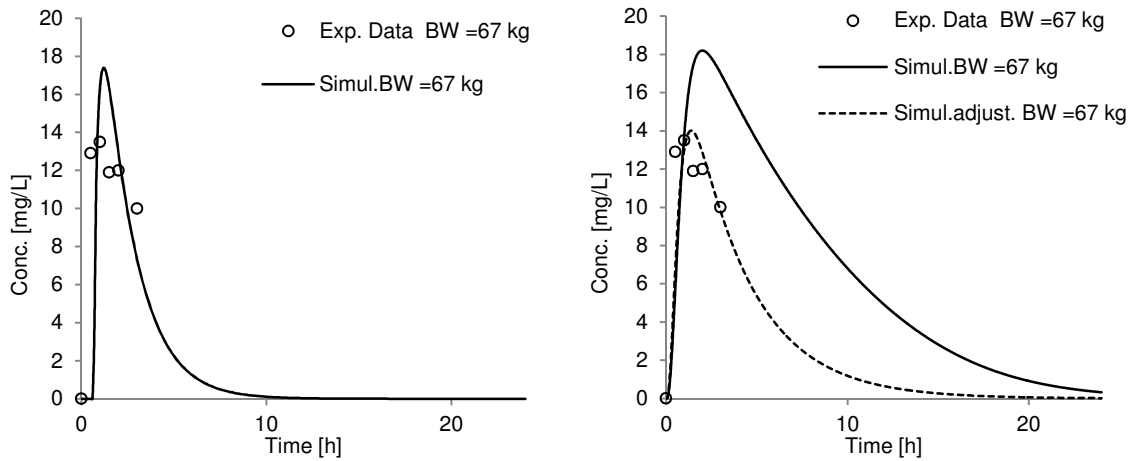


Fig 4.2.8. Simulations of caffeine plasma concentrations following oral absorption (PBTK1_orl –left, PBTK3_orl- right). Experimental data from : (Acheson et al., 1980).

Only one study of caffeine repeated dosing was found in the public literature. It was a 6-times repeated dosing of 4.2 (low) and 12 (high) mg/kg BW of caffeine as a coffee drink (Denaro et al., 1991) - **Figure 4.2.9**. The difference between the simulation performance of the models is clear in this example. The PBTK3_orl proved to be much more suitable for repeated exposure.

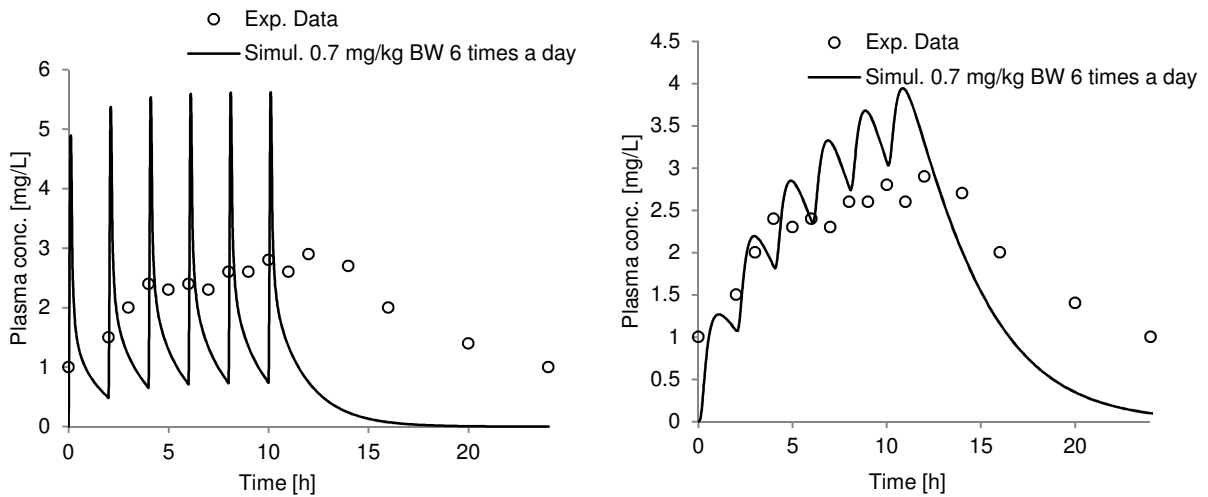


Fig 4.2.9. Simulations of caffeine plasma concentrations following repeated oral absorption (PBTK1_orl – left, PBTK3_orl- right). Experimental data from: (Denaro et al., 1991).

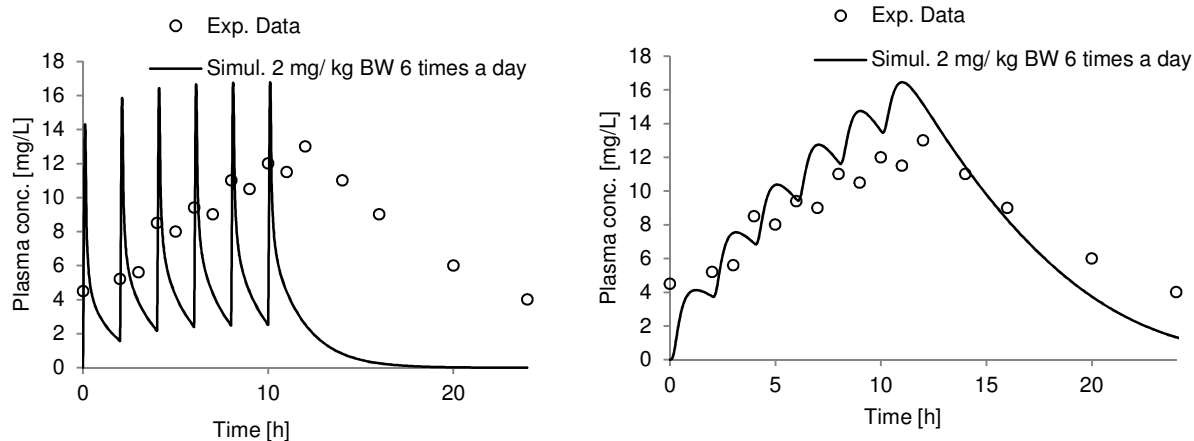


Fig 4.2.9 (continued). Simulations of caffeine plasma concentrations following repeated oral absorption (PBTK1_orl –left, PBTK3_orl- right). Experimental data from: (Denaro et al., 1991).

Table 4.2.7 shows a comparison between calculated versus experimental (if available) values of caffeine AUC in plasma by the PBTK1_orl and PBTK3_orl. The latter model structure produced higher AUC values both after single and repeated dosing and therefore closer to literature results (Lelo et al., 1986; Newton et al., 1981).

Table 4.2.7. AUC in blood following oral absorption of coumarin

AUC plasma [mg.h/L]	BW= 83 kg (single)	BW= 65 kg (single)	BW= 65 kg (single)	BW= 69 kg (single)	BW= 67 kg (single)	BW= 71 kg (repeated)
PBTK1_orl	16.783	12.320	14.325	22.425	41.915	19.659
PBTK3_orl	39.679	30.060	36.1625	57.983	139.473	63.423
Literature	26.19172 (Lelo et al., 1986) Calculated from dose/(CL*BW)	-	-	ca. 50 (Newton et al., 1981)	-	-
						41.936
						196.568

- Dermal absorption

In the case of dermal dosing, the study used (Otberg et al., 2008) was carried out on 6 human volunteers with mean results presented. In contrast to the coumarin and hydroquinone dermal studies, the increased impact of the hair follicles on overall absorption was considered here in accordance with the experimental design specified in the publication (**Figure 4.2.10**). A concentration of 4.56 mg/mL of caffeine in ethanol/propylene glycol was applied on 25 cm² area of chest for 24 h.

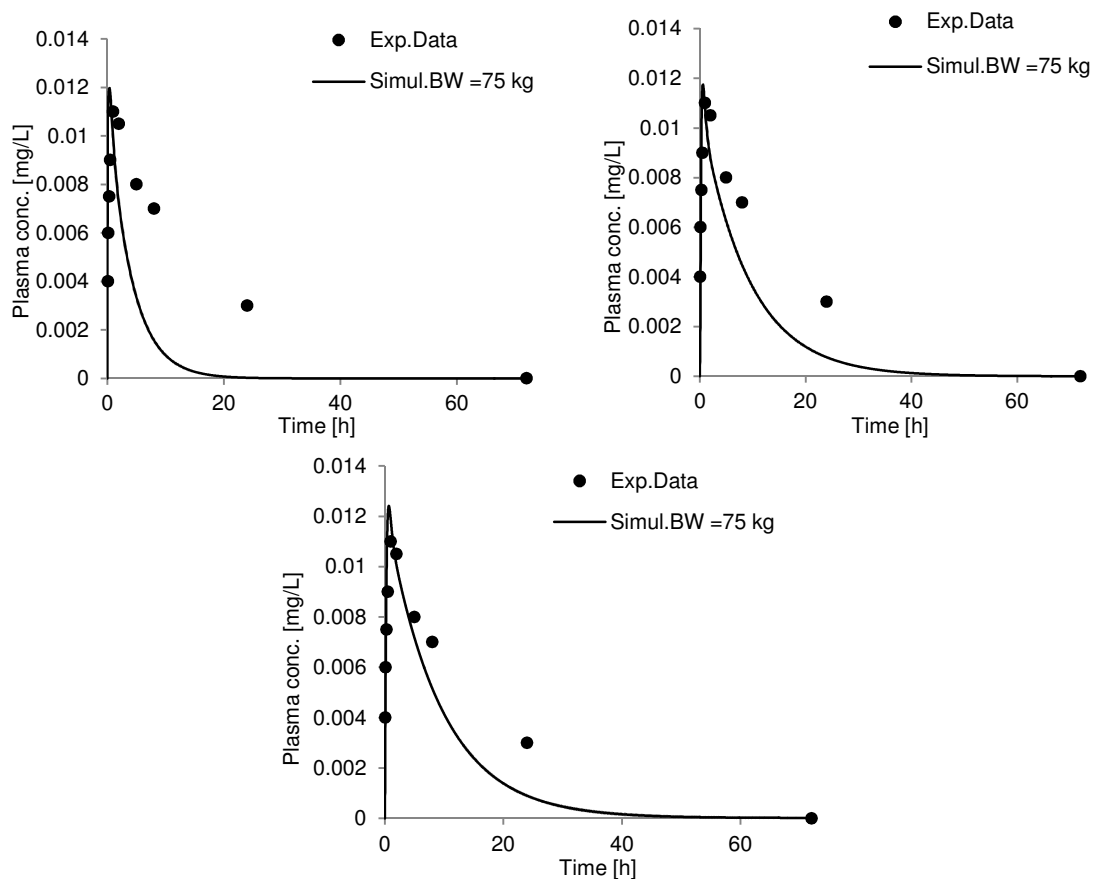


Fig 4.2.10. Simulations of caffeine plasma concentrations following dermal administration (PBTK1_skn – upper left, PBTK2_skn- upper right, PBTK3_skn- bottom). Experimental data from: (Otberg et al., 2008).

PBTK2_skn and PBTK3_skn showed similar simulation performance of caffeine concentration-time profiles in plasma. **Table 4.2.8** presents the difference between experimental and calculated total percentage of dose absorbed. All the models overpredicted the absorption when compared to experimental data. I assumed the ratio between plasma and blood to be 0.28 to obtain a better simulation of the concentration-time profile in the plasma due to lack of experimental value. The optimised ratio for oral absorption of caffeine of 0.35 would indicate much smaller caffeine levels in plasma for this study, but a smaller value than 0.28 would give the same results with smaller total absorption (due to slower rate of absorption $k_{a_{form}}$ than 0.2 mL/h – PBTK3_skn) as obtained in the experiment.

Table 4.2.8. Simulated percentage of dose absorbed and flux

BW= 75 kg	%Abs.	Flux [$\text{mg}/\text{cm}^2/\text{h}$]
PBTK1_skn	100	0.5226 (max) 0.00016 (median)
PBTK2_skn	80	0.0144 (max) 0.0003 (median)
PBTK3_skn	86.28	0.0215 (max) 0.0005 (median)
(Liu et al., 2011)	56	-

d) Isopropanol

- Oral absorption

To calibrate and validate oral absorption, two experiments were used. In (Monaghan et al., 1995) three healthy male subjects ingested 0.6 ml/kg 70% IPA in 240 ml water over a 5-min period, whereas in (Lacouture et al., 1989) three male subjects ingested 0.4 ml/kg 70% IPA in 210 ml apple juice over 10 min (Figures 4.2.11-4.2.12).

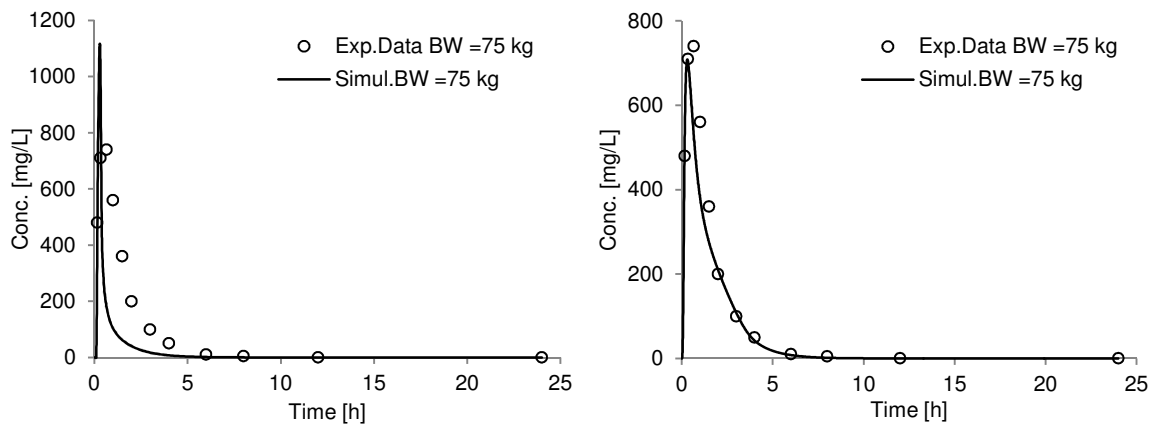


Fig 4.2.11. Simulations of caffeine plasma concentrations following oral absorption (PBTK1_orl –left, PBTK3_orl- right). Experimental data from: (Monaghan et al., 1995).

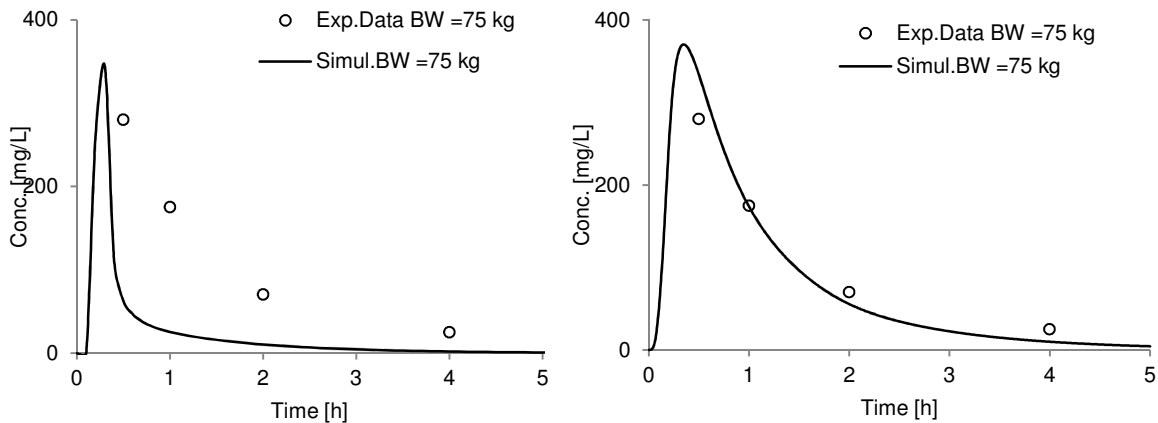


Fig 4.2.12. Simulations of caffeine plasma concentrations following oral absorption (PBTK1_orl –left, PBTK3_orl- right). Experimental data from: (Lacouture et al., 1989).

The AUC in blood of isopropanol calculated by (Monaghan et al., 1995) was compared with simulated values (Table 4.2.9). In the same manner as before, PBTK3_orl results were closer to experimental results.

Table 4.2.9. AUC of isopropanol in blood after oral absorption

AUC blood [mg/L/h]	Man (BW= 75 kg)	Man (BW= 75 kg)
PBTK1_orl	448.46	125.77
PBTK3_orl	903.3971	453.67
	1093 (mean)	-
Literature	(Monaghan et al., 1995)	

- Dermal absorption

Dermal absorption PBTK model was calibrated with respect to study of (Turner et al., 2004). 3mL of isopropyl alcohol- containing hand rub (52.6% w/w) was applied to the hands every 10 min over 4 h. Ten healthy adults participated in the experiment. Blood concentration of isopropanol after 4 h were published separately for males and females but only one experimental point after 4 h was reported (**Figure 4.2.13**).

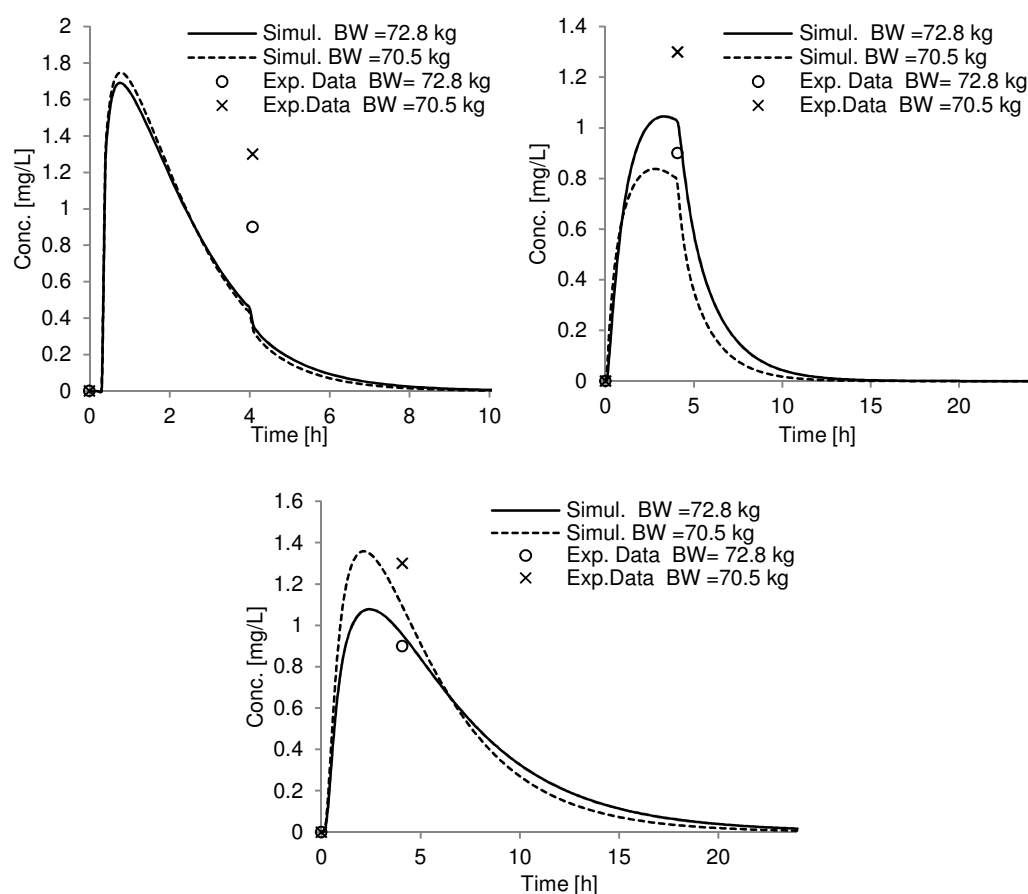


Fig 4.2.13. Simulations of isopropanol plasma concentrations following dermal administration (PBTK1_skn – upper left, PBTK2_skn- upper right, PBTK3_skn- bottom). Experimental data from: (Turner et al., 2004). PBTK1_skn simulated very fast absorption placing this experimental point almost at the end of elimination phase, whereas PBTK2_skn and PBTK3_skn indicated it shortly after the peak value slowing down absorption significantly.

Discussion

Based on the calibrated parameters in the PBTK3 model, it can be concluded that, within the investigated dose ranges, coumarin and isopropanol show the highest absorption rate from stomach and diffusion across the *stratum corneum*. Hydroquinone and isopropanol are quickly absorbed from the small intestine. Caffeine shows the highest partitioning in *stratum corneum* (the most limiting absorption step) and the lowest in viable epidermis. It tends to partition to plasma more readily than the three other substances. Neither renal clearance nor the excretion rate in bile is the most important elimination route for all the four substances. First pass metabolism in liver is a main elimination route although a certain percentage of caffeine was reported as eliminated in urine unchanged (Newton et al., 1981).

The coefficient of determination (R^2), mean squared error (MSE) and corrected Akaike's Information Criterion (AICc) (Kletting and Glatting, 2009) were used as decision criteria. As these statistics show in **Tables 4.2.10-4.2.11**, the PBTK3 model structure (with sub-compartments in the absorption stage and therefore with more parameters to determine) is better in most of the instances (11/14 in oral and 4/5 in dermal absorption), as indicated by the lower AICc value whenever individual or mean data are available for the same substance. The PBTK1 model has the advantage of fewer parameters to calibrate that can easily be set for a given set of experimental data but usually it simulates much faster absorption than *in vivo* even with a pre-defined time-lag. This misprediction can be easily seen in the case of repeated exposure data, when too fast absorption is associated with much faster elimination. In contrast, PBTK3, which consists of sub-compartments in the absorption stage (but with more parameters to determine), gives improved predictions when applied to the population, especially in the case of repeated exposure. When simulating the coumarin oral experiment, PBTK3 gave predictions comparable to PBTK1. However, I found only single administration gavage data for 3 subjects. When simulating the dermal experiment, PBTK1 did not give good results, PBTK2 was close to PBTK3 in predictions but still PBTK3 performed the best. To simulate the hydroquinone oral and dermal experiments, all model structures seem to be good candidates; however in this case there was no comparison between different subjects or different exposure conditions. The availability of many oral experimental data for caffeine makes it a good test substance for choosing the best fitting model. Additionally, different types of dosing could be considered, either pure caffeine or its mixture with herbs/substances, single or repeated dosing. PBTK1 did not perform well either in the case of pure caffeine or in case of the mixture (single dosing). This poor performance is even more obvious in the case of repeated absorption. Overall, PBTK3 gives good predictions for pure caffeine in gelatin coating but performs poorly for the second study (Csajka et al., 2005). It seems likely that either PBTK3 does not work well when applied to mixtures or the experimental results were more variable due to population effects and drug-drug interactions (e.g. use of contraceptives) which cannot be easily captured by the present PBTK model. The mean values taken from all the candidates gave a slower excretion rate of caffeine (most likely clearance rates are different) when compared to other studies. Re-calibration of liver clearance did not improve the

results significantly. Interestingly, for the higher dose (in the fifth study (Acheson et al., 1980)), PBTK3 gave good predictions only if this clearance rate was re-adjusted (increased not lowered as before). This can be explained, either by the dose itself, by different application conditions than in the previous studies for which the parameters were optimised or simply by big differences in caffeine liver clearance between subjects. In the dermal model the inclusion of the hair follicles compartment, in accordance with the experimental design (Otberg et al., 2008), helped obtain better prediction performance. However, PBTK2, without this compartment, also gave sufficiently good results (in terms of R-squared, AICc, MSE). The isopropanol case study further showed that the PBTK3 structure is more suitable for modelling oral and dermal absorption than the two other alternatives. Two oral experiments (Lacouture et al., 1989; Monaghan et al., 1995) gave much lower AICc and MSE but higher R² values for PBTK3_orl when compared to PBTK1_orl. I could not, however, calculate these measures for dermal absorption because there was only one experimental point published by (Turner et al., 2004) for males and females individually following exposure to 3 mL of isopropyl alcohol- containing hand rub (52.6% w/w).

Table 4.2.10. Goodness of fit: oral model.

Compound	BW [kg]	PBTK3			PBTK1		
		MSE (1)	R2(2)	AICc (3)	MSE (1)	R2 (2)	AICc (3)
coumarin	70	1.245·10 ⁻⁰⁵	86.736	-95.325	1.234·10 ⁻⁰⁵	86.855	-96.477
	46	2.356·10 ⁻⁰⁵	80.369	-90.861	3.514·10 ⁻⁰⁵	70.727	-89.154
	68	3.149·10 ⁻⁰⁵	83.245	-115.407	8.433·10 ⁻⁰⁵	55.129	-108.688
hydroquinone	87.7	4.091·10 ⁻⁰⁶	96.367	-133.774	2.272·10 ⁻⁰⁵	79.822	-120.491
	69	6.568·10 ⁻⁰⁵	93.225	-83.569	5.430·10 ⁻⁰⁵	94.398	-85.978
	83	0.450	90.867	-41.3517	4.158	15.560	-18.376
caffeine	65	1.828	20.923	-18.964	7.462	-222.691	-7.101
	65	1.422	38.316	-24.410	4.078	-76.849	-15.705
	69	0.8117	85.280	-34.268	9.515	-72.567	-8.443
	67	35.375	-65.490	7.932	33.647	-57.405	6.789
	71 (repeated)	0.533	-48.721	-57.537	2.425	-575.927	-47.829
isopropanol		6.402	15.382	-17.778	46.785	-518.355	-0.471
	75	12950.8	83.044	82.084	73727.8	3.474	97.926
	75	2073.45	78.692	21.990	18453.793	-89.634	30.465

(1) mean squared error

(2) coefficient of determination, R- squared

(3) Akaike's Information Criterion with the correction for a small number of data points (Kletting and Glatting, 2009)

Table 4.2.11. Goodness of fit: dermal model:

Compound	BW [kg]	PBTK3			PBTK1			PBTK2		
		MSE (1)	R2 (2)	AICc (3)	MSE (1)	R2 (2)	AICc (3)	MSE (1)	R2 (2)	AICc (3)
coumarin	78	1.274·10 ⁻⁰⁵	88.97	-123.225	1.009·10 ⁻⁰⁴	12.658	-106.809	4.379·10 ⁻⁰⁵	62.108	-112.971
	76	1.084	59.58	-103.959	1.029	61.618	-106.633	3.096	88.455	-116.090

		10^{-04}	7		10^{-04}			10^{-05}		
	91	1.381	81.90	-122.499	9.633	-26.223	-107.229	4.857	36.359	-112.037
		10^{-05}	2		10^{-05}			10^{-05}		
hydroquinone	69	1.292	92.86	-67.192	4.938	72.722	-61.008	3.221	82.209	-62.797
		10^{-05}	2		10^{-05}			10^{-05}		
caffeine	75	9.565	91.05	-163.465	2.305	-	-134.960	1.671	84.367	-159.227
		10^{-07}	2		10^{-05}	115.62		10^{-06}		
						7				

(1) mean squared error

(2) coefficient of determination, R- squared

(3) Akaike's Information Criterion with the correction for a small number of data points (Kletting and Glatting, 2009)

4.2.2 Inhalation

Two different PBTK model structures (PBTK1_inh: simple 3-compartment model with inhaled, exhaled air and lungs and PBTK3_inh: multi-compartment model) were compared in terms of their predicted ADME profiles of inhaled styrene, ethanol and isopropanol.

The multi-compartment lungs model represents 24 interconnected compartments (generation of the Weibel model) (Peterman and Longtin, 1984; Weibel, 1979). The model assumes that gas is transported through the lungs by convection and diffusion. The inhaled gas diffuses across the alveolar membrane, dissolves in the blood circulating through the lungs and is cleared from the lungs due to the blood perfusion. Three main compound-specific parameters are a part of this model: the diffusion coefficient (in generations 13-22; D_i), removal of a gas from the blood (r) and the dissolution of the gas in the blood (represented by the Ostwald solubility (λ)). Other quantities such as sinusoidal breathing pattern, convection rate, tidal volume, airways area and volumes were assumed constant. A 4-sec inhalation-exhalation process describes well the resting conditions (a tidal volume of 500 ml and a breathing rate of 15 breaths per minute) – in accordance with original implementation of the model (Peterman and Longtin, 1984). Because of the high complexity of this model and the many parameters left for optimisation the same breathing pattern was used for exercise conditions as well. The model described by Peterman and Longtin was linked here with other body compartments (used in PBTK modelling) for the first time. Peterman and Longtin showed the usefulness of the model in simulating profiles and build-up of radioactive inert gases such as T_2 and ^{133}Xe . The authors concluded that the model exhibits good predictive power regarding the rate of transport of gases through the lungs and by associating the generations with physical locations in the lungs. In this study I applied this model to simulate the profiles of organic vapours assuming that the particular stages of the multistep inhalation/exhalation process are unchanged: uptake and washout process (as described in **chapter 3.2**). In literature PBPK models of organic solvents, uptake in the respiratory tract is assumed to occur only in the alveolar region (Ramsey and Andersen, 1984). Local effects such as metabolism were added to the model. I contrasted the simulations of this complex model against the performance of a simple model by means of toxicokinetic parameters (C_{max} , AUC) and simple statistics (MSE, R^2 , AICc). The advantage of using a multi-compartment respiratory tract lies in the possibility of estimating chemical concentrations in particular segments of the tract which is especially important in cases of ongoing reactions or bioaccumulation;

however computational time is higher than for simple few-compartments models. The dynamic lungs model is also used to predict and simulate the buildup of gases in the lungs and their washout. The input dose to the PBTK model has to be provided in mg/L and due to the fact that most of inhalation studies report the exposure level in parts per million [ppm], I used the following conversion²⁶:

$$MW \left[\frac{g}{mol} \right] \cdot [ppm] = MV \left[\frac{m^3}{mol} \right] \cdot \left[\frac{mg}{m^3} \right] \quad (4.2.1)$$

Where: MV= Molar volume [m³/mol]

The number of model parameters necessary for calculating AICc values was: PBTK1_inh = 33 and PBTK3_inh = 30.

a) Styrene

Styrene is one of the most common industrial chemicals that has been studied in terms of PBTK modelling and internal concentrations following inhalation both in humans and animals. Up to 3% of the absorbed styrene vapour is exhaled unchanged, and about 90% is ultimately biotransformed to mandelic and phenylglyoxylic acid and excreted in the urine (Prieto et al., 2002). Metabolism in the liver is usually described by Michaelis-Menten kinetics (Csanady et al., 1994) and so far the liver has been assumed to be the only metabolizing organ in the modelling. However, styrene was also found to undergo metabolism in the respiratory tract (Chung et al., 2006) (the toxicity of styrene is metabolism-dependent). CYP2E1 was suggested to be one of the cytochrome P450 enzymes responsible for the bio-activation of styrene.

In this study I compare the performance of two PBTK model structures (PBTK3_inh and PBTK1_inh) in estimating internal level metrics of styrene alone. The exposure conditions and experimental data were taken from the literature – see **Table 4.2.12**.

Table 4.2.12. Inhalation exposure to styrene

Reference	Exposure time [h]	Breathing conditions	Dose [ppm] (exposure time)	Conversion [mg/L]	<i>In vivo</i> concentrations available for
(Wigaeus et al., 1984)	2	Light physical exercise(50W)	68.78	0.293 -> opt. 0.1	Arterial blood
(Ramsey and Young, 1978)	6		80	0.341	Venous blood
(Johanson et al., 2000)	2		50	0.220 -> opt. 0.4	Venous blood

²⁶ <http://ww2.unhabitat.org/wuf/2006/aqm/tool28.htm> (last access: 06.10.2014)

The model parameters are given in **Table 4.2.13**. Most of them, except for the diffusion coefficient in lungs (D_l), were taken from the literature and used unchanged. Given these values, both the PBTK1_inh and PBTK3_inh models were used to simulate blood concentrations from three different literature studies (Johanson et al., 2000; Ramsey and Young, 1978; Wigaeus et al., 1984). The predicted results were much higher than observed values for two studies (Johanson et al., 2000; Wigaeus et al., 1984). In order to better simulate the experimental values, I optimised (lowered) the constant external concentration of the chemical (see opt. in **Table 4.2.12**). The simulated versus experimental results are shown in **Figures 4.2.14-16** and internal dose metrics results in **Tables 4.2.14-16**.

Table 4.2.13 PBTK model parameters for styrene

Reference	Parameter name	Value
(Csanady et al., 1994)	V_{max} [mg/h/gliv]	0.2083
	K_m [mg/L]	1.0415
(Van Rees, 1974)	$PC_{water,air}$	4.38
(Csanady et al., 1994)	$PC_{blood,air}$	48
(Peterman and Longtin, 1984)	r [mL/s]	0.126
(Katritzky et al., 2008)	$Log\lambda$	3.852
optimised	D_l [cm ² /s]	0.04-0.08
Assumed	CLR [L/h]	0.1
Tissue-to-blood partition coefficients (PC_{org})		
	Liver	2.71
(Csanady et al., 1994)	Poorly-perfused tissues	1.96
	Highly-perfused tissues	2.60
	Adipose tissue	93.8
(Schmitt, 2008)	Lungs	1.47
	Kidney	1.75

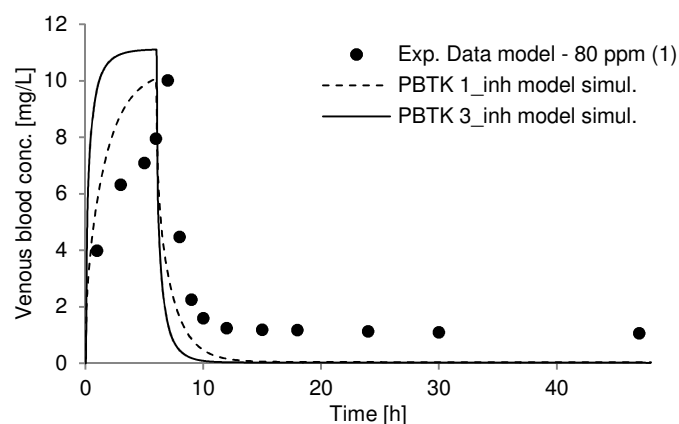


Fig 4.2.14. PBTK1_inh and PBTK3_inh model simulations of styrene concentration in venous blood.

Experimental data (1) from: (Ramsey and Young, 1978).

Table 4.2.14 Internal metrics results for styrene

Model	AUC in liver [mg.h/L]	AUC in blood [mg.h/L] (venous)	C_{max} in liver [mg/L]	C_{max} in blood (venous) [mg/L]
PBTK1_inh	207.670	58.211	38.600	10.237
PBTK3_inh	162.610	58.896	27.129	9.677

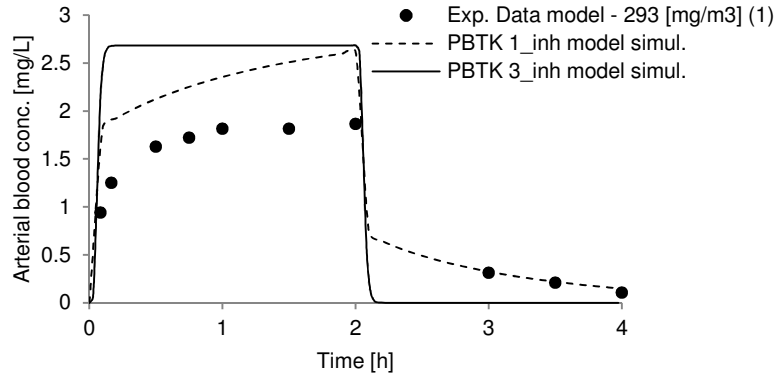


Fig 4.2.15. PBTK1_inh and PBTK3_inh model simulations of styrene concentration in arterial blood. Experimental data (1) from: (Wigaeus et al., 1984).

Table 4.2.15 Internal metrics results for styrene

Model	AUC in liver [mg.h/L]	AUC in blood [mg.h/L] (venous)	C _{max} in liver [mg/L]	C _{max} in blood (venous) [mg/L]
PBTK1_inh	7.024	3.784	3.803	1.662
PBTK3_inh	18.047	6.763	9.059	3.250

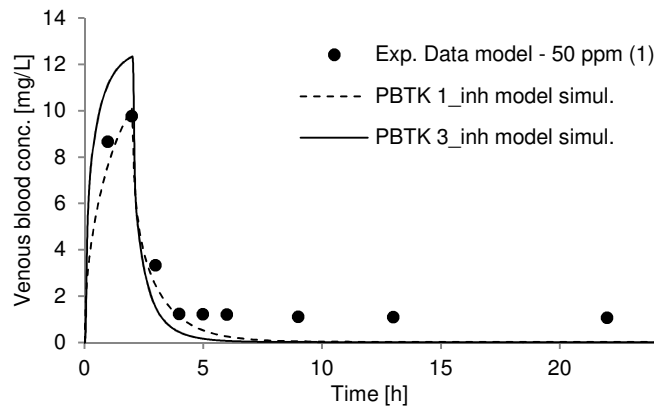


Fig 4.2.16. PBTK1_inh and PBTK3_inh model simulations of styrene concentration in venous blood. Experimental data (1) from: (Johanson et al., 2000).

Table 4.2.16 Internal metrics results for styrene

Model	AUC in liver [mg.h/L]	AUC in blood [mg.h/L] (venous)	C _{max} in liver [mg/L]	C _{max} in blood (venous) [mg/L]
PBTK1_inh	74.311	22.250	41.497	10.090
PBTK3_inh	77.489	27.731	38.834	13.231

Based on the **Tables 4.2.14-16** it can be seen that AUC values in the liver and blood calculated by the PBTK3_inh model are in most cases higher (except for Ramsey and Young study where I didn't lower an external inhaled concentration of styrene and only liver AUC calculated by the PBTK1_inh seems to higher). Peak concentrations in the blood simulated by PBTK3_inh are again higher for the last two studies but lower for the first study; whereas peak levels in the liver determined by PBTK1_inh are on average higher.

Table 4.2.17. Simulation performance of the models - statistics

Model	(Ramsey and Young, 1978)	(Wigaeus et al., 1984)	(Johanson et al., 2000)
PBTK1_inh	R ² = 14.258	R ² = 34.849	R ² = 93.453
	MSE= 7.503	MSE= 0.304	MSE= 0.715
	AICc= -17.118	AICc=-39.097	AICc= -26.564
PBTK3_inh	R ² = -23.315	R ² =-514.534	R ² = 66.428
	MSE= 10.791	MSE= 2.870	MSE= 3.664
	AICc= -14.920	AICc= -17.637	AICc= -12.574

Table 4.2.17 shows the statistics of fit to experimental data for the two models. Clearly it was difficult to obtain good matching of the data by both of them. However, it can be concluded that PBTK1_inh performs better for predicting blood concentrations while both models overestimate a clearance rate of styrene – after 10 h there is almost no styrene left in the blood according to the PBTK modelling but experimental data show that it maintains a low but constant level even up to 50 h (Wigaeus et al., 1984). Improvements to the model could be made either by introducing a changeable clearance rate (metabolism rate) in time or perhaps by using different blood-to-tissue partition coefficients that could account for the compound accumulation. More experiments would be necessary to further investigate these model refinements.

b) Isopropanol

Isopropanol has been widely used for many years mainly as a solvent, rubbing alcohol, and mild disinfectant. Therefore its inhalation occurs during the short time of contact with certain consumer products or for longer times in workplaces (in the industrial manufacturing, processing, and use of isopropanol). (Clewel Iii et al., 2001) developed a multi-route PBTK model and indicated that inhalation studies of isopropyl alcohol have demonstrated neurological effects while oral administration studies have identified developmental and reproductive effects. (Kumagai et al., 1999) carried out experiment on four healthy male volunteers who inhaled concentrations of 50, 100, or 200 ppm of isopropanol while resting for 10 min. The subjects inhaled the vapours through a mouthpiece equipped with a valve to isolate exhaled air, and samples of exhaled air were collected 1 min prior to exposure, during the 10 min- exposure, and for 5 min following exposure. Exhaled air concentrations were reported both for the average concentration over an exhalation as well as for the concentration at the end of an exhalation (which better represents air from the alveolar region). I used from this study only higher mixed-exhaled results. This is the only freely available isopropanol inhalation study I could find in the current literature. The molecular volume of isopropanol of 75.9 m³/mol²⁷ was taken for concentration conversions from ppm to mg/L – **Table 4.2.18**.

²⁷ <http://www.aqnovel.com/mytag.php?id=22963> (last access: 06.10.2014)

Table 4.2.18. Inhalation exposure to isopropanol

Reference	Exposure time [min]	Breathing conditions	Dose [ppm] (exposure time)	Conversion [mg/L]	<i>In vivo</i> concentrations available for
(Kumagai et al., 1999)	10	rest	200	0.158	exhaled air

The model parameters are given in **Table 4.2.19**. The simulated versus experimental results in the blood and exhaled air are shown in **Figure 4.2.17** and internal dose metric results in **Table 4.2.20**. To better describe the experimental results I optimised the Ostwald solubility coefficient (λ) and water/air partition coefficient ($PC_{\text{water,air}}$). I additionally introduced a first order rate of isopropanol bioconversion in the respiratory tract (optimised by PBTK1_inh) to better match the *in vivo* data.

Table 4.2.19 PBTK model parameters for isopropanol

Reference	Parameter name	value
Liver metabolism (Clewell Iii et al., 2001)	V_{max} [mg/h/kg BW ^{3/4}]	300
Metabolism in respiratory tract wall tissue- optimised (Kumagai et al., 1999)	Km [mg/L]	10
(Clewell Iii et al., 2001)	$K_{\text{met,inh}}$ [L/h]	1
(Peterman and Longtin, 1984)	$PC_{\text{water,air}}$	1500 -> opt. 10
(Katritzky et al., 2008)	$PC_{\text{blood,air}}$	848
Assumed as the one of styrene (Clewell Iii et al., 2001)	r [mL/s]	0.126
Tissue-to-blood partition coefficients (PC_{org}) (Clewell Iii et al., 2001)	$\text{Log}\lambda$	2.863 -> opt. 1
	DI [cm ² /s]	0.08
	CLR [L/h]	0.04
	Brain	1.33
	Poorly-perfused tissues	
	Skin	1.3
	Highly-perfused tissues	
	Heart	1.25
	Kidney	
	GI tract	
	Adipose tissue	0.32

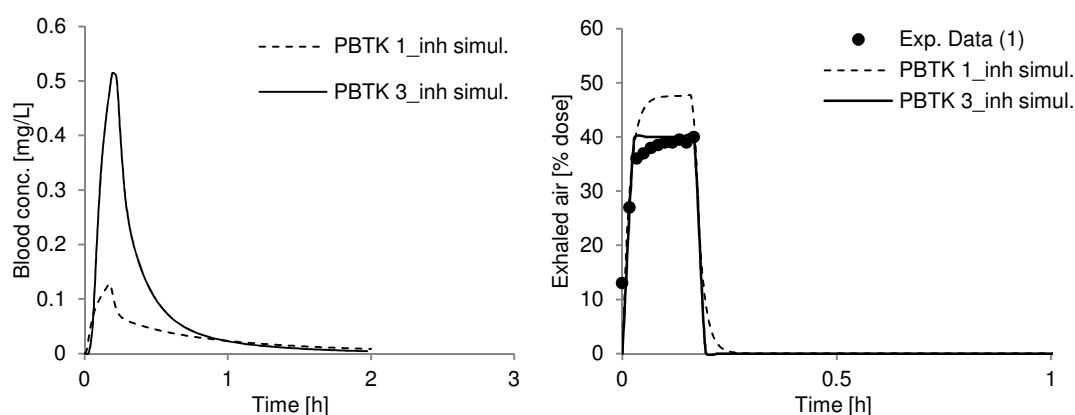


Fig 4.2.17. PBTK1_inh and PBTK3_inh model simulations of styrene concentration in venous blood (left) exhaled air (right). Experimental data (1) from: (Kumagai et al., 1999).

Table 4.2.20 Internal metrics results for isopropanol

Model	AUC in liver [mg.h/L]	AUC in blood [mg.h/L] (venous)	C _{max} in liver [mg/L]	C _{max} in blood (venous) [mg/L]
PBTK1_inh	$9.067 \cdot 10^{-06}$	0.065	$3.2 \cdot 10^{-05}$	0.128
PBTK3_inh	$1.125 \cdot 10^{-05}$	0.156	$1 \cdot 10^{-04}$	0.515

AUC and C_{max} results both in the blood and liver simulated by the PBTK3_inh model are higher than the ones simulated by the PBTK1_inh model. The statistics in **Table 4.2.21** show that it is the multi-compartmental model that produces a better fit of the exhaled data, although this fit is not the best. In fact, the PBTK3_inh model offers a better simulation of chemical concentrations in particular stages of the respiratory tract that ranges from the mouth concentrations to the alveolar region. This is important in cases when the chemical is said to produce a toxicological effect in the tract or undergoes biotransformation and when the information about concentrations of this chemical as a function of time is necessary

Table 4.2.21 Simulation performance of the models - statistics

Model	(Kumagai et al., 1999)
PBTK3_inh	R ² = 51.473 MSE= 29.443 AICc= 4.730
PBTK1_inh	R ² = -14.182 MSE= 69.278 AICc= 15.453

c) Ethanol

Ethyl alcohol, or ethanol, is found in many common consumer products. It also has many uses in work environments (fuels, solvents, disinfectants, a raw material for chemical synthesis). Beyond alcoholic beverages, ethanol is found in many professional products: paints, varnishes and inks, alcohol-based products, and biofuels. Therefore, exposure to ethanol by inhalation is very common. (Nadeau et al., 2003) reported that the occupational standard limit for ethanol exposure in air is 1000 ppm. They measured ethanol in blood and alveolar air in a group of five healthy men exposed to this level for 6 h. Unfortunately only a few experimental points were presented (at 3 and 6 h for blood and at 3, 4.5 and 6 h for expired air), which is not sufficient to evaluate statistically the performance of the models. As in the case of isopropanol, I could not find any other available *in vivo* data that could be further used to test the performance of the PBTK1_inh and PBTK3_inh models. For dose conversion (see Table 4.2.22), the molecular volume of ethanol of 58m³/mol was taken ²⁸.

²⁸ <http://chemistry.tutorcircle.com/inorganic-chemistry/molar-volume.html> (last access: 06.10.2014)

Table 4.2.22. Inhalation exposure to ethanol

Reference	Exposure time [h]	Breathing conditions	Dose [ppm] (exposure time)	Conversion [mg/L]	<i>In vivo</i> concentrations available for
(Nadeau et al., 2003)	6	Rest	1000	0.7943	Venous blood and expired air

The model parameters are given in **Table 4.2.23**. The simulated versus experimental results are shown in **Figure 4.2.18** and internal dose metrics results in **Table 4.2.24**.

Table 4.2.23 PBTK model parameters for ethanol inhalation

Reference	Parameter name	value
(Kaneko et al., 1994)	PC _{waterair}	2140
(Meulenberg and Vijverberg, 2000)	PC _{bloodair}	1352.5
(Peterman and Longtin, 1984)	r [mL/s]	0.126
(Katritzky et al., 2008)	Log λ_{cn}	2.855-> -2
assumed as the one of styrene	DI [cm ² /s]	0.08
Kmet [L/h]	Kmet [L/h]	0.15

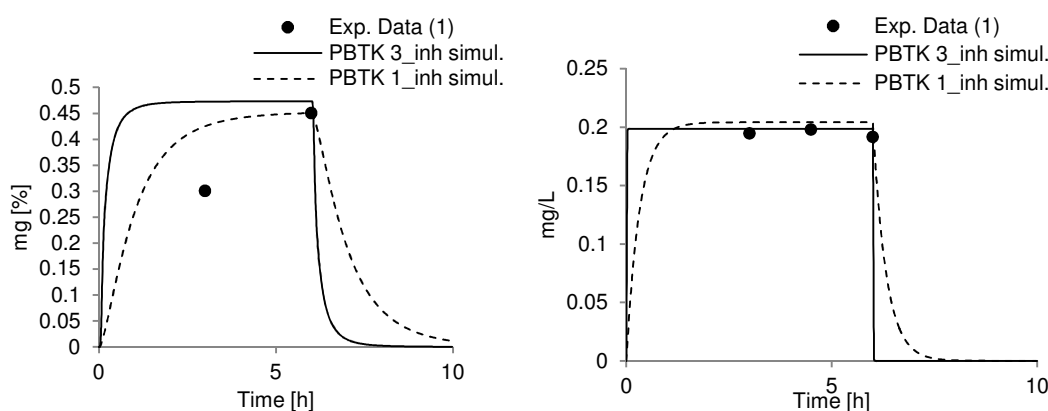


Fig 4.2.18. PBTK1_inh and PBTK3_inh model simulations of ethanol concentration in venous blood as a percentage of applied dose (2.5 dose)- left; and exhaled concentration of ethanol - right. Experimental data (1) from: (Nadeau et al., 2003).

Table 4.2.24 Internal dose metric results for ethanol

Model	AUC in liver [mg.h/L]	AUC in blood [mg.h/L] (venous)	C _{max} in liver [mg/L]	C _{max} in blood (venous) [mg/L]
PBTK1_inh	0.066	0.054	0.011	0.009
PBTK3_inh	0.039	0.056	0.0065	0.009

Based on the model simulations it can be seen that blood levels are again better described by the PBTK1_inh model, which has a slower absorption phase than PBTK3_inh. It seems that concentration in expired air is well accounted for by both of the models. It was particularly difficult to parametrise the PBTK3_inh model as the results were always much higher than the experimental ones. Assuming that only compound-specific parameters such as diffusion, Ostwald coefficients and water-air partition coefficient could be modified I had to lower the most sensitive one. The Ostwald coefficient showed the highest impact on internal (blood)

concentration results and only a very low value equal to 0.01 gave satisfactory results including also a first order metabolism rate in the air tract.

4.3 *In vitro*- to- *in vivo* correlation

Several case study compounds (coumarin, caffeine, estragole and hydroquinone) were used in this section to perform *in vitro*- to- *in vivo* correlation (IVIVC) of kinetic measures of skin penetration, liver clearance as well as dose metrics of caffeine-induced HepaRG toxicity. I applied a simple correlation factor to quantify the *in vitro* and *in vivo* differences in the amount of caffeine and coumarin permeated through the skin and concentration-time profiles of coumarin, estragole, hydroquinone and caffeine in the liver. I developed a multi-scale computational approach by linking the PBTK model with the Virtual Cell-Based Assay (VCBA) to relate an external oral and dermal dose of caffeine (only) with an internal dose-dependent liver toxicity, measured *in vitro* as HepaRG cell viability. The results revealed higher *in vivo* skin permeation profiles than those determined *in vitro* using identical *in vitro* and *in vivo* exposure conditions for all the compounds. Liver clearance of caffeine derived from *in vitro* metabolism rates was found much slower than the optimised *in vivo* clearance with respect to available caffeine plasma concentrations but the reverse was observed for coumarin, hydroquinone and estragole. Finally, HepaRG cell viability was shown to remain almost unchanged for external caffeine doses in the range of 5-400 mg (up to ca. 2 times oral NOAEL dose – see **Chapter 4.4**), assuming a concentration of 4.56 mg/mL of caffeine in ethanol/propylene glycol vehicle for both exposure types. I modelled human (reference man, BW= 75 kg) exposure to single doses of caffeine only. The goal of this analysis is to show that administration of single doses of caffeine in the range of extrapolated to human no-effect level is safe in terms of liver cells viability. Finally, I compared the results with experimental *in vitro* exposure of HepG2 to caffeine of similar concentrations as in HepaRG case. HepaRG showed a slightly higher sensitivity to caffeine than HepG2.

The approaches described in the present chapter provide a promising means of performing *in vitro* -to- *in vivo* correlations that may contribute to a reduction of animal experimentation in the chemical risk assessment process.

4.3.1 Skin penetration

The goal of this study was to calibrate the PBTK model performance with respect to *in vivo* and *in vitro* permeation profiles and correlate the *in vitro* and *in vivo* permeation results in terms of maximal amount of a substance permeated in time over exposed skin area. Caffeine and coumarin were used as case study examples. For *in vivo* case, PBTK3_skn model was used, whereas for *in vitro* case, to better simulate the *in vitro* skin absorption the model was slightly modified and simplified to include two skin layers, *stratum*

corneum and viable epidermis without hair follicles, and a receptor compartment instead of dermis (**Figure 4.3.1**). I carried out three calibration/modelling steps in determining IVIVC of skin penetration: (I) the *in vitro* skin model was optimised with respect to *in vitro* permeation results, (II) some of the *in vitro*-optimised parameters (namely diffusion coefficient in viable epidermis, partition coefficients in skin layers) were scaled up to *in vivo* values by the *in vivo* skin PBTK model basing on caffeine plasma concentrations, (III) the $IVIV_{\text{skin}}$ ratio for skin penetration was calculated (**Equation 4.3.1**) for the maximal permeated amount of caffeine estimated *in vitro* and *in vivo* using identical exposure scenarios for the *in vitro* and *in vivo* skin models.

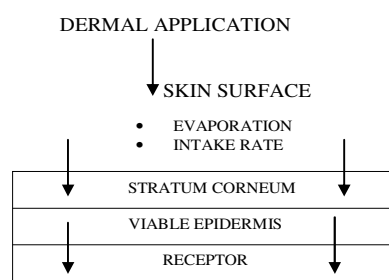


Fig 4.3.1 *In vitro* PBTK model.

$$IVIV_{\text{skin}} = \frac{A_{\text{max, in vitro}}}{A_{\text{max, in vivo}}} \quad (4.3.1)$$

a) Caffeine

There are many *in vitro* methods available in literature for measuring absorption rate, percentage and diffusion/ permeation coefficients of caffeine through various skin sites and using vehicles such as water, ethanol, acetone, propylene glycol or mixtures of some of them. (Lehman et al., 2011) studied a difference between total absorption of caffeine (percentage of applied dose) through human skin *in vivo* and *in vitro*-based on scientific literature. They calculated the *in vitro/ in vivo* (IVIV) ratio as the metric for comparison. For harmonised data sets (in terms of the anatomical skin site, compound dose, vehicle dose and composition, length of exposure/ wash time and the temperature) the average IVIV ratio was 0.96 (0.58-1.28).

It is well known that the percutaneous absorption process of a given compound depends on many factors: physicochemical characteristics, molecular size, partition coefficient, solubility, thermodynamic activity, drug-binding, vehicle type and anatomic skin site. (Rougier et al., 1987) reported difference in total amount of permeated caffeine based on different anatomic sites: abdomen, arm, postauricular and forehead showing respectively differences in total absorbed amounts within 4 days in terms of ratio 1:1.6:1.56:2.97. (Hansen et al., 2008) reported different diffusion coefficient measures of caffeine after 1, 2 and 6 h that are $3.97 \cdot 10^{-08}$, $2.98 \cdot 10^{-08}$ and $1.82 \cdot 10^{-08}$ cm^2/h respectively. (Lotte et al., 1993) concluded no statistical individual differences in percutaneous absorption of caffeine due to race. (Roskos et al., 1989) investigated the effect of aging on

percutaneous absorption in man. The authors stated that a diminished surface lipid content of “old” skin (>65 years) implies a diminished dissolution medium for compounds administered topically. This physiologic change and the typically reduced hydration of aged *stratum corneum* have an impact on permeation of compounds whose lipid solubility is low like that of caffeine. (Chambin-Remoussenard et al., 1993) measured *in vivo* absorption of caffeine from two vehicles, an emulsion and an acetone solution, in 12 human volunteers. A surface recovery technique after a 6-h-application and a stripping method after a 30-min application of caffeine were performed on the volar aspect of the forearm. The permeability coefficient for caffeine in emulsion and acetone were $1.59 \cdot 10^{-04}$ and $9.53 \cdot 10^{-08}$ cm/h, respectively (ratio equals ca 1700).

Table 4.3.1 shows *in vivo* literature studies of caffeine absorption as a percent of an absolute dose applied on the skin that were used to verify the *in vivo* simulations of the PBTK model (described below) in terms of its parameters such as caffeine intake from formulation (k_{form}) by *stratum corneum*, diffusion coefficients in *stratum corneum* (D_{SC}), viable epidermis (D_{VE}) and hair follicles (HF) (D_{HF}), partition coefficients between *stratum corneum*/vehicle (PC_{SC}), between *stratum corneum*/viable epidermis (PC_{VE}) and between hair follicles and vehicle (PC_{HF}).

Table 4.3.1 *In vivo* caffeine permeation

Dose/ vehicle	Skin site	% of dose absorbed	Reference
4 $\mu\text{g}/\text{cm}^2$ over 13 cm^2 in acetone	Forearm	47.56 (*)	(Feldmann and Maibach, 1970)
Dose= 10 $\mu\text{g}/\text{cm}^2$ Area= 25 cm^2 in ethanol/ propylene glycol	Chest	Open HF: 57.4 Closed HF: 36	(Liu et al., 2011; Otberg et al., 2008)
4 $\mu\text{g}/\text{cm}^2$ in 1:1 aq ethanol/acetone	Abdominal skin	22.1	(Franz, 1978)
60 $\mu\text{g}/\text{cm}^2$ in ethylene glycol gel; 0.5 $\mu\text{g}/\text{cm}^2$ in petrolatum; 50 $\mu\text{g}/\text{cm}^2$ in water gel Area=20-60 cm^2	Abdominal skin	40.6 55.6 4	(Bronaugh and Franz, 1986)
1 Mmol/ cm^2 ^{14}C -labeled	Asian Black Caucasian ethnic skin	1.06 1.01 and 0.96	(Lotte et al., 1993)
21.7g/L in aq.solution	Young (22-40 years) Old (>65 years)	48.2 25.2	(Roskos et al., 1989)

(*) based on urine recovery % dermal dose/ % IV dose

Table 4.3.2 provides some literature-derived *in vitro* results used to calibrate the PBTK model for simulating *in vitro* permeation profiles of caffeine. In addition, Cosmetics Europe provided the experimental results on caffeine permeation through abdominal and cadaver skin (*stratum corneum*) in terms of diffusion and partition coefficient for caffeine in ethanol/propylene glycol/water vehicle. These parameters were used to simulate caffeine permeation (see below) for comparison with literature studies but could not be disclosed in this work.

Table 4.3.2 *In vitro* caffeine permeation

Dose/ vehicle	Human skin type	Diffusion coefficient (D [cm ² /h]); Permeation coefficient (Kp [cm/h])	Partition coefficients: PC _{SC} ; PC _{VE}	Max. abs. rate [µg/cm ² /h]	% of dose absorbed	Reference
4 mg/mL in ethanol/water	Breast and abdominal skin from surgical waste– full thickness	-	-	1.75	17.3	(Wilkinson et al., 2006)
4 mg/mL in ethanol/water	Breast, abdomen, leg from surgical waste	-	-	2.24	53.7	(van de Sandt et al., 2004)
260 mg/cm ² in O/W and W/O/W* (ethylene oxide/propylene oxide + oil phase)	Abdominal biopsies	O/W:D (SC+VE) = 3.852·10 ⁻⁶ W/O/W: D (SC+VE) = 1.523·10 ⁻⁶	-	-	O/W: 3.21 W/O/W: 1.25	(Doucet et al., 1998)
2.5 g/33.898 mL in ethanol sol.	Breast- full thickness	-	-	-	11.82	(Trauer et al., 2009)
4 g/cm ² in ethanol (280 µg/mL)	Full thickness	-	-	-	Trial1: 14 Trial2: 11.4	(Pugh et al., 2004)
Dose= 10 µg/cm ² in 17.6 µL of water sol.	Breast skin- full thickness	-	-	-	Open HF: 12 Closed HF: 5	(Liu et al., 2011)
383.4 mg/mL in aloe vera 367.6 mg/mL in water	Porcine ear skin	Kp (aloe vera) = 19.22·10 ⁻⁶ Kp (water) = 29.49·10 ⁻⁶	-	-	14.2 (aloe vera)	(Cole and Heard, 2007)
12.5 mg/mL in phosphate buffers	Abdominal surgical waste – <i>stratum corneum</i>	D _{SC} = 2.98·10 ⁻⁰⁸ (median value)	-	-	-	(Hansen et al., 2008)
10 mg/mL in ethanol/propylene glycol/water	Cadaver skin - <i>stratum corneum</i>	D _{SC} = CF (**)	PC _{SC} = CF (**)	-	-	Cosmetics Europe

1% Caffeine sol. in ethanol/propylene glycol/water	Abdominal surgical waste – full thickness	$D_{SC} = CF (**)$	$PC_{SC} = CF (**)$	-	-	Cosmetics Europe
5-10 $\mu\text{L}/\text{cm}^2$ of acetone; 1:1 aq ethanol/acetone	Abdominal skin	-	-	-	24.1 10.9-46.5	(Franz, 1978)
0.5 $\mu\text{g}/\text{cm}^2$ in ethylene glycol gel; 2, 60 $\mu\text{g}/\text{cm}^2$ in petrolatum; 10, 50 $\mu\text{g}/\text{cm}^2$ in water gel	Cadaver skin	$K_p = 7.2 \cdot 10^{-4}$, $6.2 \cdot 10^{-4}$ $K_p = 2.1 \cdot 10^{-4}$ $K_p = 5.1 \cdot 10^{-4}$, $5.6 \cdot 10^{-4}$	PC_{SC} (24 h) =1.5; (96 h) 3.3 PC_{SC} (24 h) =2.3 PC_{SC} (24 h) = 3.5; (96 h) = 3.2	-	61.8, 40.6 32.2 4.7, 5.1	(Bronaugh and Franz, 1986)
25.82 mg/mL in water	Upper leg – isolated epidermis	$K_{p_{VE}} = 2.23$ - $2.58 \cdot 10^{-4}$ $D_{SC} = 1.98 \cdot 10^{-7}$	$PC_{SC} = 1.79$	-	-	(Dias et al., 1999)
In water and in acetone	<i>Stratum corneum</i> abdomen	$K_{p_{SC}} = 0.0016$ -	-	-	- 33	(Southwell et al., 1984)
In 50% aq. ethanol	Breast	-	-	-	6.2	(Greaves et al., 2012)
High:15 mg/mL Low:320 $\mu\text{g}/\text{mL}$ Area=3.14 cm^2 in acetone (50 μL)	Excised abdominal skin	-	-	0.7 0.3	-	(Treffel et al., 1993)

(*) emulsion formulas that differ in oil/water phases

(**) CF - confidential data

From **Table 4.3.2** I selected five different *in vitro* studies that, in addition to providing *in vitro* parameters measures, reported permeated amount of caffeine in time through the investigated type of human skin necessary for validation of the simulated *in vitro* permeation profile by the PBTK model. The complete set of *in vitro* absorption parameters for these studies is provided in **Table 4.3.3**. They were either measured in these studies (in bold), estimated by means of QSPRs (in italic) with median value chosen (i.e. the partition coefficient between *stratum corneum* and viable epidermis- PC_{VE}) or fitted to/ estimated from published permeation profiles of caffeine (regular font).

Table 4.3.3 PBTK model optimisation of *in vitro* parameters (measured in bold, QSPR predicted in italic).

Dose	% of dose Abs.	D_{SC}, D_{VE} [cm^2/h]	PC_{SC}, PC_{VE}	k_{form} [mL/h]	Reference
260 mg/ cm^2 1% sol. Area= 1 cm^2	0.09 (W/O/W)* 0.216 (O/W)*	$D_{(SC+VE)} = 1.523 \cdot 10^{-6}$ (WOW) $D_{(SC+VE)} = 3.852 \cdot 10^{-6}$ (OW)	$PC_{SC} = 4$ (W/O/W) $PC_{SC} = 10$ (O/W) $PC_{VE} = 0.6$	0.06	(Doucet et al., 1998)
High:15 mg/mL Low:320 $\mu\text{g}/\text{mL}$	High: 4.054 Low: 32.004	$D_{SC} = 1.4 \cdot 10^{-7}$ $D_{VE} = 1.1 \cdot 10^{-6}$	$PC_{SC} = 0.38$ (high) $PC_{SC} = 3$ (low)	0.06	(Treffel et al., 1993)

Area=3.14 cm ² in acetone (50 µL)				$PC_{VE} = 0.6$	
4 mg/mL Area= 1.5 cm ² in ethanol/water (0.15 µL)	17.3 (opt.16.211)	$D_{SC} = 1.4 \cdot 10^{-7}$ $D_{VE} = 1.1 \cdot 10^{-6}$	$PC_{SC} = 2.5$ $PC_{VE} = 0.6$	0.06	(Wilkinson et al., 2006)
10 mg/mL in ethanol/propylene glycol/water Area=1.5 cm ² (800 µL)	0.634 0.636	$D_{SC} = CF (**)$ $D_{VE} = 1.5 \cdot 10^{-6}$	$PC_{SC} = CF (**)$ $PC_{VE} = 0.6$	0.06	Cosmetics Europe
25.82 mg/mL In water (1 mL) Area= 1 cm ²	0.455	$D_{SC} = 1.98 \cdot 10^{-7}$ $D_{VE} = 1.1 \cdot 10^{-6}$	$PC_{SC} = 1.79$ $PC_{VE} = 0.25$	0.06	(Dias et al., 1999)

(*) emulsion formulas that differ in oil/water phases

(**) CF - confidential data

Figures 4.3.2-4.3.6 show simulated versus measured results for different literature experiments.

In all the simulations I assumed 1 mL of applied solution on the skin surface. In the studies of (Treffel et al., 1993) and (Wilkinson et al., 2006) I used D_{SC} of $1.4 \cdot 10^{-7}$ cm²/h and the same values of viable epidermis parameters- the difference in using different vehicles in these two works is reflected only in modified *stratum corneum*/ vehicle partition coefficients: 1.79 for water, 2.5 for ethanol/water, 4 for W/O/W vehicle or 10 O/W vehicle and 0.38 (low concentration) -3 (high concentration) for acetone. Clearly, partition coefficient between *stratum corneum* and vehicle depends on type of vehicle and a measured substance concentration in it. The experimental data from (Wilkinson et al., 2006) for ethanol/ water vehicle and (Doucet et al., 1998) with specially prepared W/O/W and O/W vehicles were well estimated by the *in vitro* PBTK model (Figures 4.3.2-4.3.3) what is indicated by a good match of experimental points.

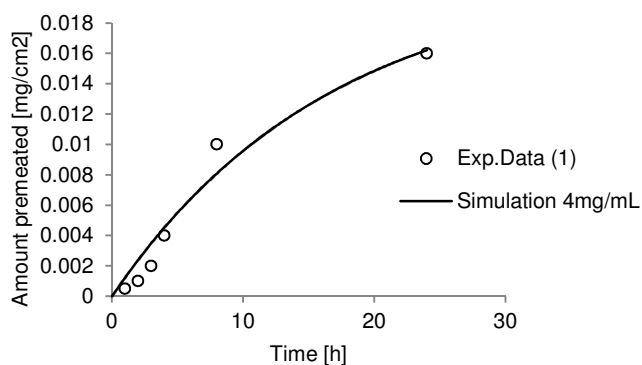


Fig 4.3.2. Simulated (*in vitro*) amount of caffeine permeated through the skin over 24 h: (1) (Wilkinson et al., 2006).

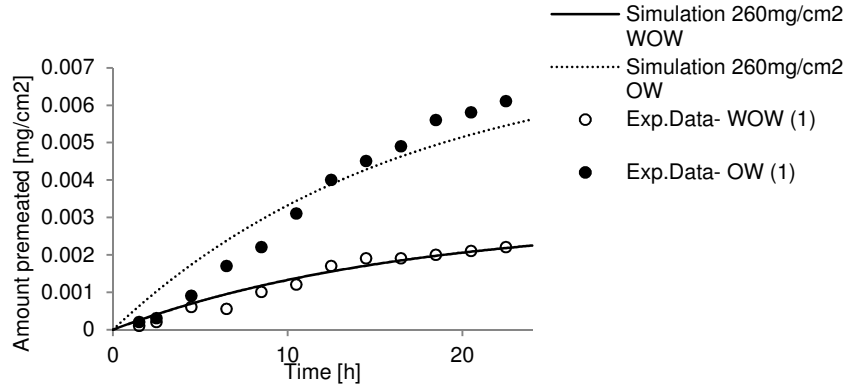


Fig 4.3.3. Simulated (*in vitro*) amount of caffeine permeated through the skin over 24 : (1) (Doucet et al., 1998).

Amount of caffeine permeated in time over skin area was well simulated also for the experimental results of (Treffel et al., 1993) under normal pressure, however only one experimental point at the end of experiment was available. Only determined timely fluxes in this study were not matched by the simulations (**Figure 4.3.4-right**). The reason could be that some of the absorption parameters such as caffeine release from vehicle (k_{form}) or diffusion coefficients (especially in *stratum corneum* as indicated by (Watkinson et al., 1992)) that are assumed constant in the model may vary with concentration of caffeine in the skin (Crank, 1975), depth of skin or time. However, calculated median values of flux over 24 h were found close to experimental ones: for 15 mg/mL: 0.000375 (experimental) and 0.000374 (simulated); and for 0.320 mg/mL: 0.000198 (experimental) and $6.38 \cdot 10^{-5}$ (simulated) $\text{mg}/\text{cm}^2/\text{h}$.

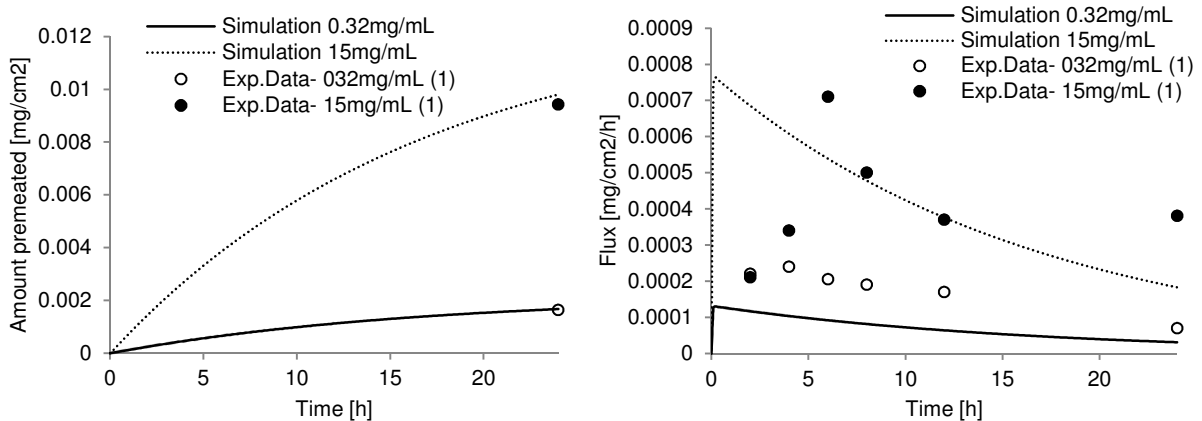


Fig 4.3.4. Simulated (*in vitro*) amount of caffeine permeated through the skin (left) and flux (right) over 24 h: (1) (Treffel et al., 1993)

Simulations of 800 μL of 10 mg/mL of caffeine applied on 1.5 cm^2 of skin over 22 h using experimentally derived parameters provided by Cosmetics Europe are presented in **Figure 4.3.5**. The experiments were performed on human frozen cadaver skin and abdominal skin. The measured parameters gave identical simulations. According to the simulations, 22 h of exposure to caffeine at given conditions results in total permeated amount of caffeine equal to 0.03 mg/cm^2 and maximal flux of 0.003 $\text{mg}/\text{h}/\text{cm}^2$ over 22 h.

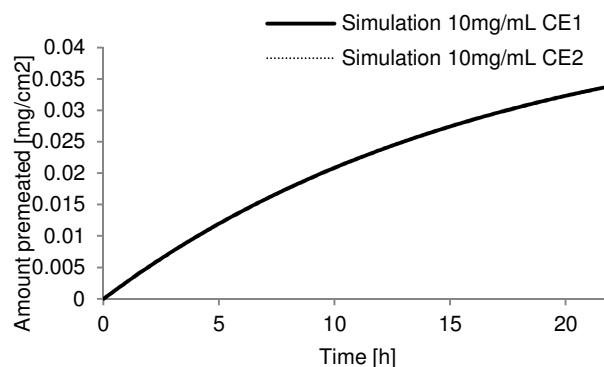


Fig 4.3.5. Simulated (*in vitro*) amount of caffeine permeated through the skin over 24: Cosmetics Europe (CE experiments 1 and 2) parameters.

(Dias et al., 1999) investigated a permeation of saturated caffeine solution in water through human viable epidermis (upper leg) providing almost complete set of absorption parameters. In this study they reported diffusion coefficient in *stratum corneum* ($1.98 \cdot 10^{-7} \text{ cm}^2/\text{h}$) together with *stratum corneum*/water partition coefficient (1.79) – for *stratum corneum* thickness of 15 μm – close to our assumed thickness of 17 μm . Permeation coefficient in viable epidermis was also provided and equal to $2.21 \cdot 10^{-4} \text{ cm}/\text{h}$ – diffusion coefficient was calculated by multiplying it by thickness of epidermis. Therefore only 2 parameters were left for optimisation: k_{form} and PC_{SCVE} (*stratum corneum*/viable epidermis partition coefficient). K_{form} of 0.06 proved to be an optimal solution also in this case but partition coefficient needed to be lowered from 0.6 to 0.25 in order to reach the estimated permeated amounts after 20 h. Unlike in the all previous studies, the experimental points were not well predicted by the PBTK model (there is a higher mismatch shown in **Figure 4.3.6**) but this is due to measured permeation only through the layer of extracted viable epidermis, whereas *in vitro* PBTK model takes into account all the skin layers excluding mix with a blood in the dermis part.

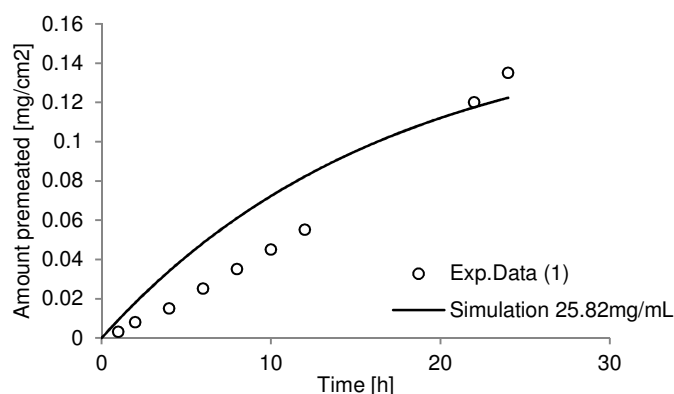


Fig 4.3.6. Simulated (*in vitro*) amount of caffeine permeated through the skin over 24 h: (1). Experimental data for permeation through viable epidermis (Dias et al., 1999).

In the second step of the correlation strategy, I used *in vivo* caffeine levels in plasma following skin absorption with open and closed hair follicles (Otberg et al., 2008) to optimise some of the parameters. **Table 4.3.4** provides the final parameter values. D_{SC} , PC_{SC} and PC_{VE} (calculated by using QSPRs) were taken from *in vitro* studies of (Wilkinson et al., 2006) because the vehicle was similar (ethanol/water vs. ethanol/ propylene glycol). Diffusion coefficient in *stratum corneum* equal to $1.40 \cdot 10^{-7} \text{ cm}^2/\text{h}$ was used as reported by (Hansen et al., 2008). The remaining parameters: D_{HF} , D_{VE} , k_{HF} and k_{form} were optimised because of obviously different permeation properties of viable epidermis *in vivo* (when linked to dermis and blood flow) and enhanced action of follicles, not considered in the *in vitro* experiment. I assumed partition coefficient between hair follicles (PC_{HF}) and solvent to be equal to 1 because of lack of information about it. Simulated versus experimental concentration-time points are shown in **Figure 4.3.7** for a reference male subject (body weight: 75 kg). The *in vivo* PBTK model uses different percentage of skin available for permeation from 100% with open hair follicles to 80% with closed hair follicles according to optimisation results best fitting the experimental values.

Table 4.3.4. PBTK model optimisation of *in vivo* parameters (taken from *in vitro* studies in bold)

Dose	% of dose Abs.	Diffusion coefficients[cm^2/h]	Partition coefficients	k_{form} [mL/h]	Reference
0.250mg in 0.06mL Ethanol/ propylene glycol	Open HF*= 87.11	$D_{SC} = 1.40 \cdot 10^{-7}$ $D_{VE} = 1.50 \cdot 10^{-5}$	$PC_{SC} = 2.5$ $PC_{VE} = 0.6$	$k_{form} = 0.2$ $k_{HF} = 0.153$	(Otberg et al., 2008)
	Closed HF*= 75.153	$D_{HF} = 1.24 \cdot 10^{-5}$	$PC_{HF} = 1$		

(*) HF-hair follicles

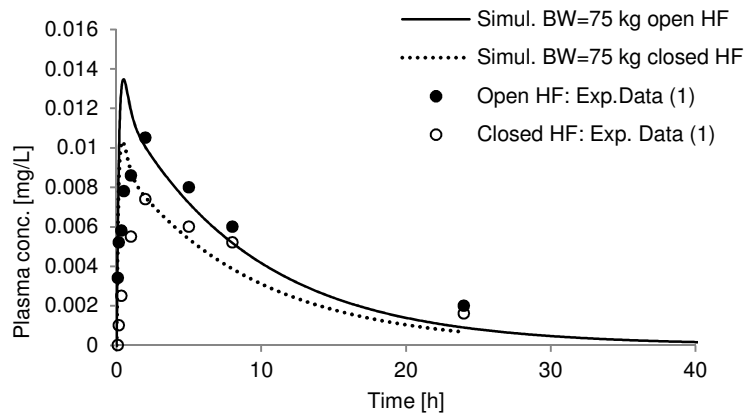


Fig 4.3.7. Plasma concentrations of caffeine after *in vivo* dermal absorption: 1.(Otberg et al., 2008).

In the third and final step, *in vitro* to *in vivo* correlation of permeated amount of caffeine in time was performed for the experimental design of (Otberg et al., 2008) with 4 h of exposure to caffeine (*in vitro* parameters of (Wilkinson et al., 2006) were used). **Figure 4.3.8** shows the permeation differences in *in vitro* and *in vivo* model simulations. *In vivo* results are ca. 6-9 times higher than *in vitro* estimates. The $IVIV_{skin}$ ratio based on the maximal permeated amount to receptor was equal to 0.133 for absorption with open follicles and 0.177 for absorption with closed follicles.

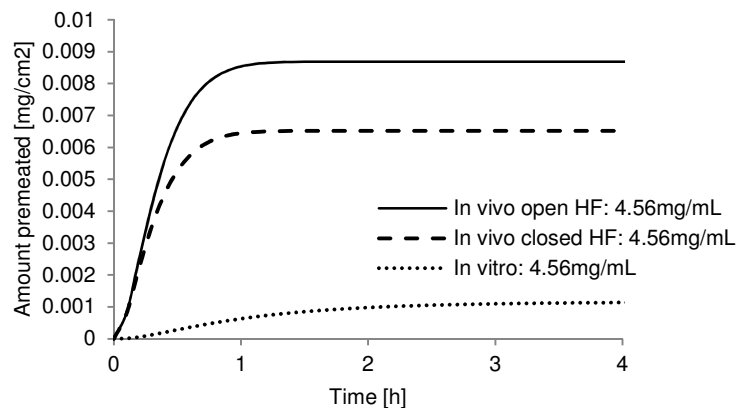


Fig 4.3.8. *In vitro*- to- *in vivo* correlation of caffeine permeation.

In vivo permeation (Otberg et al., 2008) was already concluded in literature to be higher than *in vitro* one following the same exposure settings such as concentration of caffeine, skin area, and exposure time (Liu et al., 2011). This is probably because the *in vitro* skin model under-predicts the amount absorbed due to experimental factors such as the permeability of the extracted part of the skin, the experimental temperature and the relatively semi-static conditions (periodical renewal of the acceptor medium) when compared to the *in vivo* situation, in which the systemic circulation provides a continuous perfusion of the skin compartment. I further applied the PBTK modelling validated on variety of experimental data to confirm this observation and to calculate a correlation factor ($IVIV_{skin}$).

In both *in vivo* and *in vitro* modelling the following assumptions were additionally taken: (i) the absorption parameters including formulation uptake and diffusion coefficients were assumed constant in time; however diffusion and partition coefficients were different for *stratum corneum*, viable epidermis and hair follicles (if considered- *in vivo* case only); (ii) influence of different skin anatomical origin on permeation was neglected; (iii) inter-individual differences in skin permeation were neglected.

b) Coumarin

Human exposure to coumarin via skin is very frequent as it is used as a fragrant ingredient in many cosmetic and personal care products. However, there are fewer *in vitro* and *in vivo* studies available in the literature than for caffeine. Coumarin absorption has been shown in *in vitro* studies to be largely affected by the vehicle type and exposed skin area: (i) when ethanol was used as a vehicle, 58.2 ± 2.32 % was absorbed after 6 h and 63.5 ± 0.16 % after 24 h, whereas when coumarin was applied in oil-in-water emulsion, 94.3 ± 5.41 % was absorbed after 6 h and 96.9 ± 0.01 % after 24 h (Yourick and Bronaugh, 1997); (ii) when the surface area of application was increased from 4.9 to 30 cm², absorbed percent of applied dose rose from ca. 9 up to 66 % in 24 h (hydrophilic ointment was used as a vehicle and Sprague-Dawley rats as subjects (Ritschel and Hussain, 1988)). In addition to it, the epidermal/dermal tissue represented the major limiting barrier for coumarin absorption, not *stratum corneum* (Yourick and Bronaugh, 1997). (Ford et al., 2001) carried out *in vivo* skin absorption experiment on 3 male subjects under conditions similar to those encountered while using a typical consumer product with higher coumarin concentration and alcohol as a vehicle. Exposure time of 6 h was chosen including 30 min of alcohol evaporation and occlusion afterwards. A total of ca. 59.7 % (44 % for the rat skin) of the applied dose was absorbed after 120 h (90 % of it was cleared within 24 h, 59 % was excreted in urine and 1.1 % in feces). Rat studies showed also higher coumarin elimination in feces (up to 21 % of the absorbed dose) but slightly less in urine (up to 50 % of the absorbed dose). Published results of *in vivo* experiments for humans are shown in **Table 4.3.5** and of *in vitro* studies (in bold) in **Table 4.3.6** together with QSPR predictions (in italic) and PBTK model optimised/ calculated remaining parameters (regular font) for (Ritschel et al., 1989) only (just in this work permeated amount of coumarin in time was provided). Higher absorption was found *in vitro* through scalp skin when compared to abdominal skin (Ritschel et al., 1989) – **Figure 4.3.9**.

Table 4.3.5. *In vivo* dermal absorption of coumarin

Dose/ vehicle	Skin site	% of dose absorbed	Reference
0.02 mg/cm ² in 70% aq. Ethanol	Back	54.5, 62.4, 62.2	(Ford et al., 2001)
In 70% aq ethanol	Back	59.7	(Beckley-Kartey et al., 1997)

Table 4.3.6. *In vitro* dermal absorption of coumarin (measured in bold, QSPR predicted in italic).

Dose/ vehicle	Human skin type	Diffusion coefficient (D [cm ² /h]); Permeation coefficient (Kp [cm/h])	Partition coefficients:	k _{form} [mL/h]	% of dose absorbed	Reference
0.194 mg/mL in phosphate buffer pH= 7.4	Abdominal	D_{SC}= 2.34·10⁻⁰⁷	PC _{SC} = 1.65	0.035	6.267	(Ritschel et al., 1989)
	Scalp	D_{SC}= 1.044·10⁻⁰⁶ Kp= 9.1·10⁻⁰³ Kp= 12.05·10⁻⁰³ <i>D_{VE}= 2·10⁻⁰⁵</i> <i>D_{VE}= 1·10⁻⁰⁴</i>	<i>PC_{VE}= 1.828</i>	0.046	7.648	
0.5 µCi per cell in ethanol (15 µL/cm ²) and oil-in-water (3 mg/cm ²)	Abdominal viable skin	-	-	-	58.2 (6 h), 63.5 (24 h) 94.3 (6 h), 96.9 (24 h)	(Yourick and Bronaugh, 1997)
3.7 µg/cm ² in 0.02 % in ethanol	Viable skin	-	-	-	50.4	(Beckley-Kartey et al., 1997)

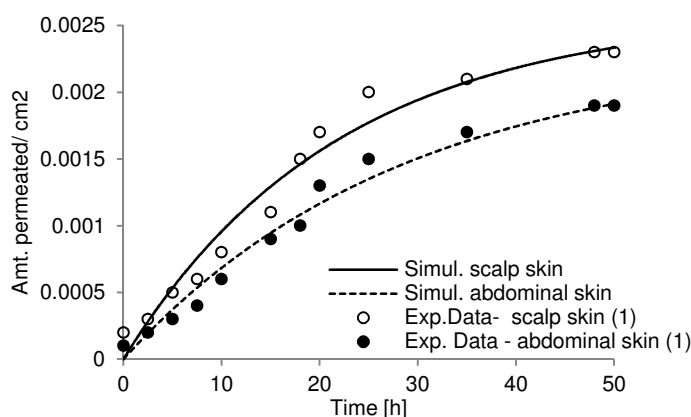


Fig 4.3.9. Coumarin permeation *in vitro*: (1) (Ritschel et al., 1989)

In vivo optimised PBTK model absorption parameters with respect to individual plasma concentrations of three male subject (Ford et al., 2001) are in **Table 4.3.7**. Diffusion coefficients and formulation uptake were scaled to higher values *in vivo* when compared to *in vitro* results, whereas similar skin partition coefficients were used in both cases even though the vehicle was different (this is an assumption due to lack of experimental results). QSPRs were used to estimate median permeability and partition coefficients of coumarin in viable epidermis. However, minimum (0.019 cm/h), instead of median (0.215 cm/h), value of QSPR predictions for permeability coefficient in viable epidermis was used because the median value was 1000 times higher from optimised permeability in *stratum corneum* what could be concluded to be rather unrealistic. **Figure 4.3.10** shows simulated versus experimental points for the three individuals.

Table 4.3.7. *In vivo* optimised parameters (measured in bold, QSPR predicted in italic).

Dose/ vehicle	Human skin type	Diffusion coefficient (D [cm ² /h])	Partition coefficients: PC _{SC} ; PC _{VE}	k _{form} [mL/h]	% of dose absorbed	Reference
0.02 mg/cm ² in 70 % aq. Ethanol Area=100 cm ²	Back	D _{SC} = 2.5 ·10 ⁻⁰⁶ D _{VE} = 9 ·10 ⁻⁰⁵	PC _{SC} = 1.65 PC _{VE} = 1.828	0.22	54.308	(Ford et al., 2001)

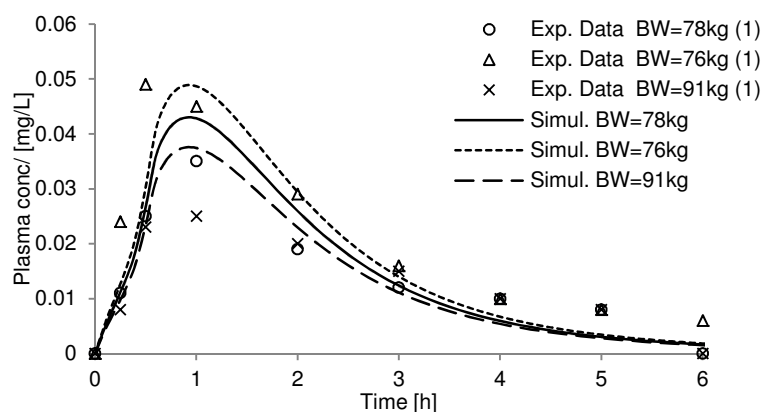


Fig 4.3.10. *In vivo* absorption of coumarin in three subjects: (1) (Ford et al., 2001).

In vitro –to- *in vivo* correlation was finally done in a similar manner to caffeine case study. Application conditions according to *in vivo* experiment (Ford et al., 2001) were used to perform PBTK model simulations with *in vivo* and *in vitro* parameters. Amount permeated in time over 100 cm² of exposed skin area is presented in **Figure 4.3.11** for both scenarios. IVIV ratio between *in vitro* maximal amount permeated and *in vivo* one was calculated to be 0.61 for the scalp skin and 0.427 for the abdominal skin- little bit higher than for caffeine. Nevertheless, *in vitro* absorption is still smaller than estimated *in vivo*. Lack of complete harmonization of both studies is again due to vehicle type (ethanol versus phosphate buffer) and anatomical skin site (abdomen and scalp skin versus back) for which the parameters were calibrated.

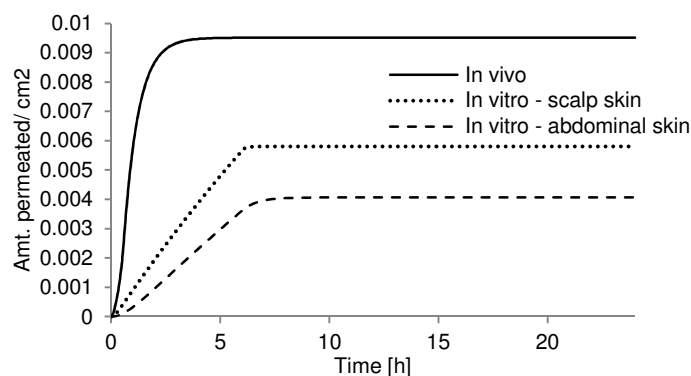


Fig 4.3.11. *In vitro* –to- *in vivo* correlation of coumarin permeation.

Skin metabolites

QSAR toolbox²⁹ (v3.1) has been used to generate potential skin metabolites of coumarin and caffeine. Skin metabolism simulator mimics the metabolism of chemicals in the skin compartment. Given the lack of reported skin metabolism data and the widespread hypotheses is that skin enzymes can metabolise absorbed xenobiotics via reactions analogous to those determined in liver, the simulator was developed as a simplified mammalian liver metabolism simulator. The skin metabolism simulator contains a list of hierarchically ordered principal transformations, which can be divided into two main types – rate-determining and non-rate-determining. The rate-determining transformations are phase I and phase II, such as C-hydroxylation, ester hydrolysis, oxidation, glutathione conjugation, glucuronidation, sulfonation. The non-rate-determining transformations include molecular transformations of highly reactive intermediates. The simulator starts by matching the parent molecule with the reaction fragments associated with the transformation having the highest probability of occurrence. This produces a set of first level metabolites. Each of these derived metabolites is then submitted to the same list of hierarchically ordered transformations, to produce a second level of metabolites. The procedure is repeated until a constraint for metabolism propagation is satisfied (e.g. low probability of obtaining a metabolite or application of Phase II reaction). The only resulting structure of potential coumarin metabolite was umbelliferone (CAS: 93-35-6) – see **Figure 4.3.12a** and of potential caffeine metabolite was caffeidine acid (CAS: 54536-15-1) - see **Figure 4.3.12b**. In case of caffeine, the 6-membered ring opening is achieved through the hydrolysis of the amide in alkaline environment. However, no experimental studies yet exist to confirm that this chemical species is indeed generated in human skin. Caffeidine acid could not be found in liver metabolism experiments or generated through liver metabolism simulators. It was only found in microbial simulators and dedicated chemical reactivity simulations (basic hydrolysis). Umbelliferone (7-HC), on the other hand, was predicted as a potential product of phase I metabolism of coumarin in the liver via hydroxylation of fused benzenes and confirmed by the experiments. Nevertheless, this compound was not confirmed as a skin metabolite. With no experimental proof of the formation of these metabolites, I did not consider them in the PBTK model simulations.

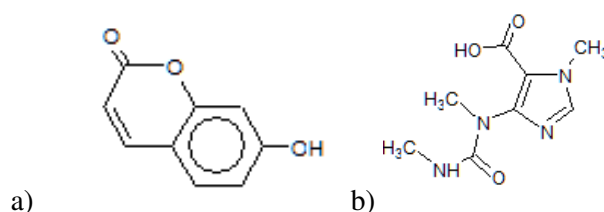


Fig 4.3.12. QSPR toolbox predicted skin metabolites of a) coumarin, b) caffeine (not considered in the PBTK model simulations).

²⁹ <http://www.QSARtoolbox.org/> (last access: 06.10.2014)

4.3.2 Liver clearance

In this section I correlated measured *in vitro* and scaled to *in vivo* differences in liver clearance for selected case study compounds (coumarin, estragole, hydroquinone and caffeine) by means of IVIV factor that indicates here a ratio between liver $AUC_{in\ vitro}$ and $AUC_{in\ vivo}$ (**Equation 4.3.2**). I believe that using AUC is more appropriate than C_{max} because it better reflects the difference in elimination phase using different rates – for lower rates the half-life of a compound is longer and it stays longer in the body what may result in different toxicological responses and bioaccumulation. I limited the study showing differences in liver concentrations following selected oral exposure scenarios only. In general, oral absorption produces higher internal concentrations of absorbed chemicals than other exposure routes and thus shows clearer differences in clearance. Liver metabolism rates (Michaelis-Menten parameters: V_{max} , K_m or first order rate of formation: K_{met}) of coumarin, hydroquinone, caffeine and estragole determined in *in vitro* experiments available in literature are presented in **Table 4.3.8**.

$$IVIV_{liver} = \frac{AUC_{in\ vitro}}{AUC_{in\ vivo}} \quad (4.3.2)$$

These rates were scaled to *in vivo* values by some of the authors (**Table 4.3.9**) for all the compounds except for caffeine. Liver *in vitro* metabolism rates of caffeine were measured in terms of recombinantly expressed enzymes V_{max}^{CYP} [$pmol \cdot h^{-1} \cdot pmol\ CYP^{-1}$]. A combination of human microsomal protein per gram liver (MPPGL) [$mg_{protein}/g_{liver}$] together with hepatic enzyme abundance ($CYP_{content}$ [$pmol\ CYP/mg_{protein}$]) was used to scale data from recombinantly expressed enzyme systems (Barter et al., 2007). A correction for any difference in intrinsic enzyme activity from that of the native enzyme in human liver would be additionally required once this information is available. V_{max} rates [$mg/h/g_{liv}$] were scaled according to:

$$V_{max}^{CYP} \cdot MW \cdot 10^{-9} \cdot CYP_{content} \cdot MPPGL$$

Where :

$$MPPGL = 10^{(-0.3 \cdot \text{LogAge} + 2.04)} \quad (4.3.3)$$

Where: age=21 (Lelo et al., 1986) giving MPPGL = 43.988.

The PBTK model was further used to validate the scaled values and/or optimise them when necessary with respect to available *in vivo* blood or plasma concentrations. Due to limited number of such data optimisation was performed only for the main metabolites formed (**Table 4.3.10**).

Liver clearance rates were calculated from Michaelis-Menten parameters: V_{max} , K_m by dividing V_{max}/K_m and scaling to a body weight for *in vivo* clearance and per gram liver for *in vitro* clearance. Independently, both *in vitro* and *in vivo* parameters were used in the oral PBTK model to simulate concentration-time profiles of caffeine in the liver and to calculate resulting AUC.

Table 4.3.8. *In vitro* metabolism rates in the liver from literature

Substance and dosing conditions	Investigated material	Metabolism rates V_{max} [mg/h/gliv] and K_m [mg/L] or K_{met} [L/h/gliv]	Overall liver clearance rate [L/h/gliv]	Reference
Coumarin (CMR) Concentrations: 0-4000 μ M in 1% (v/v) in DMSO	Liver microsomes, hepatic microsomes	CMR to o-HPA V_{max} =0.49; 0.405-1.507 K_m = 397.508; 192.908-1084.379		(Rietjens et al., 2008)
50 μ M coumarin in 1mL of potassium phosphate buffer, pH 7.4		CMR to 7-HC V_{max} = 0.644 K_m = 0.278 CMR to 3-HC K_{met} = 0.0058 o-HPA to o-HPAA V_{max} = 1.807; 1.438- 4.689 K_m = 0.140; 0.089- 23.962 o-HPA to o-HPE V_{max} = 0.761 K_m = 2.437	2.324	(Born et al., 2000) (Vassallo et al., 2004)
45, 227 and 2270 μ M of hydroquinone (HQ)	Isolated hepatocytes	HQ to HQ-SG (glutathione conjugates) V_{max} = 20.623 K_m = 30.500 HQ to HQ- Gluc (glucuronide) V_{max} = 55.976 K_m = 5.065	11.728	(Poet et al., 2004)
Caffeine (CAF) 0.05-2 mmol/L in sodium phosphate buffer pH= 7.4	Microsomal preparations from human β -lymphoblastoid cell lines Human cytochrome P-450 isoenzymes (CYPs) expressed in human B-lymphoblastoid cell lines: CYP1A1, 1A2, 2A6, 2B6, 2D6-Val, 2E1, 3A4; and microsomal epoxide hydroxylase (EH)	CAF to theobromine 1A1: V_{max} = $1.8 \cdot 10^{-4}$; K_m = 79.62 1A2: V_{max} = 0.001; K_m = 31.07 2D6-Met: V_{max} = 0.023; K_m = 3087.62 2E1: V_{max} = $1.7 \cdot 10^{-4}$; K_m = 279.63 CAF to theophylline 1A2: V_{max} = $4 \cdot 10^{-4}$; K_m = 48.55 2D6-Met: V_{max} = 0.052; K_m = 2427.38 2E1: V_{max} = $1.2 \cdot 10^{-4}$; K_m = 163.12 CAF to paraxanthine 1A1: V_{max} = $6 \cdot 10^{-4}$; K_m = 114.57 1A2: V_{max} = 0.0103; K_m = 36.90 2D6-Met: V_{max} = 0.046; K_m = 2136.09	0.0004	(Ha et al., 1996)

		CAF to trimethyluric acid 1A1: $V_{max} = 8 \cdot 10^{-4}$; $K_m = 50.49$ 1A2: $V_{max} = 7 \cdot 10^{-4}$; $K_m = 52.43$ 2D6-Met: $V_{max} = 0.017$; $K_m = 1772.96$ 2E1: $V_{max} = 0.001$; $K_m = 201.96$ 3A4: $V_{max} = 0.005$; $K_m = 8932.74$	
Estragole (EST) 10-400 μ M	Human liver microsomes	EST to 4-Allylphenol: $V_{max} = 0.108$ $K_m = 42.978$	(Punt et al., 2009)
		EST to 1'-hydroxyestragole $V_{max} = 0.208$ $K_m = 3.112$	0.096
		EST to 3'-hydroxyanethole $V_{max} = 0.384$ $K_m = 51.87$	
		EST to estragole-2',3'-oxide V_{max} [mg/h/g liver] = 0.242 $K_m = 12.301$	

Table 4.3.9. Scaled *In vivo* metabolism rates in the liver from literature

Substance and dosing conditions	Metabolism rates V_{max} [mg/h/kg BW] and K_m [mg/L] or K_{met} [L/h/kg BW]	Overall liver clearance rate [L/h/kg BW]	Reference
Coumarin (CMR) Concentrations: 0-4000 μ M in 1% (v/v) in DMSO	CMR to o-HPA $V_{max} = 12.714$ $K_m = 397.508$		(Rietjens et al., 2008)
	CMR to 7-HC: $V_{max} = 16.806$ $K_m = 0.278$	60.486	
	CMR to 3-HC: $K_{met} = 0.001$		
	o-HPA to o-HPAA: $V_{max} = 144.998$ $K_m = 0.140$		
	o-HPA to o-HPE: $V_{max} = 60.994$ $K_m = 2.437$		
Hydroquinone (HQ) 275mg	HQ to benzoquinone $V_{max} = 4.8-8.3$ (last taken) $K_m = 5.05$		(Corley et al., 2000)
	HQ to HQ-glucuronide $V_{max} = 120$ $K_m = 5$	37.644	
	HQ to HQ-sulfate $V_{max} = 60$		

	Km= 5	
	Benzoquinone to HQ-glutathione V _{max} = 20 Km= 0.5	
Estragole (EST)	EST to 4-Allylphenol: V _{max} [mg/h/gliv] =0.1037 Km= 42.978	
	EST to 1'-hydroxyestragole V _{max} [mg/h/gliv] = 0.207 Km= 3.112	0.096 L/h/gliv
	EST to 3'-hydroxyanethole V _{max} [mg/h/gliv] = 0.3853 Km= 51.87	
	EST to estragole-2',3'-oxide V _{max} [mg/h/gliv] = 0.237 Km= 12.301	(Punt et al., 2009)

Table 4.3.10. *In vivo* optimised liver metabolism by the PBTk model

Substance	Metabolism rates V _{max} [mg/h/kg BW] and Km [mg/L] or Kmet [L/h/kg BW]	Overall liver clearance rate [L/h/kg BW]
Coumarin (CMR)	CMR to 7-HC: V _{max} = 2.5 Km= 0.278	9.030
Hydroquinone (HQ)	HQ to HQ-glucuronide V _{max} = 28 Km= 5	19.240
Caffeine (CAF)	CAF to theobromine V _{max} = 0.0432 Km= 1	
	CAF to theophylline V _{max} = 0.0072 Km= 1	0.120
	CAF to Paraxanthine V _{max} = 0.3514 Km= 1	
	CAF to Trimethyluric acid Kmet= 0.001	

In vitro metabolism rates of coumarin (Born et al., 2000; Rietjens et al., 2010; Vassallo et al., 2004) were scaled using MPPGL = 35 mg/gliv as provided by the authors. Literature *in vivo* clearance was assumed equal to *in vitro* measurements scaled up to the body weight. The optimised clearance with respect to blood/plasma concentration following oral and dermal coumarin absorption (Ford et al., 2001; Ritschel et al., 1979) was found 8.1 times lower. (Ritschel et al., 1977) reported coumarin clearance rate following oral absorption to be equal to 1.354 L/h/BW what is even 5.5 times lower than the optimised result. **Figure 4.3.13** shows the differences in concentration-time profiles in the liver with *in vitro*-derived and *in vivo*- optimised

liver clearance rates of coumarin. When compared to clearance parameters of (Rietjens et al., 2010) I modified only *in vivo* V_{max} rate of coumarin to 7-HC (from 16.806 to 2.5 mg/h/kg BW). 7-HC is the main metabolite of coumarin in humans and CYP2A6 is responsible for its formation. $IVIV_{liver}$ ratio was equal to 0.147 indicating higher clearance *in vitro*.

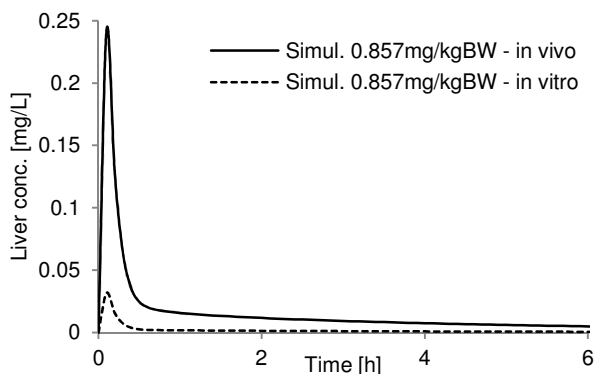


Fig 4.3.13. Coumarin concentrations in liver using *in vitro* and *in vivo* parameters. Oral dosing conditions according to (Ritschel et al., 1979).

For Hydroquinone I used *in vitro* rates determined by (Poet et al., 2004) in isolated hepatocytes. However, the rate of hydroquinone metabolism to benzoquinone was not determined (CYP450) therefore IVIV correlation was done based on sulfonation and glucuronidation only (HQ sulfate and glucuronide). *In vitro* rates were scaled to liver weight of 69kg- man. From among literature scaled to *in vivo* parameters (Corley et al., 2000), I modified V_{max} of hydroquinone to hydroquinone glucuronide from 120 to 28 mg/h/kg BW. Simulated *in vitro* (excluding metabolism to benzoquinone), literature *in vivo* and the optimised *in vivo* liver concentrations are presented in **Figure 4.3.14**. $IVIV_{liver}$ was calculated to be 0.063 indicating again higher clearance *in vitro*.

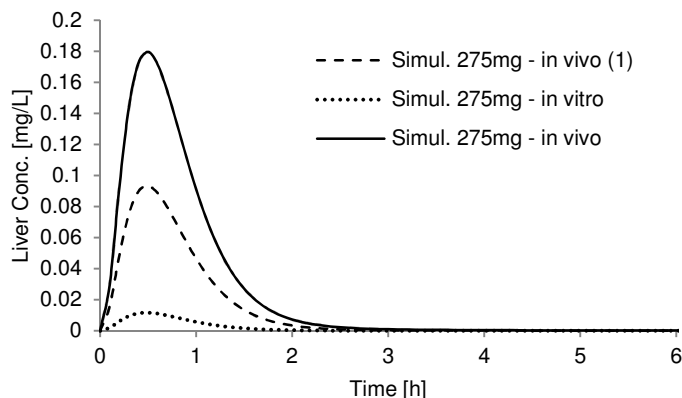


Fig 4.3.14. Hydroquinone concentrations in liver using *in vitro* and *in vivo* parameters (literature and optimised). Oral dosing conditions and *in vivo* parameters (1) according to: (Corley et al., 2000).

Caffeine undergoes 1-,3- and 7-N-demethylation and C-8-oxidation in rats. The CYP1A2 responsible for N-demethylation but C-8-oxidation of caffeine is the most important elimination route *in vivo* (catalyzed by CYP1A2, 2B1, 2E1, 3A1). In humans, in similar way, more than one CYP can be involved in caffeine biotransformation (N-demethylation, C-8-oxidation). CYP1A2 seems to have the highest intrinsic clearance cells due to its abundance in the liver and therefore it should be considered as the most important isoenzyme in caffeine metabolism. Caffeine showed comparable affinity to its homologue CYP1A1 and another important low-affinity high-capacity CYP isoenzyme - CYP2D6-Met. Paraxantine formation ca 70% of caffeine metabolism (Lelo et al., 1986). AUC in plasma after oral administration showed paraxanthine: theobromine: theophylline =42: 9: 8 % of that of unchanged caffeine (Ha et al., 1996). From the study of (Lelo et al., 1986) it could be concluded that the ratio of average plasma concentrations of paraxanthine: theobromine: theophylline equal to 1: 0.35: 0.1. The sum of all enzymes clearance rates was equal to 4.23E-05 L/h/gliv. Independently, the *in vivo* liver clearance was calibrated by fitting the PBTK model to available *in vivo* plasma concentrations, which resulted in 0.120 L/h/BW. These values were scaled with respect to 83 kg-man (and his liver weight). The latter value represents average fitting results with respect to 1-16 subjects receiving a single oral dose of caffeine (Csajka et al., 2005; Lelo et al., 1986) and validated for a similar oral absorption study (Newton et al., 1981) and dermal absorption experiment performed on 6 subjects with mean results published (Otberg et al., 2008).

Figure 4.3.15 shows liver concentrations of caffeine with *in vitro*- derived and *in vivo* -fitted caffeine clearance rates. Oral dosing conditions of 270 mg of caffeine in a gelatin capsule (Lelo et al., 1986) was used for an average body weight of 83 kg. The $IVIV_{liver}$ value was estimated to be ca. 2.3 indicating higher *in vivo* clearance when compared to previous case studies.

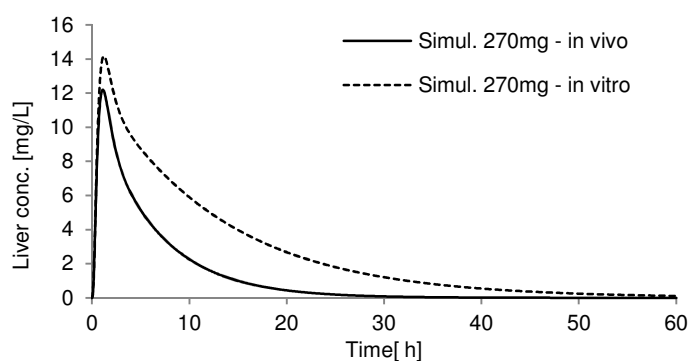


Fig 4.3.15. Caffeine concentrations in liver using *in vitro* and *in vivo* optimised parameters. Oral dosing conditions according to (Lelo et al., 1986).

Estragole phase 1 metabolism (detoxification of estragole) includes: o-demethylation, epoxidation and 3'-hydroxylation of estragole. Sulfonation of 1'-hydroxyestragole leads to formation of carcinogenic metabolite- 1'-sulfoxyestragole- that is unstable and degrades in aqueous environment to reactive carbocation able to form DNA adduct. 1'-hydroxyestragole glucuronide is a stable metabolite found in urine.

Dose dependent effects in metabolism have been observed: at low doses o-demethylation predominates, at high doses – glucuronidation of 1'-hydroxyestradiol as well as species differences: in rats sulfonation of 1'-hydroxyestradiol is more efficient (Punt et al., 2009). As suggested by some of the authors, using liver zonation in the PBTK model helps getting better predictions because metabolism doesn't occur uniformly across the liver. Only in this case, I used 3 liver zones to better quantify 1 and 2nd phases of metabolism in the following way:

For estradiol:

$$\text{- Zone 1: } \frac{dA_{liv,1}}{dt} = Fl_{GIT} + f_{liv} \cdot \left(C_{art} - \frac{C_{liv,1}}{PC_{liv}} \right) \quad (4.3.4)$$

$$\text{- Zone 2: } \frac{dA_{liv,2}}{dt} = f_{liv} \cdot \left(\frac{C_{liv,1}}{PC_{liv}} - \frac{C_{liv,2}}{PC_{liv}} \right) \quad (4.3.5)$$

$$\text{- Zone 3: } \frac{dA_{liv,3}}{dt} = f_{liv} \cdot \left(\frac{C_{liv,2}}{PC_{liv}} - \frac{C_{liv,3}}{PC_{liv}} \right) - \frac{V_{max1} \cdot \frac{C_{liv,3}}{PC_{liv}}}{Km_1 + \frac{C_{liv,3}}{PC_{liv}}} - \frac{V_{max2} \cdot \frac{C_{liv,3}}{PC_{liv}}}{Km_2 + \frac{C_{liv,3}}{PC_{liv}}} - \frac{V_{max3} \cdot \frac{C_{liv,3}}{PC_{liv}}}{Km_3 + \frac{C_{liv,3}}{PC_{liv}}} - \frac{V_{max4} \cdot \frac{C_{liv,3}}{PC_{liv}}}{Km_4 + \frac{C_{liv,3}}{PC_{liv}}} \quad (4.3.6)$$

where: V_{max1} , Km_1 refer to 4-allylphenol, V_{max2} , Km_2 refer to 1-hydroxyestradiol, V_{max3} , Km_3 refer to 3-hydroxyanethole and V_{max4} , Km_4 refer to estradiol-2,3-oxide. For 1-hydroxyestradiol:

$$\text{- Zone 1: } \frac{dA_{liv,met,1}}{dt} = f_{liv} \cdot \left(C_{art,met} - \frac{C_{liv,met,1}}{PC_{liv,met}} \right) - \frac{V_{max1,met} \cdot \frac{C_{liv,met,1}}{PC_{liv,met}}}{Km_{1,met} + \frac{C_{liv,met,1}}{PC_{liv,met}}} - \frac{V_{max2,met} \cdot \frac{C_{liv,met,1}}{PC_{liv,met}}}{Km_{2,met} + \frac{C_{liv,met,1}}{PC_{liv,met}}} \quad (4.3.7)$$

$$\text{- Zone 2: } \frac{dA_{liv,met,2}}{dt} = f_{liv} \cdot \left(\frac{C_{liv,met,1}}{PC_{liv,met}} - \frac{C_{liv,met,2}}{PC_{liv,met}} \right) \quad (4.3.8)$$

$$\text{- Zone 3: } \frac{dA_{liv,met,3}}{dt} = f_{liv} \cdot \left(\frac{C_{liv,met,2}}{PC_{liv,met}} - \frac{C_{liv,met,3}}{PC_{liv,met}} \right) - \frac{V_{max3,met} \cdot \frac{C_{liv,met,3}}{PC_{liv,met}}}{Km_{3,met} + \frac{C_{liv,met,3}}{PC_{liv,met}}} + \frac{V_{max2} \cdot \frac{C_{liv,3}}{PC_{liv}}}{Km_2 + \frac{C_{liv,3}}{PC_{liv}}} \quad (4.3.9)$$

Where: $V_{max1,met}$, $Km_{1,met}$ refer to 1-sulfoxyestradiol, $V_{max2,met}$, $Km_{2,met}$ refer to 1-hydroxyestradiol glucuronide and $V_{max3,met}$, $Km_{3,met}$ refer to 1-oxoestradiol.

Figure 4.3.16 shows the differences in simulating 1-hydroxyestradiol concentrations in the liver and plasma with respect to *in vivo* data with and without liver zonation. Unfortunately no experimental data for estradiol are currently available to further validate this concept.

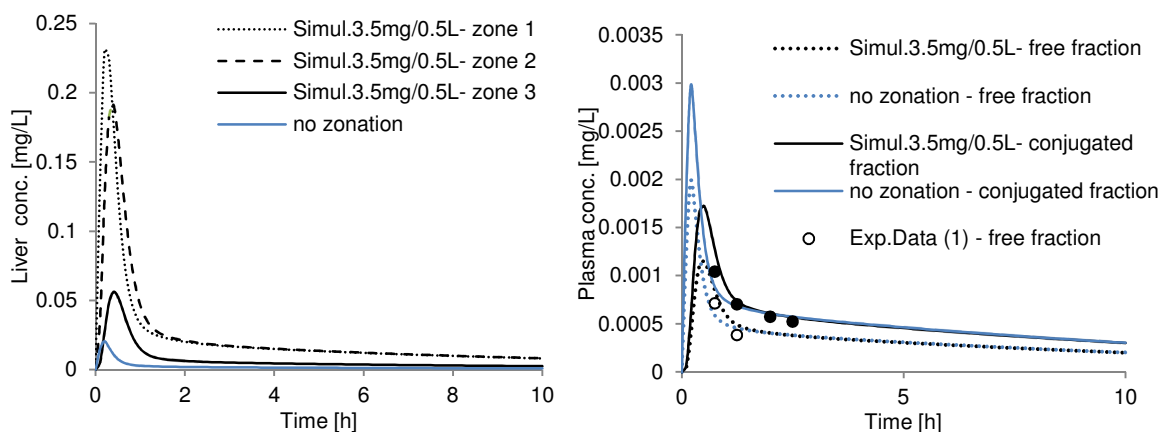


Fig 4.3.16. 1-hydroxyestragole concentrations in liver and plasma with and without liver zonation. Dosing conditions according to (1): (Zeller et al., 2009).

Liver concentrations of estragole with *in vitro* and *in vivo*-scaled parameters for the 3rd liver zone (this is where entire estragole metabolism is assumed to take place) are shown in **Figure 4.3.17**. I used only published literature scaled parameters due to lack of estragole blood concentrations needed for verification and optimisation of these parameters. Estragole *in vitro* (scaled using microsomal protein yield of 32 mg/g liver) and *in vivo* rates were taken from (Punt et al., 2009). In case of 1-hydroxyestragole no refinement of published *in vivo* rates was necessary to give a satisfactory model simulation. $IVIV_{liver}$ was calculated to be 0.844 showing only slightly higher *in vitro* clearance.

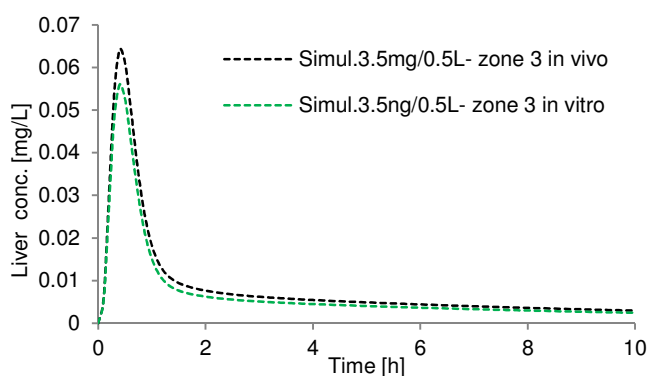


Fig 4.3.17. Estragole concentrations in liver (3rd zone) using *in vitro* (CYP1A2, CYP2D6-Met) and *in vivo* published parameters. Oral dosing conditions according to (Zeller et al., 2009).

Table 4.3.11 provides calculated AUC and C_{max} values in liver with *in vitro* and *in vivo* clearances and the compiled AUC-based $IVIV_{liver}$ ratio for all the investigated compounds. We see that the results are consistent for coumarin, hydroquinone and estragole but different for caffeine.

Table 4.3.11. *In vitro* and *in vivo* AUC and C_{max} in liver

Compound	AUC liver <i>in vitro</i>	AUC liver <i>in vivo</i>	C _{max} liver <i>in vitro</i>	C _{max} liver <i>in vivo</i>	IVIV _{liver}
Coumarin	0.0141	0.0960	0.0318	0.204	0.147
Hydroquinone	0.0103	0.163	0.0117	0.1796	0.063
Caffeine	160.812	70.437	14.158	12.205	2.283
Estragole (zone 3)	0.071	0.0841	0.056	0.064	0.844

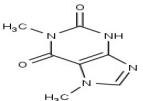
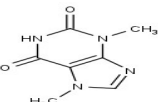
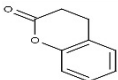
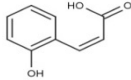
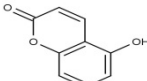
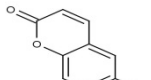
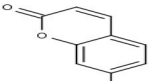
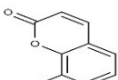
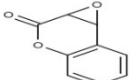
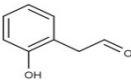
In all the four examples, I did not consider inter-individual differences in enzyme activities which would result in different clearance rates and consequently different IVIV_{liver} ratios. Notwithstanding, I would like to underline that there are many factors that contribute to inter-individual differences in total activity of specific enzymes and drug metabolism rates that are dependent on this. The maximum total activity of biotransformation enzymes is dependent on many factors such as genetic polymorphisms, prior (enzyme induction) or concomitant (enzyme stabilisation and reversible or irreversible inhibition) exposure to drugs and environmental chemicals, presence or depletion of cofactors, dietary factors, diseased states, epigenetic factors and endogenous hormonal factors, which change with age and differ between male and female subjects (Venkatakrishnan et al., 2000).

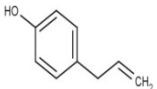
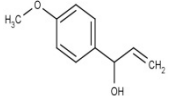
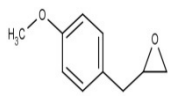
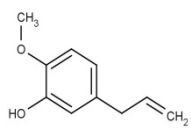
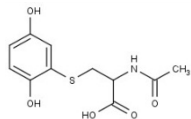
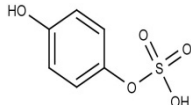
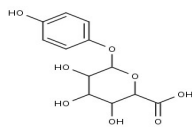
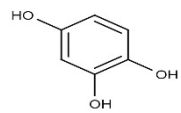
Derek meteor 1.5.2³⁰ was used to generate human metabolites in liver (only the 1st generation- direct). The results are shown in **Table 4.3.12**. The following metabolites were estimated in accordance with literature experiments:

- Caffeine: paraxanthine and theobromine
- Coumarin: o-HPA, coumarin-3,4-epoxide, 7-hydroxycoumarin
- Estragole: 4-allylphenol, 1'-hydroxyestragole, estragole-2',3'-oxide
- Hydroquinone: Hydroquinone sulfate, hydroquinone glucuronide.

³⁰ <http://www.lhasalimited.org/> (last access: 06.10.2014)

Table 4.2.12 Liver metabolites predicted by Derek meteor 1.5.2

Metabolite of	Structure	Biotransformation Name	Exact Mass	LogP	Phase	Enzyme
Caffeine		Oxidative N-Demethylation	180.0647	-0.28	Phase I	CYP450
		Oxidative N-Demethylation	180.0647	-0.67	Phase I	CYP450
Coumarin		Reduction of alpha, beta-Unsaturated Compounds	148.0524	1.63	Phase I	abKDBR
		Hydrolytic Ring Opening of Coumarins	164.0473	1.57	Phase I	Hydrolase
		Hydroxylation of Fused Benzenes	162.0317	1.62	Phase I	CYP450
		Hydroxylation of Fused Benzenes	162.0317	1.62	Phase I	CYP450
		Hydroxylation of Fused Benzenes	162.0317	1.62	Phase I	CYP450
		Hydroxylation of Fused Benzenes	162.0317	1.62	Phase I	CYP450
		Epoxidation of Z-1,2-Disubstituted Alkenes	162.0317	0.81	Phase I	CYP450
		Oxidative Ring Opening of Coumarins	136.0524	1.07	Phase I	CYP450

Estragole		Oxidative O-Demethylation	134.0732	2.55	Phase I	CYP450
		Benzylic Hydroxylation	164.0837	1.58	Phase I	CYP450
		Epoxidation of Monosubstituted Alkenes	164.0837	1.73	Phase I	CYP450
		2-Hydroxylation of 1,4-Disubstituted Benzenes	164.0837	2.4	Phase I	CYP450
Hydroquinone		Oxidation of 1,4-Dihydroquinones	271.0514	0.03	Phase II	Peroxidase, GST, GT, Peptidase, NAT
		O-Sulphation of Aromatic Alcohols	189.9936	-0.57	Phase II	SULT
		Glucuronidation of Aromatic Alcohols	286.0689	-0.99	Phase II	UGT
		2-Hydroxylation of 1,4-Disubstituted Benzenes	126.0317	0.21	Phase I	CYP450

4.3.3 Cell viability

4.3.3.1 Experimental results

a) HepaRG – *in vitro* viability data: single exposure

The results of cytotoxicity studies show that caffeine exposure to HepaRG for 24 h produced a statistical significant reduction of cell viability at concentrations higher than 3 mM. Such high concentrations of caffeine were selected to be able to observe the cell viability reduction below 10% (for 60 mM \approx 11651.4 mg/L). This concentration-response curve (**Figure 4.3.18**) was used to optimise the VCBA model parameters (no- effect concentration NEC, killing rate kt) in single exposure mode for the HepaRG cell line. The results showed: HepaRG, NEC = 0 g/g_{cell}, kt = 0.222 1/h.

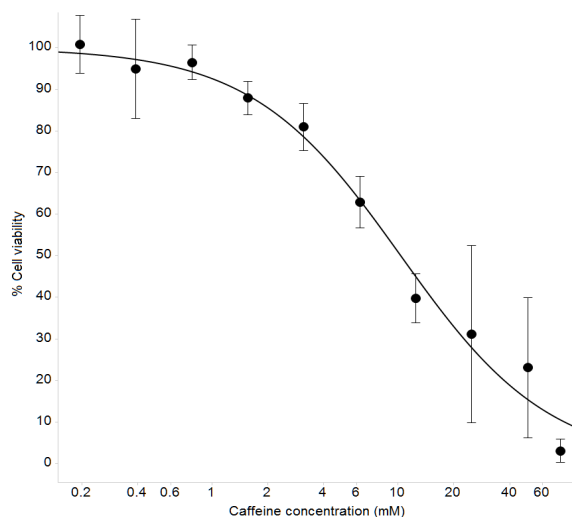


Fig 4.3.18. Caffeine effect on cell viability of HepaRG cell line (using 5 biological replicates). The plot (x scale in log units) and curve fitting (logistic regression) was performed with TIBCO Spotfire 6.0.1- performed at the JRC.

b) HepaRG – *in vitro* viability data: multiple exposure

The results (**Figure 4.3.19**) show that HepaRG exposed to Caffeine (0-9 mM) in multiple exposure (medium change and readout every 24 h) show a decrease in cell viability already at 48 h, but the drastic decrease is found starting from 2.3 mM at 72 and 96 h.

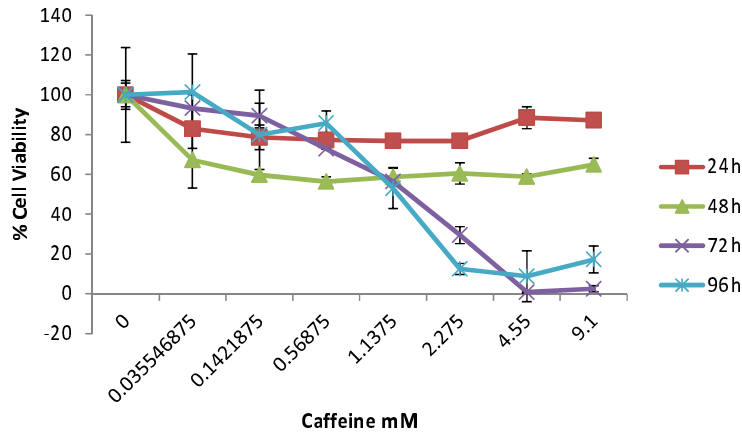


Fig 4.2.19. Caffeine effect on cell viability of HepaRG cell line (mean of three technical replicates performed at the JRC).

c) HEPG2 – *in vitro* viability data: single exposure

The results showed that caffeine exposure to HepG2 for 24 h resulted in a statistically significant reduction of cell viability at the two highest concentrations of 25 and 75 mM. This concentration-response curve (**Figure 4.3.20**), was used to optimise the VCBA model in single exposure mode for the HepG2 cell line in terms of NEC and kt values, giving: $NEC = 0 \text{ g/g}_{\text{cell}}$, $kt = 1.11 \text{ 1/h}$.

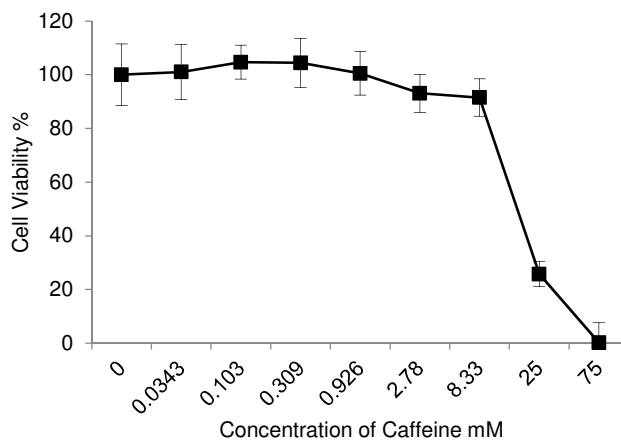


Figure 4.3.20. Caffeine effect on cell viability of HepG2 cells (mean of three biological replicates – performed at the JRC).

d) HEPG2 – *in vitro* viability data: multiple exposure

The data shown in **Figure 4.3.21**, taken from the literature (Scheers et al., 2001), represent cell viability as % to the control (set to be the PI_{50} at 24 h, PI_{50} is the concentration of compound needed to reduce the total protein content to 50 % after 24 h of treatment). Following optimisation of the VCBA model in single exposure mode, these data were used to compare the VCBA model simulations under repeated exposure conditions. The data show fast cell death at the concentration of 4.67 mM caffeine within two weeks of exposure.

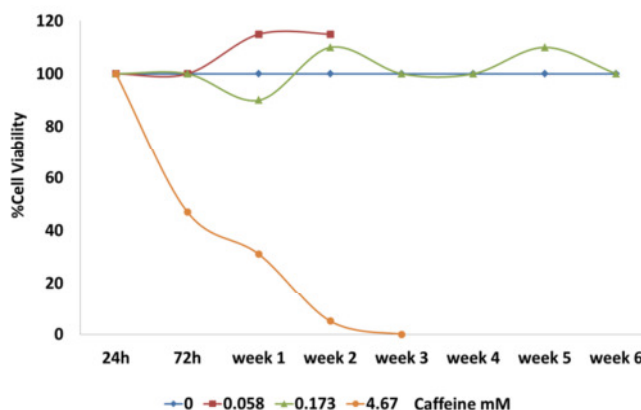


Fig 4.3.21. Caffeine effect on cell viability of HepG2 cells. Literature data from (Scheers et al., 2001).

In vitro single exposure data of HepaRG to caffeine indicated decrease of cell viability below 10 % for a concentration of more than 60 mM of caffeine (ca 155.352 mg/L/kg BW for 75-kg person). Similar was observed for a repeated exposure to 2.3 mM (ca 6 mg/L/kg BW for 75-kg person) after 72 and 96 h (3rd and 4th administration of compound). HepG2, in turn, revealed a cell viability below 10 % for a caffeine concentration of around 70 mM after single exposure and 4.67 mM after 1.5 week of exposure (3rd administration) showing slightly lower sensitivity to caffeine when compared to HepaRG.

4.3.3.2 Multi-scale modelling: cell viability of HepaRG

Dose-response modelling example is presented in this section in which human exposure to caffeine via skin and gelatin capsules given orally was translated to internal liver concentrations by PBTK model and then linked to the VCBA model to estimate HepaRG cells viability as a function of external dose. This link is facilitated via the liver compartment. The simulated liver concentrations of caffeine in time by the PBTK model are assumed to be a concentration outside the hepatic cells. I used only single applications conditions according to **Table 4.3.13** for doses 5- 400 mg (up to 2 times

human oral NOAEL dose) as a proof of concept of no observed effects in liver cell viability in this dose range. Due to model calibration domain for caffeine concentration 4.56 mg/mL only (Otberg et al., 2008) the volume of vehicle was increased accordingly.

Table 4.3.13. The liver and blood AUC simulated by the human PBK model for caffeine

Dose [mg]	Volume of vehicle [mL]	Skin area[cm ²]	Vehicle/ skin type
5	1.096	25	
10	2.192	75	
25	5.480	150	Ethanol + propylene glycol;
50	10.960	300	Chest area, open hair follicles
100	21.920	600	
200	43.840	1000	
300	65.76	1800	
400	87.68	2400	

The cell model consists of 3 compartments (lipid, protein and aqueous): the interchange of the chemical through the cell membrane occurs via diffusion and then the chemical is distributed into the 3 compartments of the cell by its partitioning. When the chemical enters into the cell a toxicokinetic process occurs which is governed by two parameters: No- Effect Concentration (NEC) and killing rate (kt) (**Figure 4.3.18**). These parameters are calculated prior to the joint PBKT-VCBA simulation by their optimisation to predicted cell viability via VCBA using the experimental results (HTS experiments). The VCBA model parameters together with their references are in **Table 4.3.14**.

Table 4.3.14. The parameters of VCBA model

Parameter type	Abbreviation used in the model	Value	Units	Ref.
Mass fraction of compartment f_x (aqueous, l-lipids, p-proteins)	f_{aq}	0.72	fraction of weight	(Zaldívar et al., 2011, 2010)
	f_L	0.012		
	f_p	0.268		
Partition coefficient within a cell (l-lipids, p-proteins)	K_l	$1.63 \cdot 10^{-4}$	m ³ /kg	
	K_p	1.36	m ³ /mol	
Uptake rate	r_{da}	35.208	L m ⁻² h ⁻¹	
Elimination rate	r_{ad}	35.208	L m ⁻² h ⁻¹	
Wet weight	W	$1.79 \cdot 10^{-9}$	gr	
Volume of the cell	V	$1.67 \cdot 10^{-15}$	m ³	

For caffeine case study, the VCBA model was optimised to minimise the error in model prediction of the no effect concentration and killing rate, using experimental values for HepaRG, in single exposure model. This resulted in the following optimised values of NEC and k_t : HepaRG, NEC = 0, k_t = 0.222.

The human PBTK model was used to simulate the liver concentrations following: i) dermal absorption of caffeine following exposure conditions according to (Otberg et al., 2008) – at caffeine concentration of 4.56 mg/mL in ethanol/propylene glycol vehicle and variable absolute dose and skin area with open hair follicles and solution application time of 4 h; ii) and oral absorption according to (Lelo et al., 1986) with caffeine release from gelatin matrix. Only single human exposure to caffeine was investigated. Simulations were performed for male subject (BW= 75 kg). The results are shown in **Table 4.3.15**.

Table 4.3.15. Link of PBTK dermal model to the VCBA- estimated HepaRG cell viability

Dermal External Dose [mg]	C _{max} Liver [mg/L]	C _{max} in liver cells [mg/g _{cell}]	Simulated Cell Viability [%]
	oral: 0	oral: 0	
0	dermal: 0	dermal: 0	
	oral: 0.187	oral: 1.18·10 ⁻¹⁰	
5	dermal: 0.050	dermal: 1.46·10 ⁻⁷	
	oral: 0.380	oral: 2.36·10 ⁻¹⁰	
10	dermal: 0.179	dermal: 4.41·10 ⁻⁷	
	oral: 0.984	oral: 5.92·10 ⁻¹⁰	Oral> 99.99
25	dermal: 0.389	dermal: 1.02·10 ⁻⁶	Dermal>99.99
	oral: 2.074	oral: 1.19·10 ⁻⁹	
50	dermal: 0.753	dermal: 2.72·10 ⁻⁶	
	oral: 4.464	oral: 2.44·10 ⁻⁹	
100	dermal: 1.402	dermal: 9.73·10 ⁻⁶	
	oral: 9.705	oral: 5.15·10 ⁻⁹	
200	dermal: 2.215	dermal: 3.72·10 ⁻⁵	
	oral: 15.175	oral: 8.34·10 ⁻⁹	
300	dermal: 3.929	dermal:0.0004	
	oral: 20.760	oral: 1.23·10 ⁻⁸	
400	dermal: 5.700	dermal:0.0016	

In the **Figure 4.3.22** presents the relationship between the HepaRG cell viability and the external doses. Even for the two highest analysed external doses of 300 and 400 mg (4.00 and 5.33 mg/kg BW for a 75 kg- male reference person) the simulated decrease in cell viability is insignificant (below 1%).

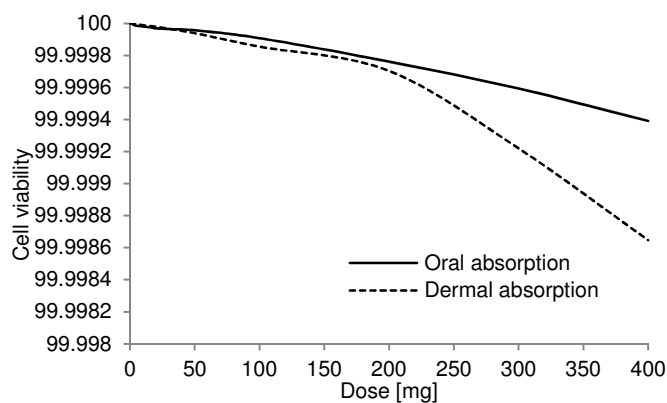


Fig 4.3.22. PBTK/VCBA simulations of HepaRG cell viability as a function of external dose of caffeine applied dermally and orally for a male subject (BW=75 kg).

A dose-response curve generated by linking the PBTK model output (liver C_{\max}) with the VCBA model allows the application of both forward and reverse dosimetry. The forward approach means that when exposed to a given external dose, the joint model predicts the corresponding effect on liver cell viability. The backward approach can be used to estimate from a given cell viability the corresponding external dose. Concentrating on the forward dosimetry approach, I found almost no effect of caffeine on HepaRG cell viability (reduction of cell viability by much less than 1%) for doses up to 400 mg. Caffeine is known to be extensively metabolised in the liver *in vivo* but the main organs affected are the brain and heart. Simulated dose-response profiles following dermal and oral caffeine absorption were similar, even though maximal liver concentrations determined by the PBTK model after oral exposure were higher (see **Table 4.3.16**, second column). I used only single doses of up to of 5.33 mg/kg BW which was more than 2 times the extrapolated NOAEL from rat studies - 2.1 mg/kg BW (for a body weight of 75 kg) – see **Chapter 4.4**. Experimental *in vitro* results showed, however, a significant decrease in HepaRG cell viability when compared to our simulations but in the latter case much smaller doses were considered. **Figure 4.3.18** shows that a caffeine concentration of ca. 2 mM (=388.4 mg/L) produces 20 % of viability loss. The maximal liver concentration that was applied as an input to the VCBA model was 20.760 mg/L following oral absorption of 400 mg. In addition, I used the PBTK dermal model with enhanced action of hair follicles regardless of the fact that while increasing the external absolute dose, I also increased proportionately the skin area. In this way, I wanted to show an extreme case of caffeine skin absorption which still produced lower liver C_{\max} values when compared to the oral case. However, interestingly, the concentration inside cells and their viability calculated by the VCBA model revealed that dermal exposure led to a slightly faster decline in cell viability (regeneration of liver cells was not simulated). This may be due to the prolonged exposure of liver to caffeine after skin absorption as the compound enters the circulation gradually and therefore stays in a body for a longer time.

In vitro experiments revealed slightly higher sensitivity of HepaRG to caffeine when compared to HepG2. Critical concentrations that produced less than 10% of remaining cell viability were for HepRG: more than 60 mM of caffeine (single exposure) and 2.3 mM (after 3rd and 4th exposure). These were external cell concentrations. Basing on PBTK model simulations showing that a single administration of highest caffeine dose of 400 mg produced a C_{\max} of 20.8 mg/L for oral absorption and 5.7 mg/L for dermal, it can be concluded that a dose of caffeine would have to be at least 100 times higher (assuming a ratio external dose/internal concentration is not altered by high doses) to produce the above critical concentrations for HepaRG cells.

4.4 Interspecies extrapolation

No-observed adverse effect level oral/dermal doses (NOAEL) and low-observed adverse effect level doses (LOAEL) determined in subchronic/ chronic rat studies are converted to human equivalent dose via PBTK modelling (PBTK3) in this chapter. Due to lack of realistic acute toxicity data, rat NOAEL doses based on repeated dose experiments were used as a surrogate. These doses together with the literature reference are given in **Table 4.4.1**. Internal dose metrics calculated by the rat PBTK model (Area Under Curve and peak concentration) serves back-extrapolation in the human PBTK model to external exposure level. Parent compounds are considered for coumarin, hydroquinone, caffeine, isopropanol, methyl iodide, ethanol and nicotine; toxic metabolites, for coumarin and hydroquinone only due to availability of information necessary for the PBTK model calibration. Oral gavage simulations were chosen in accordance to rat experiments for all the substances except for iodomethane. In the latter case, only dermal experimental rat NOAEL was found in literature, requiring simulation of skin exposure. In addition, there is a comparison with two traditional approaches (“rules of thumb” not based on PBTK modelling) in determining critical levels for humans. In this work, conversion via toxicokinetics was done only and no inter-individual differences were taken into account. The extrapolations were made for specific physiological data in the first approach and then via PBTK modelling. The reason of doing so is that PBTK conversions are always subject-dependent and there must be a consistency in results between methodologies. For coumarin case, dog NOAEL dose, as indicated in literature, was found smaller than the one of a rat (50 mg/kg BW - lowest rat NOAEL value and 10 mg/kg BW - dog NOAEL) therefore it was selected as a substitute for a rat dose to assure a safe level.

Table 4.4.1. Experimental rat NOAEL doses for selected chemicals

Compound	NOAEL [mg/kg BW/day]	LOAEL [mg/kg BW/day]	Study type	Critical effect	Reference
Coumarin	10 (oral)	-	Sub-chronic	Hepatotoxic effects	(Lungarini et al., 2008)
Hydroquinone	20, 25 (oral)	50 (oral)	Chronic Target organ: kidney	BW reduction increased severity of chronic progressive glomerulonephrop athy, significant increase of renal tubuli adenoma	(Corley et al., 2000; Kari et al., 1992; OECD SIDS, 1996)
Caffeine	10.1 (oral)	27.4 (oral)	Developmental	Teratogenic, fetotoxicity	(Collins et al., 1983; OECD SIDS, 2002a)
Ethanol	1.73 g/kg BW/day	3.16 g/kg BW/day	Sub-chronic Target organ:	Renal tubular epithelial	(ECHA, 2014a)

	(oral)	(oral)	kidney	hyperplasia in males	
Isopropanol	2 (oral)	20 (oral)	Sub-chronic Target organ: liver	Liver deposition; inclusion body intracytoplasmic irritability increase	(FDA, 1968)
Iodomethane	30 (dermal)	-	Subchronic	Secondary histopathological effects and organ weight changes; several secondary effects attributed to the severe skin irritation including changes in haematology, clinical chemistry and urinalysis	(ECHA, 2014b)
Nicotine	1.25 (oral)	2.5 (oral)	Short- and intermediate- term health risks	Episodic oral, dermal, and inhalation toxicity endpoints	(EPA, 2008)

- i) Human equivalent dose (HED) translation is based on (Reagan-Shaw et al., 2008). This study suggests using body weight and body surface (BSA) in the conversion. It is believed that BSA correlates well across several mammalian species with several parameters of biology, including oxygen utilization, caloric expenditure, basal metabolism, blood volume, circulating plasma proteins, and renal function. The human dose equivalent can be more appropriately calculated by using the **Equation 4.4.1**. The results of this approach applied to NOAEL and LOAEL doses are given in **Table 4.4.2**.

$$HED \left[\frac{mg}{kgBW} \right] = NOEL_{RAT} \text{ (or } LOAEL_{RAT} \text{)} \cdot \frac{Km_{Rat}}{Km_{Human}} \quad (4.4.1)$$

where:

$$Km_{Rat} = \frac{BW_{Rat}}{BSA_{Rat}} \approx \frac{0.15}{0.025} = 6$$

$$Km_{human} = \frac{BW_{Human}}{BSA_{Human}}$$

Table 4.4.2. Human equivalent dose conversion

Compound	NOAEL [mg/kg BW/day]	LOAEL [mg/kg BW/day]	Man BW [kg] (Km)	Converted NOAEL [mg/kg BW]	Converted LOAEL [mg/kg BW]
Coumarin	10 (dog) 50	-	80 (39.803)	1.507 7.54	-

Hydroquinone	20	50	69 (37.045)	3.239	8.098
Caffeine	10.1	27.4	75 (38.575)	1.571	4.262
Ethanol	1.73 g/kg BW/day	3.16 g/kg BW/day	75 (38.575)	0.269 g/kg BW/day	0.492 g/kg BW/day
Isopropanol	2	20	75 (38.575)	0.311	3.111
Iodomethane	30	-	85 (40.992)	4.391	-
Nicotine	1.25	2.5	71 (37.562)	0.200	0.400

- ii) Extrapolation applying traditional purely theoretical approach bases on body weight considerations only (Bessems and Geraets, 2013; WHO, 2005) (**Figure 4.4.1**). This is according to the project conducted within the Integrated Public Safety Commission (IPSC)³¹ project on the harmonization of approaches to the assessment of risk from exposure to chemicals. Results are provided in **Table 4.4.3**. As assumed before, only conversion via toxicokinetics was considered.

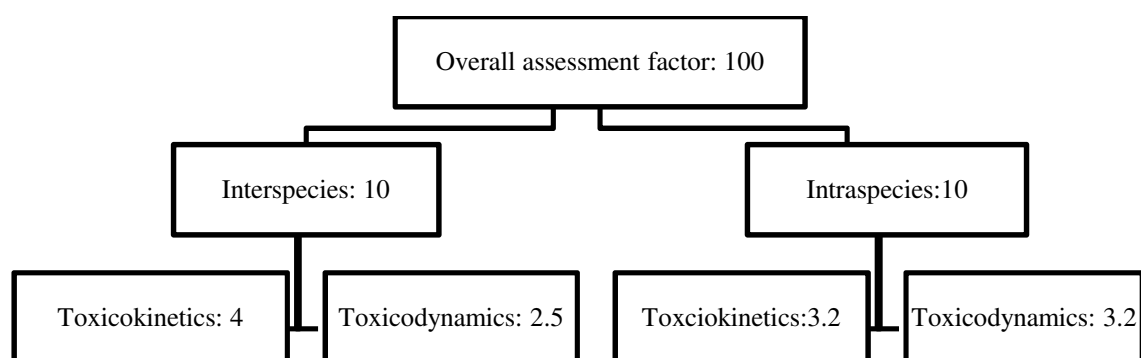


Fig 4.4.1. Traditional approach in risk assessment for converting doses between and within species.

Table 4.4.3. Traditional conversion according to WHO.

Compound	NOAEL [mg/kgBW/day]	LOAEL [mg/kg BW/day]	Converted NOAEL [mg/kg BW]	Converted LOAEL [mg/kg BW]
Coumarin	10	-	2.5	-
	50		12.5	
Hydroquinone	20	50	5	12.5
Caffeine	10.1	27.4	2.525	6.85
Ethanol	1.73	3.16	0.4325	0.79
	g/kg BW/day	g/kg BW/day	g/kg BW/day	g/kg BW/day
Isopropanol	2	20	0.5	5
Iodomethane	30	-	7.5	-
Nicotine	1.25	2.5	0.3125	0.625

³¹ <http://www.in.gov/ipsc/> (last access: 06.10.2014)

iii) Conversion via PBTK modelling (use of PBTK3)

Simple PBTK1 model for rat oral absorption (via gavage) was constructed in accordance with the literature (Mielke et al., 2011; Rietjens et al., 2008) for coumarin (validated on experimental data from (Hardt and Ritschel, 1983)), hydroquinone (validated on experimental data from (English and Deisinger, 2005)), caffeine (validated on experimental data from (Mohiuddin et al., 2009)) and nicotine (model parameters taken from (Yamazaki et al., 2010)). This simple model consists of first order rate absorption from the GI tract (single compartment). The refinement in the model structure was necessary for isopropanol and ethanol due to poor simulation of oral gavage rat data. Therefore, for isopropanol, the PBTK3 model was built in the same manner as the one of human and for ethanol according to the paper of (Pastino and Conolly, 2000). These two models were validated on *in vivo* results from (Livy et al., 2003) for ethanol and from (Corley et al., 2000) for isopropanol. Human PBTK3_orl model with sub-compartments in the GI tract was used in all the 6 case studies. Rat and human simulations were performed for 48 h. **Table 4.4.4** gives rat AUC and C_{\max} results in blood and liver and human estimated external doses that produce similar to rat results in terms of all the investigated toxicokinetic parameters for the parent compounds (coumarin, hydroquinone, caffeine, ethanol, isopropanol, nicotine) and toxic metabolites (coumarin, hydroquinone) at their NOAELs (**Tables 4.4.4-5**) and LOAELs (**Table 4.4.6-7**). For the selected chemicals, only coumarin and hydroquinone metabolites could have been analysed given available information in literature for needed for parametrization of the model. In case of caffeine, it is assumed that it is the parent compound that is most toxic. Extrapolation for iodomethane was carried out via dermal exposure. In this instance, rat PBTK dermal model was constructed in the similar way to PBTK2 (with diffusion in one skin layer) but with additional hair follicles compartment not accounted for by the PBTK2. Application time of 4 h was selected with no vehicle evaporation. Water was assumed as the vehicle due to use of water-based QSPR predictions for human skin absorption. No *in vivo* human or rat data could have been accessed in the literature. Rat exposed skin area of 25 cm² was used and the one of human was increased proportionally to the dose to keep concentration unchanged used in the model calibration step (**Table 4.4.4**).

When comparing the results of the three methods, it is clear that there are high differences in calculated final human levels and these differences are case dependent. For coumarin, caffeine and isopropanol the first approach shows the lowest values. PBTK model results are (less than) 2 times higher for coumarin and caffeine and (more than) 10 times higher for isopropanol when compared to the first method. In contrast, hydroquinone, ethanol, nicotine and methyl iodide PBTK simulations indicate the lowest extrapolated results (in case of nicotine even ca. 10 times lower). However, the

results of ethanol and hydroquinone are very close to the HED method estimations. Second method shows the highest values for the four substances. Iodomethane case is very specific due to the fact that extrapolation via dermal route requires strictly defined conditions (skin area, duration of exposure, application conditions, etc.) and therefore the inter-occasion variability in extrapolated results is higher than in case of oral absorption. In this study example, the PBTK model- extrapolated NOAEL value is 100 times lower than these estimated by the other methods at quite small exposure skin area (25 cm²).

Table 4.4.8 provides, additionally, quantity measures (based on specified body weight of a reference man) of selected consumer products administered per day equivalent to oral extrapolated to human level NOAEL doses in terms of a type of product, content of the analysed substance in it and amount of the product per day. This is done, however, only for coumarin, caffeine, ethanol and nicotine as these substances appear and food related products and are administered orally.

Conversion via PBTK modelling was performed for a reference man with the following body weights: 80 kg for coumarin, 69 kg for hydroquinone, 75 kg for caffeine, ethanol and isopropanol, 85 kg for iodomethane and 71 kg for nicotine – based on the *in vivo* data used for the calibration of the oral models.

Table 4.4.4. Rat NOAEL doses extrapolation via PBTK modelling for the parent compound

	Coumarin NOAEL = 10, 50 mg/kg BW/day	Hydroquinone NOAEL = 20 mg/kg BW/day	Caffeine NOAEL = 10.1 mg/kg BW/day	Ethanol NOAEL = 1.73 g/kg BW/day	Isopropanol NOAEL = 2 mg/kg BW/day	MEI (dermal) NOAEL = 30 mg/kg BW/day	Nicotine NOAEL = 1.25 mg/kg BW/day
internal metrics	AUC liver: 2.214, 26.773 AUC blood: 0.326, 3.760	AUC liver: 0.8187 AUC blood: 0.0806	AUC liver: 245.2845	AUC liver: 3879.408 AUC blood: 391.396	AUC liver: 11.847 AUC blood: 1.325	AUC liver: $1.6 \cdot 10^{-04}$ AUC blood: 0.295	AUC liver: 0.081 AUC blood: 0.00425
JC [L/h]	C_{max} liver: 8.241, 138.442 C_{max} blood: 0.450, 6.389	C_{max} liver: 1.037 C_{max} blood: 0.056	AUC blood: 4.728 C_{max} liver: 123.105 C_{max} blood: 1.867	C_{max} liver: 7528.954 C_{max} blood: 389.208	C_{max} liver: 38.158 C_{max} blood: 1.029	C_{max} liver: $3.09 \cdot 10^{-05}$ C_{max} blood: 0.058	C_{max} liver: 0.0826 C_{max} blood: 0.0021
estimated equivalent dose [mg/kg BW] for human	AUC liver: 3.9, 11 AUC blood: 3.1, 8.5 C_{max} liver: 4.7, 40.5 C_{max} blood: 3.1, 13.5	AUC liver: 16 AUC blood: 2.4 C_{max} liver: 13 C_{max} blood: 1.9	AUC liver: 9 AUC blood: 2.1 C_{max} liver: 30 C_{max} blood: 4.2	AUC liver: 1.15g AUC blood: 0.2g C_{max} liver: 4.9g C_{max} blood: 0.29g	AUC liver: 35 AUC blood: 15.5 C_{max} liver: 31.5 C_{max} blood: 8	AUC liver: 0.03 (25 cm²) AUC blood: 2.4 (600 cm ²) C_{max} liver: 0.03 (25 cm ²) C_{max} blood: 1.9 (475 cm ²)	AUC liver: 0.11 AUC blood: 0.014 C_{max} liver: 0.1 C_{max} blood: 0.027

Table 4.4.5. Rat NOAEL doses extrapolation via PBTK modelling for the toxic metabolite

	o-HPA	Benzoquinone
Rat internal metrics	AUC liver: 0.017, 0.130 AUC blood: 0.001, 0.0065	AUC liver: 0.029 AUC blood: 0.00346
AUC [mg/L/h]	C_{max} liver: 0.062, 0.511	C_{max} liver: 0.0342
C_{max} [mg/L]	C_{max} blood: 0.00098, 0.0077	C_{max} blood: 0.0028
Estimated equivalent dose [mg/kg BW] for human	AUC liver: 16,300 AUC blood: 22, 400 C_{max} liver: 75, >500 C_{max} blood: 60, 500	AUC liver: 28 AUC blood: 3.1 C_{max} liver: 24 C_{max} blood: 2.7

Table 4.4.6. Rat LOAEL doses extrapolation via PBTK modelling for the parent compound

	Coumarin	Hydroquinone RAT LOAEL=50 mg/kg BW/day	Caffeine RAT LOAEL=27.4 mg/kg BW/day	Ethanol RAT LOAEL=3.16 g/kg BW/day	Isopropanol RAT LOAEL=20 mg/kg BW/day	Nicotine RAT LOAEL=2.5 mg/kg BW/day
Rat internal metrics	-	AUC liver: 2.653 AUC blood: 0.266	AUC liver: 679.453 AUC blood: 13.097	AUC liver: 10241.590 AUC blood: 1029.001	AUC liver: 153.345 AUC blood: 16.995	AUC liver: 0.163 AUC blood: 0.0085
AUC		C_{max} liver: 4.34	C_{max} liver: 336.191	C_{max} liver: 15920.867	C_{max} liver: 426.767	

[mg/L/h] C _{max} [mg/L]		C _{max} blood: 0.208	C _{max} blood: 5.106	C _{max} blood: 893.160	C _{max} blood: 12.329	C _{max} liver: 0.165 C _{max} blood: 0.004
Estimated equivalent dose [mg/kg BW] for human	-	AUC liver: 37.5 AUC blood: 7.5 C _{max} liver: 35 C _{max} blood: 6.5	AUC liver: 20 AUC blood: 4.7 C _{max} liver: 70 C _{max} blood: 10.8	AUC liver: 3 AUC blood: 0.5 C _{max} liver: 10.5 C _{max} blood: 0.65	AUC liver: 123 AUC blood: 56 C _{max} liver: 130 C _{max} blood: 35.8	AUC liver: 0.22 AUC blood: 0.027 C _{max} liver: 2.00 C _{max} blood: 0.14

Table 4.4.7. Rat LOAEL doses extrapolation via PBTK modelling for the toxic metabolite

Benzoquinone	
Rat internal metrics	AUC liver: 0.0785 AUC blood: 0.009
AUC [mg/L/h] C _{max} [mg/L]	C _{max} liver: 0.1 C _{max} blood: 0.008
Estimated equivalent dose [mg/kg BW] for human	AUC liver: 75 AUC blood: 8.5 C _{max} liver: 100 C _{max} blood: 7.5

Table 4.4.8. Equivalent safe daily human exposure to consumer products acc. to extrapolated to human NOAEL doses.

Compound	Oral NOAEL [mg/kg BW/day]	Man BW [kg]	NOAEL equivalence in selected consumer products	Reference
Coumarin	3.1	80	35.58 g of Saigon cinnamon, Vietnamese Cassia, Vietnamese Cinnamon	³²
Caffeine	2.1	75	3 x a cup of espresso assuming it contains 75 mg of caffeine	³³
Ethanol	0.2 g/kg BW/day	75	¾ 500 ml 5% lager beer that contains 2.5 units of ethanol	³⁴
Nicotine	0.014	71	1 cigarette with unventilated filters per day assuming it contains 1.3mg and 76% of it is administered	(Russell et al., 1980)

³² http://cinnamonvogue.com/Types_of_Cinnamon_1.html (last access: 06.10.2014)

³³ <http://coffeetea.about.com/od/caffeinehealth/a/How-Much-Caffeine-Is-In-Coffee-Tea-Cola-And-Other-Drinks.htm> (last access: 06. 10. 2014)

³⁴ https://www.princeton.edu/~achaney/tmve/wiki100k/docs/Unit_of_alcohol.html (last access: 06.10.2014)

Coumarin and hydroquinone were further examined for existing dependencies between rat and human AUC and C_{max} at rat doses ranging from 0.5rat NOAEL to 2rat LOAEL and PBTK-extrapolated to human equivalent doses. This comparison was done for the parent compound and the toxic metabolite. For coumarin: rat doses: 5, 10, 30, 50 and 100 mg/kg BW were extrapolated to human levels at 2.1, 3.1, 5.7, 8.5 and 15.5 mg/kg BW either via C_{max} or AUC of coumarin in blood. **The Figure 4.4.2-3** show the relationships between rat and human results in terms of AUC and C_{max} in blood and liver at these extrapolated equivalent doses for coumarin and o-HPA. AUC-based relationship for coumarin seems to be more linear, whereas C_{max} -based one is more logarithmic. The nature of AUC and C_{max} dependencies for o-HPA is clearly different and exponential.

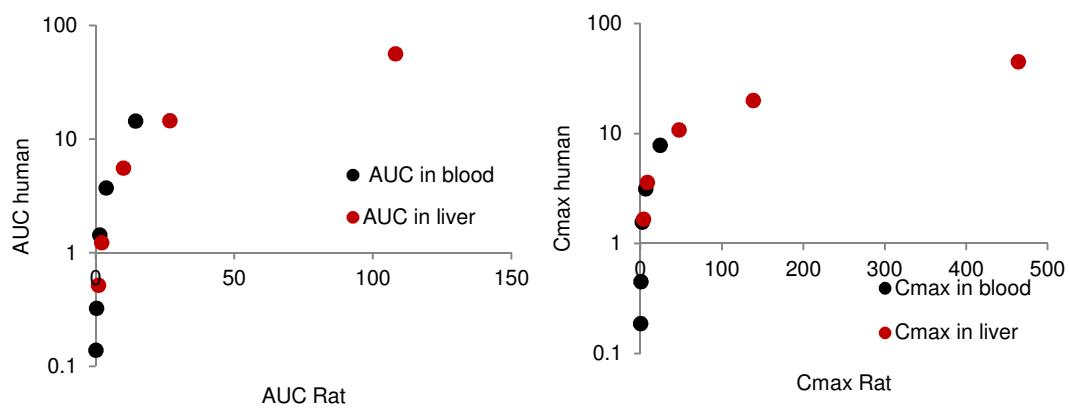


Fig 4.4.2. AUC and C_{max} relationships between rat and human at equivalent doses for coumarin.

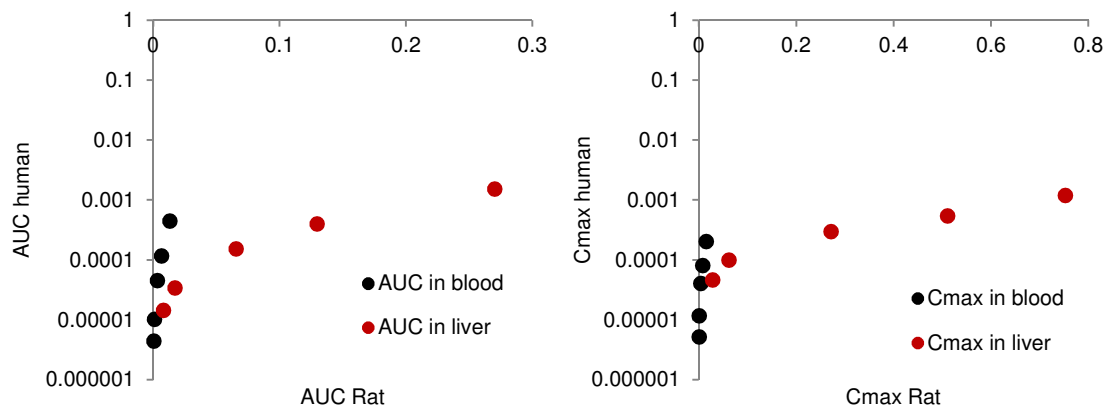


Fig 4.4.3. AUC and C_{max} relationships between rat and human at equivalent doses for o-HPA.

For hydroquinone: rat doses were: 10, 20, 50 and 100 mg/kg BW and human estimated doses based on C_{max} or AUC in blood were: 0.8, 1.9, 6.5 and 33 mg/kg BW.

Figures 4.4.4-5 show dependencies between rat and human AUC and C_{max} values in blood and liver for hydroquinone and benzoquinone. In the similar way to coumarin, hydroquinone shows behaviour close to logarithmic and benzoquinone close to exponential trend.

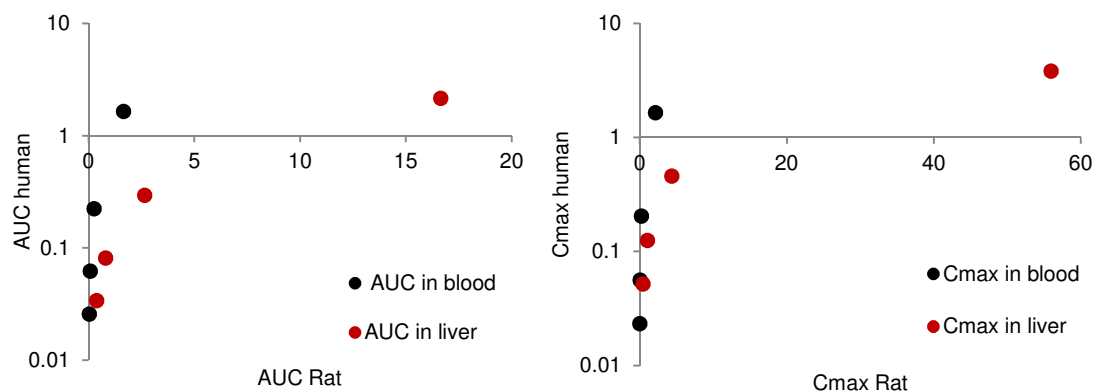


Fig 4.4.4. AUC and C_{max} relationships between rat and human at equivalent extrapolated doses for hydroquinone.

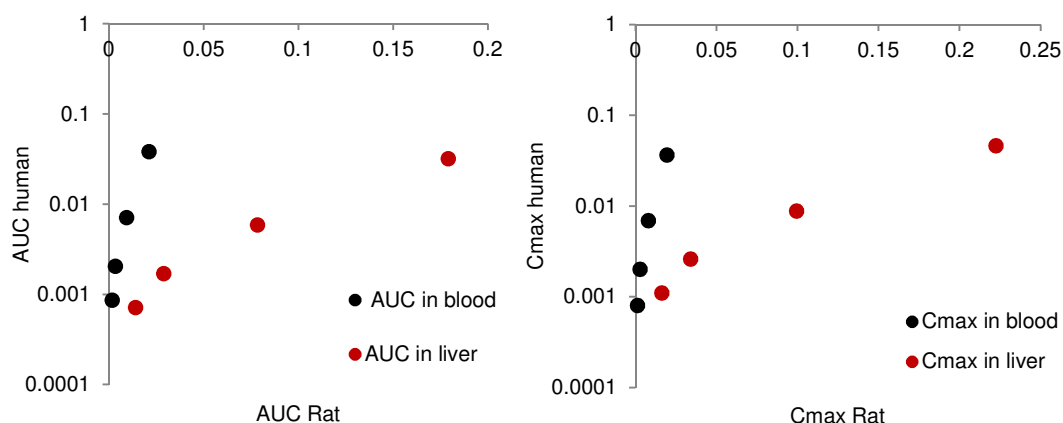


Fig 4.4.5. AUC and C_{max} relationships between rat and human at equivalent extrapolated doses for benzoquinone.

We can conclude for this that metabolites do not show the same AUC or C_{max} based pattern in blood and liver as parent compounds. For parent compounds, there is an obvious difference in absorption step described by the PBTK model. Human PBTK model with sub-compartments accounts for the saturation at higher doses, whereas the rat model shows equal absorption at all doses (first order rate of absorption). In case of metabolites, we see that human AUC and C_{max} increase faster with a dose than these of a rat and reason for this could be either ill-described GI tract absorption of a parent compound in rats; the delivery of a parent compound to the liver is higher than its clearance for humans.

4.5 Route-to-route extrapolation

Oral or dermal NOAEL experimental rat doses extrapolated to human level by the PBTK model for coumarin, hydroquinone, caffeine, ethanol, isopropanol and methyl iodide were used in this chapter to determine dermal and inhalation thresholds via route-to-route (RtR) extrapolation. The idea is to exemplify application of PBTK modelling in determination of dermal thresholds under defined experimental conditions. This is done via analysis of calculated toxicokinetic parameters such as area under curve and peak concentrations in blood and liver as previously. Only PBTK3 model is used in this section for all the substances except for inhalation of iodomethane, ethanol and isopropanol. The experimental conditions selected for inhalation, oral or dermal model simulations are given in **Tables 4.5.1-2** for all the substances. The application conditions, concentrations and vehicles were chosen in accordance with the literature source used in the calibration step with a slight modification of exposure time (2-6 h) and exposed skin area (surface area of hands= 2448 cm²), in order to be consistent for all the case studies. As the absolute amount of dose applied refers to estimated NOAEL values, the volume of vehicle had to be increased to ensure unchanged concentrations (due to the model applicability domain) and consequently the exposed skin area is larger. RtR strategy for the safe oral NOAEL dose is shown in **Figure 4.5.1** below. Dermal safe results, in case of iodomethane, were extrapolated in the similar way. All the extrapolations are done for different body weights of reference male subjects.

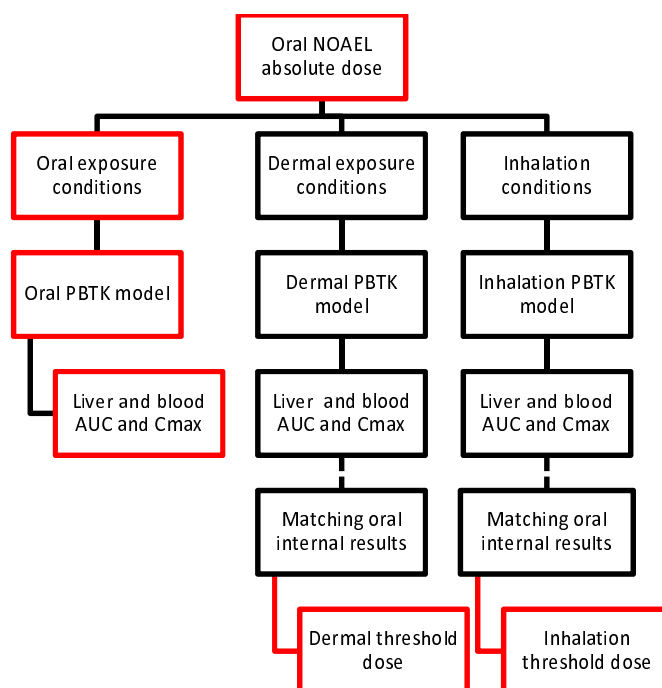


Fig 4.5.1. RtR extrapolation strategy based on oral NOAEL dose.

Table 4.5.1. Exposure conditions used in route-to-route extrapolations (part 1)

	Hydroquinone		Isopropanol		Iodomethane		
	oral	dermal	oral	dermal	inhalation	dermal	inhalation
Exposure type	oral	dermal	oral	dermal	inhalation	dermal	inhalation
Simulation time	100 h	100 h	48 h	48 h	24 h	48 h	48 h
Exposure time	-	2 h	-	every 10 min of 4 h	10 min	4 h	2 h
Administration type	drinking rate	-	drinking rate	-	-	-	-
Vehicle type	water	cream	water	hand rub	-	water	-
Concentration of formul.	-	16 mg/mL	-	413.433 mg/mL	120 ppm	10 mg/mL	10 ppm
Occlusion	-	yes	-	yes	-	yes	-
Skin Area	-	2'448 cm ²	-	2'448 cm ²	-	25 cm ²	-
Inhalation at rest	-	-	-	-	yes	-	yes

Table 4.5.2. Exposure conditions used in route-to-route extrapolations (part 2)

	Caffeine		Ethanol		Coumarin		
	oral	dermal	oral	dermal	inhalation	oral	dermal
Exposure type	oral	dermal	oral	dermal	inhalation	oral	dermal
Simulation time	48 h	48 h	24 h	24 h	24 h	24 h	24 h
Exposure time	-	2	-	4 h	6 h	-	6 h
Administration type	gelatin tablet	-	drinking rate	-	-	gavage	-
Vehicle type	-	ethanol+ propylene glycol	-	Hand rub commercial	-	-	70% ethanol
Concentration of formul.	-	4.5625 mg/mL	-	439.065 mg/mL	1000 ppm	-	2 mg/mL
Occlusion	-	After 8 h	-	no	-	-	after 30 min
Skin Area	-	2'448 cm ²	-	1500 cm ²	-	-	2'448 cm ²
Inhalation at rest	-	-	-	24 h	yes	-	-

4.5.1 Oral-to-dermal extrapolation

The first step towards extrapolation was to simulate oral and dermal human exposure to coumarin, hydroquinone, caffeine, isopropanol and ethanol (cosmetic ingredients only) separately at their extrapolated from rat oral NOAEL (absolute) doses. Oral administration was either via gavage, drinking or via gelatin tablet. Skin diffusion and partition coefficients were determined in the calibration step for specific skin sites and used unchanged in this application. Dermal thresholds were determined by comparing dermal and oral internal concentration results at the NOAEL level and then by finding a minimal absolute dermal dose (at a constant concentration) that gives a match of oral and dermal AUC or C_{\max} values in blood or liver (in the similar way to interspecies extrapolation via PBTK modelling). Case studies are presented below. It is assumed in this study that for the investigated substances only up to 5 times NOAEL absolute dose can be applied on skin area equal to 5 times area of hands (2448 cm²) in real life scenarios and this is already an extreme exposure.

a) Coumarin

Concentration-time profiles of coumarin in blood simulated by PBTK3 model at the NOAEL dose (3.1 mg/kg BW/day) are shown in **Figure 4.5.2**. Simulations were performed for a male subject, BW= 80 kg. Oral and dermal internal concentrations in terms of AUC and C_{\max} in blood and liver are shown in **Table 4.5.2** (coumarin) and **Table 4.5.3** (o-HPA). Safe oral values are marked in red.

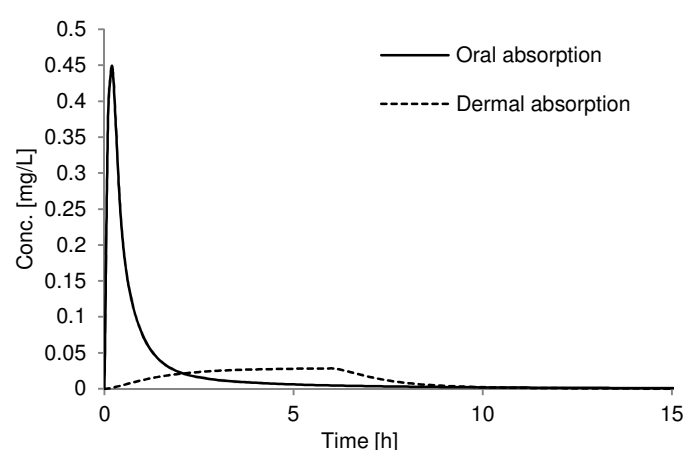


Fig 4.5.2. Coumarin profiles in blood after oral and dermal absorption of the oral NOAEL dose.

Table 4.5.2. AUC and C_{\max} of coumarin in blood and liver for oral NOAEL dose

AUC liver [mg.h/L]		AUC blood [mg.h/L]		C_{\max} liver [mg/L]		C_{\max} blood [mg/L]	
oral	dermal	oral	dermal	oral	dermal	oral	dermal
1.222	0.047	0.3215	0.174	3.592	$7.7 \cdot 10^{-03}$	0.449	0.028

Table 4.5.3. AUC and C_{max} of o-HPA in blood and liver for oral NOAEL dose

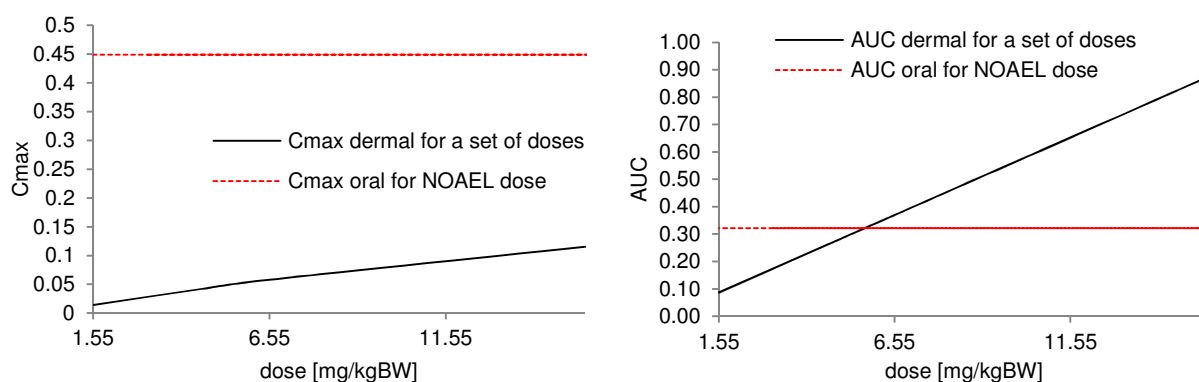
AUC liver [mg.h/L]		AUC blood [mg.h/L]		C_{max} liver [mg/L]		C_{max} blood [mg/L]	
oral	dermal	oral	dermal	oral	dermal	oral	dermal
$3.4 \cdot 10^{-05}$	$1.3 \cdot 10^{-06}$	$1.0 \cdot 10^{-05}$	$3.8 \cdot 10^{-07}$	0.0001	$2.1 \cdot 10^{-07}$	$1.2 \cdot 10^{-05}$	$6.0 \cdot 10^{-08}$

Under given exposure conditions (**Table 4.5.2**) AUC in blood following skin absorption is only slightly lower than the safe oral one. This indicates that the dermal threshold value is not much higher than the oral NOAEL when assuming AUC as more relevant for possible toxic actions than C_{max} . To find this value and to check whether other oral toxicokinetic parameters are always higher, absolute doses applied on skin were lowered up to half of the NOAEL dose and increased up to 5 times the NOAEL value.

When it comes to the toxic metabolites (o-HPA), dermal results are at least 10 times lower than the corresponding oral ones (**Table 4.5.3**). Skin area was increased in the same way as a dose.

Table 4.5.4. Dermal AUC and C_{max} for several doses

	AUC liver [mg.h/L]	AUC blood [mg.h/L]	C_{max} liver [mg/L]	C_{max} blood [mg/L]
0.5·oral NOAEL	0.023	0.0865	$3.80 \cdot 10^{-05}$	0.014
1.5·oral NOAEL	0.071	0.262	0.011	0.042
2·oral NOAEL	0.095	0.350	0.015	0.056
5·oral NOAEL	0.242	0.876	0.032	0.116

**Fig 4.5.3.** Determination of dermal threshold values via C_{max} and AUC in blood

Based on the results in **Tables 4.5.2 and 4** it can be concluded that under the analysed conditions and assumptions:

- C_{max} in blood and liver and AUC in liver are always higher for oral absorption (**Figure 4.5.3**)
- **Dermal threshold based on coumarin AUC in blood is $1.8 \cdot \text{NOAEL} = 5.58 \text{ mg/kg BW/ day}$ for the skin area: $1.8 \cdot 2448 = 1612.8 \text{ cm}^2$ over 6 h (**Figure 4.5.3**).**

b) Hydroquinone

Concentration-time profiles of hydroquinone in blood simulated by the PBTK3 model at the NOAEL dose (1.9 mg/kg BW/day) are shown in **Figure 4.5.4**. Simulations were performed for a male subject, BW= 69 kg. Oral and dermal internal concentrations in terms of AUC and C_{max} in blood and liver are shown in **Table 4.5.5** (for hydroquinone) and **Table 4.5.6** (for benzoquinone). Safe oral values are marked in red.

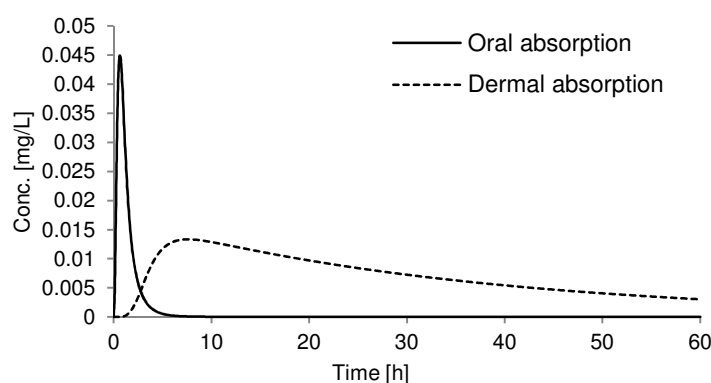


Fig 4.5.4. Concentration-time profiles of hydroquinone in blood after oral and dermal absorption of the oral NOAEL dose.

Table 4.5.5. AUC and C_{max} of hydroquinone in blood and liver for oral NOAEL dose (oral and dermal absorption)

AUC liver [mg.h/L]		AUC blood [mg.h/L]		C_{max} liver [mg/L]		C_{max} blood [mg/L]	
oral	dermal	oral	dermal	oral	dermal	oral	dermal
0.082	0.026	0.062	0.532	0.091	$6.00 \cdot 10^{-04}$	0.045	0.013

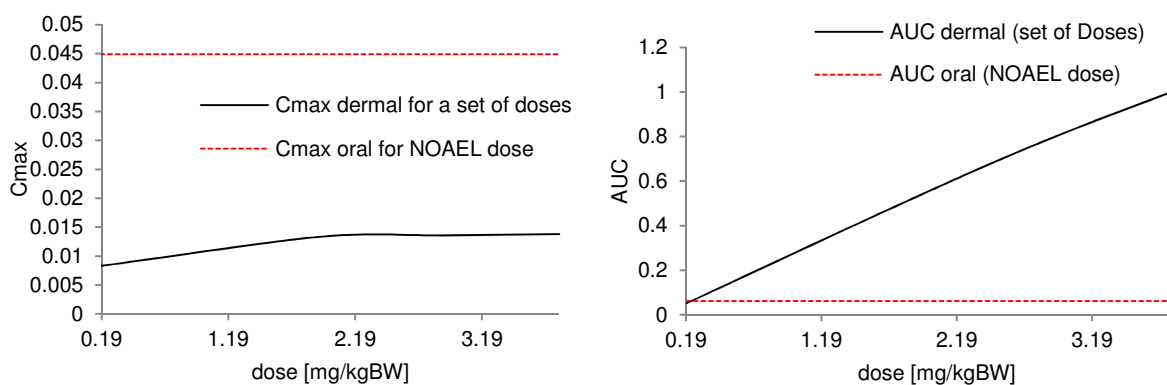
Under given exposure conditions (**Table 4.5.1**) AUC in blood following skin absorption is 10 times higher than the safe oral one. This indicates that the dermal threshold value is far below the oral NOAEL. This threshold and the behavior of other toxicokinetic parameters was further studied by changing the absolute doses applied on skin from 10 times lower the oral NOAEL dose and up to 2 times the NOAEL value (**Table 4.5.6**). Hydroquinone is not commonly used in consumer care products on every day basis therefore exposure equal to 5 times the NOAEL value was not considered. When it comes to the toxic metabolites (benzoquinone), dermal results are at least 10 times lower than the corresponding oral ones (**Table 4.5.7**). Skin area was increased in the same way as a dose.

Table 4.5.6. AUC and C_{max} of benzoquinone in blood and liver for oral NOAEL dose (oral and dermal absorption)

AUC liver [mg.h/L]		AUC blood [mg.h/L]		C_{max} liver [mg/L]		C_{max} blood [mg/L]	
oral	dermal	oral	dermal	oral	dermal	oral	dermal
0.0017	$6.0 \cdot 10^{-04}$	0.0021	$6.4 \cdot 10^{-04}$	0.002	$1.37 \cdot 10^{-05}$	0.0017	$1.64 \cdot 10^{-05}$

Table 4.5.7. Dermal AUC and C_{max} for several doses

	AUC liver [mg.h/L]	AUC blood [mg.h/L]	C_{max} liver [mg/L]	C_{max} blood [mg/L]
NOAEL/10	$2.47 \cdot 10^{-03}$	0.051	$4.0 \cdot 10^{-04}$	0.008
1.5·NOAEL	0.038	0.784	$7.0 \cdot 10^{-04}$	0.014
2·NOAEL	0.049	1.006	$7.0 \cdot 10^{-04}$	0.014

**Fig 4.5.5.** Determination of dermal threshold values via C_{max} and AUC in blood.

Based on the results in **Table 4.5.7** it can be concluded that under the analysed conditions and assumptions:

- C_{max} in blood and liver are always higher for oral absorption (**Figure 4.5.5**)
- Dermal AUC in liver becomes only slightly lower (ca. 2 times) than the oral one at 2·oral NOAEL dose.
- **Dermal threshold value based on AUC in blood for hydroquinone is: $NOAEL/9=0.211$ mg/kg BW/day applied on the skin area $(448/2)/9 = 99.56$ cm² over 2 h (Figure 4.5.5).**

c) Caffeine

Concentration-time profiles of caffeine in blood following oral and dermal absorption simulated by the PBTK3 model at the NOAEL dose (2.1 mg/kg BW/day) are shown in **Figure 4.5.6**. Simulations were performed for a male subject, BW= 75 kg. Oral and dermal internal concentrations in terms of AUC and C_{max} in blood and liver are shown in **Table 4.5.8**. Safe oral values are marked in red. In dermal exposure, additionally, hair follicles were taken into consideration.

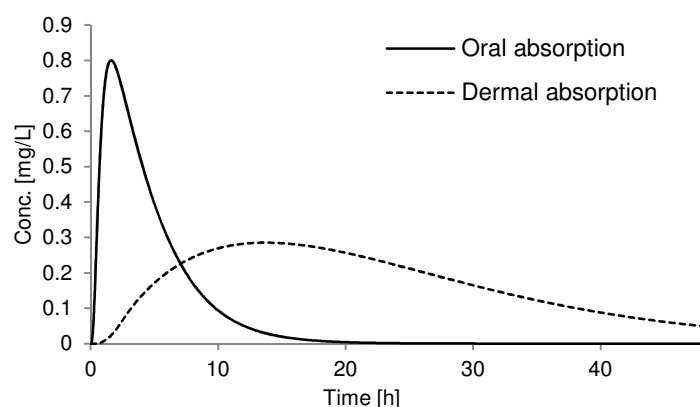


Fig 4.5.6. Concentration-time profiles of caffeine in blood after oral and dermal absorption of the oral NOAEL dose.

Table 4.5.8. AUC and C_{max} of caffeine in blood and liver for oral NOAEL dose (oral and dermal absorption)

AUC liver [mg.h/L]		AUC blood [mg.h/L]		C_{max} liver [mg/L]		C_{max} blood [mg/L]	
oral	dermal	oral	dermal	oral	dermal	oral	dermal
29.395	26.735	4.201	8.162	7.434	0.946	0.800	0.285

Under given exposure conditions (**Table 4.5.2**) AUC in blood following skin absorption is 2 times higher than the safe oral one, AUC in liver is similar in both exposures and dermal C_{max} in blood is only 3.5 times lower than the oral one. This indicates that the dermal threshold value is below the oral NOAEL. This threshold was determined by changing the absolute doses applied on skin from 5 times lower the oral NOAEL dose and up to 5 times the NOAEL value (**Table 4.5.9**). Skin area was increased in the same way as a dose.

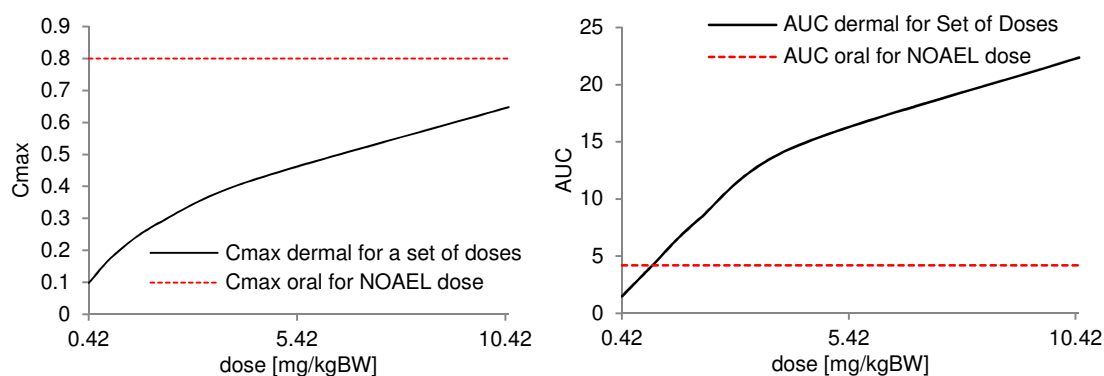


Fig 4.5.7. Determination of dermal threshold values via C_{max} and AUC in blood.

Table 4.5.9. Dermal AUC and C_{max} for several doses

	AUC liver [mg.h/L]	AUC blood [mg.h/L]	C_{max} liver [mg/L]	C_{max} blood [mg/L]
NOAEL/5	4.743	1.483	0.315	0.098
NOAEL/2	12.971	4.009	0.613	0.188

2·NOAEL	61.886	14.501	1.394	0.413
5·NOAEL	170.631	22.371	2.249	0.648

It can be concluded that under the analysed conditions and assumptions:

- C_{max} in blood and liver are always higher for oral absorption (**Figure 4.5.7**).
- Dermal AUC in liver becomes higher than the oral one at 1.2·oral NOAEL dose.
- **Dermal threshold value for caffeine based on AUC in blood is: $NOAEL/2 = 1.05 \text{ mg/kg BW/day}$ applied on the skin area $(448/2) = 448 \text{ cm}^2$ over 2 h.**

d) Ethanol

Concentration-time profiles of ethanol in blood following oral and dermal absorption simulated by PBTK3 model at the NOAEL dose (0.2 g/kg BW/day) are shown in **Figure 4.5.8**. Simulations were performed for a male subject, BW= 75 kg and a drinking time of 60 min. Oral and dermal internal concentrations in terms of AUC and C_{max} in blood and liver are shown in **Table 4.5.10**. Safe oral values are marked in red as previously. Due to lack of human experimental data for blood concentrations of acetaldehyde (potentially toxic metabolite) it was not possible to evaluate the toxicokinetic parameters for this metabolite.

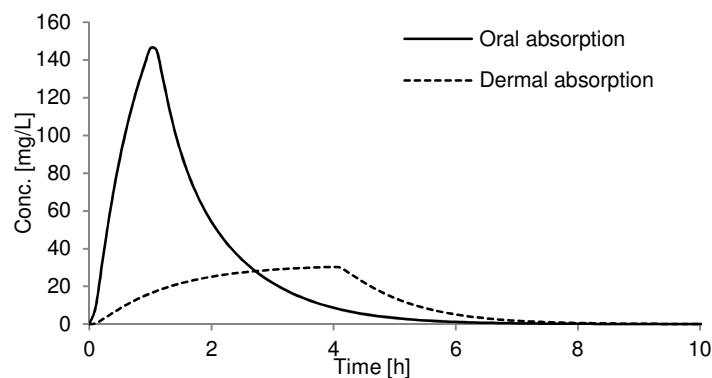


Fig 4.5.8. Ethanol profiles in blood after oral and dermal absorption of the oral NOAEL dose.

Table 4.5.10. AUC and C_{max} of ethanol in blood and liver for oral NOAEL dose (oral and dermal absorption)

AUC liver [mg.h/L]		AUC blood [mg.h/L]		C_{max} liver [mg/L]		C_{max} blood [mg/L]	
oral	dermal	oral	dermal	oral	dermal	oral	dermal
446.812	94.989	235.586	122.348	158.516	11.649	146.1895	30.341

Under given exposure conditions (**Table 4.5.2**) AUC in blood following skin absorption is only slightly lower than the oral one when compared to the other parameters that are surely within a safe limit. This indicates that the dermal threshold value is a bit above the oral NOAEL. This threshold was determined by

changing the absolute doses applied on skin from 1.5 times the oral NOAEL dose and up to 5 times the NOAEL value (**Table 4.5.11**). Skin area was increased in the same way as a dose.

Table 4.5.11. Dermal AUC and C_{max} for several doses

	AUC liver [mg.h/L]	AUC blood [mg.h/L]	C_{max} liver [mg/L]	C_{max} blood [mg/L]
1.5 NOAEL	150.923	189.888	18.278	46.538
2 NOAEL	207.807	258.110	24.704	62.320
3 NOAEL	322.547	395.249	36.488	90.999
5 NOAEL	552.496	669.861	54.956	135.980

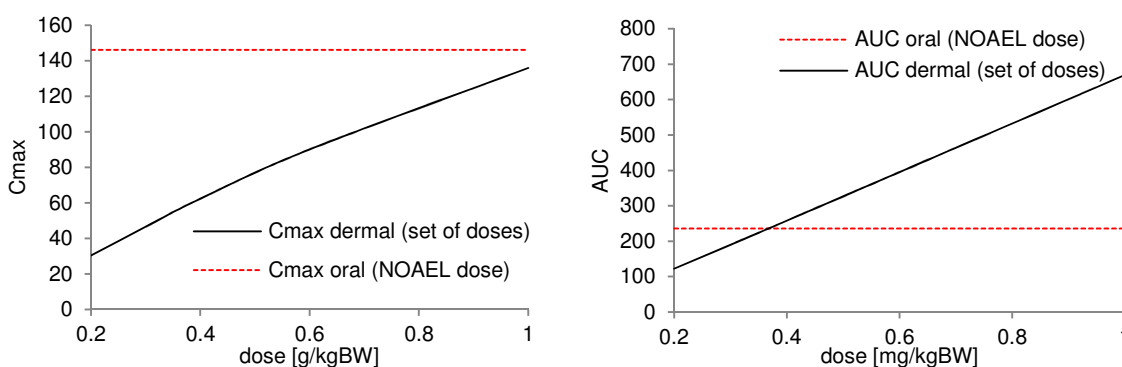


Fig 4.5.9. Determination of dermal threshold values via C_{max} and AUC in blood.

It can be concluded that under the analysed conditions and assumptions:

- C_{max} in liver and blood are higher for oral absorption for doses lower than 5 NOAEL.
- Dermal AUC in liver becomes higher than the oral one at ca. 3 NOAEL.
- **The lowest dermal threshold for ethanol based on AUC in blood is 1.8 NOAEL = 0.36 g/kg BW/day applied on the skin area $1.8 \cdot 1500 = 2700 \text{ cm}^2$ over 4 h (Figure 4.5.9).**

e) Isopropanol

Concentration-time profiles of isopropanol in blood following oral and dermal absorption simulated by PBTK3 model at the NOAEL dose (8 mg/kg BW/day) are shown in **Figure 4.5.10**. Simulations were performed for a male subject, BW= 75 kg. Oral and dermal internal concentrations in terms of AUC and C_{max} in blood and liver are shown in **Table 4.5.12**. Safe oral values are marked in red. Isopropanol is assumed to be more toxic than its metabolite acetone. Therefore acetone was not considered in the extrapolation procedure.

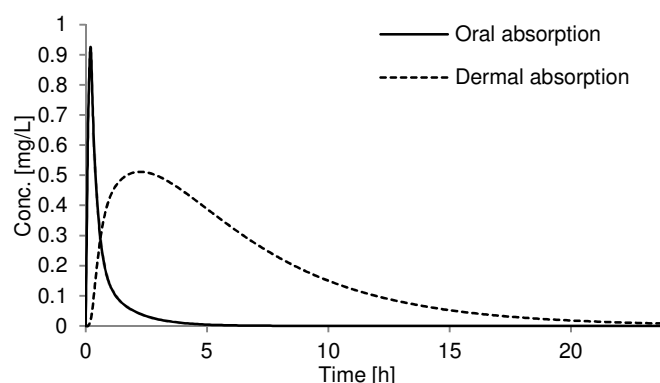


Fig 4.5.10. Isopropanol profiles in blood after oral and dermal absorption of the oral NOAEL dose.

Table 4.5.12. AUC and C_{max} of isopropanol in blood and liver for oral NOAEL dose (oral and dermal absorption)

AUC liver [mg.h/L]		AUC blood [mg.h/L]		C_{max} liver [mg/L]		C_{max} blood [mg/L]	
oral	dermal	oral	dermal	oral	dermal	oral	dermal
1.066	0.489	0.553	4.0735	3.137	0.061	0.926	0.511

Under given exposure conditions (**Table 4.5.1**) Dermal AUC in blood is ca. 10 times higher and C_{max} only slightly lower than the oral results. This indicates that the dermal threshold value is much lower than the oral NOAEL. This threshold was determined by changing the absolute doses applied on skin from 10 times lower the oral NOAEL dose and up to 5 times higher the NOAEL value (**Table 4.5.13**). Skin area was increased in the same way as a dose.

Table 4.5.13. Dermal AUC and C_{max} for several doses

	AUC liver [mg.h/L]	AUC blood [mg.h/L]	C_{max} liver [mg/L]	C_{max} blood [mg/L]
1/10 * NOAEL	0.045	0.375	0.0255	0.213
0.5 * NOAEL	0.242	2.017	0.049	0.410
2 * NOAEL	0.975	8.129	0.0735	0.611
5 * NOAEL	2.110	17.571	0.086	0.7135

It can be concluded that under the analysed conditions and assumptions:

- C_{max} in blood and liver are always higher for oral absorption (**Figure 4.5.10**).
- Dermal AUC in liver becomes higher than the oral one at a dose of ca. 2·NOAEL.
- **Dermal threshold based on AUC in blood is $1/7 \cdot \text{NOAEL} = 1.143 \text{ mg/kg BW/day}$ applied on the skin area $1/7 \cdot 2448 = 128 \text{ cm}^2$ over 4 h (Figure 4.5.11).**

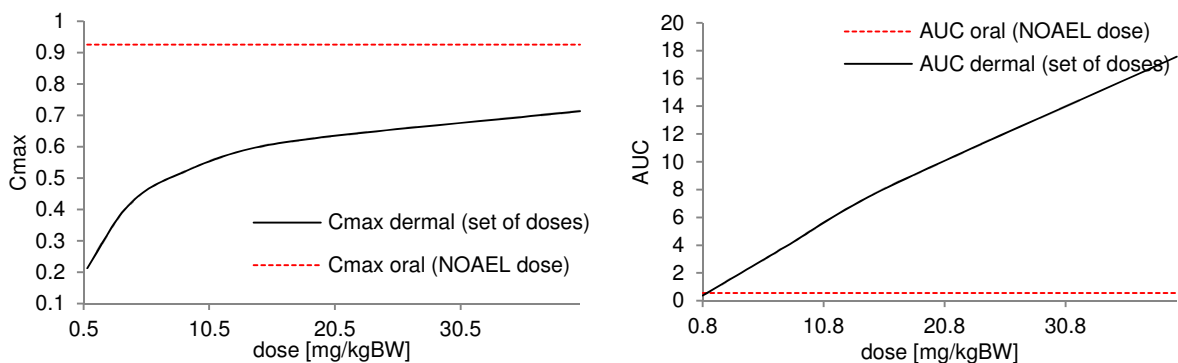


Fig 4.5.11. Determination of dermal threshold values via C_{\max} and AUC in blood.

4.5.2 Oral-to-inhalation extrapolation

Ethanol and isopropanol oral NOAEL doses were translated into internal concentration-time profiles in blood and liver via PBTK1_inh model and compared with, in contrast to previous extrapolations, inhalation results under specified conditions. Exposure limits were used unchanged as in the calibration step regardless of the oral NOAEL value (inhaled air concentrations must be kept constant due to applicability domain of the PBTK model in the similar way to skin absorption). Only time of exposure was increased up to extreme time of 12 h. In this way, the aim was to prove that a given exposure scenario is within a safe limits.

a) Ethanol

Concentration-time profiles of ethanol in blood following oral absorption of the estimated human NOAEL dose simulated by the PBTK3_orl and inhalation of the experimental (literature) concentration simulated by the PBTK1_inh are shown in **Figure 4.5.12**. Simulations were performed for a male subject, BW= 75 kg. Oral and inhalation internal concentrations in terms of AUC and C_{\max} in blood and liver are shown in **Table 4.5.14**. Safe oral values are marked in red. The model was calibrated previously for 6 h of exposure to 0.794 mg/L of ethanol in air and this concentration was used in the extrapolation. Only the exposure time was increased up to 12 h. Lack of different exposure experiments makes it difficult to establish a close to NOAEL dose and time of inhalation. However, it is clear that even 12 h of exposure to ethanol at 0.7943 mg/L is safe (**Tables 4.5.14-15**).

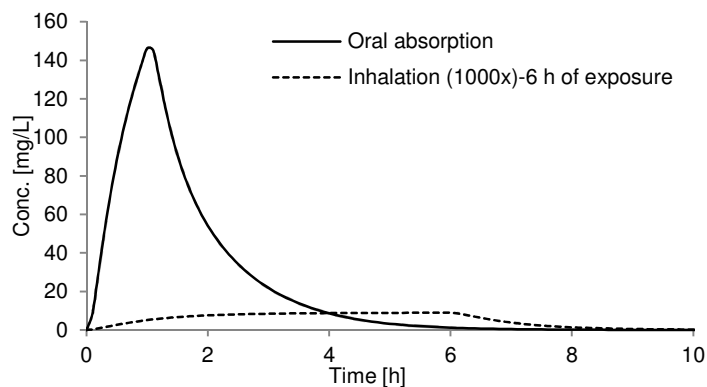


Fig 4.5.12. Ethanol profiles in venous blood after oral absorption and inhalation.

Table 4.5.14. AUC and C_{max} of ethanol in blood and liver for oral NOAEL dose (oral absorption and inhalation)

AUC liver [mg.h/L]		AUC blood [mg.h/L]		C_{max} liver [mg/L]		C_{max} blood [mg/L]	
oral	Inhalation	oral	Inhalation	oral	Inhalation	oral	Inhalation
446.812	0.067	235.586	0.054	158.516	0.011	146.1895	0.009

Table 4.5.15. Inhalation AUC and C_{max} for various exposure times

Time of exposure	AUC liver [mg.h/L]	AUC blood [mg.h/L]	C_{max} liver [mg/L]	C_{max} blood [mg/L]
8 h	0.0884	0.0719	0.011	0.009
10 h	0.111	0.090	0.011	0.009
12 h	0.133	0.110	0.011	0.009

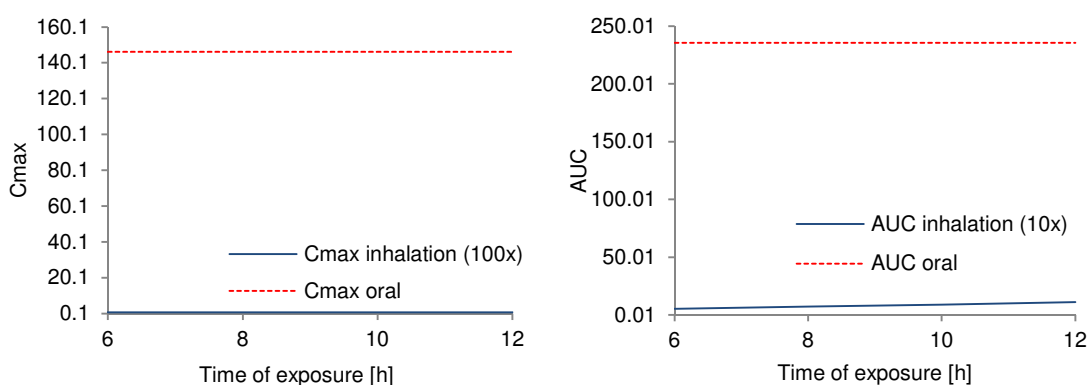


Fig 4.5.13. Determination of inhalation threshold values via C_{max} and AUC in blood.

b) Isopropanol

Concentration-time profiles of isopropanol in blood following oral absorption of the NOAEL dose and inhalation, according to available in literature exposure conditions (0.158 mg/L) were simulated by the PBTK3_orl and PBTK1_inh models respectively. Results are shown in **Figure 4.5.14**. Simulations were

performed for a male subject, BW= 75 kg. Oral and inhalation internal concentrations in terms of AUC and C_{max} in blood and liver are shown in **Table 4.5.16**. Safe oral values are marked in red. 10 min of exposure was initially used and compared with oral safe results. In the same manner, we can show that less than 2 h of exposure to isopropanol at 0.158 mg/L is safe, however, AUC in blood approaches oral safe limit (**Tables 4.5.16-17**).

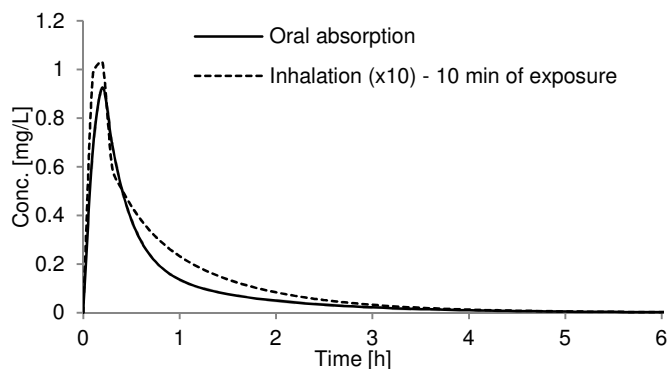


Fig 4.5.14. Isopropanol profiles in venous blood after oral absorption and inhalation.

Table 4.5.16. AUC and C_{max} of isopropanol in blood and liver for oral NOAEL dose (oral absorption and inhalation)

AUC liver [mg.h/L]		AUC blood [mg.h/L]		C_{max} liver [mg/L]		C_{max} blood [mg/L]	
oral	Inhalation	oral	Inhalation	oral	Inhalation	oral	Inhalation
1.066	$9.067 \cdot 10^{-06}$	0.553	0.065	3.137	$3.2 \cdot 10^{-05}$	0.926	0.128

Table 4.5.17. Inhalation AUC and C_{max} for exposure times

	AUC liver	AUC blood	C_{max} liver	C_{max} blood
1 h of exposure	$5.870 \cdot 10^{-05}$	0.440	$4.8 \cdot 10^{-05}$	0.313
2 h of exposure	0.0001	0.880	$5.5 \cdot 10^{-05}$	0.392
3 h of exposure	0.0002	1.320	$5.7 \cdot 10^{-05}$	0.421
6 h of exposure	0.0004	2.640	$5.9 \cdot 10^{-05}$	0.439
12 h of exposure	0.0007	5.281	$5.9 \cdot 10^{-05}$	0.440

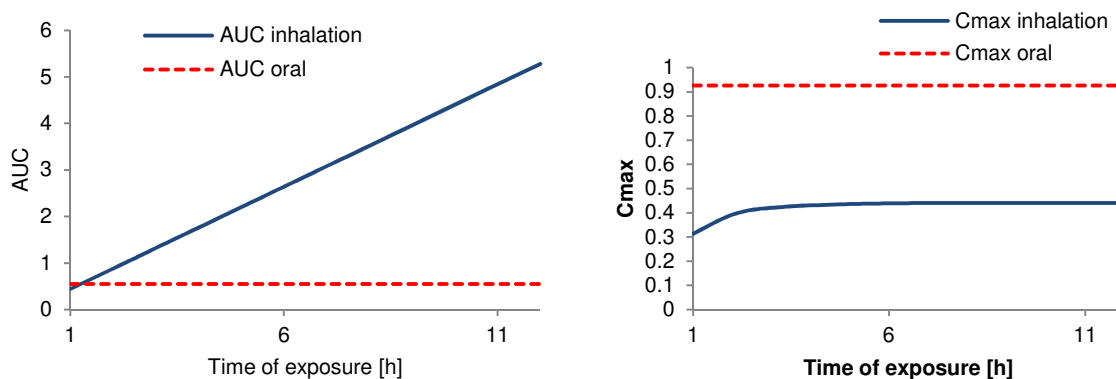


Fig 4.5.15. Determination of inhalation threshold values via C_{max} and AUC in blood.

It can be concluded that under the analysed conditions and assumptions:

Inhalation threshold based on AUC in blood is ca. 0.158 mg/L inhaled for 1.2 h (Figure 4.5.15).

4.5.3 Dermal-to-inhalation extrapolation

Methyl iodide was used to derive inhalation thresholds from dermal exposure results at dermal NOAEL dose for rat and human. This study is just a theoretical example of a different than before type of RtR extrapolation. Rat inhalation PBTK model has been calibrated with respect to *in vivo* data: 25 and 100 ppm (Himmelstein et al., 2009) but there were no data to validate the dermal one. In case of human, the only calibration possible was based on IV data of a single subject (Robertz-Vaupel et al., 1991). PBTK parameters were used from Sweeney et al. 2009 (Sweeney et al., 2009). The parameters for dermal absorptions were calculated by means of QSPRs. Due to these limitations, the following versions of PBTK models were used in the extrapolation:

- PBTK1: inhalation for both rat and human.
- PBTK1: Simple skin model was used for rat with first rate of absorption that is equal $K_{p_{skin}} \cdot Area = cm/h \cdot cm^2$. 2 times the QSPR determined median $K_{p_{skin}}$ for human was used (median $\log K_{p_{skin}} = -5.821$ cm/s).
- PBTK3: human dermal absorption.

Dermal NOAEL value was assumed in a range of 10 mg/mL for rat and for human regardless of interspecies extrapolation to better show difference between rat and human result. Skin Area, as before, was proportionally changed with a dose. Moreover, I assumed in this case study that the PBTK model can be applied to lower than calibrated exposure limits (pure water at standard temperature and pressure has a density of 1 kg/L, therefore ppm \approx mg/L but I took the value 1000 lower, so I compared 10 mg/mL for dermal absorption with 10 ppm for inhalation). Unlike previously, here concentrations of exposed chemical in air were varied.

a) Rat

Concentration-time profiles of methyl iodide in rat blood following dermal absorption and inhalation of 10 mg/mL (30 BW in 0.8 mL) simulated by PBTK1 model are shown in **Figure 4.5.16**. Simulations were performed for a male rat, BW= 0.265 kg. Oral and inhalation internal concentrations in terms of AUC and C_{max} in blood and liver are shown in **Table 4.5.18**. Safe oral values are marked in red.

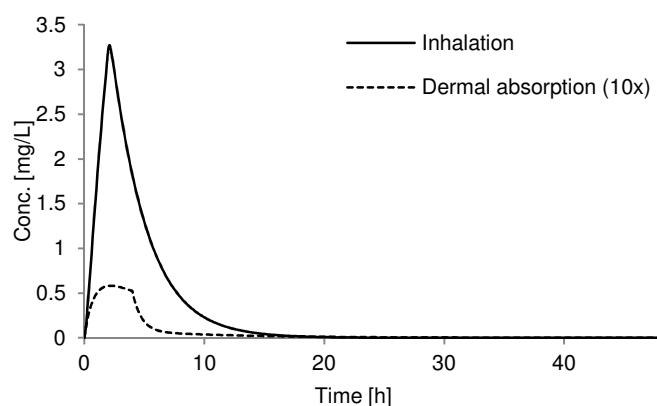


Fig 4.5.16. Concentration-time profiles of MEI in blood after inhalation and dermal absorption.

Table 4.5.18. AUC and C_{max} of MEI in blood and liver for oral NOAEL dose (oral absorption and inhalation)

AUC liver [mg.h/L]		AUC blood [mg.h/L]		C_{max} liver [mg/L]		C_{max} blood [mg/L]	
inhalation	dermal	inhalation	dermal	inhalation	dermal	inhalation	dermal
0.0832	$2.0 \cdot 10^{-04}$	13.690	0.295	0.020	$3.09 \cdot 10^{-05}$	3.271	0.058

Under given exposure conditions (**Table 4.5.1**). Inhalation AUC and C_{max} in blood are ca. 80 times higher than the dermal results. This indicates that the inhalation threshold value is much lower than the assumed dermal NOAEL of 10 mg/mL. This threshold was determined by changing the absolute doses applied on skin from 600 times lower the NOAEL dose and up to 10 times lower the NOAEL value (**Table 4.5.19**). Skin area was decreased in the same way as a dose.

Table 4.5.19. Inhalation AUC and C_{max} for different concentrations

	AUC liver	AUC blood	C_{max} liver	C_{max} blood
(10)/600	0.0001	0.018	$2.6 \cdot 10^{-05}$	0.004
(10)/100	0.0007	0.107	$2 \cdot 10^{-04}$	0.025
(10)/50	0.0013	0.216	0.0003	0.051
(10)/10	0.007	1.113	0.002	0.266

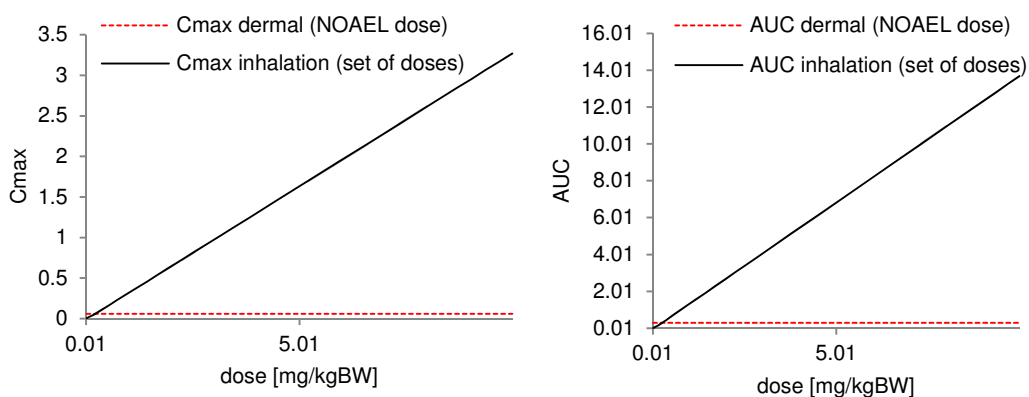


Fig 4.5.17. Determination of inhalation thresholds values via C_{max} and AUC in blood.

It can be concluded that under the analysed conditions and assumptions:

- All the investigated toxicokinetic parameters are higher after inhalation.
- **Inhalation threshold based on C_{max} in blood is 45 times lower than 10 mg/mL and equals to 0.22 mg/mL over 2 h.**

b) Human

Concentration-time profiles of methyl iodide in human blood following dermal absorption and inhalation of 10 mg/mL (0.03 BW in 0.255 mL) simulated by PBTK1 (inhalation) and PBTK3 (dermal absorption) models are shown in **Figure 4.5.18**. Simulations were performed for a male subject, BW= 85 kg. Oral and inhalation internal concentrations in terms of AUC and C_{max} in blood and liver are shown in **Table 4.5.20**. Safe oral values are marked in red.

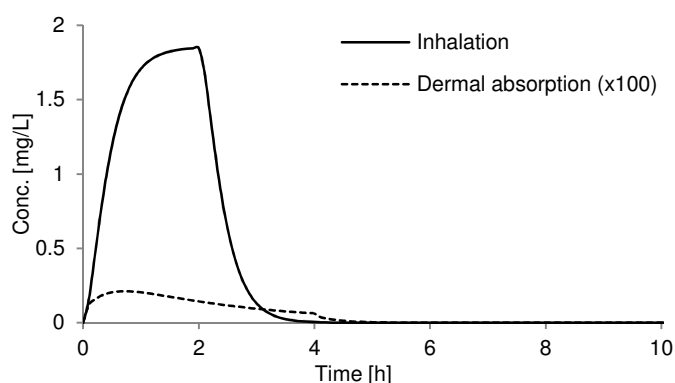


Fig 4.5.18. Concentration-time profiles of MEI in blood after inhalation and dermal absorption.

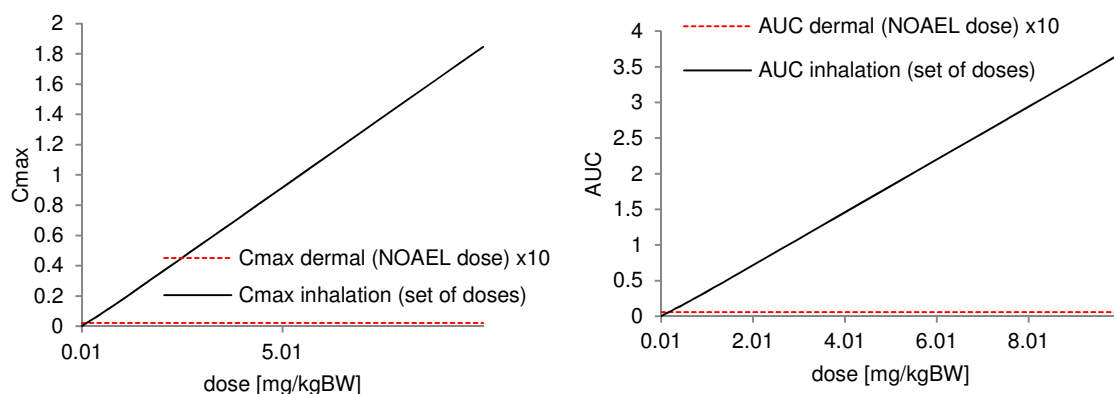
Table 4.5.20. Human AUC and C_{max} of iodomethane in blood and liver for inhalation NOAEL (inhalation and dermal absorption)

AUC liver [mg.h/L]		AUC blood [mg.h/L]		C_{max} liver [mg/L]		C_{max} blood [mg/L]	
inhalation	dermal	inhalation	dermal	inhalation	dermal	inhalation	dermal
0.249	$1.5 \cdot 10^{-04}$	3.678	0.006	0.125	$5.55 \cdot 10^{-05}$	1.847	0.002

Under given exposure conditions (**Table 4.5.1**). Inhalation toxicokinetic parameters in blood and liver are ca. 1000 times higher than the dermal results. This indicates that the inhalation threshold value is again much lower than the assumed dermal NOAEL of 10 mg/mL. This threshold was determined by changing the absolute doses applied on skin from 1000 times lower the NOAEL dose and up to 10 times lower the NOAEL value (**Table 4.5.21**). Skin area was decreased in the same way as a dose.

Table 4.5.21. Inhalation AUC and C_{max} for different concentrations

	AUC liver [mg.h/L]	AUC blood [mg.h/L]	C_{max} liver [mg/L]	C_{max} blood [mg/L]
10/1000	0.00023	0.0034	$1 \cdot 10^{-04}$	0.0017
10/600	0.0004	0.0057	$2 \cdot 10^{-04}$	0.0028
10/100	0.0023	0.0341	0.0012	0.017
10/50	0.0047	0.068	0.0023	0.034
10/10	0.024	0.3465	0.0119	0.173

**Fig 4.5.19.** Determination of inhalation thresholds values via C_{max} and AUC in blood.

It can be concluded that under the analysed conditions and assumptions:

Inhalation threshold based on C_{max} in blood is 800 times lower than 10 mg/mL and equals to 0.0125 mg/mL over 2 h.

4.6 Ethanol case studies

Two ethanol case studies are presented in this chapter: i) the application of physiologically-based toxicokinetic/pharmacokinetic (PBTK/PBPK) modelling in simulating the time-dependent concentrations of ethanol and its two minor metabolites: ethyl glucuronide and ethyl sulfate, in blood and urine, for the healthy Caucasian population; ii) modelling of ethanol skin absorption from various vehicles.

4.6.1 Simulation of ethanol metabolites in serum and urine following oral administration

In this study, I was interested to adapt the PBTK3_orl model to estimate the subject-specific EtG and EtS concentration-time profiles in human biological samples (serum and urine) with the ultimate goal to back-extrapolate to the time of alcohol intake, assuming that the dose ingested is known.

The model parameters were divided into population (constant) and subject-dependent (variable); and kinetic parameters (expressed as L or mg per h) were additionally refined to account for inter-individual variations in body mass index (BMI) and sex differences in body organ/tissue fractions of the overall body weight (in

particular adipose tissue). In this way, there were only up to four variable parameters to be fitted with respect to individual *in vivo* blood and urine data to ensure a good match of time dependent variables like peak concentration and area under curve in the considered organs and bio-fluids (more details below).

I used existing literature absorption and metabolism rates of ethanol to acetaldehyde (its main metabolite) as starting values prior to their optimisation (of all the parameters that showed sensitivity towards AUC of ethanol, EtS, EtG or creatinine- see **Table 4.6.2**) with respect to individual and median experimental data:

- Blood ethanol concentrations were taken from two drinking experiments performed by (Wilkinson et al., 1977a, 1977b), under fasting conditions: i) eight healthy adult white male volunteers received 15, 30, 45 and 60 mL of 95% ethanol in orange juice (total volume of each dose was 150mL; ii) a single adult male volunteer (74.9 kg) was given 30 and 45 mL of 95% alcohol in a total volume of 180 mL (made up with orange juice) – **Figure 4.6.1**.

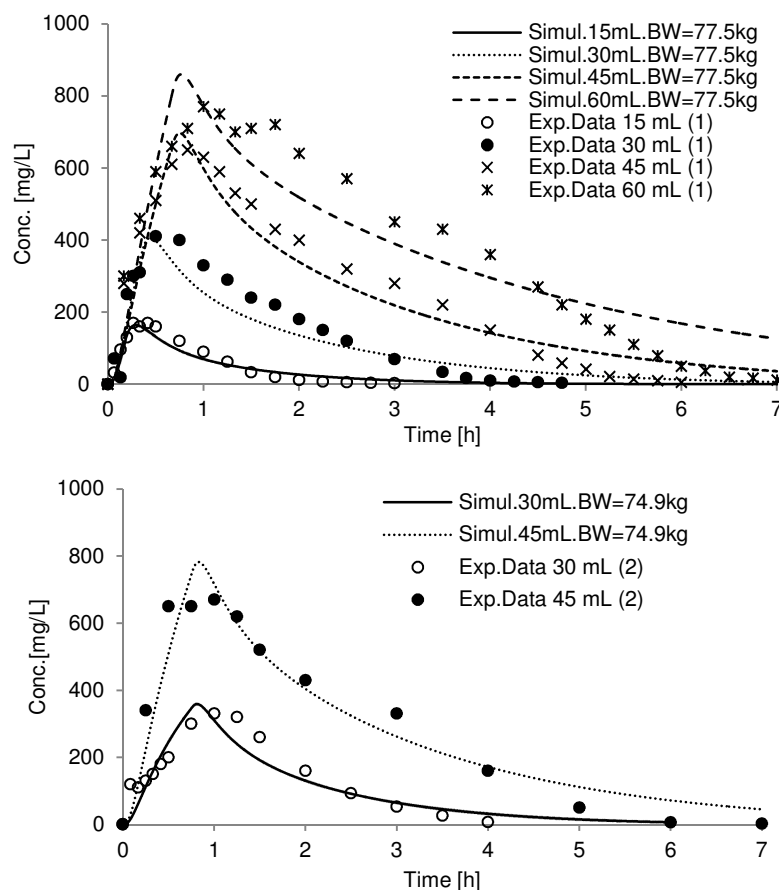


Fig 4.6.1. Concentration-time profiles of different doses of ethanol in blood according to: (1) (Wilkinson et al., 1977a), (2) (Wilkinson et al., 1977b).

- Acetaldehyde concentrations from alcohol drinking study of Jones et al. (Jones et al., 1988) were used to further refine reverse metabolism rates of ethanol to acetaldehyde (V_{rev} , $K_{m_{rev}}$).

- For the purpose of this work, EtG and EtS serum and urinary concentrations from the drinking study of (Lostia et al., 2013) were used to refine the model in terms of EtG and EtS kinetics. In this study, 18 healthy volunteers (9:9 male: female, non-Asian, 18–35 years old and with a body weight between 50 and 80 kg) participated in two separate controlled drinking experiments, with at least 1 week interval in between, and provided blood and urine samples. Asians were excluded because 40 % of the Asian population has a gene deletion and lacks the enzyme to metabolise ethanol to acetaldehyde. For each drinking experiment, volunteers abstained from alcohol during the 3 days before the study (based on self-reporting and confirmed by analysis of EtG and EtS in urine), and for 3 days after alcohol administration. In the first experiment, 4 units of alcohol (corresponding to a mean value of 0.76 g of ethanol/ kg of body weight, calculated by the Widmark equation; Widmark factors used: 0.68 for males and 0.55 for females) was administered, while in the second one, 8 units of alcohol (corresponding to a mean value of 1.53 g/kg). Ethanol was consumed at lunch time (12 a.m.) over a total period of 60 min (for 4 units, volunteers had to drink 100 mL of alcoholic drink every 15 min, while for 8 units they drank 125 mL every 15 min). Urine samples were collected after alcohol administration every hour for the first 7 h and then after 10, 24, 48 and 72 h. For each sample, all the urine volume was collected and measured. Blood samples of 15 mL were collected every hour for the first 6 h and then after 24 and 48 h. After collection, the serum fraction was isolated and used for the analysis. The following analytes were measured: EtG and EtS in serum and urine, ethanol in serum and urinary creatinine. The analysis was performed by the Drug Control Centre (King's College, London), which is accredited to ISO 17025 and by the World Anti-Doping Agency for drug testing analysis, using validated methods developed in house. In the calibration step of the PBTK model, the experimental data of 16 out of 18 volunteers were used per dose of ethanol, while data for the remaining two volunteers were used for the model validation.

The experimental data of two volunteers enrolled in the study of (Lostia et al., 2013) were used to validate the PBTK model in terms of its prediction power in simulating EtG and EtS concentration-time profiles in serum and urine samples. From the dataset composed of 18 subjects, one male administered with 4 units of alcohol and one female with 8 units were randomly selected and excluded from the training set used to calibrate the model. The training set was composed of a number of experimental values measured every hour up to 6 h in serum and 10 h in urine for each of 16 subjects, whereas the test set of the two subjects was limited to 3 random consecutive (with 1 h difference) EtG and EtS serum and urine concentrations were taken. The procedure for assigning subjects to the training and tests sets was repeated twice, and on each occasion the volunteers selected were different. The exact time of the sample collection after ethanol ingestion was assumed unknown while the dose of ethanol ingested (4 or 8 units) was used in the model prediction since the aim was to challenge the ability of the model to back-extrapolate to the time "zero" corresponding to the time of alcohol ingestion. In a real case scenario the dose of ethanol ingested would also be unknown. The primary goal of this work was thus to use PBTK modeling to predict the time of alcohol

drinking. The rationale for using three consecutive concentrations is based on the findings of (Lostia et al., 2013), and is explained more in the discussion section.

All physiological parameters for a reference man and woman were refined, for this type of study only, in terms of adipose tissue that was calculated by using the equation taken from (Deurenberg et al., 1998):

$$\frac{1.29 \cdot BMI + 0.2 \cdot Age - 8}{100} \text{ for a man and } \frac{1.29 \cdot BMI + 0.2 \cdot Age - 19.4}{100} \text{ for a woman (BMI: Body Mass Index).}$$

The kinetic parameters are: the rates of ethanol absorption in the GI tract (stomach and intestines), ethanol metabolism to acetaldehyde, EtG and EtS formation rates, renal clearance of ethanol, EtG and EtS and urinary creatinine formation and elimination. For a pragmatic implementation of the model, these parameters are distinguished into those that are assumed constant between individuals (subject-independent or population constant- optimised as population averages), and those that are subject-dependent (need to be optimised against individual experimental data). In particular, the absorption of ethanol in the GI tract, its metabolism to acetaldehyde, and renal clearance of EtS and EtG are treated as subject-independent, while the formation rates of EtG and EtS, renal clearance of ethanol and urinary creatinine formation are considered subject-dependent (explained below) -**Figure 4.6.2**. This decision was based on the results of sensitivity analysis that indicated the most sensitive parameters with respect to serum AUC.

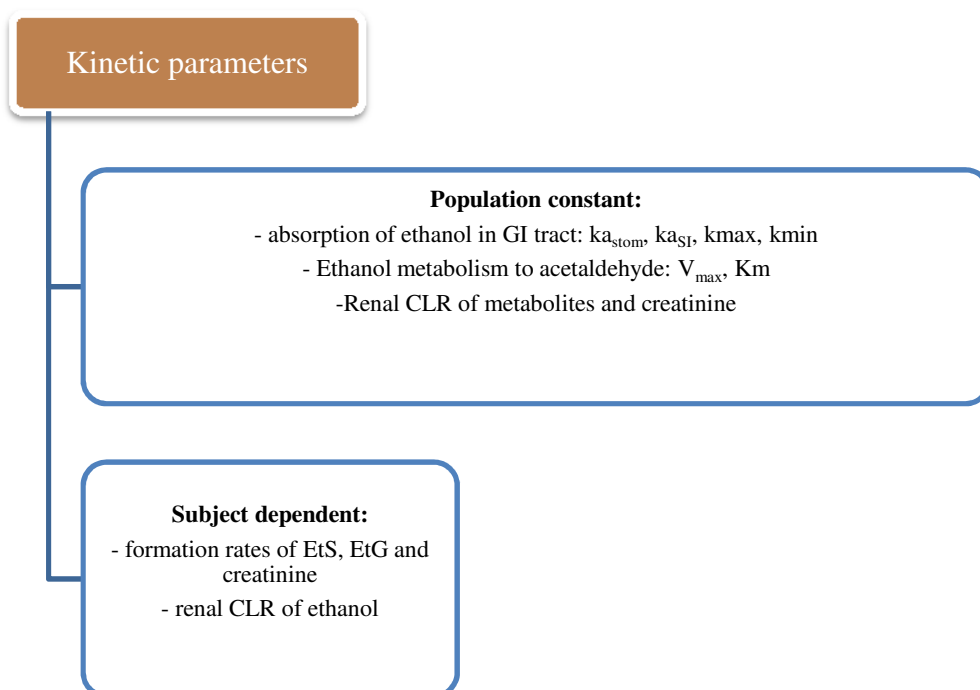


Fig 4.6.2. Kinetic parameters divided into population constant and subject-specific groups.

The following refinement and assumptions were made in developing the model:

- a) Absorption

The absorption rate of ethanol in stomach, taken from (Loizou and Spendiff, 2004), was optimised according to ethanol serum concentration from (Lostia et al., 2013) with the alcohol drinking time of 60 min.

b) Distribution

Tissue-to-blood partition coefficients (PC) for ethanol, EtG and EtS were calculated using the formula from (Schmitt, 2008) and used unchanged for all the subjects.

c) Metabolism

- Acetaldehyde

The reversible Michaelis-Menten kinetic equation (see **Equation 4.6.1**) describing the ethanol metabolism to acetaldehyde was taken from (Umulis et al., 2005). The V_{max} and K_m values of the equation were then optimised by using the ethanol blood concentrations from (Wilkinson et al., 1977a, 1977b), assumed population constant and ultimately the V_{max} was refined by BMI.

$$r_{Acet} = \frac{V_{max} \cdot \frac{C_{Eth,liv}}{PC_{Eth,liv}} - V_{rev} \cdot \frac{C_{Acet,liv}}{PC_{Acet,liv}}}{\left(Km + \frac{C_{Eth,liv}}{PC_{Eth,liv}} \right) \cdot \left(Km_{rev} + \frac{C_{Acet,liv}}{PC_{Acet,liv}} \right)} \quad (4.6.1)$$

Where:

$C_{Eth,liv}$: ethanol concentration in liver [mg/L]

$C_{Acet,liv}$: acetaldehyde concentration in liver [mg/L]

PC_{liv} : liver-to-blood partition coefficient

V_{rev} : the maximum rate of the reverse reaction of acetaldehyde to ethanol [mg/h]

Km_{rev} : reaction constant for the rate law [mg/L]

- EtG and EtS

The formation rates of EtS and EtG were calculated using serum concentrations from (Lostia et al., 2013). They follow 2nd and 0.6 orders respectively (**Equation 4.6.2**) and remained subject-specific. These two values were selected because they allow for a better fit of the concentration-time profiles than when a 1st order formation rate was used for both metabolites. Previously published kinetic (not physiologically based) models (Droenner et al., 2002; Schmitt et al., 2010) assumed 1st order formation rates for both EtG and EtS.

$$r_{EtG} = K_{formEtG}^{0.6} \cdot \frac{C_{Eth,liv}}{PC_{Eth,liv}} \quad r_{EtS} = K_{formEtS}^2 \cdot \frac{C_{Eth,liv}}{PC_{Eth,liv}} \quad (4.6.2)$$

d) Kidney elimination

- Ethanol

Subject specific ethanol renal clearance was calculated from individual serum data as a correction factor for inter-subject differences in ethanol elimination not taken into account by liver metabolism.

- EtG and EtS

Renal clearance rates of EtG and EtS were optimised by using the urinary concentrations normalised to creatinine from (Lostia et al., 2013), while the bladder emptying rate was calculated using the experimental urinary volumes. For renal clearance and bladder emptying rates, the subject-specific values were all very similar between the 16 volunteers (ranges: renal clearance: 0.6-1 L/h, bladder emptying rate: 0.08-0.12 L/h) therefore median values were calculated and used for both genders.

- Creatinine

Creatinine formation and elimination rates were optimised with respect to creatinine concentration data (Lostia et al., 2013). The formation rate remained subject-dependent and elimination was assumed equal to 5·BMI [mg/h] for the analysed population according to the model fitting results. The need for modelling creatinine came from the use of normalised to creatinine urinary experimental data.

Calculated dimensionless tissue-to- blood partition coefficients (Schmitt, 2008) for ethanol, acetaldehyde, EtS and EtG are reported in **Table 4.6.1**.

Table 4.6.1. Tissue-to-blood partition coefficients of ethanol, acetaldehyde, EtS and EtG

Tissue-to-blood partition coefficients	Ethanol	Acetaldehyde	EtS	EtG
Liver	0.86	0.83	0.84	0.83
Poorly perfused tissues	0.64	0.625	0.635	0.57
Highly perfused tissues	0.92	0.88	0.9	0.85
Lungs	0.92	0.9	0.91	0.82
Kidney	0.9	0.88	0.89	1
GI tract	0.9	0.88	-	-
Adipose tissue	0.59	0.17	0.17	0.17
Skin	0.76	0.71	0.72	0.69

Ethanol population constant kinetic parameters such as absorption rates in the GI tract, liver metabolism to acetaldehyde are given in **Table 4.6.2** together with the source (taken from literature or optimised).

Table 4.6.2. Ethanol absorption and liver metabolism parameters

	Literature value	Reference	Optimised value	Optimised with respect to
GI tract absorption of ethanol:				
Stomach abs $k_{a_{stom}}$ [1/h]	0.6584		4	Ethanol serum/blood concentrations (Lostia et al., 2013)
Intestine abs. $k_{a_{SI}}$ [1/h]	25.1	(Loizou and Spendiff, 2004)	-	-
Stomach emptying rates k_{max}, k_{min} [1/h]	8.16 0.05		-	-
Ethanol metabolism to Acetaldehyde:				
V_{max}	2.2 mmol (min ⁻¹ kg liver) ⁻¹		10 mg/h/BMI	Ethanol serum/ blood concentrations (Lostia et al., 2013)
K_m	0.4 mM		0.962 mg/L	(Wilkinson et al., 1977a, 1977b)
V_{rev}	32.6 mmol (min ⁻¹ kg liver) ⁻¹	(Umulis et al., 2005)	20 mg/h/BMI	Acetaldehyde blood conc. (Jones et al., 1988)
$K_{m_{rev}}$	1 mM		-	-
Blood-air partition coefficient for ethanol $PC_{bloodair}$	1352.5	(Meulenberg and Vijverberg, 2000)	-	-
Blood-air partition coefficient for acetaldehyde $PC_{bloodair,met}$	183	(Jones et al., 1985)	-	-

The following kinetic parameters, formation rates of EtS and EtG in liver, ethanol renal clearance and creatinine formation, were calculated for each subject and are provided in **Table 4.6.3** for the training set of 16 subjects. Statistics of fitting and median results are given in **Table 4.6.3** with a coefficient of correlation (R^2) and mean squared error (MSE).

Table 4.6.3. Parameters fitting with respect to individual concentration time profiles in blood and urine

Subject	BW	Hm	Age	$K_{formEtS}$ [L/h/BMI]	$K_{formEtG}$ [L/h/BMI]	CLR_{Eth} [L/h/BMI]	$R_{formCreat}$ [mg/h/BMI]
4 units of ethanol							
1	81	189	28	$9.10 \cdot 10^{-07}$	0.015	30	5.5
2	72	183	24	$1.80 \cdot 10^{-06}$	0.019	20	5.5
3	75	173	30	$1.30 \cdot 10^{-06}$	0.02	50	4
4	75	184	23	$3.10 \cdot 10^{-06}$	0.019	20	4
5	71.6	181	21	$1.40 \cdot 10^{-06}$	0.023	5	3.5
6	74	173	20	$1.40 \cdot 10^{-06}$	0.024	15	3
7	75.3	178	27	$2.00 \cdot 10^{-06}$	0.023	150	4
8	78.5	185	20	$2.00 \cdot 10^{-06}$	0.021	15	4
9	68	165	28	$1.70 \cdot 10^{-06}$	0.018	9	4
1	77.5	173	21	$1.30 \cdot 10^{-06}$	0.02	30	3
2	64	166	20	$9.00 \cdot 10^{-07}$	0.019	3	3

3	70	170	25	$1.50 \cdot 10^{-06}$	0.029	2	3
4	60	170	29	$1.20 \cdot 10^{-06}$	0.013	4	3
5	61	162	22	$9.00 \cdot 10^{-07}$	0.018	3	2
6	72	173	25	$1.40 \cdot 10^{-06}$	0.027	3	3
7	56	179	30	$7.50 \cdot 10^{-07}$	0.029	4	2.5
8	64	159	19	$1.10 \cdot 10^{-06}$	0.02	4	2.5
9	75	168	21	$1.10 \cdot 10^{-06}$	0.012	15	3
Median man	75	181	24	$1.80 \cdot 10^{-06}$	0.021	20	4.50
Median woman	64	170	22	$1.10 \cdot 10^{-06}$	0.019	4.0	2.50
8 units of ethanol							
1	81	189	28	$4.10 \cdot 10^{-07}$	0.024	0.5	6.5
2	72	183	24	$6.50 \cdot 10^{-07}$	0.024	2	4.5
3	75	173	30	$4.00 \cdot 10^{-07}$	0.025	1	3.5
4	75	184	23	$1.10 \cdot 10^{-06}$	0.025	1	3.5
5	71.6	181	21	$5.40 \cdot 10^{-07}$	0.025	0.1	3.5
6	74	173	20	$5.70 \cdot 10^{-07}$	0.03	1.5	3
7	75.3	178	27	$5.00 \cdot 10^{-07}$	0.015	1	3
8	78.5	185	20	$7.00 \cdot 10^{-07}$	0.025	0.5	3
9	68	165	28	$4.60 \cdot 10^{-07}$	0.02	0.5	3
1	77.5	173	21	$4.60 \cdot 10^{-07}$	0.028	0.5	2.5
2	64	166	20	$3.50 \cdot 10^{-07}$	0.022	0.1	3
3	70	170	25	$4.90 \cdot 10^{-07}$	0.028	0.5	4.5
4	60	170	29	$3.60 \cdot 10^{-07}$	0.009	0.1	2.5
5	61	162	22	$3.70 \cdot 10^{-07}$	0.021	0.1	4
6	72	173	25	$6.00 \cdot 10^{-07}$	0.04	0.1	2
7	56	179	30	$2.80 \cdot 10^{-07}$	0.033	0.1	2
8	64	159	19	$3.50 \cdot 10^{-07}$	0.02	0.1	2
9	75	168	21	$4.10 \cdot 10^{-07}$	0.014	0.1	2
Median man	75	181	24	$5.70 \cdot 10^{-07}$	0.0250	1.00	3.500
Median woman	64	170	22	$3.70 \cdot 10^{-07}$	0.0230	0.10	3.00

Table 4.6.4. Median subject-dependent parameters and statistics

Parameter	Range	Median value
Age	Men: 20-30 Women: 19-30	Men:24 Women:22
Height [cm]	Men: 165-189 Women: 159-179	Men: 181 Women: 170
BW [kg]	Men: 68-81 Women: 56-77.5	Men:75 Women:64
EtS formation rate [L/h/BMI] K_{formEtS}	Men: $4 \cdot 10^{-07}$ - $3.1 \cdot 10^{-06}$ MSE: $1.29 \cdot 10^{-05}$ -0.016 R^2 :-26.17-97 Women: $2.80 \cdot 10^{-07}$ - $1.50 \cdot 10^{-06}$ MSE: $1.4 \cdot 10^{-04}$ -0.005 R^2 :60-94.32	Men: $1.01 \cdot 10^{-06}$ MSE: $8.2 \cdot 10^{-04}$ R^2 :89.22 Women: $6.75 \cdot 10^{-07}$ MSE: 0.001 R^2 : 79.434
EtG formation rate [L/h/BMI] K_{formEtG}	Men: 0.015-0.030 MSE: $8.08 \cdot 10^{-05}$ -0.081 R^2 :-111.32-98 Women: $9.00 \cdot 10^{-03}$ -0.040 MSE: $1.04 \cdot 10^{-04}$ -0.033 R^2 :40-93.183	Men: 0.023 MSE:0.0048 R^2 :79.98 Women:0.021 MSE: 0.006 R^2 : 66.59
Ethanol renal clearance [L/h/BMI] CLR_{Eth}	Men: 0.1-150 MSE:169.647-42625.74 R^2 : 47.16-98.78 Women:0.1-30 MSE:213.22-33022.65	Men: 3.5 MSE: 5299.091 R^2 : 91.90 Women: 1.25 MSE: 7331.124

Dose dependency and inter-subjects variations

Fitting of subject-dependent parameters to individual concentration-time profiles in serum and urine showed the following:

- Ethanol renal clearance used here as a correction factor for inter-subject differences in ethanol elimination decreased with increasing dose from median 2.20 to 1 [L/h/BMI] for men and 4 to 0.1 L/h/BMI for women. EtS and creatinine formations showed similar results but, oppositely, EtG formation increased slightly with increased dose.
- There were clear gender-based differences in the fitted values – the highest for ethanol clearance and the lowest for EtG formation.

Figure 4.6.3 shows the difference in fitted formation rates of EtS and EtG and ethanol clearance among individuals and for the two ethanol doses. EtS formation rate and ethanol clearance seem to decrease with alcohol dos, whereas EtG formation rate is more or less unchanged.

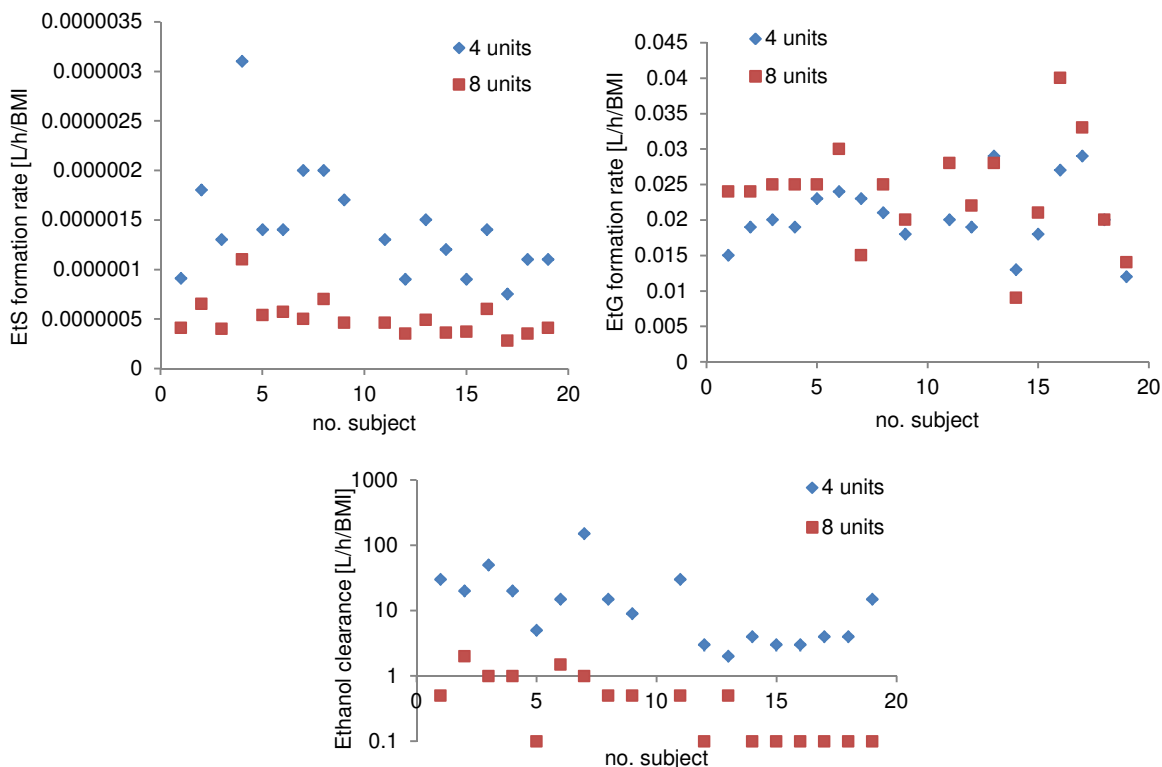


Fig 4.6.3. Inter-subject differences in EtS and EtG formation rates and ethanol clearance.

Ethanol in serum

Figure 4.6.4 shows median simulated concentration-time profiles of ethanol in serum for men and women and their experimental values. Simulations showed that ethanol reaches C_{\max} of 508 mg/L at 1.1 h (4 units, women), 314 mg/L at 1 h (4 units, men), 1312.7 mg/L at 1.1 h (8 units, women) and 1029.5 mg/L at 1.1 h (8 units, men). Based on the experimental results of (Lostia et al., 2013) a concentration threshold level of 0.01 mg/L was chosen here as the lowest possible concentration (calculated by the PBTK model) below which it is assumed that a compound is fully eliminated from the serum. Ethanol concentrations less than 0.01 mg/L were estimated at 16.7 h (4units, women), 14.9 h (4 units, men), 30.3 h (8 units, women) and 28.1 h (8 units, men). At 24 h, the model predicted in serum $1.44 \cdot 10^{-05}$ mg/L (4 units, women), $5.02 \cdot 10^{-08}$ mg/L (4 units, men), 1.85 mg/L (8 units, women) and 0.034 mg/L (8 units, men) of ethanol.

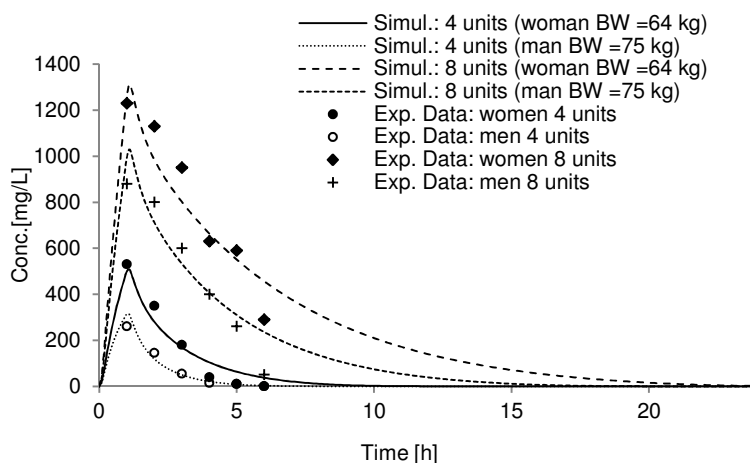


Fig 4.6.4. Simulated and experimental ethanol concentration-time profiles in serum following consumption of 4 and 8 units of alcohol: Exp. data: (Lostia et al., 2013)

EtS and in serum and urine

Simulations of EtS serum concentrations indicated the peak concentration of 0.32 mg/L at 1.4 h (4 units, women), 0.23 mg/L at 1.2 h (4 units, men), 0.69 mg/L at 2.4 h (8 units, women) and 0.55 mg/L at 2 h (8 units, men) (**Figure 4.6.5**). EtS serum levels below 0.01 mg/L were predicted after 12.9 h (4units, women), 12.5 h (4 units, men), 19.4 h (8 units, women) and 18.7 h (8 units, men). At 24 h, the estimated EtS serum concentrations were: $2.23 \cdot 10^{-04}$ mg/L (4 units, women), $3.72 \cdot 10^{-04}$ mg/L (4 units, men), 0.0021 mg/L (8 units, women and men).

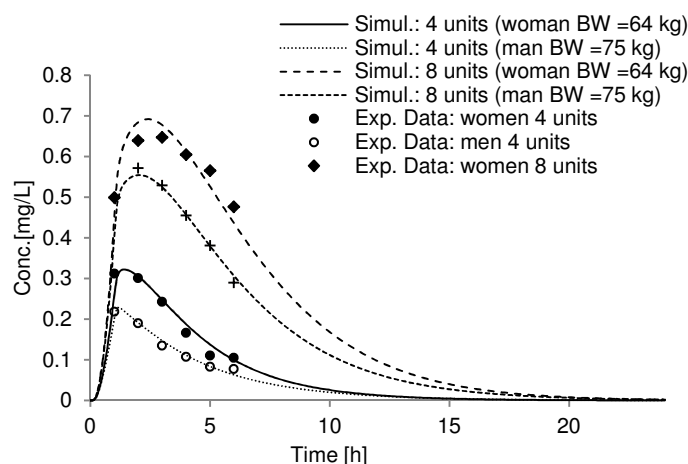


Fig 4.6.5. Simulated and experimental EtS concentration-time profiles in serum following consumption of 4 and 8 units of alcohol: Exp.Data: (Lostia et al., 2013).

Simulated urinary concentrations normalised to creatinine resulted in the peak concentration of 0.0428 at 2.1 h (4 units, women), 0.0163 at 1.9 h (4 units, men), 0.0825 at 3 h (8 units, women), 0.0579 at 2.7 h (8 units, men) (Figure 4.6.6). Women data for 4 and 8 units are particularly difficult to model due to higher fluctuations. At 24 h the urine levels of EtS were: $3.97 \cdot 10^{-05}$ (4 units, women), $3.66 \cdot 10^{-05}$ (4 units, men), $3.116 \cdot 10^{-04}$ (8 units, women) and $2.7 \cdot 10^{-04}$ (8 units, men).

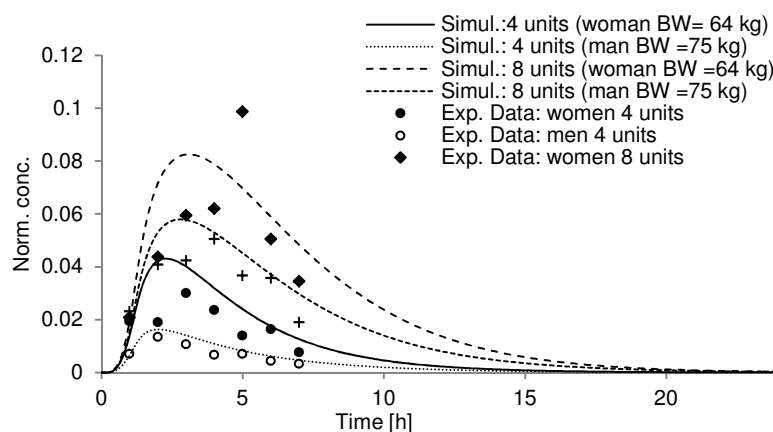


Fig 4.6.6. Simulated and experimental EtS concentration-time profiles in urine following consumption of 4 and 8 units of alcohol: Exp.Data: (Lostia et al., 2013).

EtG in serum and urine

For EtG, the serum C_{max} values were: 0.54 mg/L at 2.9 h (4 units, women), 0.37 mg/L at 2.2 h (4 units, men), 1.39 mg/L at 4.5 h (8 units, women) and 1.08 mg/L at 4.2h (8 units, men). EtG concentrations below 0.01

mg/L in serum were predicted after 18.4 h (4 units, women), 16.5 h (4 units, men), 31.5 h (8 units, women) and 28.1 h (8 units, men) (**Figure 4.6.7**). At 24 h they were equal to: 0.0013 mg/L (4 units, women), $9.66 \cdot 10^{-4}$ mg/L (4 units, men), 0.118 mg/L (8 units, women) and 0.0335 mg/L (8 units, men).

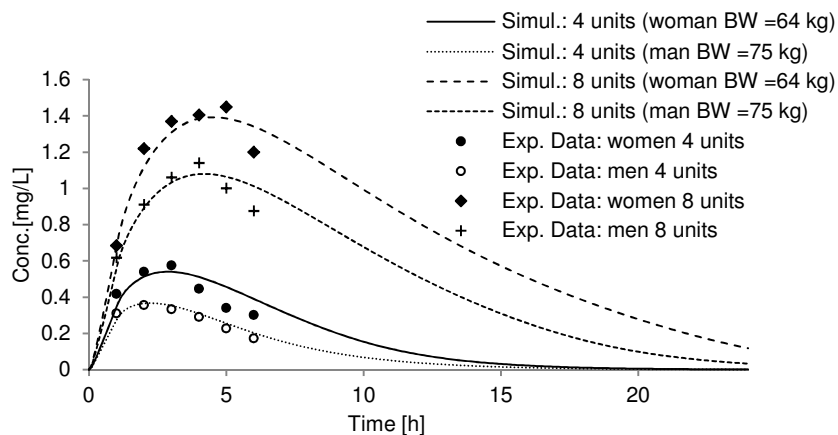


Fig 4.6.7. Simulated and experimental EtG concentration-time profiles in serum following consumption of 4 and 8 units of alcohol: Exp.Data: (Lostia et al., 2013).

In a similar way to EtS, EtG urinary concentration-time profiles revealed higher deviations from experimental data points, especially in the elimination phase (**Figure 4.6.8**).

Simulated urinary concentrations showed the peak concentration of 0.077 at 4 h (4 units, women), 0.03 at 2.8 h (4 units, men), 0.169 at 5 h (8 units, women), 0.1155 at 4.7 h (8 units, men). At 24 h, predicted urinary ratios of EtG to creatinine were: $2.41 \cdot 10^{-4}$ (4 units, women), $9.60 \cdot 10^{-5}$ (4 units, men), 0.0165 (8 units, women) and 0.0042 (8 units, men).

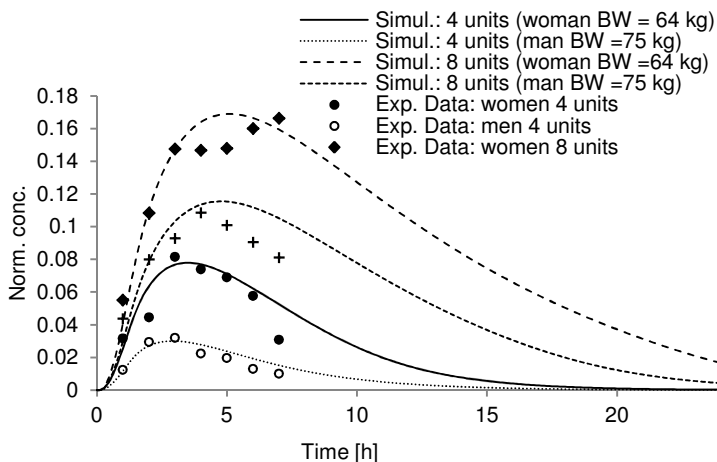


Fig 4.6.8. Simulated and experimental EtG concentration-time profiles in urine following consumption of 4 and 8 units of alcohol: Exp.Data: (Lostia et al., 2013).

Sensitivity analysis

The local sensitivity (in terms of AUC in serum) output and Monte Carlo simulations for all investigated kinetic parameters are presented in **Appendix 1**. The ranking of the most sensitive parameters with respect to ethanol, EtS and EtG serum concentrations is different. However, the following parameters are highly ranked for all of the three substances: stomach absorption rate ($k_{a_{\text{stom}}}$), ethanol metabolism rate to acetaldehyde (V_{max}) and ethanol renal clearance (CLR_{eth}) and drinking rate (Dt). Others include renal clearance rate of metabolites (CLR_{EtG} , CLR_{EtS}) and formation rates of metabolites (K_{formEtS} , K_{formEtG}).

Based on the sensitivity functions the collinearity value for a whole set of parameters was more than 20 for ethanol, EtS and EtG. The best sets for calibration (according to collinearity index) included 2-3 parameters. The following groups showed the smallest index: for ethanol: CLR_{eth} , V_{max} (3.1), CLR_{eth} , V_{max} , $k_{a_{\text{stom}}}$ (5.72), CLR_{eth} , $k_{a_{\text{SI}}}$, $k_{a_{\text{stom}}}$ (6.45), CLR_{eth} , K_m , $k_{a_{\text{SI}}}$ (7.65), CLR_{eth} , $K_{m_{\text{rev}}}$, V_{max} (8.15), CLR_{eth} , K_m , k_{min} (8.52); for EtS: $K_{\text{met}_{\text{EtS}}}$, CLR_{EtS} (1.81), $K_{\text{met}_{\text{EtS}}}$, CLR_{EtS} , $k_{a_{\text{stom}}}$ (5.56), $K_{\text{met}_{\text{EtS}}}$, $k_{a_{\text{SI}}}$, $k_{a_{\text{stom}}}$ (5.71); and for EtG: $K_{\text{met}_{\text{EtG}}}$, CLR_{EtG} (2.32), $K_{\text{met}_{\text{EtG}}}$, CLR_{EtG} , $k_{a_{\text{stom}}}$ (7.22), $K_{\text{met}_{\text{EtG}}}$, CLR_{EtG} , $k_{a_{\text{SI}}}$ (7.86). Based on these results the group of subject-dependent, variable, parameters for fitting was selected.

Finally, Monte Carlo simulations confirmed that the parameters with highest impact on the variability of serum concentrations were for ethanol, EtS and EtG: alcohol drinking rate (Dt), $k_{a_{\text{stom}}}$, V_{max} , CLR_{ETH} ; for EtS: CLR_{EtS} , Dt , $K_{\text{met}_{\text{EtS}}}$; and for EtG: CLR_{EtG} , Dt , $K_{\text{met}_{\text{EtG}}}$.

The outcome of the sensitivity analysis was then updated considering the model parameters relevant for this specific forensic application of estimating alcohol drinking time based on the knowledge of a few experimentally determined concentrations of EtG and EtS. Therefore the parameters important for the model prediction are: formation rate of EtS ($K_{\text{met}_{\text{EtS}}}$), formation rate of EtG ($K_{\text{met}_{\text{EtG}}}$) and ethanol clearance (CLR_{Eth}). The above-mentioned three parameters have been selected because are the only ones that can be measured in biological samples (serum and/or urine) collected in a real case forensic scenario to evaluate alcohol administration.

Time and dose extrapolations of new data

The median subject specific parameters were calculated for each of the 16 volunteers in the training set, separately for males and females, and were used to estimate the time course for a new and “unknown” set of data (2 volunteers excluded from the training set) as starting values. This was repeated twice resulting in two different test sets: A and B.

The following steps were carried out:

1. The PBTK model was updated upon physiological information of new subjects (BW, height, age, BMI).

2. Simulations were performed for 4 and 8 units with median subject-dependent parameters (step A: $K_{\text{formEtS}}=1.14 \cdot 10^{-06}$ (men), $7.70 \cdot 10^{-07}$ (women), $K_{\text{formEtG}}= 0.022$ (men, women), $\text{CLR}_{\text{Eth}} = 10.38$ (men), 1.8 (women) [L/h/BMI]; step B: $K_{\text{formEtS}}=1.15 \cdot 10^{-06}$ (men), $7.33 \cdot 10^{-07}$ (women), $K_{\text{formEtG}}= 0.023$ (men), 0.21 (women), $\text{CLR}_{\text{Eth}} = 9.25$ (men), 1.8 (women) L/h/BMI).
3. Euclidean distance was calculated between 3 experimental and simulated consecutive, timely separated concentrations (1 h difference in this example). The minimal distance between simulated and experimental indicated a possible time of sampled experimental concentrations.
4. Once the potential ethanol dose is estimated, refinement of subject variable parameters with respect to new *in vivo* data should be performed to improve simulated concentration-time profiles.

The model simulations for 4 and 8 units for these two subjects in test sets A and B prior to step 4 are presented in **Figure 4.6.9**. Euclidean distance (ED) criterion was used here as simple example to show the difficulty in proper identification of the sampling times (**Table 4.6.5**).

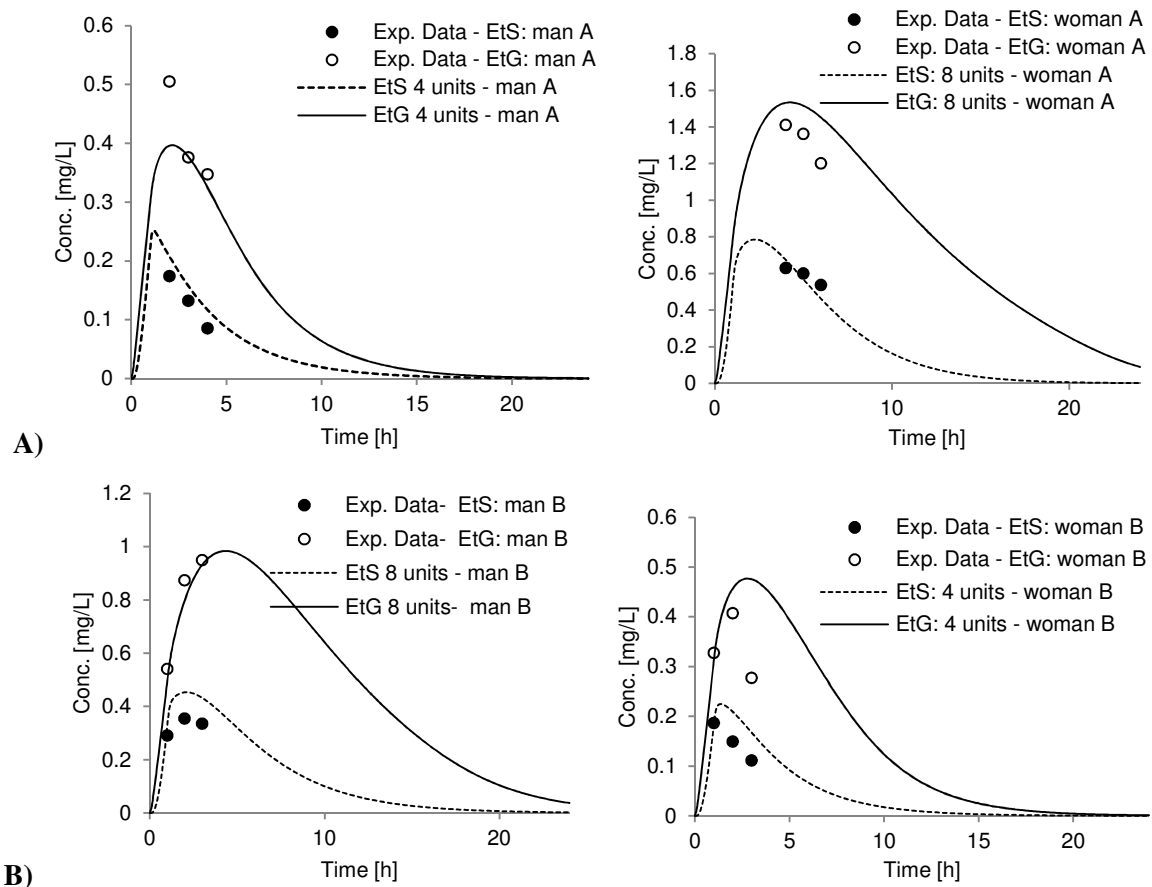


Fig 4.6.9. Simulation of EG and EtS levels in serum following consumption of 4 and 8 units of ethanol for two test sets A and B.

Table 4.6.5. Euclidean distance (ED) results

Subject	EtS 4 units	EtS 8 units	EtG 4 units	EtG 8 units
Male subject (A)	Experimental points: Hours: 2,3,4 0.174,0.132,0.085	Experimental points: -	Experimental points: Hours: 2,3,4 0.505,0.376,0.347	Experimental points: -
	ED: 0.061	-	ED: 0.112	-
	Matching hours: 2,3,4	-	Matching hours: 2,3,4	-
Female subject (A)	-	Experimental points: Hours: 4,5,6 0.628,0.599,0.535	-	Experimental points: Hours: 4,5,6 1.41,1.36,1.2
	-	ED: 0.088	-	ED: 0.081
	-	Matching hours::4,5,6	-	Matching hours:6,7,8
Male subject (B)	-	Experimental points: Hours: 1,2,3 0.291,0.354,0.335	-	Experimental points: Hours: 1,2,3 0.540,0.874,0.949
	-	ED: 0.143	-	ED= 0.138
	-	Matching hours:1,2,3	-	Matching hours:1,2,3
Female subject (B)	Experimental points: Hours: 1,2,3 0.186,0.149,0.111	-	Experimental points: Hours: 1,2,3 0.327,0.407,0.277	-
	ED: 0.029	-	ED: 0.210	-
	Matching hours:3,4,5 ED:0.095 Matching hours:1,2,3	-	Matching hours:1,2,3 ED: 0.224 Matching hours:2,3,4	-

Discussion

In this work I used for the first time the PBTK model to simulate concentration-time profiles of EtS and EtG both in serum and urine as a proof of concept to demonstrate its application in supporting the back-extrapolation of the time of alcohol intake. The goal was to present a practical application of PBTK modelling that can be of interest for forensic application with focus on determining the concentration-time profiles of a compound based on few available experimental data collected from one subject. For instance, a realistic forensic scenario to investigate would be drink driving claims or proof of drinking by courts. In this study, three consecutive serum samples were used for evaluation of the model performance since the collection of more samples, although feasible, would not be realistic.

I obtained reliable results in the model calibration step with respect to the experimental data from the study of (Lostia et al., 2013) in the training set composed of 16 subjects per dose of ethanol. In particular, the serum concentrations were well fitted by the model, whereas urinary profiles showed higher between-subject variability thus affecting the model predictive performance. Nevertheless, using a relatively simple urinary elimination profile (kidney – bladder – urine/ creatinine) a quite satisfactory prediction in urine was obtained. Another difficulty was in the modelling of excreted creatinine concentrations in time that required additional experimental information about examined subjects. Therefore I decided to use only serum samples to back extrapolate the time of drinking by model predictions. A bigger dataset for urinary concentrations might help in the future to better describe the kinetics of EtG and EtS in this biological matrix.

From the experimental and simulated data, it might be argued that the kinetic of EtG and EtS is different between males and females, with the latter showing a higher amount of alcohol in the body. This is explained by the drinking experiment layout designed in (Lostia et al., 2013) where alcohol doses were given considering only the units of alcohol ingested (1 unit corresponds to 8 g of alcohol) and not by calculating the amount of ethanol consumed per kilogram of body weight. In the latter, the amount of alcohol in the body would be very similar in all the volunteers because of the normalization against body weight. For this reason, in this dataset, the female volunteers had a mean amount of alcohol in the body almost 1.5 times higher than in males (0.88 ± 0.03 versus 0.63 ± 0.03 g/kg after 4 units; 1.76 ± 0.18 versus 1.27 ± 0.07 g/kg after 8 units). The decision of administrating alcohol as units was to obtain a more realistic drinking situation.

An advantage of the PBTK model, compared to previous kinetic models (Droenner et al., 2002; Schmitt et al., 2010), is that it includes physiological information that allows grouping the model parameters into population-constant and subject-specific. To avoid the model identifiability problem I tried to balance the minimal number of tunable parameters and good model simulation performance with respect to individual ADME profiles. Therefore, though, the model is complex and has more parameters than previously reported kinetic models (Droenner et al., 2002; Schmitt et al., 2010), it needs fitting fewer parameters with respect to individual serum and urine concentrations. Based on sensitivity analysis results, I chose four parameters to be refined with respect to new data: formation rates of EtS and EtG, ethanol renal clearance and creatinine formation. These parameters were also chosen as most sensitive because they are the most relevant for this forensic application. In fact they can be measured from biological samples, urine and serum, collected from subjects. Concentrations of the two metabolites are very low when compared to ethanol and acetaldehyde (when median population metabolism rate adjusted by BMI would work quite well for all individuals) – and therefore their formation rates show higher inter-individual variations. However, median values derived in **Table 4.6.3** may serve as a good initial estimate for unknown data prior to fitting. Based on this table, we see that there is a small variation in the formation rate of EtG in the liver and high in creatinine formation and ethanol renal clearance.

The main limitations of the PBTK model are its applicability domain and no between-subject biological differences in ADME processes other than a difference in BMI. Currently, the model can be applied for single administration of 4-8 units of ethanol (1 unit corresponds to 10 mL or ~8 g of pure ethanol) under the conditions of the above-described experimental design and would require further validation and/or refinement (in terms of subject-specific parameters) to be applicable for higher and repeated doses.

In the final stage, I applied the optimised model to new data (in the test set) to back-extrapolate the time of ethanol drinking, assuming knowledge of the dose of ethanol consumed and using median values of the subject-specific parameters. I was limited to predicting serum results only as already explained before in the discussion. I implemented a simple Euclidean distance metric to compare simulation results with experimental points to estimate the concentration-time profile. The results in **Table 4.6.6** (where simulation results are compared with experimental values) show that in most of the cases identification of accurate

sampling time based on a small ED value was possible. Nevertheless, I used the information about measured EtS/EtG concentrations ratio to decide between early (prior to concentration peak value or shortly after) or late times (far after peak value). Female subject B showed, however, two possibilities for early consecutive times which illustrates that the PBTK model itself and mathematical matching strategy should not (in its current formulation) be used on its own if a precise estimation of these times is necessary.

The choice of using only three consecutive concentrations was based on the findings of the study of (Lostia et al., 2013). The authors observed that, both in serum and urine samples, the EtG/EtS ratio rose with time after alcohol administration, mainly over the first 4 h. Although they were not able to confirm whether EtG/EtS might be a useful marker to calculate time since alcohol administration, they postulated that two or three consecutive urine or serum samples with increasing EtG/EtS might indicate recent drinking within the last 6–10 h depending on the biological specimen used for the investigation. Instead, two or three consecutive decreasing EtG/EtS values might suggest drinking before the previous 10 or even more hours. The authors, however, made it clear that a larger number of volunteers and more time-points samples would be needed to confirm the findings. Therefore currently these 3 consecutive points would help only to decide between the simulated results in the absorption (early times) and elimination (late times) phases.

At its current stage, the PBTK model is not intended to be a standalone tool to predict the exact time of ethanol ingestion based on a limited number of serum samples with known EtG and EtS concentrations. However, the model is a valuable method that in a forensic weight of evidence approach can provide further evidence, together with evaluation of increasing or decreasing EtG/EtS ratios over time, to estimate the time of alcohol ingestion.

4.6.2 Effect of different concentrations and vehicles on skin absorption of ethanol

The ethanol dermal absorption study of (Kramer et al., 2007) was used to evaluate PBTK model simulation performance when different ethanol concentrations are applied on the skin. The authors measured ethanol absorption from 3 hygienic and 3 surgical hand disinfections using different alcohol-based hand-rubs. 12 volunteers (6 male and 6 female) participated in the experiment and median blood concentrations of ethanol and acetaldehyde were published. The following parameters of the model were to be calibrated: diffusion coefficients in *stratum corneum* and viable epidermis (D_{sc} , D_{ve} [cm^2/h]), ethanol intake by the skin from the solution (k_{form} [mL/h]) and skin partition coefficients (PC_{sc} , PC_{ve}). QSPRs were used to determine diffusion coefficient in *stratum corneum* and partition coefficient in viable epidermis. QSPR prediction for diffusion coefficient in viable epidermis was not considered because it was far too high (0.3831 cm/h) when compared to the available *in vitro* permeation coefficient through the full- abdominal skin thickness (0.000317 cm/h (Scott et al., 1991)). *Stratum corneum*/ vehicle partition coefficient was assumed variable for different concentrations in order to better match ethanol blood concentrations. **Figure 4.6.10** shows the experimental results for 4 different formulations with a contact time of 10 min: 4 mL of 95% ethanol sol. (total 60 g), 4

mL of 85 % ethanol sol. (total 56.2 g), 4 mL of 55 % ethanol sol. (total 39.6 g); and with a contact time of 30 min: 20 mL of 95 % ethanol sol. (total 149.9 g) , 20 mL of 85 % ethanol sol. (total 140 g) and 20 mL of 55 % ethanol sol. (total 99 g). Based on these results we can conclude that ethanol absorption depends on absolute amount of ethanol in a rub and most likely other physicochemical properties of the solution that may alter permeation of ethanol through the skin (4 mL 55% < 20 mL 55% < 4 mL 85% < 20 mL 95% < 4 mL 95% < 20 mL 85%). We see that 20mL of 95% ethanol sol. – although it was the highest amount of ethanol (149.9 g) – it didn't produce the highest peak concentration in the blood. Because the shape of concentration-time profiles was more or less similar in all the cases (except for 20 mL of 55 % sol.- see **Figure 4.6.10**), with a difference in magnitude of peak values but similar peak times – I assumed in the modelling that diffusion coefficients and uptake rate by the skin were unchanged – not dependent upon concentration of the solution -and the only difference was in the *stratum corneum*/ vehicle partition coefficient fitted with respect to each profile (**Table 4.6.6**).

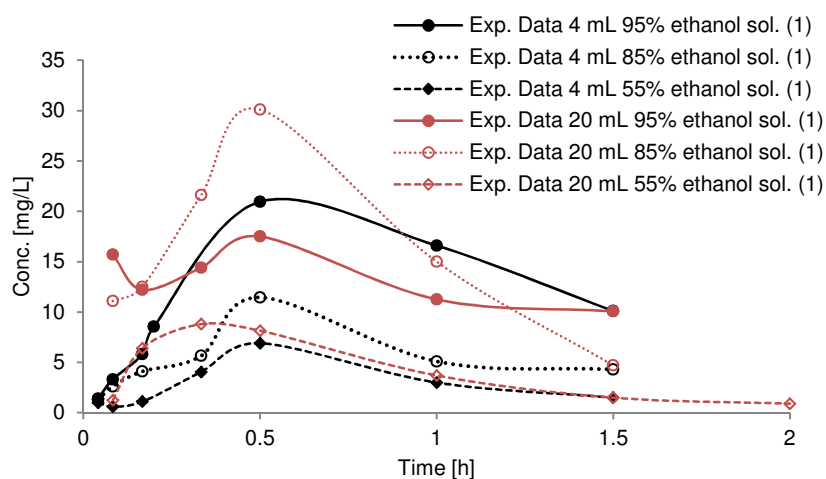


Fig 4.6.10. Experimental ethanol concentrations after absorption from different solutions: (1) (Kramer et al., 2007).

Based on this table, the best fit was obtained from PCsc ranging from 3 (4 mL 55 % sol.) to 8 (20 mL 85 % sol.). Other parameters such as: D_{ve} , k_{form} were fitted with respect to 4mL of 95 % sol. and used unchanged for the others.

Table 4.6.6. Calibrated PBTK model absorption parameters for different hand rubs.

Ethanol %	Volume [mL]	Dsc [cm ² /h]	Dve [cm ² /h]	PCsc	PCve	k _{form} [mL/h]
4 mL 95	4			5.5		
4 mL 85	4			3.2		
4 mL 55	4			3		
20 mL 95	20	$9.96 \cdot 10^{-06}$	$5.87 \cdot 10^{-05}$	6	0.2	0.2
20 mL 85	20	(QSPRs)		8	(QSPRs)	
20 mL 55	20			4		

PBTK model simulations of experimental values are shown in **Figure 4.6.11**– of ethanol and in **Figure 4.6.12** of acetaldehyde. We see that predicted acetaldehyde concentrations were in accordance with measures ones only in the first case. There could be several reasons for that:

- The experiments were repeated shortly after each other, therefore there was a base-line value of acetaldehyde present in blood, not considered by the model.
- These are median values for males and females. Previous study (**chapter 4.6.1**) showed the difference in ethanol ADME profiles between genders and subjects. In the model I used median metabolism rates fitted for men for 4 units of ethanol (because it was the smallest dose considered) and created a median male subject with a body weight of 70 kg. Therefore, no inter-subject differences are considered in this case study.
- Although ethanol concentrations were quite well simulated by the model – there was often a mismatch of ethanol elimination phase, most likely indicating that faster metabolism rates should be used here. In the oral absorption experiment I fitted ethanol clearance to blood concentration resulting from different dosing (4 and 8 units) and it was clear that it decreases with increased dose. In this work for ethanol internal concentrations up to ca. 2 % of 149.9 g = 2.998 g (dermally absorbed) I used metabolism and renal clearance parameters fitted for 31.572 g (there was almost complete oral absorption).

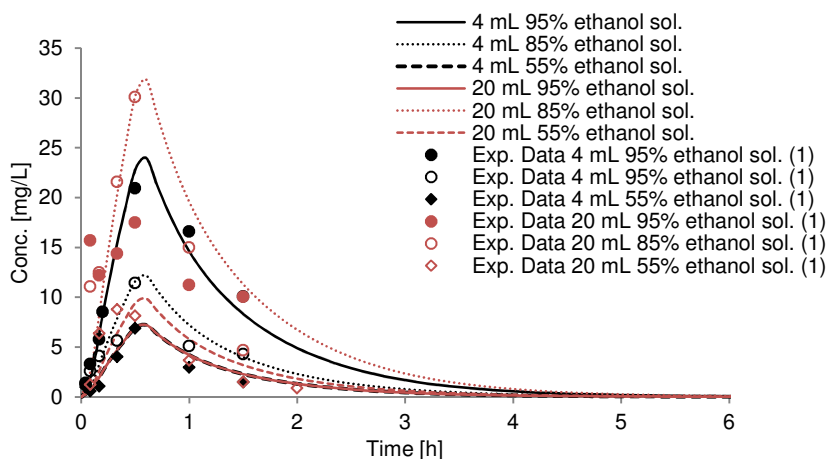


Figure 4.6.11. Simulated and experimental concentrations of ethanol after exposure to different hand rubs: (1) (Kramer et al., 2007).

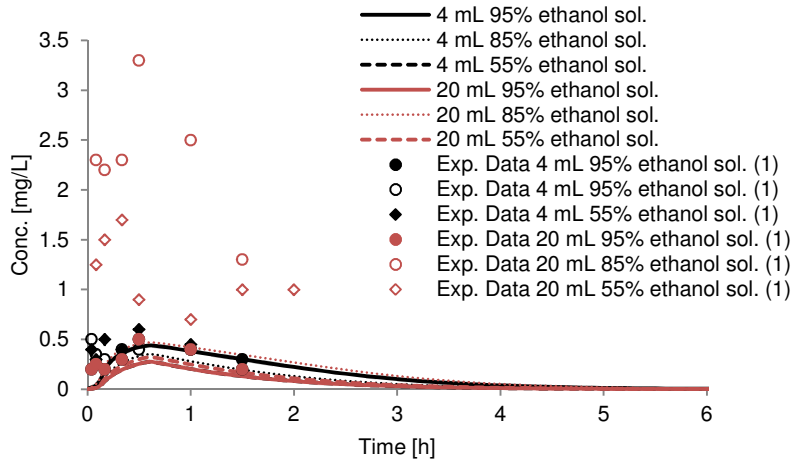


Figure 4.6.12. Simulated and experimental concentrations of acetaldehyde after exposure to different hand rubs: (1) (Kramer et al., 2007).

Table 4.6.7 provides simulated AUC and C_{max} in the blood and liver for both ethanol and acetaldehyde and percentage of ethanol absorption via skin. This absorption is also presented in **Figure 4.6.13** for all the hand rubs. This clearly shows that the highest absorption was for 4 mL of 95 % ethanol sol. and the lowest for 20 mL 55 % ethanol sol – as described in the paper (Kramer et al., 2007) – however, the calculated percentage values by the model was slightly higher than the ones published calculated roughly according to: absorbed amount [mg] = BW [kg] · r (0.7 for males and 0.6 for females) · C_{max} in blood [mg/L].

Table 4.6.7. Toxicokinetic results of the model simulations for ethanol and acetaldehyde

Ethanol %	Volume [mL]	AUC liver	AUC blood	C_{max} liver	C_{max} blood	% Abs
95	4	Ethanol: 21.229	Ethanol: 28.722	Ethanol: 9.195	Ethanol: 23.994	3.883
		Acet: 3.081	Acet: 0.891	Acet: 0.7305	Acet: 0.438	
85	4	Ethanol: 9.894	Ethanol: 14.128	Ethanol: 4.438	Ethanol: 12.168	2.133
		Acet: 2.017	Acet: 0.583	Acet: 0.584	Acet: 0.3505	
55	4	Ethanol: 5.540	Ethanol: 8.236	Ethanol: 2.519	Ethanol: 7.224	1.821
		Acet: 1.388	Acet: 0.401	Acet: 0.457	Acet: 0.2743	
95	20	Ethanol: 23.768	Ethanol: 31.917	Ethanol: 10.238	Ethanol: 26.556	1.716
		Acet: 3.261	Acet: 0.943	Acet: 0.749	Acet: 0.449	
85	20	Ethanol: 29.168	Ethanol: 38.659	Ethanol: 12.410	Ethanol: 31.868	2.199
		Acet: 3.600	Acet: 1.041	Acet: 0.780	Acet: 0.4681	
55	20	Ethanol: 7.817	Ethanol: 11.346	Ethanol: 3.534	Ethanol: 9.865	0.986
		Acet: 1.743	Acet: 0.504	Acet: 0.533	Acet: 0.320	

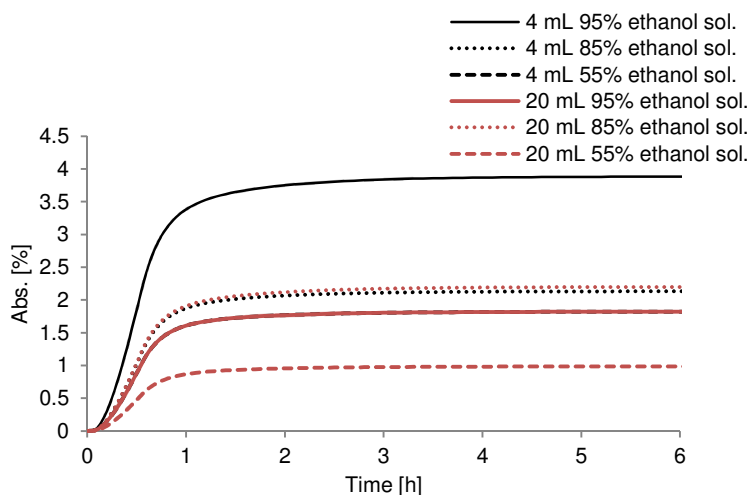


Figure 4.6.13. Simulated absorption percentage of ethanol in time.

4.7 Joint toxicokinetic and toxicodynamic modelling of single and multiple doses

In this chapter, various simulated ADME profiles of two case study compounds, caffeine and nicotine, are linked to toxicodynamic responses. This includes modelling of acute cardiovascular effects such as heart rate and blood pressure at rest and during exercise. The choice of substances has been based on experimental data availability in the literature on kinetic and dynamic effects after single and repeated exposure and the similarity in nature and intensity of these effects.

Caffeine and nicotine, two commonly used stimulants and psychoactive substances, despite differences in chemical structure, are known to cause similar effects such as increased heart rate, nervous system effects and influences on other biological processes including behavioral effects and metabolic responses (Damerchi et al., 2009; Grundy et al., 1981). They are both addictive, and consistent users are likely to develop tolerance and dependence. Nicotine is however a more addictive drug and cigarette smoking as a delivery mechanism is inherently more likely to produce addiction. Interestingly, there is an increasing human exposure to these substances via more than one exposure route (caffeine is present in various skin care products such as body creams, soaps, scrubs, shampoos and rollers; nicotine replacement therapy includes coated tablets, chewing gum, nasal spray, inhalator, microtablets and transdermal patches).

4.7.1 Nicotine

The PBTK model for humans, calibrated and validated by using literature *in vivo* blood/plasma concentrations, was applied to simulate selected daily exposure scenarios of nicotine (both in terms of cigarette smoking and nicotine replacement therapy), selected based on available online statistical data on

nicotine consumption. The internal blood and liver concentrations are defined by Area Under Curve (AUC) and peak concentration (C_{max}) and are linked to TD model estimating one of the common acute effects, mean heart rate at rest and during exercise (use of nicotine in a dermal patch measured on cycling endurance) and mean arterial pressure (MAP) at rest (due to lack of data for exercise condition). This study builds on previous work by further applying PBTK/TD modelling to analyse nicotine ADME profiles resulting from various exposure scenarios (Porchet et al., 1988; Robinson et al., 1992), with the addition of sub-compartments in the skin and GI tract and modification to the effect model.

Venous blood concentrations of nicotine (its free fraction), as a surrogate for effect-site concentration, after single and/or multiple infusion, inhalation, oral and dermal absorption are used to measure intensity of an effect and a developed tolerance. **Table 4.7.1** provides nicotine input parameters to the PBTK model and **Table 4.7.2** parameters to the PBTD model.

Table 4.7.1. ADME parameters for nicotine

Parameter	Value	Reference
Liver metabolism		
To cotinine: V_{max} [mg/h/BW]	28.1 nmol/mg of protein/h → 319.785 mg/h → 11.260 [mg/h/BW]	Optimised for (Fattinger et al., 1997; Porchet et al., 1988)
	For scaling up: microsomal protein yield: 34-42 mg/gliver (I took mean) 38mg/gliver	Originally from (Messina et al., 1997) scaled up according to (Pelkonen and Turpeinen, 2007)
To cotinine: K_m [mg/L]	10.52 (mean 64.9 μ M)	(Messina et al., 1997)
To other metabolites: K_{met} [L/h/BW]	0.1674	(Teeguarden et al., 2013)
Renal clearance [L/h/BW]	0.036	(Teeguarden et al., 2013)
Tissue-to-blood partition coefficients		
Liver	1.42	
Poorly-perfused tissues	0.39	
Highly-perfused tissues	1.62	
Skin	0.38	
Brain	2.63	(Schmitt, 2008)
Lungs	1.32	
Kidney	1.34	
GI tract	0.58	
Adipose tissue	0.19	
Oral model		
Dissolution from formulation	0.235	Optimised
Diss [1/h]		
absorption rate from stomach	0.006	Optimised
$k_{a_{stm}}$ [1/h]		
$k_{a_{SI}}$ [1/h]	0.1 (tablet) 1 (straw)	Optimised
Stomach emptying rates: k_{max} [1/h]	8.16	(Loizou and Spendiff, 2004)
Stomach emptying rates: k_{min} [1/h]	0.005	(Loizou and Spendiff, 2004)
$k_{a_{LI}}$ [1/h]	0.1	Assumed
$k_{e_{LI}}$ [1/h]	0.1	assumed
Dermal model		
Diffusion coefficient in <i>stratum corneum</i> D_{SC} [cm ² /h]	0.00016	Optimised
Diffusion coefficient in viable epidermis D_{VE} [cm ² /h]	0.00096	QSPR predicted (see text)
Release of nicotine from patch	0.06	Optimised

k [1/h]		
Partition coefficient between patch and <i>stratum corneum</i> PC_{SC}	0.4	Optimised
Partition coefficient between <i>stratum corneum and viable epidermis</i> PC_{SCVE}	1.518	QSPR predicted (see text)
Blood-to-plasma concentration ratio RBP	1.2	ADMET predictor (1)
Inhalation model		
Blood/air partition coefficient $\log PC_{blood,air}$	4.743	QSPR predicted (Buist et al., 2012)
Water/air partition coefficient $PC_{water,air}$	6000	Optimised

(1) <http://www.simulations-plus.com/Products.aspx?pID=13> (last access: 06.10.2014)

Table 4.7.2. Toxicodynamic parameters for nicotine at rest and during exercise

Parameter	Value	Reference
Heart rate		
E_0 [bpm]	At rest: 61.2 At rest: 64 during exercise: 145	(Porchet et al., 1988) (Fattinger et al., 1997) (Mündel and Jones, 2006)
S [bpm/mg/L]	1000	(Porchet et al., 1988)
$k_{a,Ant}$ [mg/L]	3	optimised
$k_{el,Ant}$ [mg/L]	6	optimised
$C_{50,Ant}$ [mg/L]	0.007	(Porchet et al., 1988)
y	1 (at rest) 0.6 (during exercise)	optimised
Mean arterial blood pressure (MAP)		
E_0 [mmHg]	At rest: 83.5 At rest: 81.7	(Fattinger et al., 1997) (Sofuoglu et al., 2012)
S [mmHg/mg/L]	600	optimised
$k_{a,Ant}$ [mg/L]	3	See heart rate
$k_{el,Ant}$ [mg/L]	6	See heart rate
$C_{50,Ant}$ [mg/L]	0.00772	(Porchet et al., 1988)
y	1 (at rest)	-

a) Nicotine infusion

In accordance with three different experimental protocols specified in the publications (Fattinger et al., 1997; Porchet et al., 1988; Sofuoglu et al., 2012), pure nicotine was administered via one and two intravenous injections. The modelling results are shown in **Figures 4.7.1-3** together with estimated heart rate and MAP. The two infusions of the same nicotine dose of 2.5 $\mu\text{g/kg BW}$ were separated by 1, 2 and 3.5 h (Porchet et al., 1988), of 0.7-1 $\mu\text{g/kg BW}$ separated by 30 min (Sofuoglu et al., 2012) and of 0.7 $\mu\text{g/kg BW}$ applied only once (Fattinger et al., 1997). The plasma experimental data of (Porchet et al., 1988) were used to calibrate the metabolism rate of nicotine to cotinine, whereas heart-rate measures of (Porchet et al., 1988) were used to calibrate parameters of the PBTD model (tolerance formation, elimination, S). The other two studies were used to validate the sigmoid model.

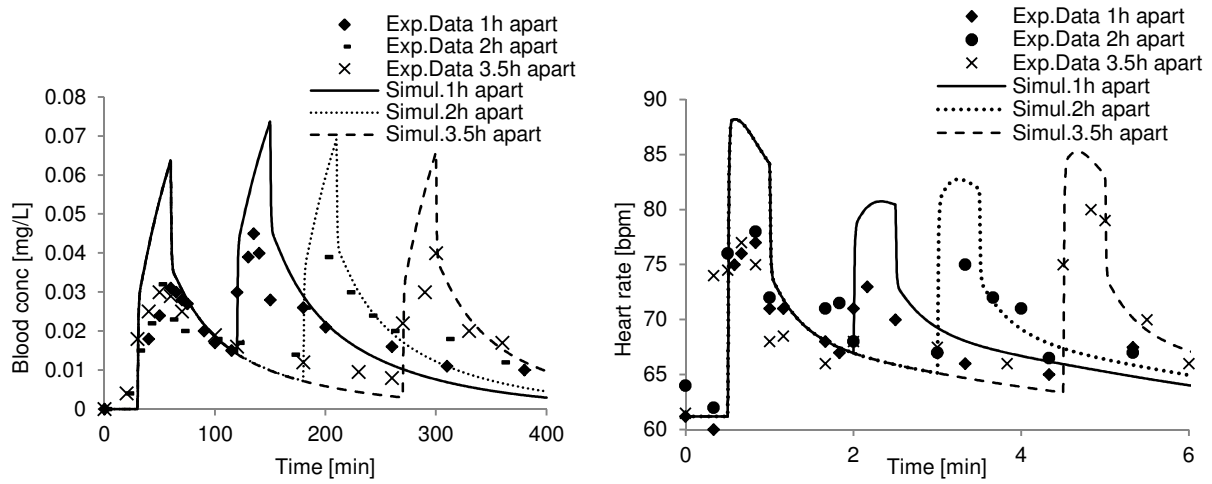


Fig 4.7.1. Two i.v. injection – blood concentrations and predicted heart rate at rest: Exp.Data: (Porchet et al., 1988).

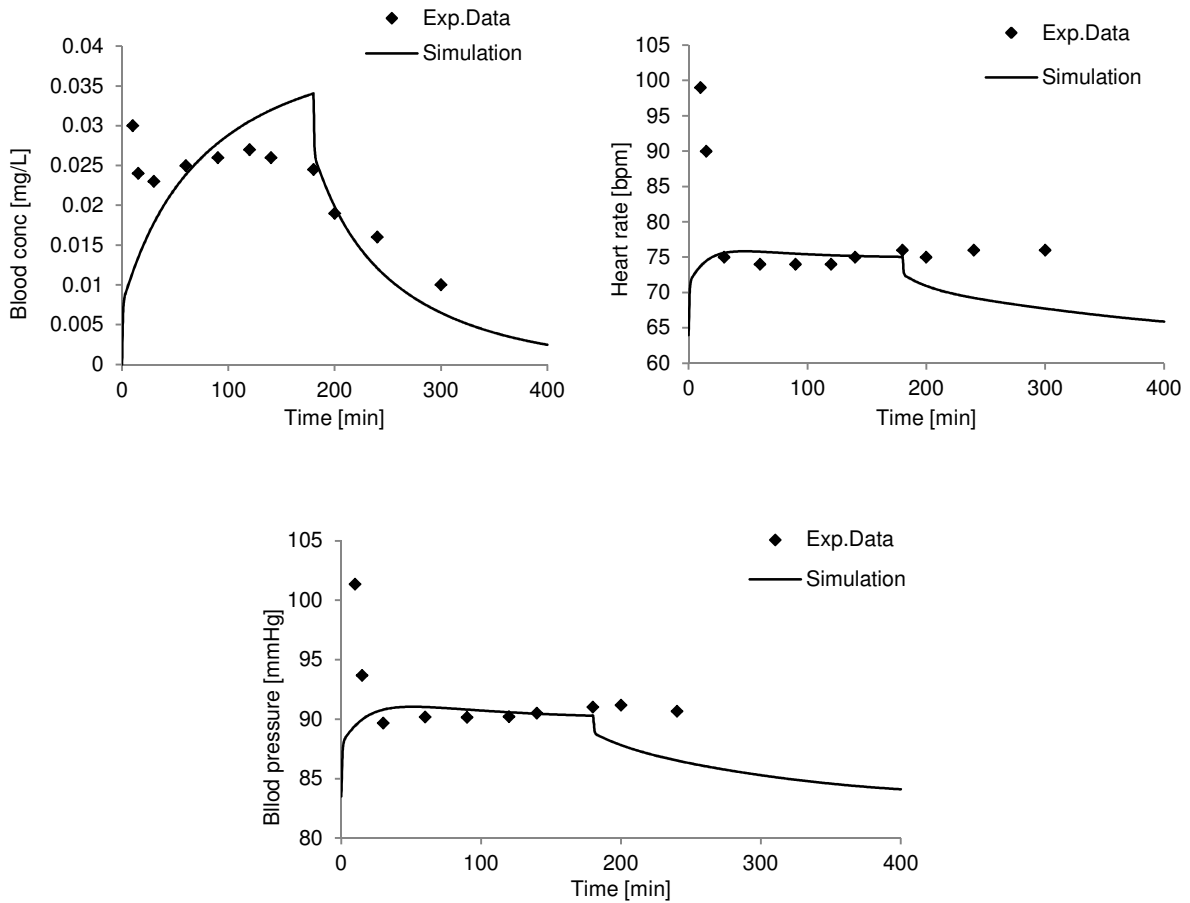


Fig 4.7.2 One i.v. injection – blood concentrations and predicted heart rate and MAP at rest. Exp. Data: (Fattinger et al., 1997)

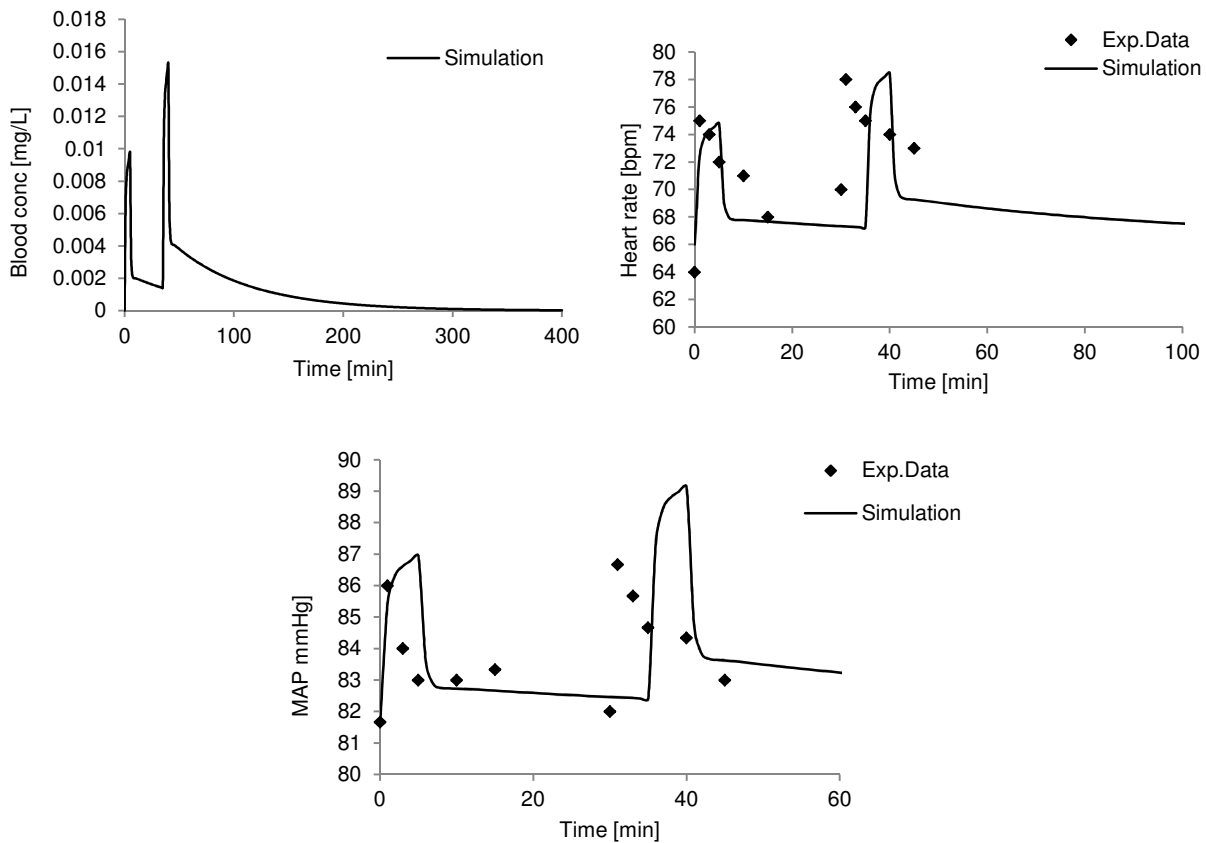


Fig 4.7.3. Two i.v. injections – blood concentrations, predicted heart rate and MAP at rest. Exp. Data: (Sofuoglu et al., 2012).

b) Oral absorption of nicotine

Experimental and simulated plasma concentrations of nicotine following oral administration with the straw (a nicotine replacement product) are shown in **Figure 4.7.4a** for single dose applications and **Figure 4.7.4b** for repeated dosing in accordance with experimental design specified in the reference source (D’Orlando and Fox, 2004). This data set was used to calibrate nicotine absorption and distribution in the GI tract. In this experiment it was noted that 8-times repeated administration of the highest dose of 12 mg did not show significant differences in plasma concentrations when compared to lower dosing of 8 mg. The authors explain that it is not clear whether it is due to limitations in the absorption of nicotine or simply variability in the patient population. The model simulations with assumed unchanged and constant parameters give much higher results for the highest dose than the experimental values

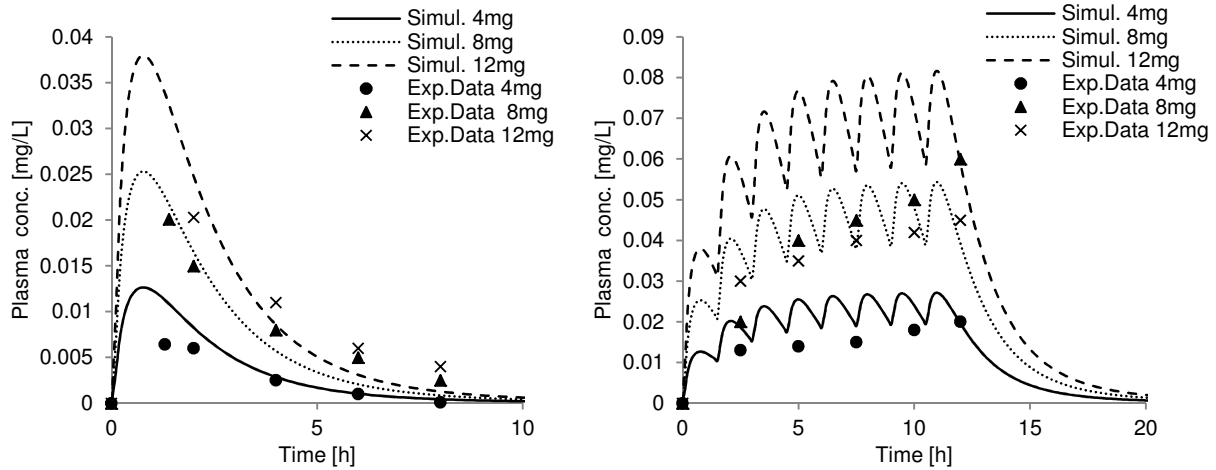


Fig 4.7.4. Single (a) and repeated (b) oral absorption of nicotine using the Straw. Experimental data: (D’Orlando and Fox, 2004).

In addition to modelling toxicokinetics, the link to potential heart-rate effects is shown in **Figure 4.7.5**, using toxicodynamic parameters calibrated for nicotine infusion (Porchet et al., 1988) at rest.

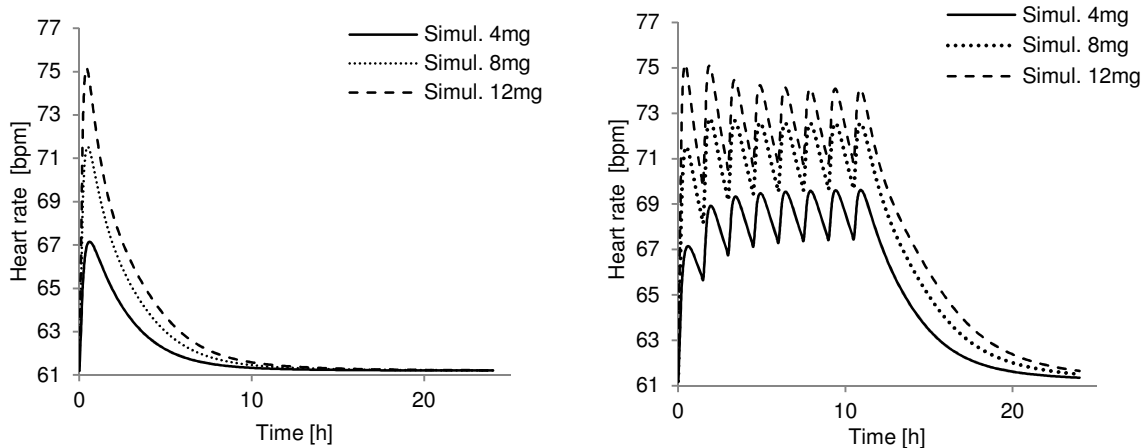


Fig 4.7.5. Single (a) and repeated (b) oral absorption of nicotine using the Straw. Estimated heart rate at rest.

Oral absorption of nicotine in capsules (Green et al., 1999) with modelled dissolution from a coated matrix used for PBTK model validation is shown in **Figure 4.7.6**. In this experiment (in contrast to all other nicotine studies) only nonsmokers participated therefore PBTK model simulations (with optimised parameters for smokers) clearly show lower clearance than expected. Metabolism for nonsmokers would require ca. 1.2 times faster liver metabolism of nicotine to cotinine provided there is no other elimination route - **Figure 4.7.6b**. Renal clearance of nicotine was not among the most sensitive model parameters and its increase would not give better presentation of nicotine concentration-time profile in serum of non-smokers.

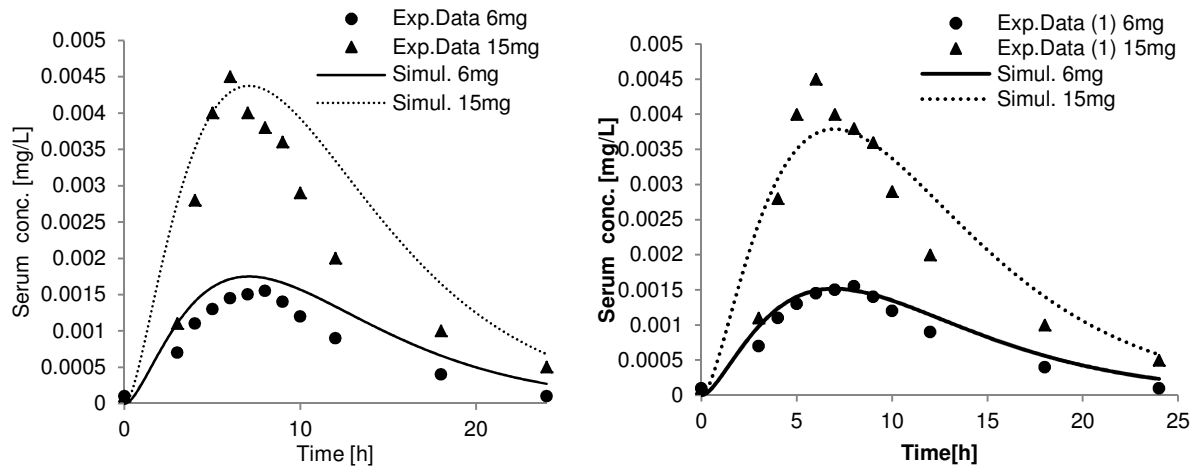


Fig 4.7.6. Oral absorption of nicotine in capsules (single dose) in nonsmokers. Experimental data: (Green et al., 1999) (right plot: liver metabolism $-V_{\max}$ 1.2 times higher).

In similar manner as before, there is an estimated increase of heart rate at rest shown in **Figure 4.7.7** for two nicotine doses applied in capsules. We see that, when comparing administration of 6 mg with 4 mg of nicotine with the straw results, the effect here is smaller.

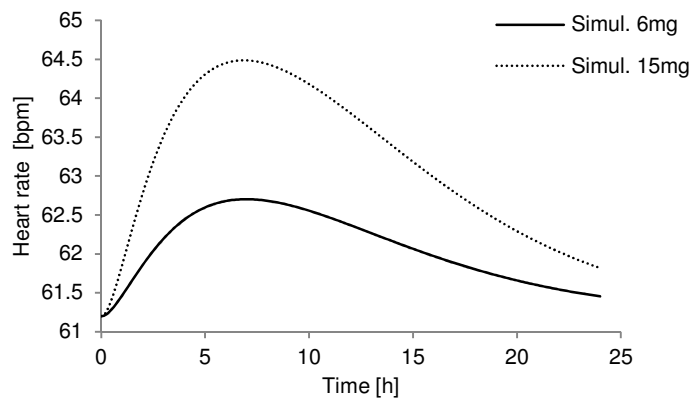


Fig 4.7.7. Estimated heart rate following oral absorption of nicotine in capsules (single dose) in nonsmokers.

c) Inhalation of nicotine

Figure 4.7.8 shows blood concentrations of smokers after repeated smoking (inhalation) every 30 min for 4 min (0.4, 1.2 mg of nicotine) and for 3 min (2.5 mg of nicotine) using simple PBTK1 model for inhalation. In this way I tried to mimic a smoking profile. I assumed that there was a constant inhaled nicotine concentration of $[\text{absolute dose}]/0.05$ mg/L and average smoking time of 4 min for low and regular doses, and 3 min of high dose, to obtain better representation of experimental data. Moreover, there is no metabolism of nicotine in the respiratory tract. I predicted the acute increase of heart rate as before (**Figure 4.7.9**).

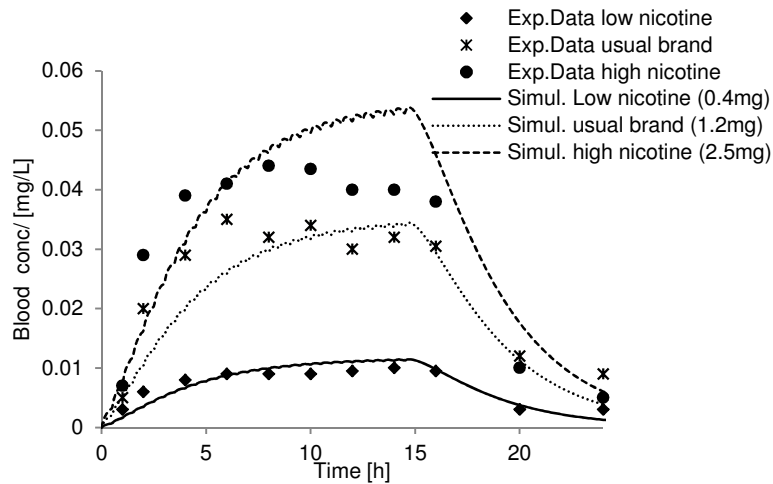


Fig 4.7.8. Concentration-time profile of nicotine in blood following inhalation of nicotine via repeated smoking in smokers. Experimental data: (Benowitz et al., 1982).

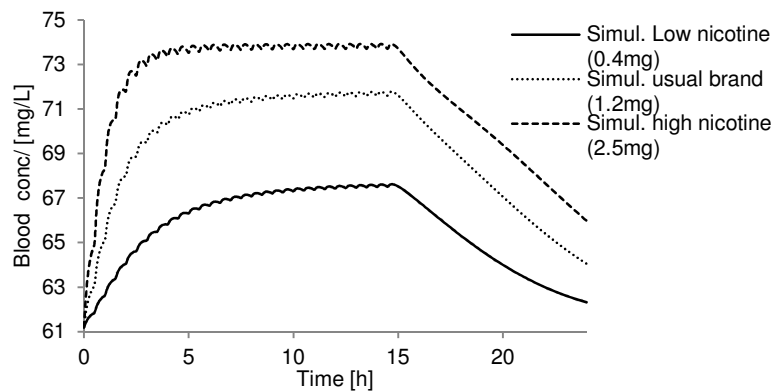


Fig 4.7.9. Inhalation of nicotine via repeated smoking in smokers. Estimated heart rate at rest.

d) Dermal absorption of nicotine

Finally, the results of dermal absorption of nicotine from patches containing different absolute doses of nicotine are given in **Figure 4.7.10a** for single 24- hour- exposure and in **Figure 4.7.10b** for prolonged exposure up to 200 h (once per day) used in the calibration step (Bannon et al., 1989). In case of prolonged exposure, the model simulations are only slightly higher than the sampled experimental results. These experimental points are measured plasma concentrations prior to application of a new nicotine patch (at the end of 24 h). They are not peak concentrations resulting after a given application. That is why the model simulations, at first glance, appear ca. 4 times higher. There were small differences reported between measured plasma AUC of nicotine on day 1 and day 7 (Bannon et al., 1989) indicating no significant nicotine accumulation following chronic transdermal delivery. The model validation was done for a single application of 35mg of nicotine in a patch (Gupta et al., 1993).

Estimated heart rate at rest and during exercise is shown in **Figure 4.7.11**. The experimental data used to calibrate the sigmoid model for the effect of nicotine on heart rate during cycling exercise are shown in **Figure 4.7.12** (Mündel and Jones, 2006), where the increased heart rate in 12 healthy, non-smoking men is measured following application of 7mg- nicotine patch.

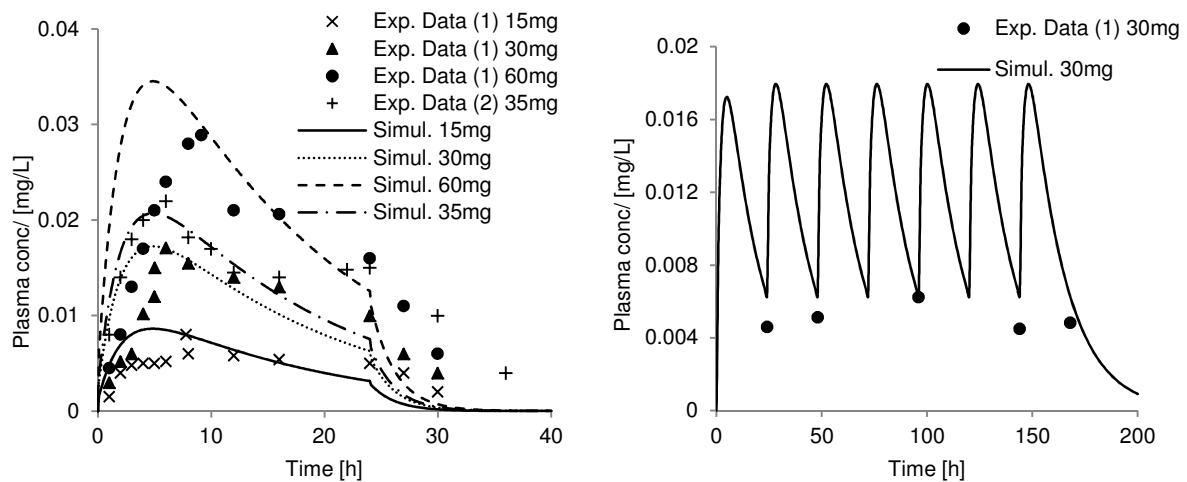


Fig 4.7.10. Simulated concentration-time profiles in plasma for single (left) and repeated (right) applications of nicotine patch in smokers. Experimental data (1) are taken from (Bannon et al., 1989) and (2) from (Gupta et al., 1993).

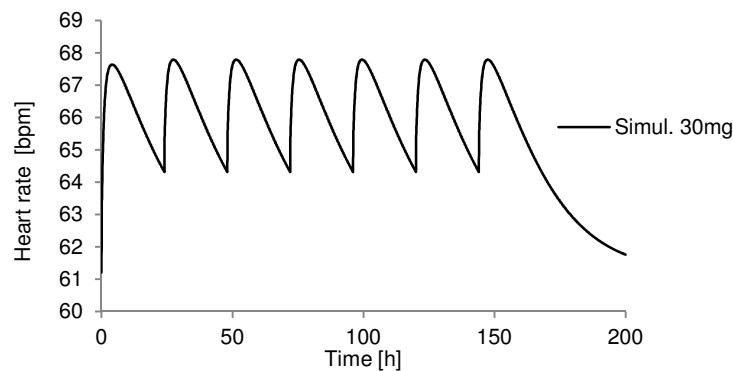


Fig 4.7.11. Simulated concentration-time profiles in plasma for repeated applications of nicotine patch in smokers. Estimated heart rate at rest.

I observed that the toxicodynamic parameters used for nicotine, obtained after intravenous nicotine injection, that include tolerance formation and elimination, S ratio of E_{max} (maximal effect) / $(C_{ven,50})^y$ and $C_{Ant,50}$ (but with different base-line effect recorded in this experiment (Damirchi et al., 2009)) work well also in case of dermal absorption during exercise but an exponent smaller than 1 would be necessary to obtain good fitting of experimental data. However, additional experiments would be necessary to confirm this assumption.

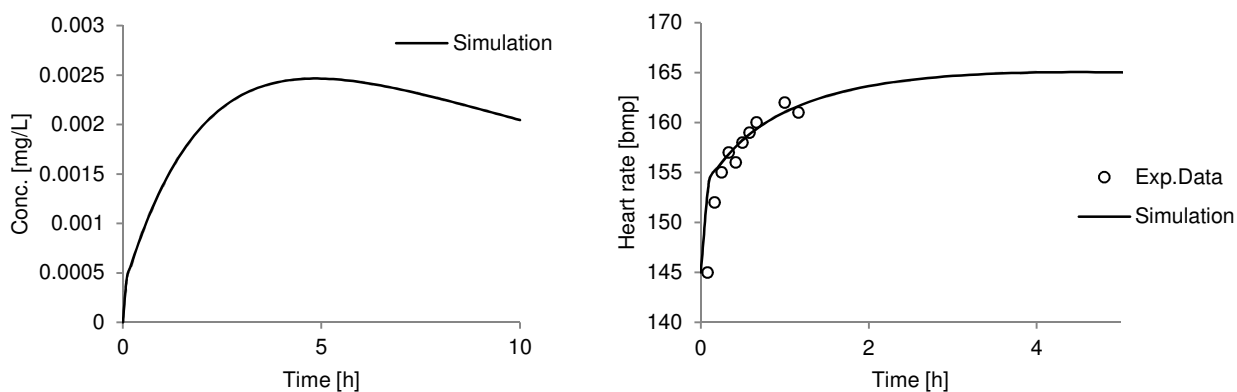


Fig 4.7.12. Simulated concentration-time profiles in plasma for single application of nicotine patch in non-smokers. Estimated heart rate during cycling exercise. Experimental data: (Mündel and Jones, 2006).

Daily exposure design

Selected daily dosing conditions for nicotine together with web and literature references are presented in **Table 4.7.3**. Various information about statistics of nicotine consumption in Europe, found online, was compiled and used to create common exposure profiles. This includes the following measures on:

- a) smoked cigarettes per day of usual brand (1.2 mg over 4 min) (Benowitz et al., 1982):
 - Occasional smokers - between 1 and 5 cigarettes per day (average 3 per day, one every 4 h)
 - Light smokers - between 6 and 10 cigarettes per day (average 8 per day, one every 2 h)
 - Regular smokers - between 11 and 20 cigarettes per day (assume 14 per day, one every 1 h)
 - Heavy smokers - 21 or more cigarettes per day (assume 21 per day, one every 30 min)
- b) nicotine patches:
 - nicotine transdermal patch 42 mg (2 patches: 21 mg + 21 mg) applied once daily (Area=2·22= 44cm²)
 - nicotine transdermal patch 21 mg applied once daily (Area= 22 cm²)
 - nicotine transdermal patch 14 mg applied once daily (Area= 22 cm²)
 - nicotine transdermal patch 7 mg applied once daily (Area= 22 cm²)
- c) nicotine lozenges – I assume dissolution rate from matrix calibrated according to (Green et al., 1999)
 - 4-mg and 2 mg-nicotine applied lozenges every 1 to 2 hours for 10 hours. In this way, no more than 20 lozenges are used per day.
- d) nicotine inhaler - modelled in the similar way to mechanism of smoking
 - I selected so called “the best effect achieved” by frequent, continuous puffing for 20 minutes. A cartridge delivers about 4 mg of nicotine, though only 2 mg are actually absorbed. I considered 4 (every 3 h), 6 (every 2 h) and 10 (every 1 h) cartridges/ day.

Table 4.7.3. Selected average daily exposure to nicotine

Exposure route	Exposed amount	Number per day	Reference
Cigarettes	1.2 mg (usual brand) per 4 min	3,8,14,21	(Benowitz et al., 1982; Fagerström, 2005; National Tobacco Control Office, 2002)
Dermal patch	7,14,21,42 mg (over 22 cm ²) per 24 h	1	(emc, 2014; Hamilton Health Sciences, 2014)
Oral capsule	2, 4 mg	5, 10	(MedlinePlus, 2014)
Nicotine lozenges			
Nicotine inhaler	2 mg	4, 6, 10	(QuitNet, 2013)

In all the daily simulations of nicotine, I used a base-line heart rate of 61.2 bpm (Porchet et al., 1988) at rest and 145 bpm during exercise (Mündel and Jones, 2006).

Concentration-time profile simulations of the daily exposure scenarios for cigarette smoking, nicotine patches, nicotine lozenges and inhaler are shown in **Figures 4.7.13-16**, whereas the simulated effects on heart rate (both at rest and during exercise) are given in **Figures 4.7.17-20**. **Table 4.7.4** shows calculated AUC and peak concentrations for each exposure profile. Cigarette smoking and nicotine inhalation via inhaler were simulated for different respiratory rates at rest and during exercise. This is why there are different blood concentrations in the case of cigarette smoking when compared to other exposure routes – increasing respiratory rate from 840 l/h to 1080 l/h produces ca. 1.5 times higher AUC values and only slightly higher C_{max} values when compared to resting conditions. However, no changes in toxicokinetic parameters and in the resulting heart rate were found in the case of inhaler.

Table 4.7.5 provides estimates of mean heart rates over the duration of experiment (400 min-48 h) for all four exposure routes.

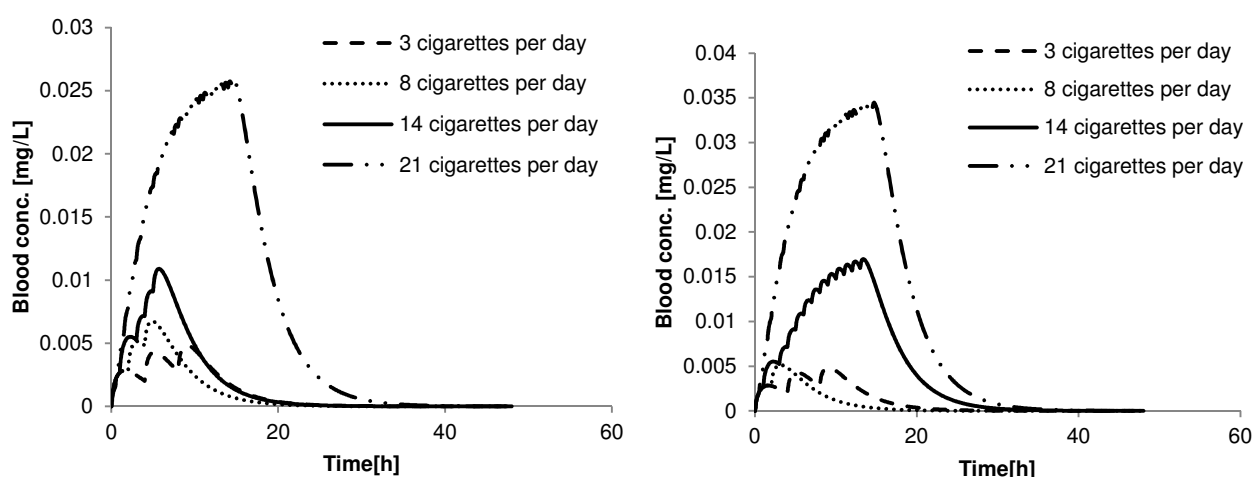


Fig 4.7.13. Simulated blood concentrations of nicotine for selected daily repeated exposure to cigarettes (1.2 mg over 4 min per cigarette at rest –left- and exercise- right).

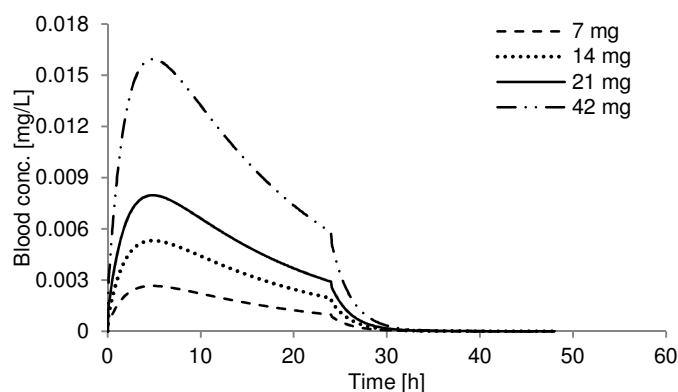


Fig 4.7.14. Simulated blood concentrations of nicotine for selected daily single exposure to nicotine patch.

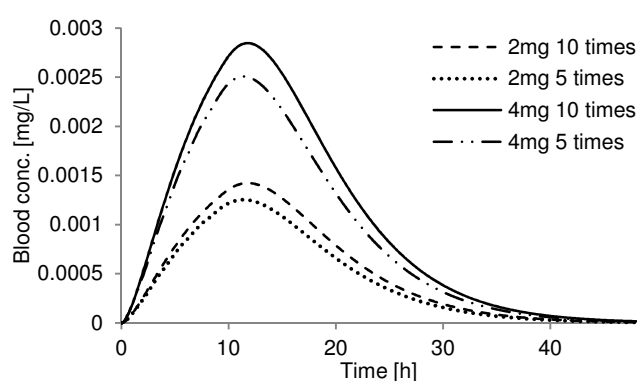


Fig 4.7.15. Simulated blood concentrations of nicotine for selected daily repeated exposure to nicotine lozenges.

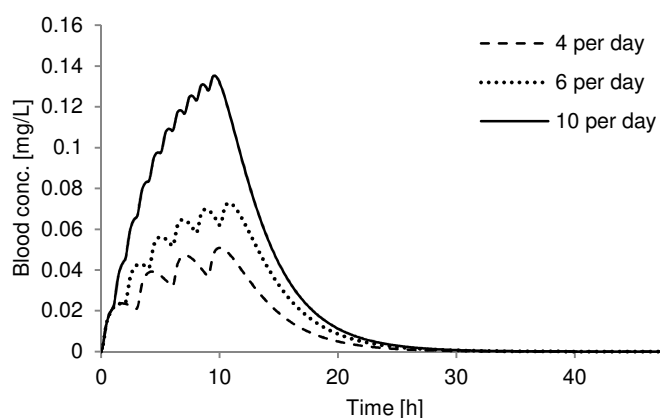


Fig 4.7.16. Simulated blood concentrations of nicotine for selected daily exposures to nicotine inhaler.

Table 4.7.4. AUC and C_{max} values for all the exposures to nicotine

Exposure route	AUC liver [mg.h/L]	AUC blood [mg.h/L]	C_{max} liver [mg/L]	C_{max} blood [mg/L]
Cigarettes (1.2mg)				
3 per day	0.072 (rest)	0.053 (rest)	0.0068 (rest)	0.0048 (rest)
	0.072 (exercise)	0.053 (exercise)	0.0068 (exercise)	0.0048 (exercise)
8 per day	0.072 (rest)	0.053 (rest)	0.0095 (rest)	0.0067 (rest)

14 per day	0.0482 (exercise) 0.121 (rest)	0.035 (exercise) 0.088 (rest)	0.0073 (exercise) 0.0153 (rest)	0.0051 (exercise) 0.0109 (rest)
21 per day	0.314 (exercise) 0.543 (rest)	0.228 (exercise) 0.394 (rest)	0.024 (exercise) 0.0358 (rest)	0.017 (exercise) 0.0258 (rest)
	0.724 (exercise)	0.526 (exercise)	0.0478 (exercise)	0.0325 (exercise)
Dermal patches				
7 mg	0.159	0.046	0.009	0.003
14 mg	0.318	0.091	0.018	0.005
21 mg	0.477	0.137	0.028	0.008
42 mg	0.956	0.274	0.056	0.016
Nicotine lozenges				
2 mg (every 2 h)	0.102	0.043	0.0062	0.0026
2 mg (every 1 h)	0.204	0.086	0.0124	0.0051
4 mg (every 2 h)	0.204	0.086	0.0125	0.0052
4 mg (every 1 h)	0.409	0.172	0.0249	0.0103
Nicotine inhaler				
2 mg				
4 per day	0.805 (rest)	0.584 (rest)	0.072 (rest)	0.051 (rest)
	0.805 (exercise)	0.584 (exercise)	0.072 (exercise)	0.051 (exercise)
6 per day	1.209 (rest)	0.877 (rest)	0.102 (rest)	0.073 (rest)
	1.209 (exercise)	0.877 (exercise)	0.102 (exercise)	0.073 (exercise)
10 per day	2.022 (rest)	1.465 (rest)	0.1895 (rest)	0.135 (rest)
	2.022 (exercise)	1.465 (exercise)	0.1895 (exercise)	0.1353 (exercise)

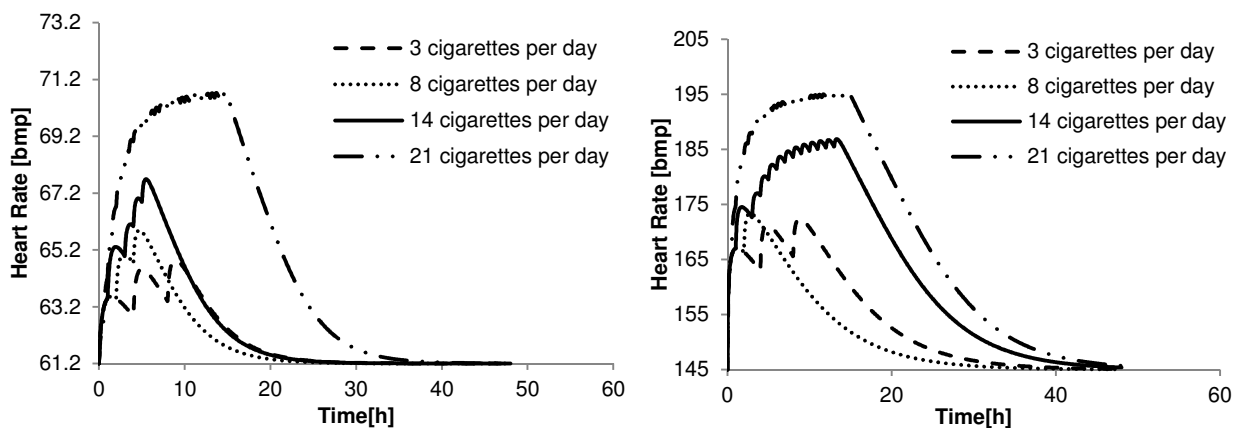


Fig 4.7.17. Simulated mean heart rate following cigarettes smoking at rest (left) and during exercise (right).

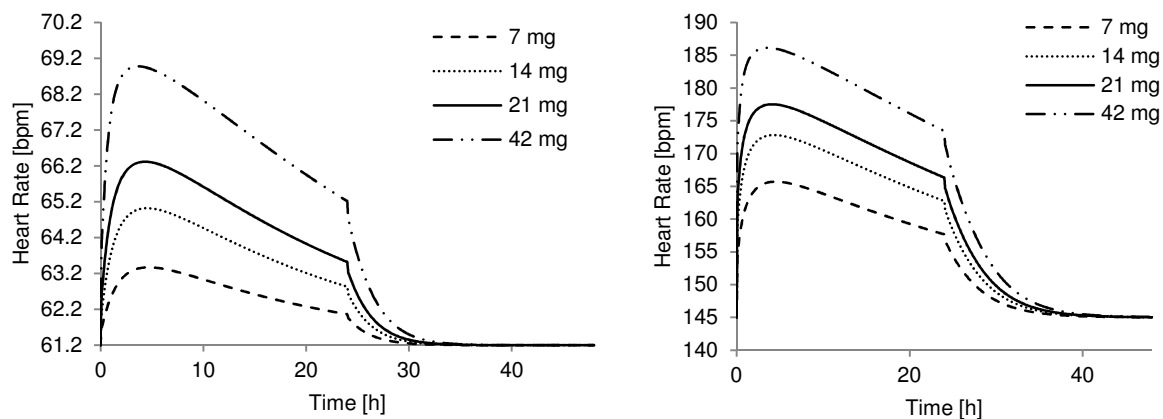


Fig 4.7.18. Simulated mean heart rate following application of nicotine patches at rest (left) and during exercise (right).

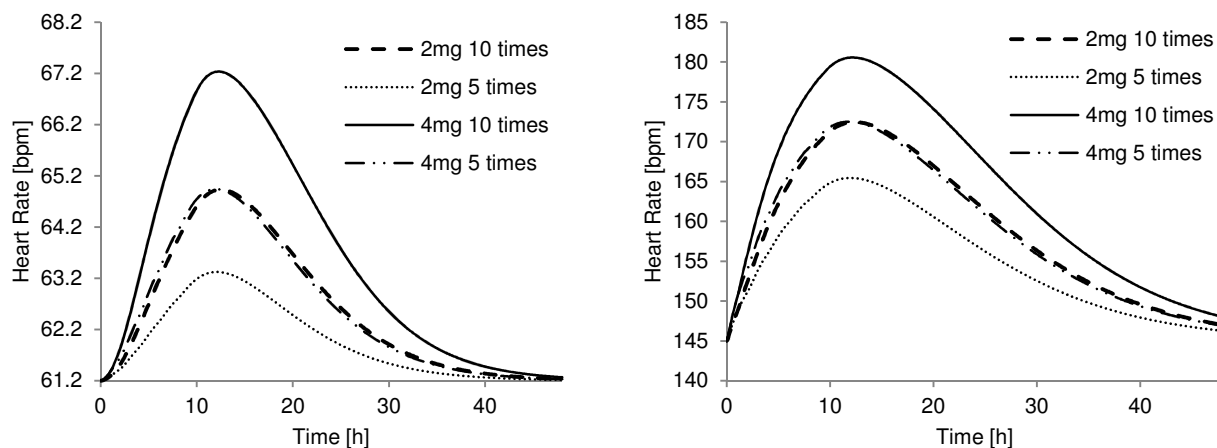


Fig 4.7.19. Simulated mean heart rate following application of nicotine lozenges at rest (left) and during exercise (right).

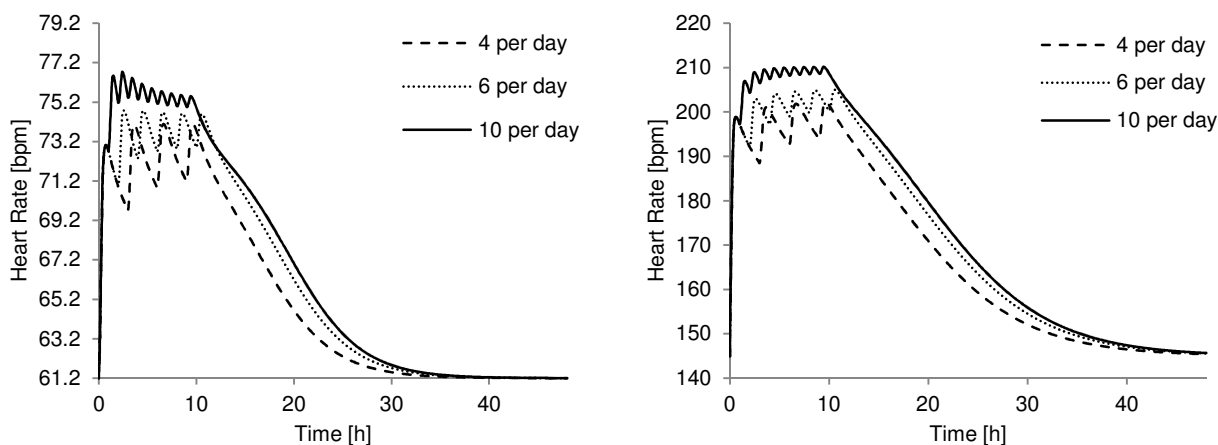


Fig 4.7.20. Simulated mean heart rate following inhalation of nicotine at rest (left) and during exercise (right).

Table 4.7.5 shows calculated mean heart rate and MAP values over the duration of experiment (400min-48h).

Table 4.7.5. Predicted mean heart rates and MAPs over simulation time for 4 administration routes

Dose	Administration route	Base-line heart rate (E0) [bpm]	Mean heart rate at rest [bpm]	Mean heart rate during exercise [bpm]	Mean MAP at rest [mmHg]
2.5 $\mu\text{g}/\text{BW}$ per 30 min 1 h apart	i.v.	at rest = 61.2	69.206	-	-
2.5 $\mu\text{g}/\text{BW}$ per 30 min 2 h apart	i.v.	at rest = 61.2	69.558	-	-
2.5 $\mu\text{g}/\text{BW}$ per 30 min 3.5 h apart	i.v.	at rest = 61.2	69.196	-	-
0.7 $\mu\text{g}/\text{BW}$ for 180 min	i.v.	at rest = 64	71.350	-	87.8834

0.7 µg/BW for 5 min 30 min later: 1 µg/BW for 5 min	i.v.	at rest=66	66.989	-	82.260
Dermal patches					
7 mg	dermal	at rest = 61.2	62.008	154.508	
14 mg		during exercise	62.666	158.079	-
21 mg		=145	63.215	160.531	
42 mg			64.436	165.256	
Cigarettes (1.2 mg)		at rest = 61.2			
3 per day	Inhalation	during exercise	61.798	154.008	-
8 per day		=145	62.505	151.417	
14 per day			63.215	161.235	
21 per day			65.493	164.713	
Nicotine inhaler					-
2mg	Inhalation	at rest = 61.2	65.334	168.023	
4 per day		during exercise	66.079	171.234	
6 per day		=145	66.676	173.826	
10 per day					
Nicotine lozenges		at rest = 61.2	61.968	155.157	
2 mg (every 2h)	Oral	during exercise	62.606	159.138	-
2 mg (every 1h)		=145	63.156	159.153	
4 mg (every 2h)			63.621	164.147	
4 mg (every 1h)					

Discussion

Simulating the toxicokinetic and dynamic behaviour of nicotine is complex even when the investigations are limited to the adult Caucasian population. The first modelling difficulty arises in accounting for differences in nicotine kinetics with respect to gender (i.e. varying nicotine and cotinine clearance), smoker-nonsmoker status (i.e. clearance of nicotine, nicotine binding to tissues, expression of metabolizing enzymes) and type of smoking – cigar smokers, users of snuff and chewing tobacco (i.e. rate of rise of nicotine) (Hukkanen et al., 2005). This, apart from pharmacodynamic issues, results in differences in blood/plasma concentrations (especially in the elimination phase) after single and prolonged exposure to nicotine.

When comparing predicted concentrations with experimental ones it is clear that the PBTK model performs best for exposure via the inhalation (cigarette smoking) and oral (with the straw) routes. Oral nicotine administration in carbomer capsules was also quite well represented by assuming a first-order rate of nicotine release from the tablet coating in the stomach. However, the model parameters calibrated previously for smokers did not produce a good match for the concentration-time profiles of nonsmokers. Absorption was simulated faster and elimination slower than observed (Green et al., 1999) – ca 1.2 times faster metabolism would produce better results. Experimental peak concentrations were achieved 7 h after nicotine dosing in the designed carbomer (Green et al., 1999) and 1-2 h after dosing with the straw (D'Orlando and Fox, 2004). Simulated peak levels were at 6.8 and 0.8h respectively indicating slightly faster calculated absorption than the observed one. Dermal exposure was the most difficult to model especially in the absorption phase.

Experiments showed a peak concentration at 8 h (Bannon et al., 1989), whereas simulations indicated it at 4.9 h. One of the explanations could be that either the diffusion coefficient in skin or the rate of nicotine release are not constant over time or that there is a time delay in nicotine release from the patch. In fact, the measured *in vivo* release profiles of nicotine are not constant. They were found to be relatively linear for the first 8 hours but then the absorption rate declined (Bannon et al., 1989). Experimental data for repeated smoking of low, average and high- nicotine brands of cigarettes resulted in nicotine concentrations in blood rising over the first 4 to 6 h after which they tended to plateau until smoking stopped (Benowitz et al., 1982). The PBTK model estimated an increase in blood levels up to the last cigarette (at 15 h) but this growth was ca. 5.3 times higher within the first 7 h. The major limitations of PBTK modelling in this study were in the underlying assumptions that: (i) there are no inter-individual and smoker-nonsmoker differences in the ADME model parameters; (ii) there is no nicotine in blood prior to exposure; and (iii) exposure is via only a single route; (iv) the model includes constant absorption parameters from the GI tract, respiratory tract and release from a patch and constant diffusion coefficient of nicotine through the skin; (v) there is a need for using QSPRs to predict partitioning between *stratum corneum* and viable epidermis as well as diffusion in epidermis due to lack of experimental data.

I applied the PBTK-TD model to various exposure scenarios: specified in the literature with experimental data published (blood or plasma concentrations) or estimated based on statistical information available online in exposure reports on nicotine smoking and replacement therapy. In the second case, I obtained the following results (**Figure 4.7.21**):

- C_{\max} , AUC and heart rate (peak and mean) results are the highest in the extreme case of nicotine inhaler.
- As expected, AUC and C_{\max} in the blood were higher after smoking 21 cigarettes per day (every 30 min) when compared to other exposure routes (AUC in blood was ca 34% higher than that of 42mg patch at rest and 92% higher with faster respiratory rate; C_{\max} in blood was 103% (both at rest and during exercise) higher than after extreme dermal exposure).
- AUC and C_{\max} in the liver were the highest for dermal application of two nicotine patches (42mg) for 24 h over 44 cm² skin area (AUC in liver compared to that of smoking 21 cigarettes was found 86 % (rest) and 32 % (exercise) higher, whereas C_{\max} in liver was 24 % (rest) and 18 % (exercise) higher).
- 2 mg of nicotine given orally every hour (10 times a day) is equivalent to 4mg given orally every 2 hours (5 times a day) in terms of AUC and C_{\max} -based results.
- Assuming that the nicotine blood concentration, both in terms of AUC and C_{\max} , is more relevant for systemic toxic effects, comparable exposure results were estimated for: 3 cigarettes per day \approx 1 dermal patch 7 mg \approx 2 mg of lozenges every 2 h (5 altogether); 8 cigarettes per day \approx 14 mg dermal patch \approx 4 mg of lozenges (5 altogether) or 2 mg lozenges (10 altogether) – **Figure 4.7.21**.

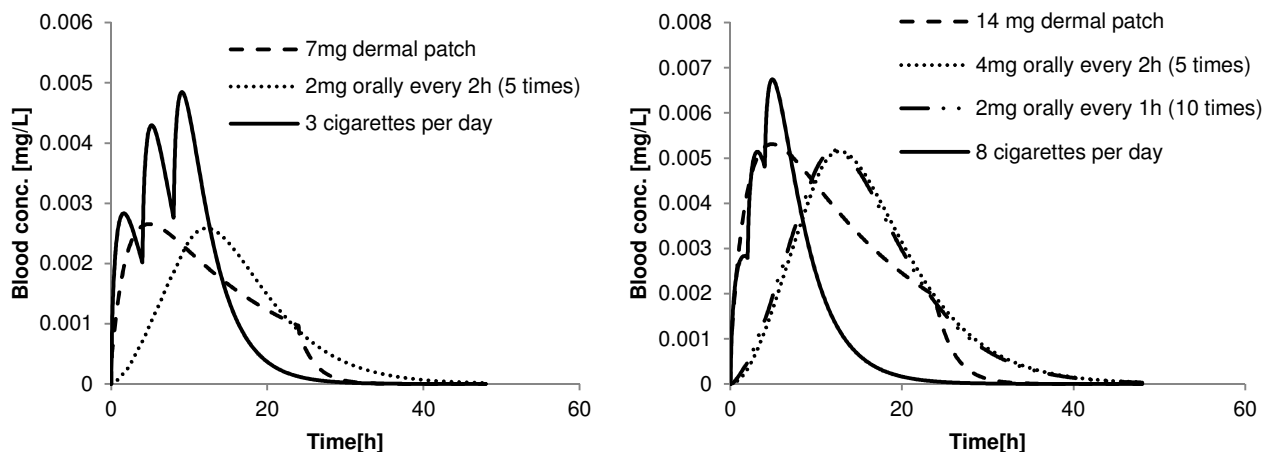


Fig 4.7.21. Comparable exposure scenarios in terms of toxicokinetics – blood results.

My choice of 4-min smoking time in these daily scenarios was based on the model calibrations with respect to *in vivo* data (Benowitz et al., 1982) and other literature studies such as the one of (Mendelson et al., 2008) in which the tested subjects smoked each cigarette for 4 min and took one 5-s-puff every 30 s. I assumed the same smoking duration for the exercise conditions and changed only the respiratory rate. By using a smoking time of 4 min I accounted for the worst-case scenario which is thus a conservative one in a safety assessment. In reality, there might be an increase in the puff frequency that makes a cigarette burn out faster; therefore a shorter time than 4 min could be more appropriate. To simulate a shorter smoking time would require, however, the availability of suitable data to verify the model performance in accurately estimating blood concentrations following smoking during exercise.

As shown in the results, the heart rate is well-described by a two-compartment PBTD model, as indicated in the literature (Porchet et al., 1988), but a modification (introduction of an exponent in relating the nicotine and antagonist concentrations to observable effect) might be necessary to obtain a better representation of heart rate increase during exercise conditions using the TD parameters calibrated for i.v. injection at rest (except for a base-line value). The need for this modification may arise from a variety of factors such as ongoing exercise, population effects, differences between smokers and non-smokers in terms of nicotine effects on heart rate, quality of experimental data, exposure route or combination of them.

TD model simulations indicate that the highest heart rate is achieved after heavy smoking of 21 cigarettes a day and equals 71.5 [bpm] (at rest, increase by 10.3 [bpm] from base effect) and 196 (during exercise, increase by 51 [bpm] from the base effect) and by nicotine inhaler: 76.2 (at rest, increase by 15 [bpm]) and 210 (increase by 65 [bpm]). My simulated heart rate values were in the range of experimental results published by (Papathanasiou et al., 2013) for smokers during exercise: 191-193 bpm. At resting conditions our simulations indicated lower heart rates due to lower assumed base-line values than the ones of (Papathanasiou et al., 2013) (61.2 vs. 72.8-76.4 bpm).

When comparing mean heart rate estimates (**Table 4.7.5**) over up to 48 h, it is a dermal absorption that causes long-lasting higher heart rate (excluding inhaler that shows the highest results: 67 at rest and 174 during exercise). The reason behind it is probably pro-longed nicotine release from a patch and therefore a longer nicotine half-life in blood.

For modelling the effects on blood pressure further validation would be necessary to confirm that the sigmoid model works well. In this study, I have predicted MAP only following i.v. injections, for which there are experimental data in literature. As a result, we see that average MAP over 400 min may rise upon 15-17 mmHg from its base-line value after infusion of 0.7-1 $\mu\text{g}/\text{BW}$ of nicotine for up to 180 min.

The development of acute tolerance to various effects of nicotine after i.v. injection was studied in the paper of (Fattinger et al., 1997). The rates of tolerance formation and elimination were found to vary considerably depending on the effect. As a result, half-lives of tolerance were concluded to be different for heart rate and pressure effects, which might be related to differences in the rate of desensitization of various subtypes of nicotinic receptors and/or differences in mechanisms of tolerance for various nicotinic effects. Nicotine was shown to increase heart rate, systolic and diastolic blood pressure. Tolerance to systolic blood pressure was said to develop relatively slowly (with half-life ≈ 70 min for systolic blood pressure), requiring several hours to reach a maximal tolerance, whereas tolerance to heart rate acceleration formed relatively rapidly (with half-life ≈ 21 min). This difference should be reflected in the tolerance compartment of the PBTD model calibrated to estimate a given effect. However, to do so, more experimental data would be necessary as there are 4-5 parameters to be optimised provided the sigmoid model is still appropriate. In my model, due to the availability of only two data sets, I had to assume that tolerance formation and elimination is the same for both cardiovascular responses. Only the ratio of E_{max} to nicotine venous blood concentration causing half of the effect (S) was optimised due to its high sensitivity to the model output. I always measured effect that is an average for a group of subjects. (Fattinger et al., 1997) additionally pointed that even if there was different modelling of tolerance for different effects, a misfit of the population model of blood pressure responses was still obtained. In contrast, using individual data did not show this misfit because inter-individual differences in average measurements were excluded. Regardless of these observations, that are based on i.v. injections only, in the current study a satisfactory fit of MAP values was found, given the stated assumptions and limitations of the model. The authors outlined that nicotinic receptors are present in varying concentrations in different parts of the brain, and nicotine receptors modulate release of different neurotransmitters, including dopamine, norepinephrine, acetylcholine, serotonin, glutamate, b-endorphin and others. Therefore, venous blood concentration should be replaced with better quantitative description of an effect-site concentration.

4.7.2 Caffeine

In this section, I used caffeine to model toxicokinetic-toxicodynamic effects – mean population heart rate and arterial blood pressure - following single and repeated exposure. As before, I took both experimental exposure data from the literature (blood or plasma concentrations) and estimated daily exposure based on statistical information available online in exposure reports on caffeine consumption as a beverage or active ingredient in cosmetics. It is assumed in the PBTD modelling that the free caffeine fraction that causes an effect is 65% based on published experimental results (Yamazaki and Kanaoka, 2004).

Toxicodynamic parameters for blood pressure and heart rate are given in **Table 4.7.6**. In modelling of blood pressure and heart rate I always assume first order rates of formation and elimination of antagonist due to insufficient experimental information necessary to better describe the kinetics of tolerance. In case of heart rate, the toxicodynamic parameters of tolerance are the same as of nicotine. However, in contrast to nicotine, there were more experimental MAP values available in literature so that the formation and elimination rates of tolerance were optimised independently of those used for heart rate effects. To estimate both pharmacological responses I used venous blood concentrations (unbound fraction) as a surrogate for effect-site concentrations in the same manner as for nicotine.

Table 4.7.6. Toxicodynamic parameters for heart rate and blood pressure for caffeine

Parameter	Value	Reference
Mean arterial blood pressure (MAP)		
E_0 [mmHg]	At rest: 83.30 At rest: 80.67 At rest: 78 During exercise :85	(Shi, 1993) (Karatzis et al., 2005) (Daniels et al., 1998)
S [mmHg/mg/L]	20.6	(Shi, 1993)
$k_{a, Ant}$ [L/h]	3.48	Optimised with respect to (Shi, 1993)
$k_{el, Ant}$ [L/h]	4.86	
$C_{Ant,50}$ [mg/L]	0.24	(Shi, 1993)
y	-	-
Heart rate		
E_0 [bpm]	At rest: 50 During exercise:100 During exercise:125 During exercise: 104.56	(Daniels et al., 1998) (Ping et al., 2010) (Damirchi et al., 2009)
S [bpm/mg/L]	200	Optimised with respect to (Daniels et al., 1998) at rest
$k_{a, Ant}$ [L/h]	3	See nicotine
$k_{el, Ant}$ [L/h]	6	See nicotine
$C_{Ant,50}$ [mg/L]	0.00772	See nicotine
y	At rest: 1 During exercise: 0.4	Optimised with respect to (Damirchi et al., 2009)

- **Mean heart rate**

Heart rate recordings following administration of caffeine containing gelatin capsule (5 mg/kg BW) in 6 lean men were used to calibrate the PBTD model (tolerance development, exponent in the sigmoid model) during exercise (Damirchi et al., 2009). Mean values of heart rate were recorded throughout the treadmill exercise (30 min- running at constant relative load). **Figure 4.7.22** shows the estimated caffeine concentration in blood and mean heart rate.

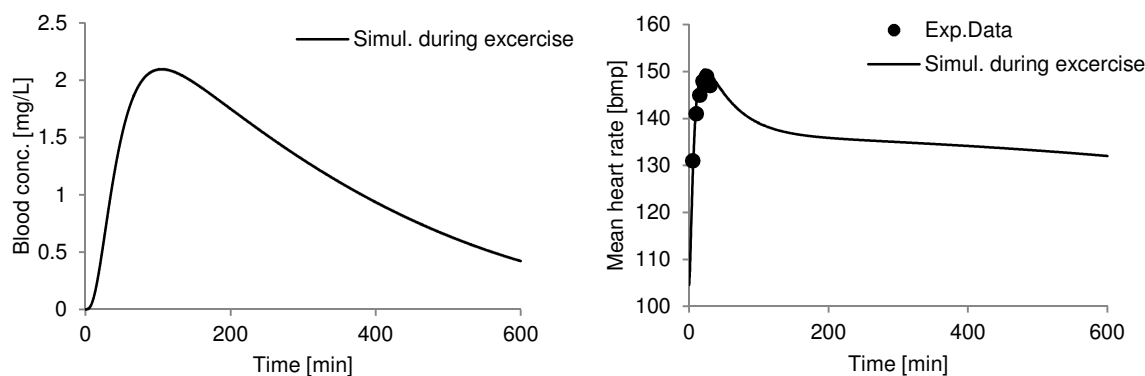


Fig 4.7.22. Simulated caffeine concentration in blood and resulting increase in heart rate during heavy exercise. Experimental data: (Damirchi et al., 2009).

(Mousavi et al., 2011) used the same dose to measure the mean heart rate of 20 female athletes (over entire duration of experiment) at rest and during cycling exercise and reported 85.55 bpm at rest and 141.50 bpm during exercise. Calculating mean heart rate values over 600 min in the experiment of (Damirchi et al., 2009), I obtained: 53.412 bpm (with E_0 at 50 bpm) at rest and 127.675 (with $E_0= 104.56$ bpm) during exercise. These results are lower than the ones of (Mousavi et al., 2011) but the differences may be, excluding experimental errors, in: base-line values, gender effects and intensity of the exercise.

(Daniels et al., 1998) measured the effect of 6 mg/kg BW of caffeine in gelatin capsules on the heart rate of trained cyclists (7 women and 3 men) at rest and during dynamic leg exercise. (Ping et al., 2010) reported effect of 7 mg/kg BW of caffeine in capsules on heart rate of nine male Malaysian recreational runners during endurance running in hot & humid climate. **Figure 4.7.23** shows the simulated toxicokinetic and toxicodynamic results versus experimental points.

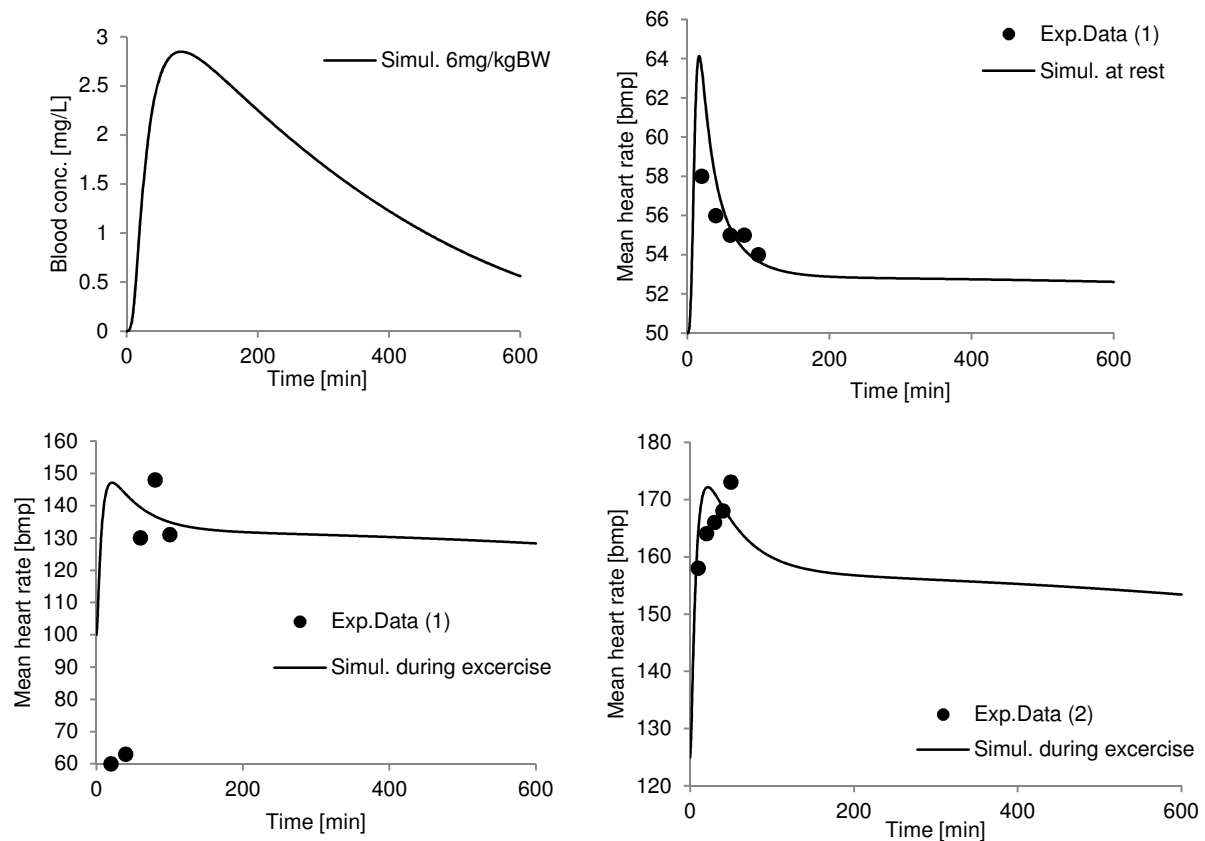


Fig 4.7.23. Caffeine concentration and resulting increase in heart rate during exercise and at res.

Experimental data: 1. (Daniels et al., 1998) and 2. (Ping et al., 2010).

- **Mean arterial blood pressure (MAP)**

Four experimental studies were used to model blood pressure. In the first one (Shi, 1993), used for the PBTD model calibration, the acute effect of a cup of instant coffee containing 80 mg of caffeine (administered to eight men and eight women within 10 min) was investigated on aortic blood pressure (**Figure 4.7.24**). Central and peripheral systolic (Sys) and diastolic (Dias) pressure recordings were provided. However, in this study only central pressure measurements were used and mean arterial pressure (MAP) was calculated as follows: $MAP = (Sys - Dias) / 3 + Dias$ (Shi, 1993). In the second study (Karatzis et al., 2005), 8 healthy men received 4 mg/kg of caffeine added to decaffeinated coffee. Drinking time of 5 min was assumed (300 mL). Mean arterial pressure results at resting conditions were published (**Figure 4.7.25**). Regardless of resting or exercise conditions, I used the same sigmoid model structure and its parameters, changing only the base-line value. This decision was made based on the fact that several literature studies showed that caffeine caused similar MAP increases at rest and exercise (Daniels et al., 1998) or the difference was not clearly stated.

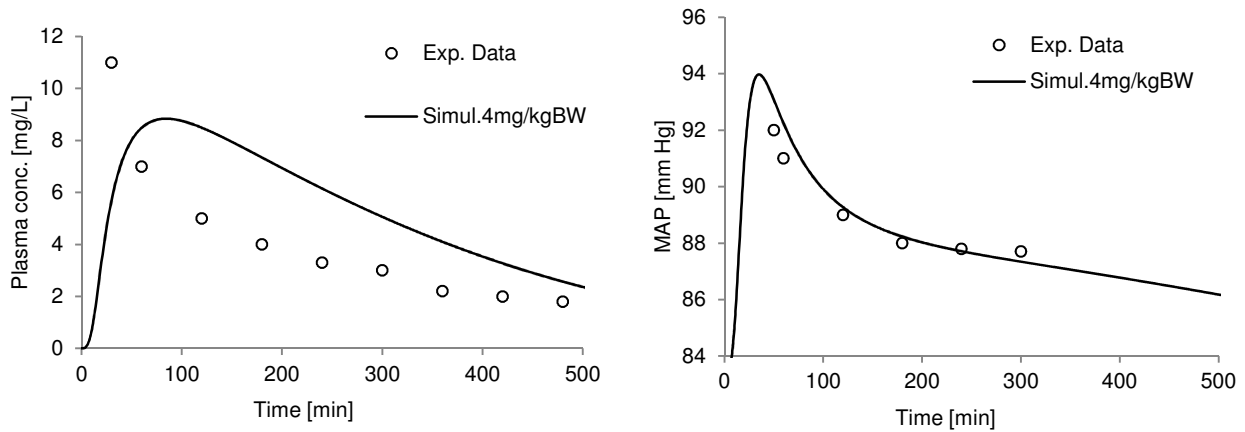


Fig 4.7.24. Caffeine concentration and resulting increase in blood pressure after administration of 4mg/kg BW of caffeine in beverage. Experimental data: (Shi, 1993).

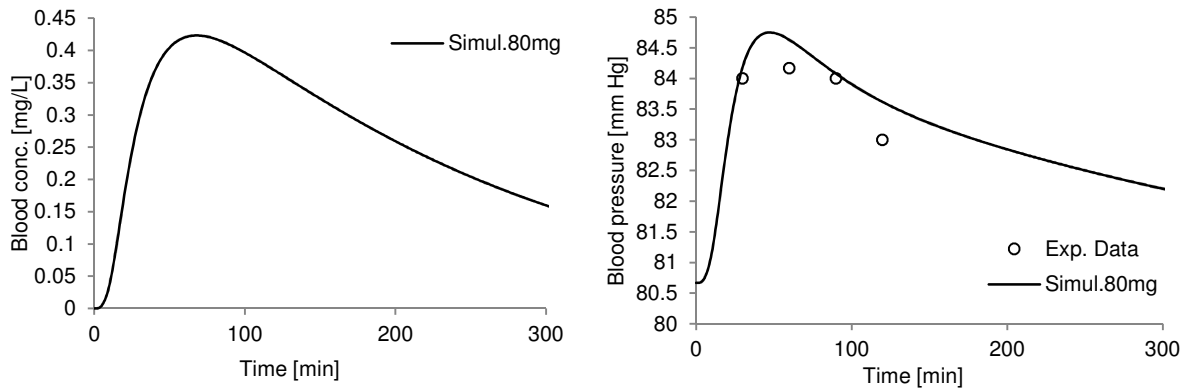


Fig 4.7.25. Caffeine concentration and resulting increase in blood pressure after administration of 80mg of caffeine in coffee. Experimental data: (Karatzis et al., 2005).

Two other studies showed the limitations of using a simple sigmoid model to accurately predict mean group MAP results. In the work of (Daniels et al., 1998) blood pressure was measured after administration of 6 mg/ kg BW of caffeine at rest and during dynamic leg exercise. In both cases, it was rather difficult to match the mean experimental points because of their high fluctuation. The authors reported calculated MAP values averaged for men and women: non-habitual coffee users, all nonsmokers, because of stated no significant differences in the response to caffeine between genders (**Figure 4.7.26**).

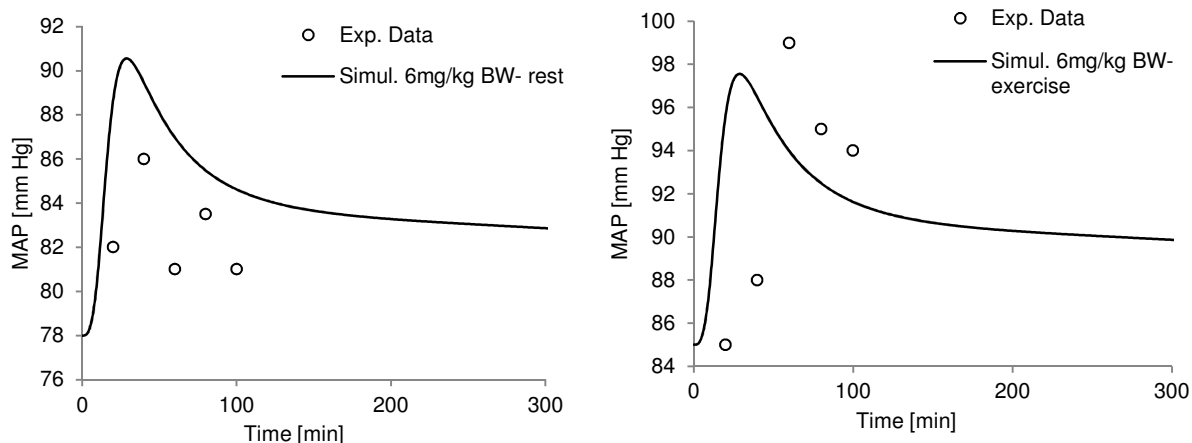


Fig 4.7.26. Caffeine concentration and resulting increase in blood pressure after administration of 6 mg/kg BW of caffeine in coffee. Experimental data (1): (Daniels et al., 1998).

In the paper of (Mousavi et al., 2011), where the subjects were 20 Iranian female athletes that received 5mg/kg BW of caffeine in capsules, the effect of caffeine on MAP was evaluated at rest and during cycling exercise and the following results were published over the duration of the experiment: mean MAP at rest = 91.67, mean MAP during exercise = 92.683 mmHg. Assuming baseline MAP values of 80.67 at rest and 85 during exercise, the PBTD simulations gave slightly lower results: mean MAP at rest = 85.466 and mean MAP at exercise = 89.799 mmHg.

- Caffeine with repeated dosing

While toxicokinetics of caffeine after repeated dosing was relatively easy to simulate, the toxicodynamic effect – MAP - was particularly difficult to fit. (Denaro et al., 1991) carried out the following experiment: nine healthy subjects were given, in randomised 5-day blocks, low (0.7 mg/kg BW) and high (1 mg/kg BW) doses of caffeine in a coffee 6 times per day. Plasma concentrations were measured over 24 h on the first day. MAP values for a subject with and without complete tolerance to caffeine effects were recorded on the 5th day. Due to the developed tolerance, blood pressure recordings on the last day were claimed to be, on average, similar in all treatment blocks. **Figure 4.7.27** presents plasma concentrations, whereas **Figure 4.7.28** MAP simulations. Clearly, there was a higher difference between MAP values measured once ca 4 hours than in the model predictions. In this case, high inter-individual variability, not accounted for by the model, or different kinetics of antagonist than the modelled one (calibrated for the first hours after ca. 48-h abstinence from caffeine (Shi, 1993)) or combination of both of them could cause this mismatch. A particularly high difference between simulated and experimental points was found for a subject without a complete tolerance to caffeine effects.

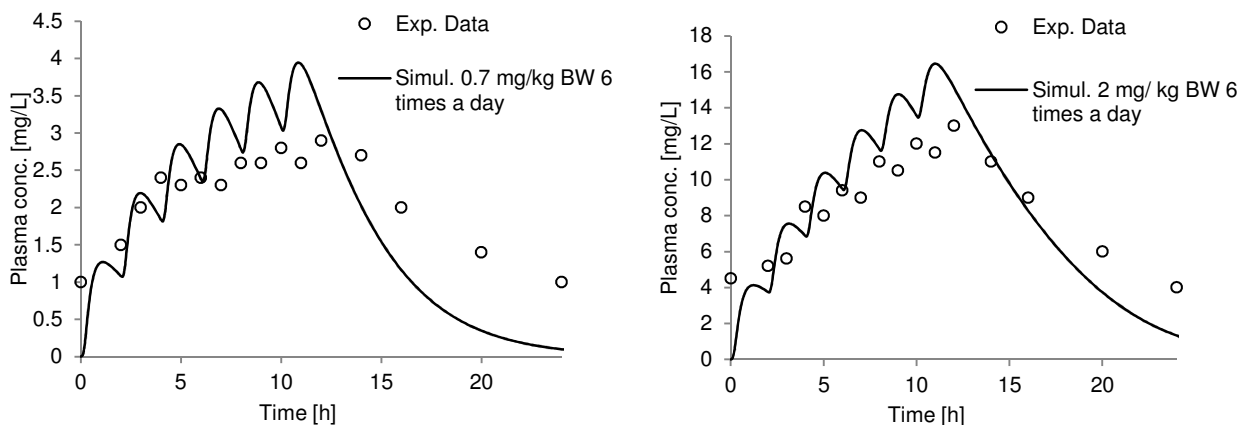


Fig 4.7.27. Plasma concentration following repeated dosing of low (left) and high (right) doses of caffeine 6 times per day. Experimental data: (Denaro et al., 1991).

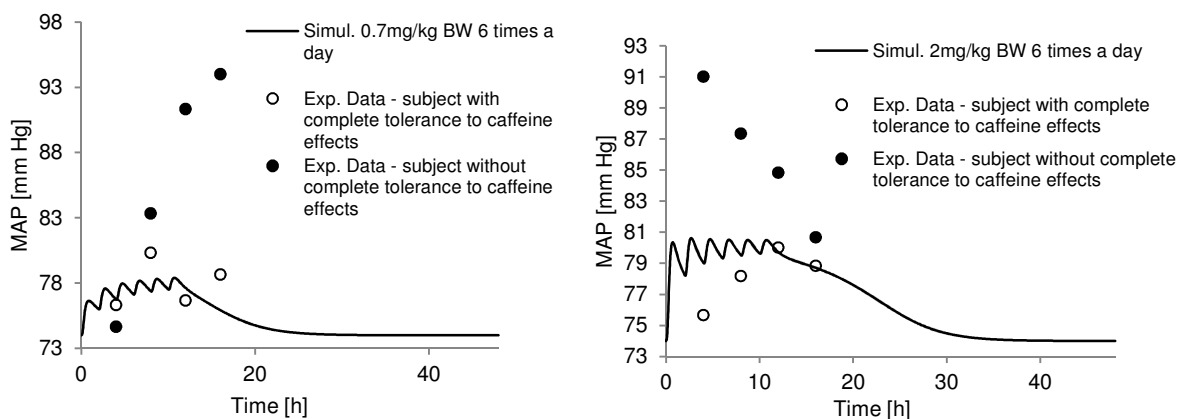


Fig 4.7.28. MAP after repeated dosing of low (left) and high (right) dose of caffeine. Experimental data: (Denaro et al., 1991).

Daily exposure design

Daily exposure to caffeine was estimated based on available web information. **Table 4.7.7** provides the experimental design for repeated exposure to caffeine via skin and consumption of coffee.

For oral absorption I assume that: i) instant coffee containing 62 mg of caffeine is consumed 4 times per day, once every 2 hours; ii) Starbucks Coffee Grande containing 320 mg of caffeine is consumed 2 and 4 times per day, every 4 and 2 hours respectively.

For dermal absorption I take: i) Vichy Destock Stomach product containing 5 % of caffeine anhydrous that is applied on 150 cm² of skin and provides, in a single dose, 30mg of caffeine in 6.575 mL of vehicle. This condition is limited by the PBTK model applicability to caffeine concentration in a vehicle of 4.5645 mg/mL, although, overall caffeine content might be around 7.5 mL:1.23 (density of caffeine) g/mL =9225 mg in 150 mL. Dosing is done twice per day, every 10 hours for 4 hours; ii) Shower shock, within 8 min,

200 mg of caffeine is spread on 1000 cm² of skin area (vehicle volume= 43.836 mL). Application is done twice per day 12 h apart. Diffusion and skin partition coefficients used in both cases have been calibrated based on the ethanol+ propylene glycol vehicle. The dermal absorption of caffeine in humans follows an extreme condition where hair follicles contribute to overall absorption rate (Liu et al., 2011; Otberg et al., 2008) – permeation through open hair follicles and less extreme absorption under closed hair follicles.

Both results in terms of AUC and C_{max} of caffeine in the blood and liver are placed in the **Table 4.7.8**. The total absorption of caffeine in Vichy Destock Stomach product after repeated dose reaches around 62.907% with open hair follicles and 55.04% with closed hair follicles; whereas, in case of shower shock, absorption reaches 2.197% with open hair follicles and 1.932% with closed hair follicles.

Table 4.7.7. Selected average daily exposure to caffeine

Exposure route	Exposed amount per day	No. per day	Ref.
Oral instant coffee (62 mg)	248 mg (every 2 h) 200 mL cup in 5 min	4	(Fitness, 2014)
Starbucks Coffee Grande (320 mg)	640 (every 4 h) and 1280 mg (every 2 h) 200 mL cup in 5 min	2, 4	(Fitness, 2014)
Dermal (Vichy Destock Stomach)	30 mg on 150 cm ² for 4 h, 10 h apart	2	(“Caffeine informer,” 2014)
Shower shock	200 mg on ca.1000 cm ² for 8 min, 12 h apart	2	(“Caffeine informer,” 2014)

All the PBTK-TD simulations were performed for a male subject (BW= 70 kg) with a heart rate base-line value of 50 bpm at rest and 104.56 bpm during exercise over 48 h. I restricted my study to simulating the heart rate due to the better sigmoid model performance when compared to MAP estimations. Blood concentrations are shown and compared in **Figure 4.7.29** and heart rates in **Figure 4.7.30**. **Figure 4.7.31**, in turn, presents the difference in blood concentrations following dermal absorption with open and closed hair follicles.

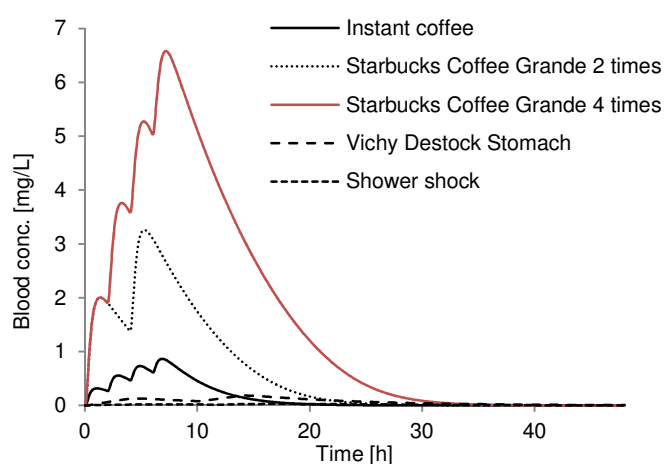


Fig 4.7.29. Simulated blood concentrations of caffeine following defined daily exposure scenarios (dermal absorption with open hair follicles).

Table 4.7.8. AUC and C_{max} of caffeine in blood and liver following selected exposure scenarios

Exposure route	AUC liver	AUC blood	C_{max} liver	C_{max} blood
Oral instant coffee	50.014	7.147	6.952	0.866
Starbucks Coffee Grande	2 times: 207.293 4 times: 537.952	2 times: 29.623 4 times: 76.875	2 times: 27.785 4 times: 50.536	2 times: 3.260 4 times: 6.580
Vichy Destock Stomach	Open HF*: 10.882 Closed HF*: 7.919	Open HF*: 3.360 Closed HF*: 2.457	Open HF*: 0.601 Closed HF*: 0.450	Open HF*: 0.184 Closed HF*: 0.139
Shower shock	Open HF*: 2.285 Closed HF*: 1.718	Open HF*: 0.717 Closed HF*: 0.539	Open HF*: 0.094 Closed HF*: 0.075	Open HF*: 0.030 Closed HF*: 0.024

(*) HF= hair follicles

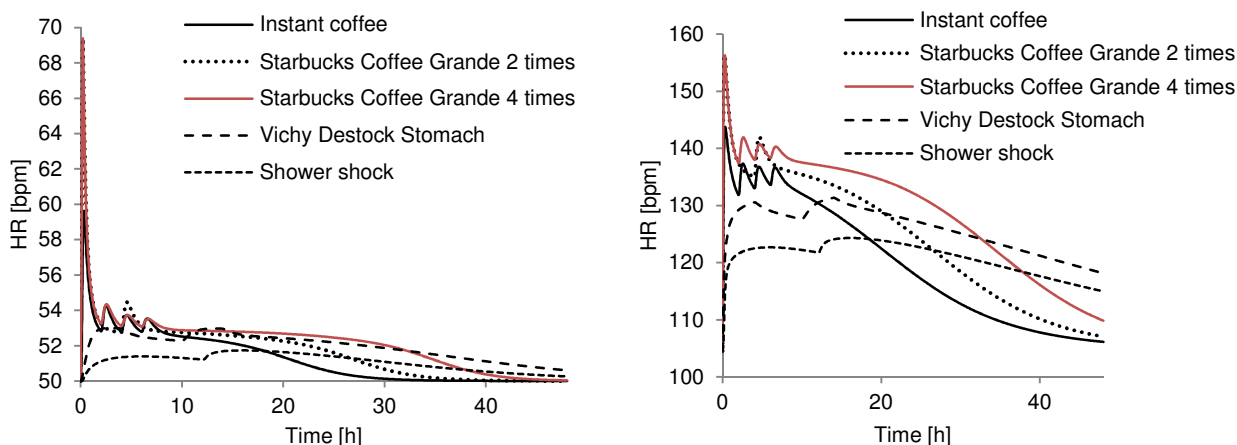


Fig 4.7.30. Simulated mean heart rate after daily exposure to caffeine at rest (left) and throughout the treadmill exercise (right).

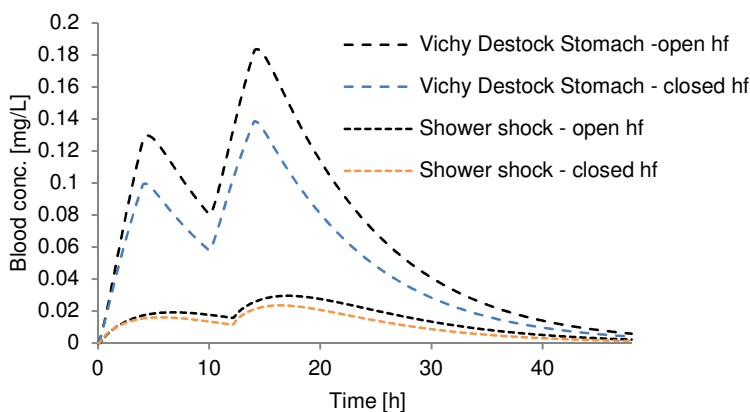


Fig 4.7.31. Simulated caffeine concentration in blood following absorption with open and closed follicles.

Discussion

The cardiovascular pharmacodynamics of caffeine is quite complex and not fully understood. In general, caffeine increases cardiovascular responses after an interval of caffeine abstinence and tolerance develops within a short period of time with repeated dosing of caffeine. But the magnitude, rate of development, and

disappearance of tolerance have not been quantified so far. However, more recently it has been reported that habitual caffeine use does not necessarily lead to complete tolerance. Effect data are more variable because of relatively large inter-individual variability, measurement error, sensitivity to caffeine between normotensive and hypertensive subjects, age and other factors such as psychological and behavioral stress. It has been diagnosed that hypertensive men had peripheral systolic blood pressure (SBP) responses >1.5 times greater than normotensives, and thus caffeine effects on peripheral SBP depend on baseline blood pressure and are not expected to be significant in normal subjects. The blood pressure was found to increase more in older than in younger subjects after caffeine consumption. As tolerance develops, the increase of cardiovascular responses, such as blood pressure, after administration of doses of caffeine will be greatly reduced, but even with daily coffee drinking the blood pressure may still remain slightly elevated compared to the situation with absence to caffeine (Shi, 1993).

Measureable effects in some of the subjects may have a relatively small signal to noise ratio, or conversely, it may produce extreme estimates because "noise" was present at informative time points, thus distorting the apparent pharmacodynamic response. To smooth these disturbances and to facilitate modelling, normally, average data from all subjects at each time point are calculated.

In the literature, based on experimental results, the following observations about the heart rate were reported:

- No significant differences were found between the effects of caffeine (6 mg/kg caffeine) on heart rate at rest and during exercise, explained by the fact that caffeine can alter the cardiovascular response to dynamic exercise by modifying regional blood flow and forearm vascular conductance (Daniels et al., 1998).
- Caffeine was shown to decrease heart rate in low intensity exercises or at rest but in heavy, submaximal exercises heart rate would remain unchanged (Damirchi et al., 2009).
- Postdrug baseline showed that caffeine decreased heart rate during exercise in normotensive healthy young men (Sung et al., 1990).
- Caffeine at low doses (ca. 1.5 and 3.0 mg/kg BW) significantly decreased heart rate during low to moderate intensity cycle exercise in non-habitual caffeine users. These low doses of caffeine did not significantly affect heart rate at rest nor did they affect it during maximal exercise (McClaran and Wetter, 2007).
- The mean heart rate at rest and after exercise increased after caffeine consumption (5 mg/kg BW) compared to placebo use with mean of 85.55 vs. 82.40 and 141.50 vs. 139.95 beat/ minute, respectively; however, these changes were not statistically significant. Caffeine can increase heart rate during recovery (Mousavi et al., 2011).
- After 5 days of caffeine consumption a complete tolerance developed to the effects of caffeine on heart rate (Denaro et al., 1991).

And about the mean arterial (MAP), systolic (SBP) and diastolic (DBP) blood pressure:

- SBP and MAP were found higher during exercise with caffeine but these increases were secondary to the effects of caffeine on resting blood pressure (Daniels et al., 1998).
- Caffeine consumption in healthy young adults leads to an acute: increase in central SBP without affecting significantly peripheral SBP.
- It is possible that both peripheral DBP and central BP of healthy young adults are more sensitive to the effect of low doses of caffeine, and larger quantities need to be consumed before peripheral SBP becomes affected (Karatzis et al., 2005).
- Caffeine acutely elevates SBP and DBP at rest and during mental and exercise stress.
- Most recent long-term studies have shown an independent positive association of caffeine consumption and higher BP, indicating that tolerance to caffeine is not complete. Several short-term studies have also provided evidence that tolerance is not complete.
- Caffeine appears to affect blood pressure via adenosine receptor inhibition and increased release of some neurotransmitters. Caffeine significantly increased the SBP especially in obese subjects, who are known to be at higher risk of hypertension than lean ones. The combined rise in blood pressure induced by exercise and caffeine did not significantly increase the SBP compared with the post-exercise value in obese men receiving placebo (Damirchi et al., 2009).
- Data indicate that caffeine increases BP additively during submaximal exercise and may cause excessive BP responses at maximal exercise for some individuals. The pressor effects of caffeine appear to be due to increasing vascular resistance rather than cardiac output (Sung et al., 1990).
- At low doses caffeine had no effect on SBP during exercise and this result differs from previous studies showing increased SBP during submaximal exercise intensity (McClaran and Wetter, 2007).
- SBP and DBP at rest showed an increase after caffeine consumption compared with placebo (mean systolic blood pressure of 122.20 vs. 115.95 mmHg and diastolic blood pressure of 76.40 vs. 65 mmHg). SBP and DBP at the end of practice were higher after taking caffeine compared with placebo (mean systolic blood pressure of 132.15 vs. 130.50 mmHg and diastolic blood pressure of 75.75 vs. 70.25 mmHg), however, this difference was not statistically significant ($P > 0.05$). Although increased blood pressure by caffeine is well established in various studies, the cardiovascular mechanisms that cause these effects are not yet clear (Mousavi et al., 2011).
- After 5 days of caffeine consumption a complete tolerance developed to the effects of caffeine on blood pressure (Denaro et al., 1991).

Analysed daily exposure scenarios of caffeine, based entirely on simulations, showed the following results:

- AUC and C_{max} results in the blood and liver are, not surprisingly, highest for caffeine-rich Starbucks Coffee Grande.
- 2 dermal applications of Vichy Destock Stomach gave 4.6 times smaller AUC of caffeine in the liver and only 2.13 times smaller AUC in the blood when compared to 4 cups of instant coffee (open hair follicles case). When similar application conditions are used in both exposure routes - 4 times a day

every 4 h for dermal absorption and every 2 h for oral; dermal exposure with open hair follicles gives the following results: AUC in liver: 24.886, AUC in blood: 7.533 (slightly higher than oral result- see **Table 4.7.8**), C_{max} in liver: 1.242 and C_{max} in blood: 0.370 (**Figure 4.7.32**).

- Short shower shock (with 8 min of caffeine on the skin surface) could have been simulated only for the skin area up to 1000 cm² because of the model applicability domain. Though the results seem relatively small even for extreme scenario, in real cases much higher body surface area is exposed to the shower shock. However, different permeability properties of different skin sites and temperature may be compensated for by using a smaller surface but with enhanced transport via hair follicles.
- Comparable magnitudes of heart rates were shown at rest and during exercise for instant coffee and Vichy Destock Stomach with the difference that dermal absorption, both in the case of Vichy and Shower Shock, caused long-lasting heart rate alterations.

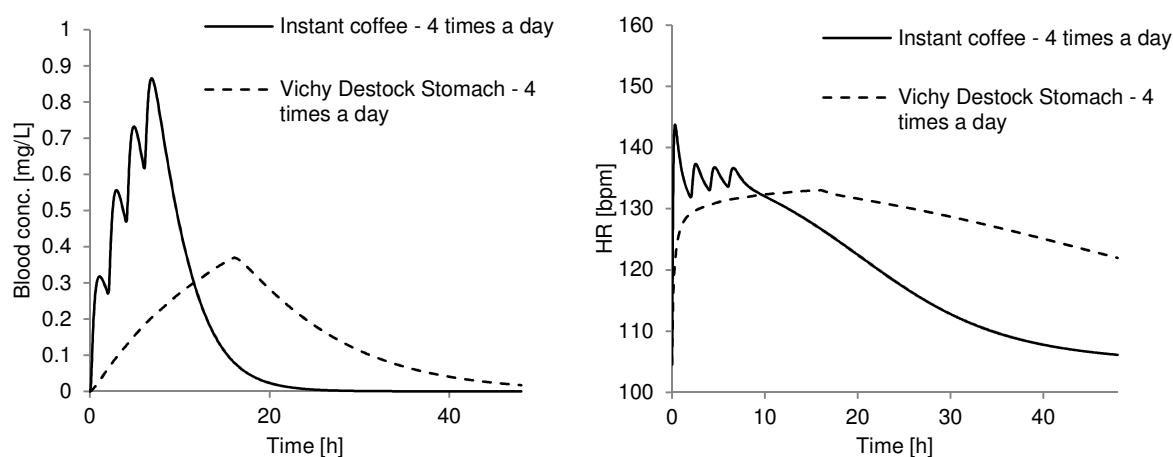


Fig 4.7.32. Oral and dermal application of caffeine 4 times a day every 2h (open hair follicles): Blood concentrations and mean heart rate during exercise.

5. Evaluation of uncertainty in input parameters to the PBTK-TD models

The error in model predictions that is often referred to as uncertainty can be decomposed into variability and true uncertainty.

Variability refers to the natural variability in a quantity that is distributed within a defined population, such as inter-individual differences in physiological parameters and inter-occasion differences in exposure durations. These quantities are inherently variable and cannot be represented by a single value, but can nevertheless be characterised in statistic terms (e.g. mean, variance, skewness). In contrast, true uncertainty refers to a parameter that has a single value, but which cannot be known with precision due to measurement

or estimation error. Thus uncertainty can be reduced by experimentation whereas variability is a fact of life (Lavé et al., 2007).

Uncertainty in model predictions arises from a number of sources, including specification of the problem, formulation of conceptual and computational models, estimation/measurement of input values, and calculation and interpretation of the results. In general, the focus of uncertainty analysis in PBTK-TD modelling is on: i) the uncertainty in measuring or estimating the “true” value of the model parameters; and ii) the variability representing inter-individual and inter-occasion differences. As described in previous chapters, the model parameters are either taken from the literature (experimental measures, optimisation results from the modelling of case studies), predicted by means of QSPRs or fitted to *in vivo* blood or plasma concentrations. The fitted value may implicitly capture and indirectly compensate for model processes that are not explicitly accounted for such as: delayed distribution of a compound from plasma to the site of action, irreversible binding to the receptor (PBTD case), metabolite interactions, indirect mechanisms of action, changes in protein binding and other effects. Thus, the fitted value may differ from the “true” value. This is the case also when a parameter value is not measured directly so that a value of another variable is attributed to this parameter (eg. skin absorption parameters). Uncertainty relating to the model structure is not considered in this chapter as comparison with other simpler models was performed in **Chapter 4.2** and more complex structures could not be used due to insufficient available information about investigated compounds in literature. In general, there is a trade-off between simpler and more complex models in terms of accuracy of prediction versus the number of parameters that need to be determined. For the purposes of chemical risk assessment, different model structures can be applicable in different circumstances (hence the importance of problem formulation). In general, the model structure should be “fit for purpose”, i.e. be accurate enough to characterise hazard, exposure or risk, without the need to capture every biological detail. It is important to bear in mind that chemical risk assessments are often based on animal data (e.g. NOAEL values) that show a high degree of variability.

A frequent problem with PBTK model parameterization is identifiability. This is a problem when more than one set of parameter values can be used to provide similar predictions. In this case, a selection of the parameter value depends on the extent to which unique determination of a parameter has an impact on predicting the internal dose metric (what can be assessed by the sensitivity analysis of this parameter). If the parameter of interest is not sensitive to the outcome but cannot be uniquely identified, then its individual impact on the dose metric may not be problematic. If the opposite case is true, i.e., a parameter is very sensitive to outcome but not uniquely identifiable, then a range of dose metric determinations are reported based on the range of biologically plausible values for this parameter (McLanahan et al., 2012).

Variation among average parameters measurements from different experiments and variation between individual measurements of the same experiment is another source of uncertainty. In many cases, the missing parameters in the PBTK model that consists of population average parameters are optimised to individual blood/plasma concentrations.

The parameters (P) in the PBTK model include: physiological information (blood flow rates, organ weights), absorption rates, tissue-to-blood partition coefficients, metabolism and renal clearance rates and other parameters such as blood-to-air or water-to-air partition coefficients, etc. The parameters of the PBTD model are estimations of base-line and maximal effects, plasma protein binding, concentration of a chemical causing half of the effect, tolerance formation and elimination rates and additive effects of a substance and exercise. In the context of chemical risk assessment, uncertainty in estimates of these parameters can propagate into uncertainty of derived toxicokinetic parameters such as simulated tissue/organ concentrations and AUC, uncertainty in, toxicodynamic responses, and uncertainty in the eventual the characterization of hazard, exposure and risk.

The uncertainty in this work was quantified: i) as the uncertainty factors (UFs) for the selected average physiological properties: using ranges provided by (Brown et al., 1997)) in a way that the interval < av. value/UFs; av. value/UFs> is considered highly probable (with assumed probability of 95%) in accordance to (Farrar et al., 1989). UFs represent variability within an adult healthy Caucasian population only; ii) as the uncertainty range (UR) for ADME parameters determined either by means of Monte-Carlo simulations (distribution = normally distributed random samples) identifying minimal and maximal value leading to an average deviation of 18% of peak blood concentrations (Huizer et al., 2012) or based on available literature data if this effect is not caused by the investigated parameters (due to its low sensitivity) when its value is varied by up to assumed $\pm 80\%$. If there is no literature information and parameter does not have the effect on simulated blood concentration, then its uncertainty could not be determined (ND).

I limited the analysis of uncertainty in parameters estimations for the compounds that have been used broadly in this thesis in route-to-route and *in vitro*-to-*in vivo* extrapolation (and for which there is more literature information available): coumarin, hydroquinone, ethanol, isopropanol, caffeine and nicotine.

Physiological properties

Table 5.1 provides the mean parameter values used in this work together with their UFs. To minimise the uncertainty in estimating percentage of skin, fat and alveolar ventilation rate for a given subject, they were calculated based on age, BW and BMI.

Table 5.1. UFs in physiological parameters for a reference man and woman.

Organ weight fractions	Reference woman (UFs)	Reference man (UFs)
Average Body Weight (BW) [kg]	64	75
Age	25	25
Liver	0.026 (1.35)	0.026 (1.35)
Lungs	0.0105 (1.5)	0.012 (1.5)
Brain	0.02 (1.25)	0.02 (1.25)
Heart	0.0044 (1.25)	0.0044 (1.25)

Kidney	0.0044 (1.25)	0.0044 (1.25)
GI tract:	0.0265 (1.3)	0.025 (1.3)
Poorly perfused tissues	0.44 (1.04)	0.52 (1.04)
Blood	0.065 (1.5)	0.072 (1.5)
Skin	$\frac{BSA \cdot L_{skn} \cdot \rho_{skn}}{10^3 \cdot BW}$ ca. 0.08 (1.2)	$\frac{BSA \cdot L_{skn} \cdot \rho_{skn}}{10^3 \cdot BW}$ ca. 0.105 (1.2)
Adipose tissue	$1.29 \cdot BMI + 0.2 \cdot Age - 11.4 \cdot Gender - 8$ ca.025 (1.3)	$1.29 \cdot BMI + 0.2 \cdot Age - 11.4 \cdot Gender - 8$ ca.015 (1.3)
Rest of body	Variable ca. 0.13 (1.5)	Variable ca. 0.16 (1.5)
Regional blood flow rates (fraction of cardiac output)		
Total cardiac output [L/h]	$15 \cdot BW^{0.74}$ (1.12)	$15 \cdot BW^{0.74}$ (1.12)
Liver	0.25 (1.35)	0.24 (1.35)
Adipose tissue	0.055 (1.09)	0.04 (1.09)
Lungs	0.025 (1.25)	0.025 (1.25)
Brain	0.114 (1.25)	0.114 (1.25)
Heart	0.04 (1.25)	0.04 (1.25)
Skin	0.05 (1.1)	0.05 (1.1)
Kidney	0.19 (1.25)	0.2 (1.25)
Poorly perfused tissues	0.135 (1.1)	0.16 (1.1)
GI tract	0.14 (1.25)	0.13 (1.25)
Rest of body	ca. 0.001 (1.04)	ca. 0.001 (1.04)
ALV [L/h]	$BW \cdot (0.7 \cdot 0.332 \cdot BW^{0.74})$ ca. 289 (1.2)	$BW \cdot (0.7 \cdot 0.332 \cdot BW^{0.74})$ ca. 340.35 (1.2)
RR [1/h]	820 (1.2)	840 (1.2)
L	0.204 (1.3)	0.2906 (1.3)
L _{SC}	0.0018 (1.5)	0.0017 (1.5)
L _{VE}	0.0032 (1.5)	0.0047 (1.5)

Tissue-to-blood partition coefficients

Estimated tissue-to-blood partition coefficients (in case of coumarin, caffeine, ethanol) according to (Schmitt, 2008) are compared with literature ranges in **Table 5.2**. Monte Carlo simulations were used to identify the parameter ranges that produce $\pm 18\%$ of change in blood (plasma) concentrations. If this effect was not observed within the range $\langle P-0.8P, P+0.8P \rangle$ and no literature information was available UR could not be defined (ND).

Table 5.2. URs for tissue-to-blood partition coefficients.

Tissue-to-blood partition coefficients		Value	Literature range	Ref.	UR
Coumarin					
	Liver	2.38	0.57-1.3		0.57-2.5
	Poorly perfused tissues	0.355	0.23-1.1		0.23-1.1
	Brain	2.09	0.73-1.3	(Mielke et al., 2011; Rietjens et al., 2008)	0.73-2.09
	Skin	0.68	0.77-1.1		0.77-1.1
	Lungs	0.51	0.57-1.3		0.5-1.3
	Kidney	2.08	0.51-1.3		0.51-2.08
	GI tract	0.62	0.57-1.3		0.57-1.3
	Adipose tissue	1.24	4.20-9.0		1.24-9.0
	Heart	1.63	0.57-1.3		0.57-1.63
Hydroquinone					
	Liver	0.8	0.8		0.26-1.5
	Poorly perfused tissues	0.8	0.8	(Corley et al., 2000)	ND
	Brain	0.8	0.8		ND
	Skin	0.8	0.8		0.18-1
	Lungs	0.68	0.68		0.24-0.68
	Kidney	0.71	0.71		0.25-0.71
	GI tract	0.8	0.8		0.11-1
	Adipose tissue	0.8	0.8		0.15-1
	Heart	0.8	0.8		ND
Caffeine					
	Liver	4.25	0.78		0.78-4.5
	Poorly perfused tissues	0.995	0.69	(Ginsberg et al., 2004)	ND
	Brain	1	0.79		ND
	Skin	1	-		0.8-1.2
	Lungs	1.23	0.79		ND
	Kidney	3.76	0.80		ND
	GI tract	1.49	0.79		0.7-1.5
	Adipose tissue	0.68	0.39		0.3-0.7
	Heart	3.69	0.79		ND
Ethanol					
	Liver	0.86	0.81-1		0.81-1
	Poorly perfused tissues	0.64	0.80-1	(Loizou and Spendiff, 2004; MacDonald et al., 2002)	0.6-1
	Brain	0.92	0.87-1		0.87-1
	Skin	0.76	0.80-1		0.7-1
	Lungs	0.92	0.95-1		0.9-1
	Kidney	0.9	0.95-1		0.9-1
	GI tract	0.9	0.81-1		0.81-1
	Adipose tissue	0.59	0.11-1		0.11-1
	Heart	0.83	0.95-1		0.8-1
Isopropanol					
	Liver	1.16	1.16		1-1.5
	Poorly perfused tissues	1.3	1.3	(Clewell Iii et al., 2001)	ND
	Brain	1.33	1.33		ND
	Skin	1.3	1.3		0.7-1.5
	Lungs	1.25	1.25		ND
	Kidney	1.25	1.25		ND
	GI tract	1.25	1.25		1-1.5
	Adipose tissue	0.32	0.32		0.2-0.8
	Heart	1.25	1.25		ND
Nicotine					
	Liver	1.42	1.42-9		1.4-3
	Poorly perfused tissues	0.39	0.39-5.6	(Robinson et al., 1992), (Teeguarden	ND
	Brain	2.63	1.4-3		ND
	Skin	0.38	0.38-2.5		0.38-2.5

Lungs	1.32	0.87-2	et al., 2013)	0.87-2
Kidney	1.34	1.34-15		ND
GI tract	0.58	0.5-2		0.5-2
Adipose tissue	0.19	0.19-1		0.19-1
Heart	1.62	0.49-3		ND

GI tract, skin and respiratory tract parameters

Absorption parameters were analysed in a similar way to blood-to-tissue partition coefficient (**Table 5.3**). Stomach emptying parameters were used in accordance to (Loizou and Spendiff, 2004) – k_{\max} [1/h] = 8.16, k_{\min} = 0.005 1/h. The authors say that the gastric emptying rates are usually taken to be constant unless the compound causes inhibition of gastric peristalsis. Absorption (ka_{LI}) and elimination rates (kel_{LI}) from large intestine were assumed to be equal ca. 0.01 L/h due to lack of literature information and therefore their uncertainty could not be determined. In the same manner, absorption rate (ka_{HF}), diffusion coefficient (D_{HF}) and partition coefficient (PC_{HF}) in hair follicles used for caffeine only were assumed to be equal to 0.153, $1.24 \cdot 10^{-5}$ and 1 respectively due to model fitting of starting values equal to viable epidermis results. Removal rate of gases from lungs was assumed to be equal to 0.126 mL/s as specified by (Peterman and Longtin, 1984) for ethanol, isopropanol and styrene.

Table 5.3. URs for the absorption parameters.

Absorption parameters	Value	Literature range	Ref.	UR
Coumarin				
Stomach abs ka_{stom} [1/h]	1.8	-		1-2
Intestine abs. ka_{SI} [1/h]	0.1	-	(Ritschel et al., 1989)	0.08-0.2
D_{SC} [cm ² /h]	$2.5 \cdot 10^{-06}$	$2.34 \cdot 10^{-07}$ - $1.044 \cdot 10^{-06}$		$1-3 \cdot 10^{-06}$
D_{VE} [cm ² /h]	$9 \cdot 10^{-05}$	-		$5-9 \cdot 10^{-05}$
ka_{form} [mL/h]	0.22	-		0.1-0.25
PC_{SC}	1.65	-		1.5-1.8
PC_{VE}	1.829	-		1.5-2
RBP	0.25	-		0.2-0.3
Hydroquinone				
Stomach abs ka_{stom} [1/h]	0.1	-		0.1-0.5
Intestine abs. ka_{SI} [1/h]	3	0.75-1.75	(Barber et al., 1995; Corley et al., 2000)	0.75-3
D_{SC} [cm ² /h]	$4 \cdot 10^{-08}$	$1.6794 \cdot 10^{-08}$		$1.6-4 \cdot 10^{-08}$
D_{VE} [cm ² /h]	$8 \cdot 10^{-06}$	-		$6-9 \cdot 10^{-06}$
ka_{form} [mL/h]	0.038	-		0.03-0.04
PC_{SC}	1	-		0.9-1.2
PC_{VE}	0.8	-		0.7-0.9
RBP	0.15	-		0.12-0.2
Caffeine				
Dissolution from a coated matrix Diss [1/h]	3.2	-		3-3.5
Stomach abs ka_{stom} [1/h]	0.2	-		0.1-0.8
Intestine abs. ka_{SI} [1/h]	1.5	-	(Hansen et al., 2008), (Dias et al., 1999),	1-2

	D_{SC} [cm^2/h]	$1.4 \cdot 10^{-07}$	$1.4-5.34 \cdot 10^{-07}$	Cosmetics Europe, (Bronaugh and Franz, 1986)	$1.4-5.34 \cdot 10^{-07}$
	D_{VE} [cm^2/h]	$1.5 \cdot 10^{-05}$	$7.13 \cdot 10^{-07}-1.1 \cdot 10^{-06}$		$8 \cdot 10^{-06}-2 \cdot 10^{-05}$
	ka_{form} [mL/h]	0.2	-		0.1-0.3
	PC_{SC}	2.5	1.5-5.9		1.5-5.9
	PC_{VE}	0.6	-		0.2-1
	RBP	0.28-0.35	-	0.2-0.4	
Ethanol					
	Stomach abs ka_{stom} [1/h]	0.6584	0.6584		0.5-0.7
	Intestine abs. ka_{SI} [1/h]	25.1	10.2-25.1	(Loizou and Spendiff, 2004;	10.2-25.1
	D_{SC} [cm^2/h]	$9.96 \cdot 10^{-06}$	-	MacDonald et al., 2002),	$7-9.96 \cdot 10^{-06}$
	D_{VE} [cm^2/h]	$5.87 \cdot 10^{-05}$	-	(Katritzky et al., 2008)	$4-6 \cdot 10^{-06}$
	ka_{form} [mL/h]	0.2	-		0.1-0.4
	PC_{SC}	4.95	-		3-8
	PC_{VE}	0.2	-		0.1-0.4
	RBP	1	-		ND
	Blood-air partition coefficient for ethanol	1352.5	1265-2195		1265-2195
	PC_{bloodair}				
	Water-air partition coefficient for ethanol	2140	2140		-
	PC_{waterair}				
	DI [cm^2/s]	0.08	-		ND
	$\log \lambda$	-2	2.855		-2-0.1
Isopropanol					
	Stomach abs ka_{stom} [1/h]	4.7	1		1-5
	Intestine abs. ka_{SI} [1/h]	10	-	(Clewel Iii et al., 2001),	8-10
	D_{SC} [cm^2/h]	$3 \cdot 10^{-07}$	-	(Kumagai and Matsunaga, 1995),	$1-5 \cdot 10^{-07}$
	D_{VE} [cm^2/h]	$5.20 \cdot 10^{-05}$	-	(Katritzky et al., 2008)	$3-7 \cdot 10^{-05}$
	ka_{form} [mL/h]	0.12	-		0.1-0.2
	PC_{SC}	1.343	-		1-1.5
	PC_{VE}	0.778	-		0.7-0.8
	RBP	1	-		ND
	Blood-air partition coefficient	848	848		-
	PC_{bloodair}				
	Water-air partition coefficient	10	1500		8-100
	PC_{waterair}				
	DI [cm^2/s]	0.08	-		ND
	$\log \lambda$	1	2.863		1-2.863
Nicotine					
	Dissolution from a coated matrix Diss [1/h]	0.235	-		0.15-0.3
	Stomach abs ka_{stom} [1/h]	0.006	-		0.004-0.008
	Intestine abs. ka_{SI} [1/h]	0.1-1	1.4	(Teeguarden et al., 2013)	0.1-1.4
	D_{SC} [cm^2/h]	0.00016	-		0.0001-0.0002
	D_{VE} [cm^2/h]	0.00096	-		0.0005-0.001
	ka_{form} [mL/h]	0.06	-		0.03-0.09
	PC_{SC}	0.4	-		0.3-0.5
	PC_{VE}	1.518	-		1.2-1.6
	RBP	1.2	-		1-1.3
	Blood-air partition coefficient	4.743	-		4-6
	$PC_{\text{blood,air}}$				
	Water-air partition coefficient f	6000	-		5000-6500

Liver metabolism and renal clearance

In the uncertainty analysis I considered only phase I of the liver metabolism because rates of phase II (coumarin, hydroquinone) were mainly taken from literature including renal clearance of metabolites. **Table 5.4** gives the URs for V_{\max}/K_m ratios based on literature and Monte-Carlo simulations, whenever possible.

Table 5.4. URs for the clearance parameters.

Clearance parameters	Value	Literature range	Ref.	UR for V_{\max}/K_m
Coumarin				
V_{\max} (o-HPA) [mg/h/kg BW], K_m (o-HPA) [mg/L]	$V_{\max}=12.714$ $K_m=397.508$ $V_{\max}/K_m=0.032$	$V_{\max}=12.71-$ $1.48 \cdot 10^{14}$ $K_m=397.5081-$ $20.9 \cdot 10^{13}$ $V_{\max}/K_m=0.032-$ 0.71	(Mielke et al., 2011; Rietjens et al., 2008)	0.032-0.71
V_{\max} (7-HC) [mg/h/kg BW], K_m (7-HC) [mg/L]	$V_{\max}=2.5$ $K_m=0.278$ $V_{\max}/K_m=8.99$	$V_{\max}=14.81 -16.81$ $K_m=0.2777$ $V_{\max}/K_m=53.33-$ 60.53		8-60.53
V_{\max} (3-HC) [mg/h/kg BW], K_m (3-HC) [mg/L], K_{met} [L/h/kg BW]	$K_{met}=0.001$	$V_{\max}=118.8627$ $K_m=397.5081$ $V_{\max}/K_m=0.07-0.3$		0.07-0.3
CLR [L/h/kg BW]	0.08	-		ND
Hydroquinone				
V_{\max} (BQ) [mg/h/kg], K_m (BQ) [mg/L]	$V_{\max}=8.4$ $K_m=5.05$ $V_{\max}/K_m=1.64$	$V_{\max}=4.8-8.3$ $K_m=5.05$ $V_{\max}/K_m=0.95-1.64$	(Corley et al., 2000)	0.95-1.64
V_{\max} (HQ glucuronide) [mg/h/kg], K_m (HQ glucuronide) [mg/L]	$V_{\max}=28$ $K_m=5$ $V_{\max}/K_m=24$	$V_{\max}=120$ $K_m=5$ $V_{\max}/K_m=24$		5.6-24
V_{\max} (HQ sulfate) [mg/h/kg], K_m (HQ sulfate) [mg/L]	$V_{\max}=60$ $K_m=5$ $V_{\max}/K_m=12$	$V_{\max}=60$ $K_m=5$ $V_{\max}/K_m=12$		-
CLR [L/h]	0.08	-		ND
Caffeine				
V_{\max} (Paraxanthine) [mg/h], K_m (Paraxanthine) [mg/L]	$V_{\max}=0.3514$ $K_m=1$ $V_{\max}/K_m=0.3514$	-	-	ND
V_{\max} (Theobromine) [mg/h], K_m (Theobromine) [mg/L]	$V_{\max}=0.0432$ $K_m=1$ $V_{\max}/K_m=0.0432$	-		ND
V_{\max} (Theophylline) [mg/h], K_m (Theophylline) [mg/L]	$V_{\max}=0.0072$ $K_m=1$ $V_{\max}/K_m=0.0072$	-		ND
K_{met} (1,3,7-trimethyluric acid) [L/h]	$K_{met}=0.001$	-		ND
CLR [L/h]	0.08	-		ND
Ethanol				
V_{\max} (ethanol) [mg/h/BMI], K_m (ethanol) [mg/L]	$V_{\max}=10$ $K_m=0.962$ $V_{\max}/K_m=10.39501$	V_{\max} [mg/h/kg BW] $=2.86-337.77$ $K_m=18.427-81.8$ $V_{\max}/K_m=0.035-$		0.035-18.33

		18.33	(Loizou and Spendiff, 2004; Umulis et al., 2005; Wilkinson et al., 1977a)	17.16-171.6
V_{rev} (acetaldehyde) [mg/h/BMI], K_{rev} (acetaldehyde) [mg/L]	$V_{rev} = 20$ $K_{rev} = 44.053$	V_{rev} [mg/h/kg BW] = 755.942-7559.419 $K_{rev} = 44.053$ $V_{rev}/K_{rev} = 17.16-171.6$		
$K_{form_{EtS}}$ [L/h/BMI]		-		$2.80 \cdot 10^{-07}$ - $3.1 \cdot 10^{-06}$
$K_{form_{EtG}}$ [L/h/BMI]	$8.425 \cdot 10^{-07}$	-		$9.00 \cdot 10^{-03}$ - 0.040
CLR_{ETH} [L/h/BMI]	0.022	-		0.1-150
CLR_{EtS} [L/h/BMI]	2.375	-		0.6-1
CLR_{EtG} [L/h/BMI]	0.8	-		0.6-1
Isopropanol				
V_{max} (acetone) [mg/h/(kg BW) ^{3/4}], K_m (acetone) [mg/L]	$V_{max}=300$ $K_m=10$	$V_{max}=300$ $K_m=10$	(Clewel Iii et al., 2001)	ND
CLR [L/h]	$V_{max}/K_m=30$ 0.004	$V_{max}/K_m=30$ 0.004		ND
Nicotine				
V_{max} (cotenine) [mg/h/kg BW], K_m (cotenine) [mg/L]	$V_{max}= 11.260$ $K_m= 10.52$ $V_{max}/K_m=1.07$	$V_{max}/K_m= 0.7719$	(Teeguarden et al., 2013)	0.77-1.07
K_{met} (rest of metabolites) [L/h/ kg BW]	0.1674	0.1674		-
CLR [L/h]	0.036	0.036		-

Toxicodynamic parameters

The uncertainty ranges for toxicodynamic parameters are given in **Table 5.5**. The uncertainty in estimating base-line (E_0) values can be specified with the following URs based on studied literature: for heart rate at rest UR: 61.2- 80.67 [bpm] (Karatzis et al., 2005; Porchet et al., 1988), during the treadmill exercise: UR: 124-151 [bpm] (Damirchi et al., 2009); for mean arterial blood pressure at rest: UR: 81.67-83.5 [mmHg] (Fattinger et al., 1997; Sofuoglu et al., 2012).

Table 5.5. URs for the toxicodynamic parameters.

Toxicodynamic parameters	Value	Literature range	Ref.	UR
Nicotine				
Heart rate (HR), Blood pressure (BP)				
S [bpm/mg/L] (HR)	1000 (HR)	1000		
S [mmHg/mg/L] (BP)	600 (BP)			600-1200
$k_{a,Ant}$ [mg/L]	3	-	(Porchet et al., 1988),	ND
$k_{el, Ant}$ [mg/L]	6	-	(Yamazaki and Kanaoka, 2004)	ND
$C_{Ant,50}$ [mg/L]	0.00772	0.00772		-
γ (HR)	1 (at rest)			
		-		0.4-1
	0.6 (during exercise)			
f_u	0.95	0.95		-

Caffeine

Heart rate (HR), Blood pressure (BP)

S [bpm/mg/L] (HR)	200 (HR)	20.6 (BP)		
S [mmHg/mg/L] (BP)	20.6 (BP)			20.6-200
$k_{a, Ant}$ [mg/L]	3 (HR) 3.48 (BP)	-	(Shi, 1993), (Yamazaki and Kanaoka, 2004)	ND
$k_{el, Ant}$ [mg/L]	6 (HR) 4.86 (BP)	-		ND
$C_{Ant,50}$ [mg/L]	0.00772 (HR) 0.24 (BP)	0.24 (BP)		0.007-0.24
γ (HR)	At rest: 1 During exercise: 0.4	-		0.4-1
f_u	0.65	0.65		-

6. Conclusions

The following conclusions were made in this thesis:

a) On quantitative structure-property relationships (QSPRs):

Literature QSPRs (based on simple physicochemical properties) for skin permeation, plasma protein binding and blood-to-air partition coefficient were applied to 9 case study substances. The best performing models, based on a median estimate calculated from a set of equations, were close to experimental value for skin and *stratum corneum* permeation coefficients and blood-to-air partition coefficients. The highest variation in predicted results was found in the case of the skin partition coefficients (in particular for viable epidermis) and maximal flux. However, these variations may arise from the use of different solvents, chemical concentrations, application conditions and skin type in the training set used to build the QSPRs compared with those applied for the selected case study chemicals.

b) On modelling refinement of skin, gastrointestinal and respiratory tracts

The use of GI and skin sub-compartments in the PBTK model gives a better simulation of *in vivo* absorption of the cosmetic ingredients than simple model structures, as supported by statistical measures such as AICc, R^2 and MSE. This is especially important if the time of peak concentration needs to be determined accurately. The difference in simulated concentration-time profiles is even more obvious in the case of repeated dosing, as shown in the caffeine example. The simple version of the PBTK model for inhalation, in turn, gives better results for styrene, isopropanol and ethanol *in vivo* blood concentrations. However, the refined PBTK model with 24 Weibel generations (diffusion/ convection sub-compartments) offers more simulated information (such as concentrations at particular stages of the respiratory tract) and therefore better estimates the exhaled concentrations.

c) On *in vitro* – to – *in vivo* correlations of skin penetration, liver clearance and hepatotoxicity of caffeine

- Simulated skin permeation of caffeine and coumarin using *in vitro* parameters was found ca. 6-9 and ca. 1.5-2.5 times lower than the estimated *in vivo* permeation respectively. Both case studies indicate that *in vitro* absorption results, whenever used to indicate a safe limit for *in vivo* scenarios, should be multiplied by a factor of 10 as indicated in the traditional risk assessment approaches. This is important when *in vitro* experimental results are to be used to establish safe external exposure levels and margins of safety for a given substance.

- *In vitro* – to – *in vivo* correlation of liver clearance is more complex than correlating skin absorption parameters. On average *in vitro* clearance rates, calculated as a sum of V_{\max}/K_m ratios of all formed metabolites, were higher than clearance rate optimised *in vivo* for all the compounds except for caffeine. Of course, different experimental protocols and V_{\max} and K_m determinations might have affected these results.
- The multi-scale modelling approach (PBTK+VCBA models) revealed almost no effect of caffeine after oral and dermal absorption (up to 5.33 mg/kg BW what equals ca. 2 times NOAEL dose extrapolated for 75 kg- male subject) on the viability of liver (HepaRG) cells regardless of the absorption route (oral and dermal absorption). *In vitro* experiments revealed a slightly higher sensitivity of HepaRG to caffeine when compared to HepG2. Critical liver concentrations that caused less than 10% of the remaining cell viability were for HepaRG: more than 60mM (single exposure) and 2.3 mM (after 3rd and 4th exposure) of caffeine that would require a caffeine external dose of more than 1000mg.

d) On route-to-route extrapolations

The oral-to-dermal extrapolations for coumarin, hydroquinone, caffeine, ethanol and isopropanol revealed that AUC in blood is the most sensitive parameter and therefore it was used to determine dermal thresholds. Under defined exposure conditions, these thresholds are higher than oral NOAEL values (oral NOAEL doses are protective) for coumarin and ethanol but lower for hydroquinone, caffeine and isopropanol. Hydroquinone, which appears to be the most toxic compound among other cosmetic ingredients, requires dermal thresholds 9 times lower than its safe oral NOAEL value. However, quite extreme exposure conditions were considered in this work (including exposed skin area and duration of exposure).

Dermal-to- inhalation extrapolation of methyl iodide in rat and human indicated the C_{\max} in blood to be the most sensitive parameter and therefore it was used to determine dermal thresholds. Inhalation thresholds under assumed exposure are 45 (rat) and 800 (human) times lower than dermal results (concentration of solutions, exposed skin area and duration of exposure were the same for rat and human). However, a different absolute amount of chemical was applied: 7.68 mg onto the rat skin and 2.55 mg onto the human skin (over 4 h) at equally same inhaled concentration of 10 ppm (over 2 h). The inhaled concentration was 1000 lower than the one applied on skin but skin area was only of 25 cm².

e) On ethanol case studies

- The refined PBTK model for oral absorption has been successfully applied in simulating concentration–time profiles of ethanol, and its two metabolites, ethyl sulfate (EtS) and ethyl glucuronide (EtG), in blood and urine (dose of ethanol: 4 and 8 units). In contrast to previous

literature modelling approaches, this model gives more simulated information with a smaller number (4) of kinetic parameters that need tuning with respect to *in vivo* data. I proposed different formation kinetics of EtS and EtG in the liver (to better simulate their *in vivo* serum concentrations) and used PBTK modelling to estimate the urine concentrations for the first time. Finally, I linked the PBTK model simulations with the Euclidean-based strategy to help back extrapolate the time of ethanol consumption for new data. At its current stage, the model is not intended to be a standalone tool to predict the exact time of ethanol ingestion based on a limited number of serum samples with known EtG and EtS concentrations. However, in a forensic weight of evidence approach the model can provide further evidence, together with evaluation of increasing or decreasing EtG/EtS ratios over time, to estimate the time of alcohol ingestion.

- Simulations of the dermal absorption of ethanol from different hand rubs (that differ in ethanol absolute amount and its concentration) showed that there were differences in skin permeation of ethanol that resulted not only from different ethanol absolute doses – therefore to meet these differences, the PBTK model absorption parameters cannot be assumed constant. I showed that varying the *stratum corneum*/ vehicle partition coefficient (PC_{SC}) would be enough and its values ranged from from 3 (4 mL 55% sol.) to 8 (20 mL 85% sol.). The difficulty of simulating acetaldehyde concentrations and ethanol elimination phase further confirmed previous conclusions about inter-individual and dose-dependent differences in ethanol metabolism.

f) On toxicodynamic studies of nicotine and caffeine

A joint PBTK-TD model for humans, calibrated and validated by using various published nicotine blood/plasma concentrations (single and repeated dosing) was applied to estimate and compare several daily exposure scenarios: cigarette smoking, oral and dermal absorption, and their effects on acute increase in heart rate at rest and during exercise. Frequent cigarette smoking shows high AUC and C_{max} in the blood, and nicotine-rich dermal patches produce high AUC and C_{max} in the liver. The resulting toxicokinetics in blood after smoking of 3 cigarettes per day was found comparable to the use of a single 7mg-dermal patch and 5 2mg-lozenges every 2 hours whereas smoking of 8 cigarettes per day was found comparable to a single use of 14-mg dermal patch or 10 2-mg lozenges every hour. However, the effects of smoking on heart rate are definitely higher than any of the investigated methods for nicotine therapy. Maximal heart rate while smoking was estimated to be ca. 1.35 times higher than a base-line value during a cycling exercise and ca. 1.17 times higher at rest. Multi-route exposure to nicotine has not been investigated in this study and would require further experiments.

In different studies, caffeine was reported to have no effect (or slightly increasing) or decreasing effect on heart rate during exercise and at rest. Only during recovery after exercise was caffeine observed to increase heart rate. Since it is probably impact of exercise itself on increased heart rate, the exponent in the sigmoid

model was modified for the exercise condition to better fit the pharmacological response. However, the fitting was performed with respect to experimental data of (Damirchi et al., 2009) resulting in a value of 0.4, so its applicability may include only a given intensity of exercise – 30-min running at a constant relative load (60% VO_2 max- see (Damirchi et al., 2009)) of lean men. The cardiovascular mechanisms that affect blood pressure are not entirely understood. Some studies have reported that MAP, SBP and DBP increase during exercise, whereas others have found no relevant effects. At rest, most of the studies indicate an increase in blood pressure due to caffeine. Due to variability in experimental results and an unclear distinction between caffeine effects at rest and during exercise the same sigmoid model was applied to predict BP in both cases (difference was only in base-line values). Not all of the model simulations produced a satisfactory match to mean experimental values. The simulation of blood pressure seems more difficult than heart rate; probably because the inter-individual variability is much higher and also effects of other phenomena (like stress or fitness) have a significant effect on the measured values. Clearly, more biological information should be included in the toxicodynamic model (perhaps with a decision-tree based algorithm to select an effect equation adjusted to given physiological and experimental conditions) to make it more robust and reliable. AUC in the blood after four 4-h-dermal applications of caffeine (4.563 mg/mL over 150 cm², with open hair follicles) was found slightly higher than oral intake of instant coffee (62 mg of caffeine in a cup per day). Milder but long-lasting increases of heart rate following dermal absorptions were simulated. However, these findings need to be supported by experimental results, before firm conclusions can be drawn concerning the physiological effects of the caffeine-containing products.

Literature

- Abraham, M.H., Martins, F., 2004. Human skin permeation and partition: General linear free-energy relationship analyses. *J. Pharm. Sci.* 93, 1508–1523.
- Acheson, K.J., Zahorska-Markiewicz, B., Pittet, P., Anantharaman, K., Jéquier, E., 1980. Caffeine and coffee: Their influence on metabolic rate and substrate utilization in normal weight and obese individuals. *Am. J. Clin. Nutr.* 33, 989–997.
- Anissimov, Y.G., Roberts, M.S., 2004. Diffusion Modeling of Percutaneous Absorption Kinetics: 3. Variable Diffusion and Partition Coefficients, Consequences for Stratum Corneum Depth Profiles and Desorption Kinetics. *J. Pharm. Sci.* 93, 470–487.
- Bannon, Y.B., Corish, J., Corrigan, O.I., Devane, J.G., Kavanagh, M., Mulligan, S., 1989. Transdermal delivery of nicotine in normal human volunteers: A single dose and multiple dose study. *Eur. J. Clin. Pharmacol.* 37, 285–290.
- Barber, E.D., Hill, T., Schum, D.B., 1995. The percutaneous absorption of hydroquinone (HQ) through rat and human skin in vitro. *Toxicol. Lett.* 80, 167–172.
- Barratt, M.D., 1995. Quantitative structure-activity relationships for skin permeability. *Toxicol. Vitr.* 9, 27–37.
- Barter, Z.E., Bayliss, M.K., Beaune, P.H., Boobis, A.R., Carlile, D.J., Edwards, R.J., Houston, J.B., Lake, B.G., Lipscomb, J.C., Pelkonen, O.R., Tucker, G.T., Rostami-Hodjegan, A., 2007. Scaling factors for the extrapolation of in vivo metabolic drug clearance from in vitro data: Reaching a consensus on values of human microsomal protein and hepatocellularity per gram of liver. *Curr. Drug Metab.* 8, 33–45.
- Beckley-Kartey, S.A.J., Hotchkiss, S.A.M., Capel, M., 1997. Comparative in vitro skin absorption and metabolism of coumarin (1,2-benzopyrone) in human, rat, and mouse. *Toxicol. Appl. Pharmacol.* 145, 34–42.
- Benowitz, N.L., 1990. Pharmacokinetic considerations in understanding nicotine dependence. *Ciba Found. Symp.* 152, 186–200; discussion 200.
- Benowitz, N.L., Kuyt, F., Jacob III, P., 1982. Circadian blood nicotine concentrations during cigarette smoking. *Clin. Pharmacol. Ther.* 32, 758–764.
- Bessems, J.G.M., Geraets, L., 2013. Proper knowledge on toxicokinetics improves human hazard testing and subsequent health risk characterisation. A case study approach. *Regul. Toxicol. Pharmacol.* 67, 325–334.
- Bicker, W., Lämmerhofer, M., Keller, T., Schuhmacher, R., Krska, R., Lindner, W., 2006. Validated method for the determination of the ethanol consumption markers ethyl glucuronide, ethyl phosphate, and ethyl sulfate in human urine by reversed-phase/weak anion exchange liquid chromatography-tandem mass spectrometry. *Anal. Chem.* 78, 5884–5892.

- Billoir, E., Péry, A.R.R., Charles, S., 2007. Integrating the lethal and sublethal effects of toxic compounds into the population dynamics of *Daphnia magna*: A combination of the DEBtox and matrix population models. *Ecol. Modell.* 203, 204–214.
- Blaauboer, B.J., 2010. Biokinetic modeling and in vitro-in vivo extrapolations. *J. Toxicol. Environ. Heal. - Part B Crit. Rev.* 13, 242–252.
- Blaauboer, B.J., 2001. Toxicodynamic modelling and the interpretation of in vitro toxicity data. *Toxicol. Lett.* 120, 111–123.
- Bogen, K., Keating, G., 2000. The Santiago (Chile) Symposium, in: *Dermal Absorption from Short-Term Exposure to Contaminated Water. Interdisciplinary Perspectives on Drinking Water Risk Assessment and Management.*
- Bookout Jr., R.L., Quinn, D.W., McDougal, J.N., 1997. Parallel dermal subcompartments for modeling chemical absorption. *SAR QSAR Environ. Res.* 7, 259–279.
- Born, S.L., Caudill, D., Smith, B.J., Lehman-McKeeman, L.D., 2000. In vitro kinetics of coumarin 3,4-epoxidation: Application to species differences in toxicity and carcinogenicity. *Toxicol. Sci.* 58, 23–31.
- Brcic Karaconji, I., 2005. FACTS ABOUT NICOTINE TOXICITY. *Arh Hig Rada Toksikol* 56, 363–371.
- Brent, R.L., Christian, M.S., Diener, R.M., 2011. Evaluation of the reproductive and developmental risks of caffeine. *Birth Defects Res. Part B - Dev. Reprod. Toxicol.* 92, 152–187.
- Broeders, J.J.W., 2013. Biokinetics and repeated exposure in in vitro assays : A detailed study into the behaviour of chlorpromazine and diazepam in different cell systems.
- Bronaugh, R.L., Franz, T.J., 1986. Vehicle effects on percutaneous absorption: In vivo and in vitro comparisons with human skin. *Br. J. Dermatol.* 115, 1–11.
- Bronaugh, R.L., Stewart, R.F., Congdon, E.R., 1982. Methods for in vitro percutaneous absorption studies. II. Animal models for human skin. *Toxicol. Appl. Pharmacol.* 62, 481–488.
- Bronaugh, Robert L. Raymond, F.S., Congdon, E.R., 1983. Differences in permeability of rat skin related to sex and body site. *Soc. Cosmet. Chem.* 34, 127–135.
- Brown, R.P., Delp, M.D., Lindstedt, S.L., Rhomberg, L.R., Beliles, R.P., 1997. Physiological parameter values for physiologically based pharmacokinetic models. *Toxicol. Ind. Health* 13, 407–484.
- Brun, R., Reichert, P., Künsch, H.R., 2001. Practical identifiability analysis of large environmental simulation models. *Water Resour. Res.* 37, 1015–1030.
- Buck, D., C.E., M., 2007. Physiologically based approaches towards the prediction of pharmacokinetics: in vitro-in vivo extrapolation. *Expert Opin Drug Metab Toxicol.* 3, 865–78.

- Buckell, M., 1950. The Toxicity of Methyl Iodide: 1. Preliminary Survey. *Br J Ind Med.* 7, 122–124.
- Buist, H.E., Wit-Bos, L.D., Bouwman, T., Vaes, W.H.J., 2012. Predicting blood:Air partition coefficients using basic physicochemical properties. *Regul. Toxicol. Pharmacol.* 62, 23–28.
- Bungay, P.J., Tweedy, S., Howe, D.C., Gibson, K.R., Jones, H.M., Mount, N.M., 2011. Preclinical and clinical pharmacokinetics of PF-02413873, a nonsteroidal progesterone receptor antagonist. *Drug Metab. Dispos.* 39, 1396–1405.
- Caffeine informer [WWW Document], 2014. URL <http://www.caffeineinformer.com/caffeine-and-skin-care-products>
- Cairns, D., 2008. *Essentials of pharmaceutical chemistry*, Third. ed. London.
- Cardot, J.M., Beyssac, E., 2013. In Vitro–In Vivo Correlation. *Encycl. Pharm. Sci. Technol.* Fourth Ed.
- Carlton, B.D., Aubrun, J.-C., Simon, G.S., 1996. Effects of coumarin following perinatal and chronic exposure in sprague-dawley rats and CD-1 mice. *Toxicol. Sci.* 30, 145–151.
- Chambin-Remoussenard, O., Treffel, P., Bechtel, Y., Agache, P., 1993. Surface recovery and stripping methods to quantify percutaneous absorption of caffeine in humans. *J. Pharm. Sci.* 82, 1099–1101.
- Chambin-Remoussenard, O., Treffel, P., Bechtel, Y., Agache, P., 1982. Surface recovery and stripping methods to quantify percutaneous absorption of caffeine in humans. *J. Pharm. Sci.* 11, 1099–1101.
- Chandrasekaran, S.K., Campbell, P.S., Watanabe, T., 1980. Application of the “dual sorption” model to drug transport through skin. *Polym. Eng. Sci.* 20, 36–39.
- Chinery, R.L., Gleason, A.K., 1993. A compartmental model for the prediction of breath concentration and absorbed dose of chloroform after exposure while showering. *Risk Anal.* 13, 51–62.
- Chiu, W.A., White, P., 2006. Steady-state solutions to PBPK models and their applications to risk assessment I: Route-to-route extrapolation of volatile chemicals. *Risk Anal.* 26, 769–780.
- Chung, J.-K., Yuan, W., Liu, G., Zheng, J., 2006. Investigation of bioactivation and toxicity of styrene in CYP2E1 transgenic cells. *Toxicology* 226, 99–106.
- Cleek, R.L., Bunge, A.L., 1993. A new method for estimating dermal absorption from chemical exposure. 1. General approach. *Pharm. Res.* 10, 497–506.
- Clewell Iii, H.J., Gentry, P.R., Gearhart, J.M., Covington, T.R., Banton, M.I., Andersen, M.E., 2001. Development of a physiologically based pharmacokinetic model of isopropanol and its metabolite acetone. *Toxicol. Sci.* 63, 160–172.

- Clothier, R., Gómez-Lechón, M.J., Kinsner-Ovaskainen, A., Kopp-Schneider, A., O'Connor, J.E., Prieto, P., Stanzel, S., 2013. Comparative analysis of eight cytotoxicity assays evaluated within the ACuteTox Project. *Toxicol. Vitro*. 27, 1347–1356.
- Cole, L., Heard, C., 2007. Skin permeation enhancement potential of Aloe Vera and a proposed mechanism of action based upon size exclusion and pull effect. *Int. J. Pharm.* 333, 10–16.
- Collins, T.F.X., Welsh, J.J., Black, T.N., Ruggles, D.I., 1983. A study of the teratogenic potential of caffeine ingested in drinking-water. *Food Chem. Toxicol.* 21, 763–777.
- Comenges, J.-M.Z Wambaugh, J., Judson, R., 2012. Modeling in vitro cell-based assays experiments: Cell population dynamics. *Dev. Environ. Model.* 25, 51–71.
- Corley, R.A., English, J.C., Hill, T.S., Fiorica, L.A., Morgott, D.A., 2000. Development of a physiologically based pharmacokinetic model for hydroquinone. *Toxicol. Appl. Pharmacol.* 165, 163–174.
- Costa, P., Sousa Lobo, J., 2001. Modeling and comparison of dissolution profiles. *Eur J Pharm Sci* 13.
- Crank, J., 1975. *The mathematics of diffusion*, 2nd ed. Oxford.
- Cronin, M.T.D., Dearden, J.C., Moss, G.P., Murray-Dickson, G., 1999. Investigation of the mechanism of flux across human skin in vitro by quantitative structure-permeability relationships. *Eur. J. Pharm. Sci.* 7, 325–330.
- Csajka, C., Haller, C.A., Benowitz, N.L., Verotta, D., 2005. Mechanistic pharmacokinetic modelling of ephedrine, norephedrine and caffeine in healthy subjects. *Br. J. Clin. Pharmacol.* 59, 335–345.
- Csanady, G.A., Mendrala, A.L., Nolan, R.J., Filser, J.G., 1994. A physiologic pharmacokinetic model for styrene and styrene-7,8-oxide in mouse, rat and man. *Arch. Toxicol.* 68, 143–157.
- D'Orlando, K.J., Fox, B.S., 2004. Tolerability and pharmacokinetics of single and repeated doses of nicotine with The Straw, a novel nicotine replacement product. *Nicotine Tob. Res.* 6, 63–70.
- Damirchi, A., Rahmani-Nia, F., Mirzaie, B., Hasan-Nia, S., Ebrahimi, M., 2009. Effect of caffeine on metabolic and cardiovascular responses to submaximal exercise in lean and obese men. *Biomed. Hum. Kinet.* 1, 31–35.
- Daniels, J.W., Molé, P.A., Shaffrath, J.D., Stebbins, C.L., 1998. Effects of caffeine on blood pressure, heart rate, and forearm blood flow during dynamic leg exercise. *J. Appl. Physiol.* 85, 154–159.
- Dayan, N., 2005. Pathways for Skin Penetration. *Cosmet. Toilet.* 120.
- De Landoni, J.H., 1991. IPSC INCHEM: Nicotine [WWW Document]. URL <http://www.inchem.org/documents/pims/chemical/nicotine.htm>

- Degim, I.T., Pugh, W.J., Hadgraft, J., 1998. Skin permeability data: Anomalous results. *Int. J. Pharm.* 170, 129–133.
- DeJongh, J., Verhaar, H.J.M., Hermens, J.L.M., 1997. A quantitative property-property relationship (QPPR) approach to estimate in vitro tissue blood partition coefficients of organic chemicals in rats and humans. *Arch. Toxicol.* 72, 17–25.
- Denaro, C.P., Brown, C.R., Jacob III, P., Benowitz, N.L., 1991. Effects of caffeine with repeated dosing. *Eur. J. Clin. Pharmacol.* 40, 273–278.
- Deurenberg, P., Yap, M., Van Staveren, W.A., 1998. Body mass index and percent body fat: A meta analysis among different ethnic groups. *Int. J. Obes.* 22, 1164–1171.
- Dias, M., Farinha, A., Faustino, E., Hadgraft, J., Pais, J., Toscano, C., 1999. Topical delivery of caffeine from some commercial formulations. *Int. J. Pharm.* 182, 41–47.
- Doucet, O., Ferrero, L., Garcia, N., Zastrow, L., 1998. O/W emulsion and W/O/W multiple emulsion: Physical characterization and skin pharmacokinetic comparison in the delivery process of caffeine. *Int. J. Cosmet. Sci.* 20, 283–295.
- Dresen, S., Weinmann, W., Wurst, F.M., 2004. Forensic confirmatory analysis of ethyl sulfate - A new marker for alcohol consumption - By liquid-chromatography/electrospray ionization/tandem mass spectrometry. *J. Am. Soc. Mass Spectrom.* 15, 1644–1648.
- Droenner, P., Schmitt, G., Aderjan, R., Zimmer, H., 2002. A kinetic model describing the pharmacokinetics of ethyl glucuronide in humans. *Forensic Sci. Int.* 126, 24–29.
- ECHA, 2014a. Ethanol. Study report. Exp Key Repeated dose toxicity: oral.001.
- ECHA, 2014b. Iodomethane. Study report. Exp Key Repeated dose toxicity: dermal.001.
- ECHA, 2012. Guidance on information requirements and chemical safety assessment.
- EFSA, 2004. Opinion of the scientific panel on food additives, flavourings, processing aids and materials in contacts with food (AFC) on a request from the commission related to coumarin. Question number EFSA-Q-2003-118. *EFSA J.* 104, 1–36.
- Ellenhorn, M., 1988. Diagnostics and Treatment of Human Poisoning, in: Elsevier Science Publishers, Ed. 1. pp. 912–920.
- emc, 2014. NiQuitin 21 mg transdermal patches [WWW Document]. URL <http://www.medicines.org.uk/emc/medicine/15340/SPC/NiQuitin+21+mg+transdermal+patches>
- English, J.C., Deisinger, P.J., 2005. Metabolism and disposition of hydroquinone in Fischer 344 rats after oral or dermal administration. *Food Chem. Toxicol.* 43, 483–493.
- EPA, 2008. Reregistration Eligibility Decision (RED) Document for Nicotine. List B. Case no. 2460.

- Fagerström, K., 2005. The nicotine market: An attempt to estimate the nicotine intake from various sources and the total nicotine consumption in some countries. *Nicotine Tob. Res.* 7, 343–350.
- Farrar, D., Allen, B., Crump, K., Shipp, A., 1989. Evaluation of uncertainty in input parameters to pharmacokinetic models and the resulting uncertainty in output. *Toxicol. Lett.* 49, 371–385.
- Fattinger, K., Verotta, D., Benowitz, N.L., 1997. Pharmacodynamics of acute tolerance to multiple nicotinic effects in humans. *J. Pharmacol. Exp. Ther.* 281, 1238–1246.
- Favretto, D., Nalesso, A., Frison, G., Viel, G., Traldi, P., Ferrara, S.D., 2010. A novel and an effective analytical approach for the LC-MS determination of ethyl glucuronide and ethyl sulfate in urine. *Int. J. Legal Med.* 124, 161–164.
- FDA, 1968. Internal report ref. SBJ000051 2.
- Feldmann, R.J., Maibach, H.I., 1970. Absorption of some organic compounds through the skin in man. *J. Invest. Dermatol.* 54, 399–404.
- Fitness, N.C. on S.&, 2014. Caffeine Consumption Among Children and Adolescents [WWW Document]. URL <http://www.ncsf.org/enev/articles/articles-CaffeineConsumptionChildrenAdolescents.aspx>
- Flynn, G., 1990. Physiochemical determinants of skin absorption, in: *Principles of Route to Route Extrapolation for Risk Assessment*. New York, NY, USA, pp. 93–127.
- Ford, R.A., Hawkins, D.R., Mayo, B.C., Api, A.M., 2001. The in vivo dermal absorption and metabolism of [4-¹⁴C]coumarin by rats and by human volunteers under simulated conditions of use in fragrances. *Food Chem. Toxicol.* 39, 153–162.
- Franz, T.J., 1978. The finite dose technique as a valid in vitro model for the study of percutaneous absorption in man. *Curr. Probl. Dermatol.* 7, 58–68.
- Frasch, H.F., 2002. A random walk model of skin permeation. *Risk Anal.* 22, 265–276.
- Geinoz, S., Guy, R.H., Testa, B., Carrupt, P.A., 2004. Quantitative Structure-Permeation Relationships (QSPeRs) to Predict Skin Permeation: A Critical Evaluation. *Pharm. Res.* 21, 83–92.
- Gentry, P.R., Covington, T.R., Andersen, M.E., Clewell III, H.J., 2002. Application of a physiologically based pharmacokinetic model for isopropanol in the derivation of a reference dose and reference concentration. *Regul. Toxicol. Pharmacol.* 36, 51–68.
- Gérard, C., Goldbeter, A., 2009. Temporal self-organization of the cyclin/Cdk network driving the mammalian cell cycle. *Proc. Natl. Acad. Sci. U. S. A.* 106, 21643–21648.
- Ghafourian, T., Amin, Z., 2013. QSAR models for the prediction of plasma protein binding. *BioImpacts* 3, 21–27.
- Gibaldi, M., Koup, J.R., 1981. Pharmacokinetic concepts: Drug binding, apparent volume of distribution and clearance. *Eur. J. Clin. Pharmacol.* 20, 299–305.

- Ginsberg, G., Hattis, D., Russ, A., Sonawane, B., 2004. Physiologically based pharmacokinetic (PBPK) modeling of caffeine and theophylline in neonates and adults: Implications for assessing children's risks from environmental agents. *J. Toxicol. Environ. Heal. - Part A* 67, 297–329.
- Goutelle, S., Maurin, M., Rougier, F., Barbaut, X., Bourguignon, L., Ducher, M., Maire, P., 2008. The Hill equation: A review of its capabilities in pharmacological modelling. *Fundam. Clin. Pharmacol.* 22, 633–648.
- Greaves, L., Wilkinson, S., Williams, F., 2012. Factors affecting percutaneous absorption of caffeine in vitro. *Toxicology* 178, 65–66.
- Green, J.T., Evans, B.K., Rhodes, J., Thomas, G.A.O., Ranshaw, C., Feyerabend, C., Russell, M.A.H., 1999. An oral formulation of nicotine for release and absorption in the colon: Its development and pharmacokinetics. *Br. J. Clin. Pharmacol.* 48, 485–493.
- Große, J., Anielski, P., Sachs, H., Thieme, D., 2009. Ethylglucuronide as a potential marker for alcohol-induced elevation of urinary testosterone/epitestosterone ratios. *Drug Test. Anal.* 1, 526–530.
- Grundy, S.M., Mok, H.Y.I., Zech, L., Berman, M., 1981. Influence of nicotinic acid on metabolism of cholesterol and triglycerides in man. *J. Lipid Res.* 22, 24–36.
- Gupta, S.K., Benowitz, N.L., Jacob III, P., Rolf, C.N., Gorsline, J., 1993. Bioavailability and adsorption kinetics of nicotine following application of a transdermal system. *Br. J. Clin. Pharmacol.* 36, 221–227.
- Ha, H.R., Chen, J., Krähenbühl, S., Follath, F., 1996. Biotransformation of caffeine by cDNA-expressed human cytochromes P-450. *Eur. J. Clin. Pharmacol.* 49, 309–315.
- Hallifax, D., Foster, J., Houston, J., 2010. Prediction of human metabolic clearance from in vitro systems: retrospective analysis and prospective view. *Pharm Res.* 27, 2150–61.
- Halter, C.C., Dresen, S., Auwaerter, V., Wurst, F.M., Weinmann, W., 2008. Kinetics in serum and urinary excretion of ethyl sulfate and ethyl glucuronide after medium dose ethanol intake. *Int. J. Legal Med.* 122, 123–128.
- Hamilton Health Sciences, 2014. Adult Nicotine Replacement Therapy (NRT) Order Set.
- Hansen, S., Henning, A., Naegel, A., Heisig, M., Wittum, G., Neumann, D., Kostka, K.H., Zbytovska, J., Lehr, C.M., Schaefer, U.F., 2008. In-silico model of skin penetration based on experimentally determined input parameters. Part I: Experimental determination of partition and diffusion coefficients. *Eur. J. Pharm. Biopharm.* 68, 352–367.
- Hansson, L., Choudry, N.B., Karlsson, J.-A., Fuller, R.W., 1994. Inhaled nicotine in humans: Effect on the respiratory and cardiovascular systems. *J. Appl. Physiol.* 76, 2420–2427.

- Hardt, T.J., Ritschel, W.A., 1983. Dose-related pharmacokinetics of coumarin, 7-hydroxycoumarin and 7-hydroxycoumarin glucuronide upon intraperitoneal administration of coumarin and 7-hydroxycoumarin in the rat. *Arzneimittel-Forschung/Drug Res.* 33, 1442–1446.
- Helander, A., Beck, O., 2005. Ethyl sulfate: A metabolite of ethanol in humans and a potential biomarker of acute alcohol intake. *J. Anal. Toxicol.* 29, 270–274.
- Helander, A., Beck, O., Jones, A.W., 1996. Laboratory testing for recent alcohol consumption: Comparison of ethanol, methanol, and 5-hydroxytryptophol. *Clin. Chem.* 42, 618–624.
- Herman, A., Herman, A.P., 2012. Caffeine's mechanisms of action and its cosmetic use. *Skin Pharmacol. Physiol.* 26, 8–14.
- Himmelstein, M.W., Kegelman, T.A., Delorme, M.P., Everds, N.E., O'Connor, J.C., Kemper, R.A., Nabb, D.L., Mileson, B.E., Bevan, C., 2009. Two-day inhalation toxicity study of methyl iodide in the rat. *Inhal. Toxicol.* 21, 480–487.
- Høiseth, G., Yttredal, B., Karinen, R., Gjerde, H., Mørland, J., Christophersen, A., 2010. Ethyl glucuronide concentrations in oral fluid, blood, and urine after volunteers drank 0.5 and 1.0 g/kg doses of ethanol. *J. Anal. Toxicol.* 34, 319–324.
- Hostynek, J.J., Magee, P.S., 1997. Modelling in vivo human skin absorption. *Quant. Struct. Relationships* 16, 473–479.
- Houston, J.B., Rowland-Yeo, K., Zanelli, U., 2012. Evaluation of the novel in vitro systems for hepatic drug clearance and assessment of their predictive utility. *Toxicol. In Vitro* 26, 1265–1271.
- Hui, X., Wester, R.C., Magee, P.S., Maibach, H.I., 1995. Partitioning of chemicals from water into powdered human stratum corneum (Callus): A model study. *Vitr. Toxicol. J. Mol. Cell. Toxicol.* 8, 159–167.
- Huizer, D., Oldenkamp, R., Ragas, A.M.J., van Rooij, J.G.M., Huijbregts, M.A.J., 2012. Separating uncertainty and physiological variability in human PBPK modelling: The example of 2-propanol and its metabolite acetone. *Toxicol. Lett.* 214, 154–165.
- Hukkanen, J., Jacob III, P., Benowitz, N.L., 2005. Metabolism and disposition kinetics of nicotine. *Pharmacol. Rev.* 57, 79–115.
- Jennen, D., Magkoufopoulou, C., Ketelslegers, H., van Herwijnen, M., Kleinjans, J., van Delft, J., 2010. Comparison of HepG2 and HepaRG by whole-genome gene expression analysis for the purpose of chemical hazard identification. *Toxicol Sci.* 115, 66–79.
- Johanson, G., Ernstgard, L., Gullstrand, E., Lof, A., Osterman-Golkar, S., Williams, C.C., Sumner, S.C.J., 2000. Styrene oxide in blood, hemoglobin adducts, and urinary metabolites in human volunteers exposed to 13C8-styrene vapors. *Toxicol. Appl. Pharmacol.* 168, 36–49.
- Jones, A.W., Jorfeldt, L., Hjertberg, H., Jonsson, K.A., 1990. Physiological variations in blood ethanol measurements during the post-absorptive state. *J. Forensic Sci. Soc.* 30, 273–283.

- Jones, A.W., Neiman, J., Hillbom, M., 1988. Concentration-time profiles of ethanol and acetaldehyde in human volunteers treated with the alcohol-sensitizing drug, calcium carbimide. *Br. J. Clin. Pharmacol.* 25, 213–221.
- Jones, A.W., Sato, A., Forsander, O.A., 1985. Liquid/air partition coefficients of acetaldehyde: Values and limitations in estimating blood concentrations from analysis of breath. *Alcohol. Clin. Exp. Res.* 9, 461–464.
- Jonsson, F., Johanson, G., 2002. Physiologically based modeling of the inhalation kinetics of styrene in humans using a Bayesian population approach. *Toxicol. Appl. Pharmacol.* 179, 35–49.
- Kaneko, T., Wang, P., Sato, A., 1994. Partition coefficients of some acetate esters and alcohols in water, blood, olive oil, and rat tissues. *Occup. Environ. Med.* 51, 68–72.
- Karatzis, E., Papaioannou, T.G., Aznaouridis, K., Karatzi, K., Stamatelopoulos, K., Zampelas, A., Papamichael, C., Lekakis, J., Mavrikakis, M., 2005. Acute effects of caffeine on blood pressure and wave reflections in healthy subjects: Should we consider monitoring central blood pressure? *Int. J. Cardiol.* 98, 425–430.
- Kari, F.W., Bucher, J., Eustis, S.L., Haseman, J.K., Huff, J.E., 1992. Toxicity and carcinogenicity of hydroquinone in F344/N rats and B6C3F1 mice. *Food Chem. Toxicol.* 30, 737–747.
- Katritzky, A.R., Dobchev, D.A., Fara, D.C., Hür, E., Tämm, K., Kurunczi, L., Karelson, M., Varnek, A., Solov'ev, V.P., 2006. Skin permeation rate as a function of chemical structure. *J. Med. Chem.* 49, 3305–3314.
- Katritzky, A.R., Kuanar, M., Stoyanova-Slavova, I.B., Slavov, S.H., Dobchev, D.A., Karelson, M., Acree Jr., W.E., 2008. Quantitative structure-property relationship studies on Ostwald solubility and partition coefficients of organic solutes in ionic liquids. *J. Chem. Eng. Data* 53, 1085–1092.
- Kenyon, E.M., 2012. Interspecies extrapolation. *Methods Mol. Biol.* 929, 501–520.
- Khalil, F., Lær, S., 2011. Physiologically Based Pharmacokinetic Modeling: Methodology, Applications, and Limitations with a Focus on Its Role in Pediatric Drug Development. *J. Biomed. Biotechnol.* 2011, 1–13.
- Kletting, P., Glatting, G., 2009. Model selection for time-activity curves: The corrected Akaike information criterion and the F-test. *Z. Med. Phys.* 19, 200–206.
- Kostewicz, E.S., Aarons, L., Bergstrand, M., Bolger, M.B., Galetin, A., Hatley, O., Jamei, M., Lloyd, R., Pepin, X., Rostami-Hodjegan, A., Sjögren, E., Tannergren, C., Turner, D.B., Wagner, C., Weitschies, W., Dressman, J., 2014. PBPK models for the prediction of in vivo performance of oral dosage forms. *Eur. J. Pharm. Sci.* 57, 300–321.
- Kramer, A., Below, H., Bieber, N., Kampf, G., Toma, C.D., Huebner, N.-O., Assadian, O., 2007. Quantity of ethanol absorption after excessive hand disinfection using three commercially available hand rubs is minimal and below toxic levels for humans. *BMC Infect. Dis.* 7.

- Krauss, M., Burghaus, R., Lippert, J., Niemi, M., Neuvonen, P., Schuppert, A., Willmann, S., Kuepfer, L., Görlitz, L., 2013. Using Bayesian-PBPK modeling for assessment of inter-individual variability and subgroup stratification. *Silico Pharmacol.* 1.
- Kroes, R., Renwick, A.G., Feron, V., Galli, C.L., Gibney, M., Greim, H., Guy, R.H., Lhuguenot, J.C., van de Sandt, J.J.M., 2007. Application of the threshold of toxicological concern (TTC) to the safety evaluation of cosmetic ingredients. *Food Chem. Toxicol.* 45, 2533–2562.
- Krüse, J., Golden, D., Wilkinson, S., Williams, F., Kezic, S., Corish, J., 2007. Analysis, interpretation, and extrapolation of dermal permeation data using diffusion-based mathematical models. *J. Pharm. Sci.* 96, 682–703.
- Kubota, K., Ishizaki, T., 1986. A diffusion-diffusion model for percutaneous drug absorption. *J. Pharmacokinet. Biopharm.* 14, 409–439.
- Kumagai, S., Matsunaga, I., 1995. Physiologically based pharmacokinetic model for acetone. *Occup. Environ. Med.* 52, 344–352.
- Kumagai, S., Oda, H., Matsunaga, I., Kosaka, H., Akasaka, S., 1999. Uptake of 10 polar organic solvents during short-term respiration. *Toxicol. Sci.* 48, 255–263.
- Lacouture, P.G., Heldreth, D.D., Shannon, M., Lovejoy Jr., F.H., 1989. The generation of acetonemia/acetoneuria following ingestion of a subtoxic dose isopropyl alcohol. *Am. J. Emerg. Med.* 7, 38–40.
- Lake, B.G., 1999. Coumarin metabolism, toxicity and carcinogenicity: Relevance for human risk assessment. *Food Chem. Toxicol.* 37, 423–453.
- Lavé, T., Parrott, N., Grimm, H.P., Fleury, A., Reddy, M., 2007. Challenges and opportunities with modelling and simulation in drug discovery and drug development. *Xenobiotica* 37, 1295–1310.
- Lehman, P.A., Raney, S.G., Franz, T.J., 2011. Percutaneous absorption in man: In vitro-in vivo correlation. *Skin Pharmacol. Physiol.* 24, 224–230.
- Lelo, A., Birkett, D.J., Robson, R.A., Miners, J.O., 1986. Comparative pharmacokinetics of caffeine and its primary demethylated metabolites paraxanthine, theobromine and theophylline in man. *Br. J. Clin. Pharmacol.* 22, 177–182.
- Li, A.P., 2001. Screening for human ADME/Tox drug properties in drug discovery. *Drug Discov. Today* 6, 357–366.
- Lian, G, Chen, L., Han, L., 2008. An evaluation of mathematical models for predicting skin permeability. *J. Pharm. Sci.* 97, 584–598.
- Lian, Guoping, Chen, L., Han, L., 2008. An Evaluation of Mathematical Models for Predicting Skin Permeability 97, 584–598. doi:10.1002/jps

- Lien, E.J., Gao, H., 1995. QSAR analysis of skin permeability of various drugs in man as compared to in vivo and in vitro studies in rodents. *Pharm. Res.* 12, 583–587.
- Liu, X., Grice, J.E., Lademann, J., Otberg, N., Trauer, S., Patzelt, A., Roberts, M.S., 2011. Hair follicles contribute significantly to penetration through human skin only at times soon after application as a solvent deposited solid in man. *Br. J. Clin. Pharmacol.* 72, 768–774.
- Livy, D.J., Parnell, S.E., West, J.R., 2003. Blood ethanol concentration profiles: A comparison between rats and mice. *Alcohol* 29, 165–171.
- Loizou, G.D., Spendiff, M., 2004. A human PBPK model for ethanol describing inhibition of gastric motility. *J. Mol. Histol.* 35, 687–696.
- Lopes, C., Péry, A.R.R., Chaumot, A., Charles, S., 2005. Ecotoxicology and population dynamics: Using DEBtox models in a Leslie modeling approach. *Ecol. Modell.* 188, 30–40.
- Lostia, A.M., Vicente, J.L., Cowan, D.A., 2013. Measurement of ethyl glucuronide, ethyl sulphate and their ratio in the urine and serum of healthy volunteers after two doses of alcohol. *Alcohol* 48, 74–82.
- Lotte, C., Wester, R.C., Rougier, A., Maibach, H.I., 1993. Racial differences in the in vivo percutaneous absorption of some organic compounds: A comparison between black, Caucasian and Asian subjects. *Arch. Dermatol. Res.* 284, 456–459.
- Lungarini, S., Aureli, F., Coni, E., 2008. Coumarin and cinnamaldehyde in cinnamon marketed in Italy: A natural chemical hazard? *Food Addit. Contam. - Part A Chem. Anal. Control. Expo. Risk Assess.* 25, 1297–1305.
- MacDonald, A.J., Rostami-Hodjegan, A., Tucker, G.T., Linkens, D.A., 2002. Analysis of solvent central nervous system toxicity and ethanol interactions using a human population physiologically based kinetic and dynamic model. *Regul. Toxicol. Pharmacol.* 35, 165–176.
- Magee, R., 1998. Some novel approaches to modeling transdermal penetration and reactivity with epidermal proteins. J. Devillers (ed.), *Comp. QSAR*. Taylor Fr. London 137–168.
- Magnusson, B.M., Anissimov, Y.G., Cross, S.E., Roberts, M.S., 2004. Molecular size as the main determinant of solute maximum flux across the skin. *J. Invest. Dermatol.* 122, 993–999.
- Malson, J.L., Sims, K., Murty, R., Pickworth, W.B., 2001. Comparison of the nicotine content of tobacco used in bidis and conventional cigarettes. *Tob. Control* 10, 181–183.
- Mathes, S., Ruffner, H., Graf-Hausner, U., 2014. The use of skin models in drug development. *Adv Drug Deliv Rev.* 69, 81–102.
- McCarley, K.D., Bunge, A.L., 2001. Pharmacokinetic models of dermal absorption. *J. Pharm. Sci.* 90, 1699–1719.
- McClaran, S.R., Wetter, T.J., 2007. Low doses of caffeine reduce heart rate during submaximal cycle ergometry. *J. Int. Soc. Sports Nutr.* 4.

- McGregor, D., 2007. Hydroquinone: An evaluation of the human risks from its carcinogenic and mutagenic properties. *Crit. Rev. Toxicol.* 37, 887–914.
- McKone, T.E., Howd, R.A., 1992. Estimating dermal uptake of nonionic organic chemicals from water and soil: I. Unified fugacity-based models for risk assessments. *Risk Anal.* 12, 543–557.
- McLanahan, E.D., El-Masri, H.A., Sweeney, L.M., Kopylev, L.Y., Clewell, H.J., Wambaugh, J.F., Schlosser, P.M., 2012. Physiologically based pharmacokinetic model use in risk assessment—Why being published is not enough. *Toxicol. Sci.* 126, 5–15.
- MedlinePlus, 2014. Nicotine Lozenges [WWW Document]. URL <http://www.nlm.nih.gov/medlineplus/druginfo/meds/a606019.html>
- Mendelson, J.H., Goletiani, N., Sholar, M.B., Siegel, A.J., Mello, N.K., 2008. Effects of smoking successive low- and high-nicotine cigarettes on hypothalamic-pituitary-adrenal axis hormones and mood in men. *Neuropsychopharmacology* 33, 749–760.
- Mennecozzi, M., Landesmann, B., Harris, G.A., Liska, R., Whelan, M., 2011. Hepatotoxicity Screening Taking a Mode-Of-Action Approach Using HepaRG Cells and HCA. *Altex Proceedings*, 1/12, Proc. WC8.
- Messina, E.S., Tyndale, R.F., Sellers, E.M., 1997. A major role for CYP2A6 in nicotine C-oxidation by human liver microsomes. *J. Pharmacol. Exp. Ther.* 282, 1608–1614.
- Meulenberg, C.J.W., Vijverberg, H.P.M., 2000. Empirical relations predicting human and rat tissue: Air partition coefficients of volatile organic compounds. *Toxicol. Appl. Pharmacol.* 165, 206–216.
- Mielke, H., Abraham, K., Götz, M., Vieth, B., Lampen, A., Luch, A., Gundert-Remy, U., 2011. Physiologically based toxicokinetic modelling as a tool to assess target organ toxicity in route-to-route extrapolation—The case of coumarin. *Toxicol. Lett.* 202, 100–110.
- Mileson, B.E., Sweeney, L.M., Gargas, M.L., Kinzell, J., 2009. Iodomethane human health risk characterization. *Inhal. Toxicol.* 21, 583–605.
- Mitragotri, S., 2002. A theoretical analysis of permeation of small hydrophobic solutes across the stratum corneum based on Scaled Particle Theory. *J. Pharm. Sci.* 91, 744–752.
- Mohiuddin, M., Azam, A.T.M.Z., Amran, M.S., Hossain, M.A., 2009. In vivo effects of gliclazide and metformin on the plasma concentration of caffeine in healthy rats. *Pakistan J. Biol. Sci.* 12, 734–737.
- Monaghan, M.S., Olsen, K.M., Ackerman, B.H., Fuller, G.L., Porter, W.H., Pappas, A.A., 1995. Measurement of serum isopropanol and the acetone metabolite by proton nuclear magnetic resonance: Application to pharmacokinetic evaluation in a simulated overdose model. *J. Toxicol. - Clin. Toxicol.* 33, 141–149.
- Moré, J.J., 1978. The Levenberg-Marquardt algorithm: implementation and theory. *Lect. Notes Math.* 630, 105–116.

- Morgan, A., Morgan, D.J., Evans, J.C., Lister, B.A., 1967. Studies on the retention and metabolism of inhaled methyl iodide. II. Metabolism of methyl iodide. *Health Phys.* 13, 1067–1074.
- Morgan, D.J., Morgan, A., 1967. Studies on the retention and metabolism of inhaled methyl iodide. I. Retention of inhaled methyl iodide. *Health Phys.* 13, 1055–1065.
- Moss, G.P., Cronin, M.T.D., 2002. Quantitative structure-permeability relationships for percutaneous absorption: Re-analysis of steroid data. *Int. J. Pharm.* 238, 105–109.
- Mousavi, A., Koushki Jahromi, M., Salesi, M., Daryanoush, F., Khoshnam, E., A, N., Hemati, M., 2011. Impact of caffeine on heart rate and blood pressure at rest and during exercise. *J. Jahrom Univ. Med. Sci.* 9.
- Mündel, T., Jones, D.A., 2006. Effect of transdermal nicotine administration on exercise endurance in men. *Exp. Physiol.* 91, 705–713.
- Nadeau, V., Lamoureux, D., Beuter, A., Charbonneau, M., Tardif, R., 2003. Neuromotor effects of acute ethanol inhalation exposure in humans: A preliminary study. *J. Occup. Health* 45, 215–222.
- Nair, J., Chatterjee, K., 2010. Methyl iodide poisoning presenting as a mimic of acute stroke: A case report. *J. Med. Case Rep.* 4.
- Nakayama, Y., Kishida, F., Nakatsuka, I., Matsuo, M., 2005. Simulation of the toxicokinetics of trichloroethylene, methylene chloride, styrene and n-hexane by a toxicokinetics/toxicodynamics model using experimental data. *Env. Sci* 12, 21–32.
- National Tobacco Control Office, 2002. Promoting a tobacco free society: Cigarette Smoking Trends [WWW Document]. URL <http://www.ntco.ie/research.asp>
- Newton, R., Broughton, L.J., Lind, M.J., Morrison, P.J., Rogers, H.J., Bradbrook, I.D., 1981. Plasma and salivary pharmacokinetics of caffeine in man. *Eur. J. Clin. Pharmacol.* 21, 45–52.
- Nitsche, J., Kasting GB, 2007. Biophysical models for skin transport and absorption, in: *Dermal Absorption and Toxicity Assessment*.
- OECD SIDS, 2002a. Caffeine: SIDS Initial assessment report for SIAM 14.
- OECD SIDS, 2002b. Caffeine 58-08-2.
- OECD SIDS, 1996. Hydroquinone.
- OECD SIDS, n.d. 2-PROPANOL: SIDS INITIAL ASSESSMENT PROFILE.
- Omlin, M., Brun, R., Reichert, P., 2001a. Biogeochemical model of Lake Zürich: Sensitivity, identifiability and uncertainty analysis. *Ecol. Modell.* 141, 105–123.
- Omlin, M., Reichert, P., Forster, R., 2001b. Biogeochemical model of Lake Zürich: Model equations and results. *Ecol. Modell.* 141, 77–103.

- Otberg, N., Patzelt, A., Rasulev, U., Hagemester, T., Linscheid, M., Sinkgraven, R., Sterry, W., Lademann, J., 2008. The role of hair follicles in the percutaneous absorption of caffeine. *Br. J. Clin. Pharmacol.* 65, 488–492.
- Papathanasiou, G., Georgakopoulos, D., Papageorgiou, E., Zerva, E., Michalis, L., Kalfakakou, V., Evangelou, A., 2013. Effects of smoking on heart rate at rest and during exercise, and on heart rate recovery, in young adults. *Hell. J. Cardiol.* 54, 168–177.
- Parkar, S.R., Mayanil, T.S., 2012. Neuropsychiatric manifestations of methyl iodide. *Indian J. Occup. Environ. Med.* 16, 38–39.
- Pastino, G.M., Conolly, R.B., 2000. Application of a physiologically based pharmacokinetic model to estimate the bioavailability of ethanol in male rats: Distinction between gastric and hepatic pathways of metabolic clearance. *Toxicol. Sci.* 55, 256–265.
- Pelkonen, O., Turpeinen, M., 2007. In vitro-in vivo extrapolation of hepatic clearance: Biological tools, scaling factors, model assumptions and correct concentrations. *Xenobiotica* 37, 1066–1089.
- Pepelko, W.E., Withey, J.R., 1985. Methods for route-to-route extrapolation of dose. *Toxicol. Ind. Health* 1, 153–175.
- Peterman, B.F., Longtin, A., 1984. Multicompartment model of lung dynamics. *Comput. Biomed. Res.* 17, 580–589.
- Piller, N.B., Schmitt, L.H., 1977. An electrophoretic investigation of the binding of 3-14C coumarin to rat serum proteins. *Experientia* 33, 1072–1074.
- Ping, W.C., Keong, C.C., Bandyopadhyay, A., 2010. Effects of acute supplementation of caffeine on cardiorespiratory responses during endurance running in a hot & humid climate. *Indian J. Med. Res.* 132, 36–41.
- Poet, T.S., Carlton, B.D., Deyo, J.A., Hinderliter, P.M., 2010. Hydroquinone PBPK model refinement and application to dermal exposure. *Food Chem. Toxicol.* 48, 3085–3092.
- Poet, T.S., Wu, H., English, J.C., Corley, R.A., 2004. Metabolic rate constants for hydroquinone in F344 rat and human liver isolated hepatocytes: Application to a PBPK model. *Toxicol. Sci.* 82, 9–25.
- Polak, S., Ghobadi, C., Mishra, H., Ahamadi, M., Patel, N., Jamei, M., Rostami-Hodjegan, A., 2012. Prediction of concentration-time profile and its inter-individual variability following the dermal drug absorption. *J. Pharm. Sci.* 101, 2584–2595.
- Politi, L., Morini, L., Groppi, A., Poloni, V., Pozzi, F., Poletini, A., 2005. Direct determination of the ethanol metabolites ethyl glucuronide and ethyl sulfate in urine by liquid chromatography/electrospray tandem mass spectrometry. *Rapid Commun. Mass Spectrom.* 19, 1321–1331.

- Porchet, H.C., Benowitz, N.L., Sheiner, L.B., 1988. Pharmacodynamic model of tolerance: Application to nicotine. *J. Pharmacol. Exp. Ther.* 244, 231–236.
- Potts, R.O., Guy, R.H., 1992. Predicting skin permeability. *Pharm. Res.* 9, 663–669.
- Pouillot, A., Dayan, N., Polla, A.S., Polla, L.L., Polla, B.S., 2008. The stratum corneum: A double paradox. *J. Cosmet. Dermatol.* 7, 143–148.
- Prieto, M.J., Marhuenda, D., Cardona, A., 2002. Analysis of styrene and its metabolites in blood and urine of workers exposed to both styrene and acetone. *J. Anal. Toxicol.* 26, 23–28.
- Pugh, G., Moyer, G.O., Raabe, H.A., Harbell, J.W., Bagley, D.M., 2004. The impact of ethanol on the in vitro penetration rates of caffeine in engineered skin constructs. Baltimore, MD.
- Pugh, W.J., Degim, I.T., Hadgraft, J., 2000. Epidermal permeability-penetrant structure relationships: 4, QSAR of permeant diffusion across human stratum corneum in terms of molecular weight, H-bonding and electronic charge. *Int. J. Pharm.* 197, 203–211.
- Pugh, W.J., Roberts, M.S., Hadgraft, J., 1996. Epidermal permeability - penetrant structure relationships: 3. The effect of hydrogen bonding interactions and molecular size on diffusion across the stratum corneum. *Int. J. Pharm.* 138, 149–165.
- Punt, A., Paini, A., Boersma, M.G., Freidig, A.P., Delatour, T., Scholz, G., Schilter, B., van Bladeren, P.J., Rietjens, I.M.C.M., 2009. Use of physiologically based biokinetic (PBBK) modeling to study estragole bioactivation and detoxification in humans as compared with male rats. *Toxicol. Sci.* 110, 255–269.
- QuitNet, 2013. MEDICATION Guide Nicotine Replacement Therapy (NRT) [WWW Document]. URL <http://www.quitnet.com/library/guides/nrt/inhaler.jtml>
- Qvist, M.H., Hoeck, U., Kreilgaard, B., Madsen, F., Frokjaer, S., 2000. Evaluation of Gottingen minipig skin for transdermal in vitro permeation studies. *Eur. J. Pharm. Sci.* 11, 59–68.
- Ramchandani, V.A., Bosron, W.F., Li, T.K., 2001. Research advances in ethanol metabolism. *Pathol. Biol.* 49, 676–682.
- Ramsey, J.C., Andersen, M.E., 1984. A physiologically based description of the inhalation pharmacokinetics of styrene in rats and humans. *Toxicol. Appl. Pharmacol.* 73, 159–175.
- Ramsey, J.C., Young, J.D., 1978. Pharmacokinetics of inhaled styrene in rats and humans. *Scand. J. Work. Environ. Heal.* 4, 84–91.
- Ramsey, J.C., Young, J.D., Karbowski, R.J., Chenoweth, M.B., McCarty, L.P., Braun, W.H., 1980. Pharmacokinetics of inhaled styrene in human volunteers. *Toxicol. Appl. Pharmacol.* 53, 54–63.
- Reagan-Shaw, S., Nihal, M., Ahmad, N., 2008. Dose translation from animal to human studies revisited. *FASEB J.* 22, 659–661.

- Reddy, M., Clewell, H., Lave, T., Andersen, M., 2013. Physiologically Based Pharmacokinetic Modeling: A Tool for Understanding ADMET Properties and Extrapolating to Human, in: Pharmacology, Toxicology and Pharmaceutical Science.
- Renwick, A.G., 2005. Toxicokinetics. pp. 24–41.
- Rietjens, I.M.C.M., Boersma, M.G., Zaleska, M., Punt, A., 2008. Differences in simulated liver concentrations of toxic coumarin metabolites in rats and different human populations evaluated through physiologically based biokinetic (PBBK) modeling. *Toxicol. Vitro*. 22, 1890–1901.
- Rietjens, I.M.C.M., Punt, A., Schilter, B., Scholz, G., Delatour, T., van Bladeren, P.J., 2010. In silico methods for physiologically based biokinetic models describing bioactivation and detoxification of coumarin and estragole: Implications for risk assessment. *Mol. Nutr. Food Res.* 54, 195–207.
- Ritschel, W.A., Brady, M.E., Tan, H.S.I., 1979. First-pass effect of coumarin in man. *Int. J. Clin. Pharmacol. Ther. Toxicol.* 17, 99–103.
- Ritschel, W.A., Brady, M.E., Tan, H.S.I., Hoffmann, K.A., Yiu, I.M., Grummich, K.W., 1977. Pharmacokinetics of coumarin and its 7-hydroxy-metabolites upon intravenous and peroral administration of coumarin in man. *Eur. J. Clin. Pharmacol.* 12, 457–461.
- Ritschel, W.A., Hussain, S.A., 1988. Transdermal absorption and topical bioavailability of coumarin. *Methods Find. Exp. Clin. Pharmacol.* 10, 165–169.
- Ritschel, W.A., Sabouni, A., Hussain, A.S., 1989. Percutaneous absorption of coumarin, griseofulvin and propranolol across human scalp and abdominal skin. *Methods Find. Exp. Clin. Pharmacol.* 11, 643–646.
- Roberts, M.S., Pugh, W.J., Hadgraft, J., 1996. Epidermal permeability: Penetrant structure relationships. 2. The effect of H-bonding groups in penetrants on their diffusion through the stratum corneum. *Int. J. Pharm.* 132, 23–32.
- Roberts, M.S., Pugh, W.J., Hadgraft, J., Watkinson, A.C., 1995. Epidermal permeability-penetrant structure relationships: 1. An analysis of methods of predicting penetration of monofunctional solutes from aqueous solutions. *Int. J. Pharm.* 126, 219–233.
- Robertson, D., Wade, D., Workman, R., Woosley, R.L., Oates, J.A., 1981. Tolerance to the humoral and hemodynamic effects of caffeine in man. *J. Clin. Invest.* 67, 1111–1117.
- Robertz-Vaupel, G.-M., Bierl, R., Von Unruh, G., 1991. Intravenous methyl iodide intoxication - detoxication by haemoperfusion [INTRAVENOSE METHYLJODIDINTOXIKATION - DETOXIKATION DURCH HAMOPERFUSION]. *Anesthesiol. Intensivmed. Notfallmedizin Schmerztherapie* 26, 44–47.
- Robinson, D.E., Balter, N.J., Schwartz, S.L., 1992. A physiologically based pharmacokinetic model for nicotine and cotinine in man. *J. Pharmacokinet. Biopharm.* 20, 591–609.

- Ronald, M.D., 2011. Pharmacodynamics: The Study of Drug Action, in: Bartlett, J.& (Ed.), Pharmacology for Nurse Anesthesiology.
- Roskos, K. V, Maibach, H.I., Guy, R.H., 1989. The effect of aging on percutaneous absorption in man. *J. Pharmacokinet. Biopharm.* 17, 617–630.
- Rougier, A., Lotte, C., Dupuis, D., 1987. An original predictive method for in vivo percutaneous absorption studies. *J. Soc. Cosmet. Chem.* 38, 397–417.
- Roy, A., Georgopoulos, G., 1997. Mechanistic Modeling of Transport and Metabolism in Physiological Systems.
- Russell, L.M., Guy, R.H., 2009. Measurement and prediction of the rate and extent of drug delivery into and through the skin. *Expert Opin. Drug Deliv.* 6, 355–369.
- Russell, M.A.H., Jarvis, M., Iyer, R., Feyerabend, C., 1980. Relation of nicotine yield of cigarettes to blood nicotine concentrations in smokers. *Br. Med. J.* 280, 972–976.
- Sarangapani, R., Teeguarden, J.G., Cruzan, G., Clewell, H.J., Andersen, M.E., 2002. Physiologically based pharmacokinetic modeling of styrene and styrene oxide respiratory-tract dosimetry in rodents and humans. *Inhal. Toxicol.* 14, 789–834.
- Sarkola, T., Eriksson, C.J.P., 2003. Testosterone increases in men after a low dose of alcohol. *Alcohol. Clin. Exp. Res.* 27, 682–685.
- SCCP, 2006. Basic criteria for the in vitro assessment of dermal absorption of cosmetic ingredients.
- Scheers, E.M., Ekwall, B., Dierickx, P.J., 2001. In vitro long-term cytotoxicity testing of 27 MEIC chemicals on Hep G2 cells and comparison with acute human toxicity data. *Toxicol. Vitro.* 15, 153–161.
- Schmitt, G., Halter, C.C., Aderjan, R., Auwaerter, V., Weinmann, W., 2010. Computer assisted modeling of ethyl sulfate pharmacokinetics. *Forensic Sci. Int.* 194, 34–38.
- Schmitt, W., 2008. General approach for the calculation of tissue to plasma partition coefficients. *Toxicol. Vitro.* 22, 457–467.
- Scott, R.C., Corrigan, M.A., Smith, F., Mason, H., 1991. The influence of skin structure on permeability: An intersite and interspecies comparison with hydrophilic penetrants. *J. Invest. Dermatol.* 96, 921–925.
- Seidl, S., Wurst, F.M., Alt, A., 2001. Ethyl glucuronide - A biological marker for recent alcohol consumption. *Addict. Biol.* 6, 205–212.
- Shi, J., 1993. Pharmacokinetic-pharmacodynamic modeling of caffeine: Tolerance to pressor effects. *Clin. Pharmacol. Ther.* 53, 6–14.
- Sinhaa, V.K., Snoeysb, J., Van Osselaerc, N., Van Peera, A., Mackied, C., Healde, D., 2012. From preclinical to human - Prediction of oral absorption and drug-drug interaction potential using

physiologically based pharmacokinetic (PBPK) modeling approach in an industrial setting: A workflow by using case example. *Biopharm. Drug Dispos.* 33, 111–121.

Soetaert, K., 2010. R package FME: inverse modelling, sensitivity, Monte Carlo - applied to a dynamic simulation model.

Soetaert, K., Petzoldt, T., 2010. Inverse Modelling, Sensitivity and Monte Carlo Analysis in R Using Package FME. *J. Stat. Softw.* 33, 1–28.

Sofuoglu, M., Herman, A.I., Nadim, H., Jatlow, P., 2012. Rapid nicotine clearance is associated with greater reward and heart rate increases from intravenous nicotine. *Neuropsychopharmacology* 37, 1509–1516.

Southwell, D., Barry, B.W., Woodford, R., 1984. Variations in permeability of human skin within and between specimens. *Int. J. Pharm.* 18, 299–309.

Stoick, K., Nitschke, K., Sandusky, C., 2007. 6th World Congress on Alternatives & Animal Use in the Life Sciences, in: Systemic Testing by the Dermal Route Can Be Precluded by New Non-Animal Percutaneous Absorption Strategies.

Sung, B.H., Lovallo, W.R., Pincomb, G.A., Wilson, M.F., 1990. Effects of caffeine on blood pressure response during exercise in normotensive healthy young men. *Am. J. Cardiol.* 65, 909–913.

Sweeney, L.M., Kirman, C.R., Gannon, S.A., Thrall, K.D., Gargas, M.L., Kinzell, J.H., 2009. Development of a physiologically based pharmacokinetic (PBPK) model for methyl iodide in rats, rabbits, and humans. *Inhal. Toxicol.* 21, 552–582.

Tayar, N.E., Tsai, R.S., Testa, B., Carrupt, P.A., Hansch, C., Leo, A., 1991. Percutaneous penetration of drugs: A quantitative structure-permeability relationship study. *J. Pharm. Sci.* 80, 744–749.

Teeguarden, J.G., Housand, C.J., Smith, J.N., Hinderliter, P.M., Gunawan, R., Timchalk, C.A., 2013. A multi-route model of nicotine-cotinine pharmacokinetics, pharmacodynamics and brain nicotinic acetylcholine receptor binding in humans. *Regul. Toxicol. Pharmacol.* 65, 12–28.

Ten Berg, W., 2014. QSARs for skin permeation of chemicals [WWW Document]. URL 29. <http://home.wxs.nl/~wtberge/qsarperm.html>

Ten Berge, W., 2009. A simple dermal absorption model: Derivation and application. *Chemosphere* 75, 1440–1445.

The Metabolomics Innovation Centre, 2013. metabocard for Coumarin (HMDB01218) [WWW Document]. Hum. Metabolome Database. URL <http://www.hmdb.ca/metabolites/HMDB01218>

Tibaldi, R., ten Berge, W., Drolet, D., 2011. IH SkinPerm Help Manual.

- Tojo, K., 1987. MATHEMATICAL MODELING OF TRANSDERMAL DRUG DELIVERY. *J. Chem. Eng. Japan* 20, 300–308.
- Tornero-Velez, R., Rappaport, S.M., 2001. Physiological modeling of the relative contributions of styrene-7,8-oxide derived from direct inhalation and from styrene metabolism to the systemic dose in humans. *Toxicol. Sci.* 64, 151–161.
- Toutain, P.L., Bousquet-Melou, A., 2004. Plasma clearance. *Ther. J. vet. Pharmacol.* 27, 415–425.
- Trauer, S., Patzelt, A., Otberg, N., Knorr, F., Rozycki, C., Balizs, G., Büttemeyer, R., Linscheid, M., Liebsch, M., Lademann, J., 2009. Permeation of topically applied caffeine through human skin - A comparison of in vivo and in vitro data. *Br. J. Clin. Pharmacol.* 68, 181–186.
- Treffel, P., Panisset, F., Humbert, P., Remoussenard, O., Bechtel, Y., Agache, P., 1993. Effect of pressure on in vitro percutaneous absorption of caffeine. *Acta Derm. Venereol.* 73, 200–202.
- Turner, P., Saeed, B., Kelsey, M.C., 2004. Dermal absorption of isopropyl alcohol from a commercial hand rub: Implications for its use in hand decontamination. *J. Hosp. Infect.* 56, 287–290.
- Tutka, P., Mosiewicz, J., Wielosz, M., 2005. Pharmacokinetics and metabolism of nicotine. *Pharmacol. Reports* 57, 143–153.
- Umulis, D.M., Gürmen, N.M., Singh, P., Fogler, H.S., 2005. A physiologically based model for ethanol and acetaldehyde metabolism in human beings. *Alcohol* 35, 3–12.
- Vajda, S., Rabitz, H., Walter, E., Lecourtier, Y., 1989. Qualitative and Quantitative Identifiability Analysis of Nonlinear Chemical Kinetic Models. *Chem. Eng. Commun.* 83, 191–219.
- Van de Sandt, J., van Burgsteden, J., Cage, S., Carmichael, P., Dick, I., Kenyon, S., Korinth, G., Larese, F., Limasset, J., Maas, W., Montomoli, L., Nielsen, J., Payan, J., Robinson, E., Sartorelli, P., Schaller, K., Wilkinson, S., Williams, F., 2004. In vitro predictions of skin absorption of caffeine, testosterone, and benzoic acid: a multi-centre comparison study. *Regul Toxicol Pharmacol.* 39, 271–81.
- Van Iersel, M., Henderson, C., Walters, D., Price, R., Wolf, C., Lake, B., 1994. Metabolism of [3-¹⁴C]coumarin by human liver microsomes. *Xenobiotica* 8, 795–803.
- Van Rees, H., 1974. The partition coefficients of styrene between blood and air and between oil and blood. *INT.ARCH.ARBEITSMED.* 33, 39–47.
- Vassallo, J.D., Hicks, S.M., Daston, G.P., Lehman-McKeeman, L.D., 2004. Metabolic detoxification determines species differences in coumarin-induced hepatotoxicity. *Toxicol. Sci.* 80, 249–257.
- Venkatakrishnan, K., Von Moltke, L.L., Court, M.H., Harmatz, J.S., Crespi, C.L., Greenblatt, D.J., 2000. Comparison between cytochrome P450 (CYP) content and relative activity approaches to scaling from CDNA-expressed CYPs to human liver microsomes: Ratios of accessory

proteins as sources of discrepancies between the approaches. *Drug Metab. Dispos.* 28, 1493–1504.

Wang, L., Chen, L., Lian, G., Han, L., 2010. Determination of partition and binding properties of solutes to stratum corneum. *Int. J. Pharm.* 398, 114–122.

Watkinson, A.C., Bunge, A.L., Hadgraft, J., Naik, A., 1992. Computer simulation of penetrant concentration-depth profiles in the stratum corneum. *Int. J. Pharm.* 87, 175–182.

Webster, G.D., Gabler, H.C., 2008. Modeling of transdermal transport of alcohol: Effect of body mass and gender. *Biomed. Sci. Instrum.* 44, 361–366.

Weibel, E.R., 1979. Morphometry of the human lung: The state of the art after two decades. *Clin. Respir. Physiol.* 15, 999–1013.

Wester, R.C., Melendres, J., Hui, X., Cox, R., Serranzana, S., Zhai, H., Quan, D., Maibach, H.I., 1998. Human in vivo and in vitro hydroquinone topical bioavailability, metabolism, and disposition. *J. Toxicol. Environ. Heal. - Part A* 54, 301–317.

Wetmore, B.A., Wambaugh, J.F., Ferguson, S.S., Sochaski, M.A., Rotroff, D.M., Freeman, K., Clewell, H.J., Dix, D.J., Andersen, M.E., Houck, K.A., Allen, B., Judson, R.S., Singh, R., Kavlock, R.J., Richard, A.M., Thomas, R.S., 2012. Integration of dosimetry, exposure, and high-throughput screening data in chemical toxicity assessment. *Toxicol. Sci.* 125, 157–174.

WHO, 2005. Chemical-specific adjustments factors for interspecies differences and human variability: guidance document for use of data in dose/concentration- response assessment. Geneva.

Wigaeus, E., Lof, A., Byfalt Nordqvist, M., 1984. Uptake, distribution, metabolism, and elimination of styrene in man. A comparison between single exposure and co-exposure with acetone. *Br. J. Ind. Med.* 41, 539–546.

Wilkinson, P.K., Sedman, A.J., Sakmar, E., Kay, D.R., Wagner, J.G., 1977a. Pharmacokinetics of ethanol after oral administration in the fasting state. *J. Pharmacokinet. Biopharm.* 5, 207–224.

Wilkinson, P.K., Sedman, A.J., Sakmar, E., Lin, Y.-J., Wagner, J.G., 1977b. Fasting and nonfasting blood ethanol concentrations following repeated oral administration of ethanol to one adult male subject. *J. Pharmacokinet. Biopharm.* 5, 41–52.

Wilkinson, S.C., Maas, W.J.M., Nielsen, J.B., Greaves, L.C., van de Sandt, J.J.M., Williams, F.M., 2006. Interactions of skin thickness and physicochemical properties of test compounds in percutaneous penetration studies. *Int. Arch. Occup. Environ. Health* 79, 405–413.

Wilschut, A., Ten Berge, W.F., Robinson, P.J., McKone, T.E., 1995. Estimating skin permeation. The validation of five mathematical skin permeation models. *Chemosphere* 30, 1275–1296.

Wurst, F.M., Dresen, S., Allen, J.P., Wiesbeck, G., Graf, M., Weinmann, W., 2006. Ethyl sulphate: A direct ethanol metabolite reflecting recent alcohol consumption. *Addiction* 101, 204–211.

- Wurst, F.M., Kempter, C., Metzger, J., Seidl, S., Alt, A., 2000. Ethyl glucuronide: A marker of recent alcohol consumption with clinical and forensic implications. *Alcohol* 20, 111–116.
- Wurst, F.M., Metzger, J., 2002. The ethanol conjugate ethyl glucuronide is a useful marker of recent alcohol consumption. *Alcohol. Clin. Exp. Res.* 26, 1114–1119.
- Wurst, F.M., Skipper, G.E., Weinmann, W., 2003a. Ethyl glucuronide - The direct ethanol metabolite on the threshold from science to routine use. *Addiction* 98, 51–61.
- Wurst, F.M., Vogel, R., Jachau, K., Varga, A., Alling, C., Alt, A., Skipper, G.E., 2003b. Ethyl glucuronide discloses recent covert alcohol use not detected by standard testing in forensic psychiatric inpatients. *Alcohol. Clin. Exp. Res.* 27, 471–476.
- Yamaguchi, K., Mitsui, T., Aso, Y., Sugibayashi, K., 2008. Structure-permeability relationship analysis of the permeation barrier properties of the stratum corneum and viable epidermis/dermis of rat skin. *J. Pharm. Sci.* 97, 4391–4403.
- Yamashita, F., Hashida, M., 2003. Mechanistic and empirical modeling of skin permeation of drugs. *Adv. Drug Deliv. Rev.* 55, 1185–1199.
- Yamazaki, H., Horiuchi, K., Takano, R., Nagano, T., Shimizu, M., Kitajima, M., Murayama, N., Shono, F., 2010. Human blood concentrations of cotinine, a biomonitoring marker for tobacco smoke, extrapolated from nicotine metabolism in rats and humans and physiologically based pharmacokinetic modeling. *Int. J. Environ. Res. Public Health* 7, 3406–3421.
- Yamazaki, K., Kanaoka, M., 2004. Computational prediction of the plasma protein-binding percent of diverse pharmaceutical compounds. *J. Pharm. Sci.* 93, 1480–1494.
- Yourick, J.J., Bronaugh, R.L., 1997. Percutaneous absorption and metabolism of coumarin in human and rat skin. *J. Appl. Toxicol.* 17, 153–158.
- Yun, H.-Y., Seo, J.-W., Choi, J.-E., Baek, I.-H., Kang, W., Kwon, K.-I., 2008. Effects of smoking on the pharmacokinetics and pharmacodynamics of a nicotine patch. *Biopharm. Drug Dispos.* 29, 521–528.
- Zaldívar, J.M., Menecozzi, M., Macko, P., Rodriguez, R., Bouhifd, M., Baraibar Fentanes, J., 2011. A Biology-Based Dynamic Approach for the Modelling of Toxicity in Cell Assays: Part II: Models for Cell Population Growth and Toxicity.
- Zaldívar, J.M., Mennecozzi, M., Marcelino Rodrigues, R Bouhifd, M., 2010. A biology-based dynamic approach for the modelling of toxicity in cell-based assays. Part I: Fate modelling.
- Zandvliet, A.S., Huitema, A.D.R., De Jonge, M.E., Den Hoed, R., Sparidans, R.W., Hendriks, V.M., Van Den Brink, W., Van Ree, J.M., Beijnen, J.H., 2005. Population pharmacokinetics of caffeine and its metabolites theobromine, paraxanthine and theophylline after inhalation in combination with diacetylmorphine. *Basic Clin. Pharmacol. Toxicol.* 96, 71–79.

Zanelli, U., Caradonna, N.P., Hallifax, D., Turlizzi, E., Houston, J.B., 2012. Comparison of cryopreserved HepaRG cells with cryopreserved human hepatocytes for prediction of clearance for 26 drugs. *Drug Metab. Dispos.* 40, 104–110.

Zeller, A., Horst, K., Rychlik, M., 2009. Study of the metabolism of estragole in humans consuming fennel tea. *Chem. Res. Toxicol.* 22, 1929–1937.

Zhang, Q., Grice, J.E., Li, P., Jepps, O.G., Wang, G.J., Roberts, M.S., 2009. Skin solubility determines maximum transepidermal flux for similar size molecules. *Pharm. Res.* 26, 1974–1985.

APPENDIX 1

Sensitivity Analysis of the ethanol case study

Effect of the following parameters was measured on concentrations of ethanol, EtS and EtG in the serum: V_{max} , K_m , V_{rev} , K_{rev} , $K_{formEtS}$, $K_{formEtG}$, CLR_{Eth} , Dt , ka_{SI} , ka_{stm} , k_{max} , k_{min} , CLR_{EtS} , CLR_{EtG} . The median estimated population values were used and examined on average man (BW= 75 kg, height =181 cm, age= 24) and woman (BW= 64 kg, height= 170 cm, age= 22) based on 18 subjects that took part in the ethanol drinking experiment. The parameters (P) were varied by $P \pm P50\%$ for the Monte Carlo simulations (**Figures: A1.1-16**), whereas, in case of local Sensitivity Analysis each parameter value was perturbed as $\max(10^{-8}, P)(1+10^{-8})$ –the default setting in the function -and the parameters were scaled by the mean of the simulated serum concentrations (**Tables: A1.1-3**).

Local Sensitivity Analysis

Local sensitivity analysis identified the following parameters, that were evaluated individually in a very small region close to their nominal value, to be top sensitive (based on sum of L1, L2): for ethanol: V_{max} , CLR_{Eth} and ka_{stm} ; for EtS: Dt , CLR_{Eth} , V_{max} ; for EtG: V_{max} , ka_{stm} and CLR_{Eth} .

Table A1.1 Summary of local Sensitivity Analysis for ethanol concentrations (most sensitive parameters)

Parameter	4 units man		4 units woman		8 units man		8 units woman	
	L1	L2	L1	L2	L1	L2	L1	L2
V_{max} [mg/h]	0.28	0.062	0.005	$7.3 \cdot 10^{-4}$	$2.0 \cdot 10^{-2}$	$3.6 \cdot 10^{-3}$	$8.1 \cdot 10^{-3}$	$9.4 \cdot 10^{-4}$
ka_{stm} [1/h]	0.17	0.043	0.018	$3.1 \cdot 10^{-3}$	$1.5 \cdot 10^{-2}$	$3.3 \cdot 10^{-3}$	$6.2 \cdot 10^{-3}$	$7.5 \cdot 10^{-4}$
Dt [L/h]	0.12	0.023	0.058	$7.3 \cdot 10^{-3}$	$9.8 \cdot 10^{-3}$	$1.8 \cdot 10^{-3}$	$7.9 \cdot 10^{-3}$	$9.4 \cdot 10^{-4}$
CLR_{Eth}	0.22	0.06	0.006	$8.1 \cdot 10^{-4}$	$1.5 \cdot 10^{-2}$	$2.8 \cdot 10^{-3}$	$3.4 \cdot 10^{-4}$	$4.0 \cdot 10^{-5}$

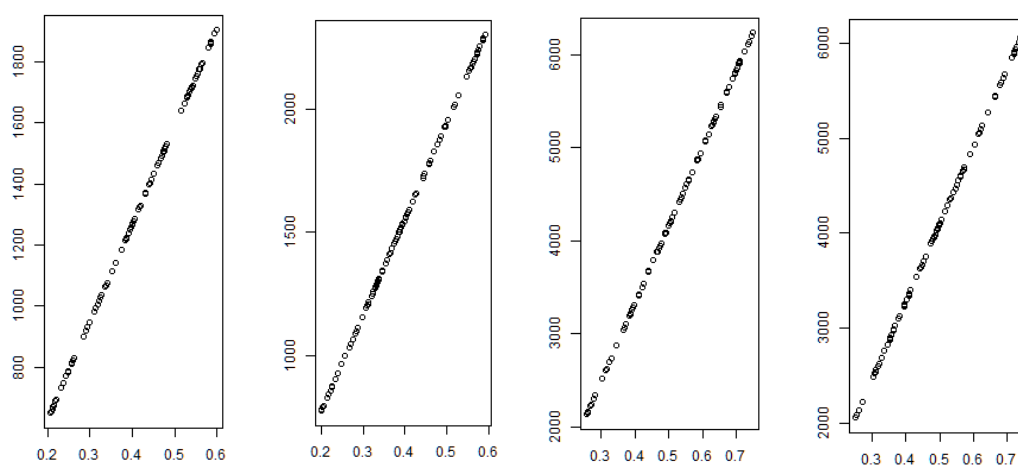
Table A1.2 Summary of local Sensitivity Analysis for EtS concentrations (most sensitive parameters)

Parameter	4 units man		4 units woman		8 units man		8 units woman	
	L1	L2	L1	L2	L1	L2	L1	L2
V_{\max} [mg/h]	25.03	3.02	6.49	2.41	20.71	3.08	26.17	3.04
ka_{stm} [1/h]	15.14	1.84	18.15	3.72	11.39	2.03	18.38	2.31
Dt [L/h]	17.21	2.053	56.06	6.80	10.01	1.44	21.21	2.51
CLR_{Eth}	49.87	5.94	7.22	2.87	9.43	1.78	0.87	0.18
CLR_{EtS}	1.46	0.27	22.49	4.78	1.17	1.36	1.54	0.64
$K_{\text{form}_{\text{EtS}}}$	2.33	0.26	1.94	0.22	0.67	0.07	0.66	0.07

Table A1.3 Summary of local Sensitivity Analysis for EtG concentrations (most sensitive parameters)

Parameter	4 units man		4 units woman		8 units man		8 units woman	
	L1	L2	L1	L2	L1	L2	L1	L2
V_{\max} [mg/h]	4.15	0.52	0.57	0.17	2.77	0.54	3.26	0.38
ka_{stm} [1/h]	7.54	0.94	0.29	-0.015	0.56	-0.84	1.83	0.28
Dt [L/h]	2.65	0.33	0.95	7.92	0.27	0.23	0.29	-2.41
CLR_{EtH}	2.16	0.36	0.21	-0.47	3.01	0.67	0.25	0.04
CLR_{EtG}	0.37	0.05	0.04	-0.27	0.01	-0.08	0.08	0.01
$K_{\text{form}_{\text{EtG}}}$	0.87	0.097	0.09	0.78	0.03	0.21	0.25	0.03

High effect of drinking rate on resulting ethanol concentrations in serum was caused mostly due to higher/lower amount and rate of ethanol reaching the stomach (drinking time was unchanged 60 min in all the instances) with mean 0.4 L/h for 4 units and 0.5 L/h for 8 units. This effect was also clear for EtS and EtG.

**Fig A1.1.** Effect of drinking rate (Dt) on serum concentrations of ethanol for: 4 units average man, 4 units average woman, 8 units average man, 8 units average woman (from left).

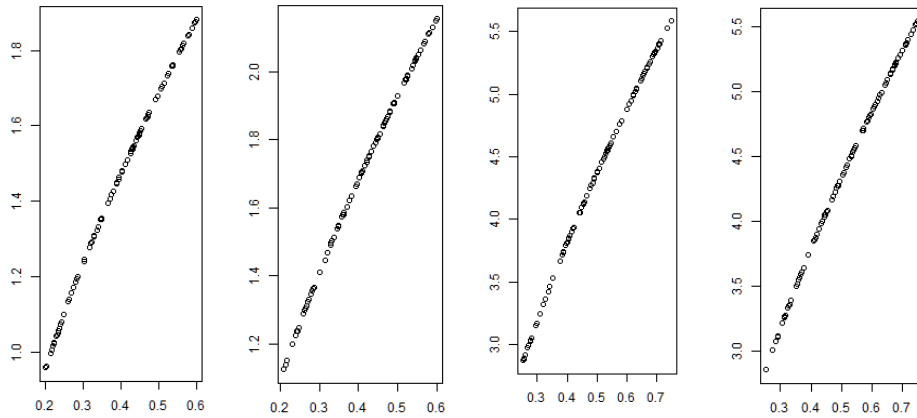


Fig A1.2. Effect of ethanol drinking rate Dt on serum concentrations of EtG for: 4 units average man, 4 units average woman, 8 units average man, 8 units average woman (from left).

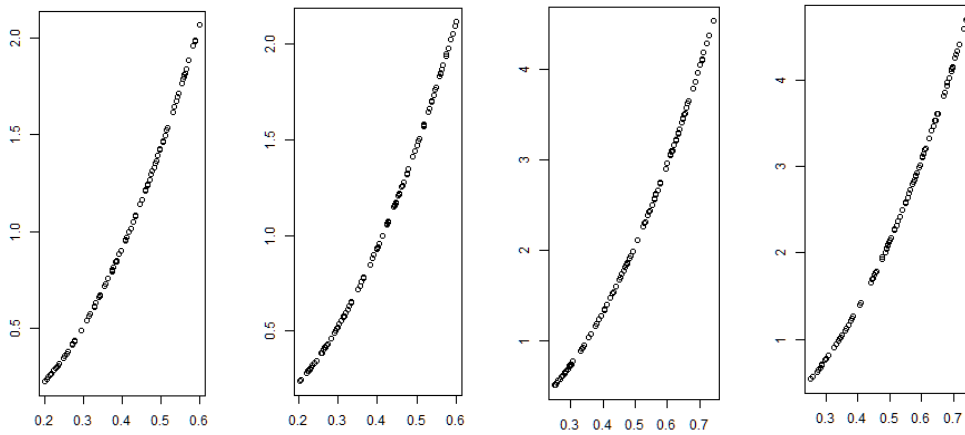


Fig A1.3. Effect of ethanol drinking rate (Dt) on serum concentrations of EtS for: 4 units average man, 4 units average woman, 8 units average man, 8 units average woman (from left).

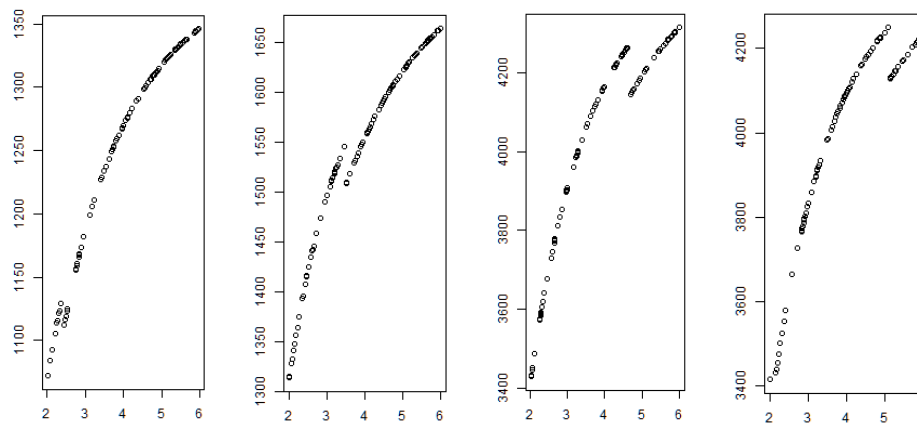


Fig A1.4. Effect of stomach absorption rate (k_{a_stm}) on serum concentrations of ethanol for: 4 units average man, 4 units average woman, 8 units average man, 8 units average woman (from left).

Stomach absorption rate of ethanol was evaluated in the range 2:6 1/h (with a mean of 41/h) for both 4 and 8 units of ethanol. Its effect, however, was higher for 8 units of ethanol in terms of ethanol concentrations in serum and almost the same for the two metabolites.

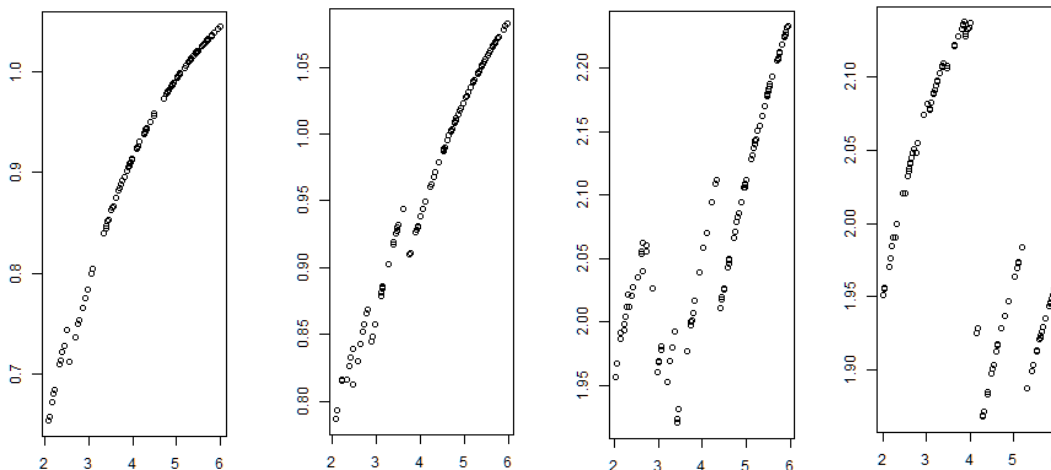


Fig A1.5. Effect of ethanol absorption rate from stomach ($k_{a_{stm}}$) on serum concentrations of EtS for: 4 units average man, 4 units average woman, 8 units average man, 8 units average woman (from left).

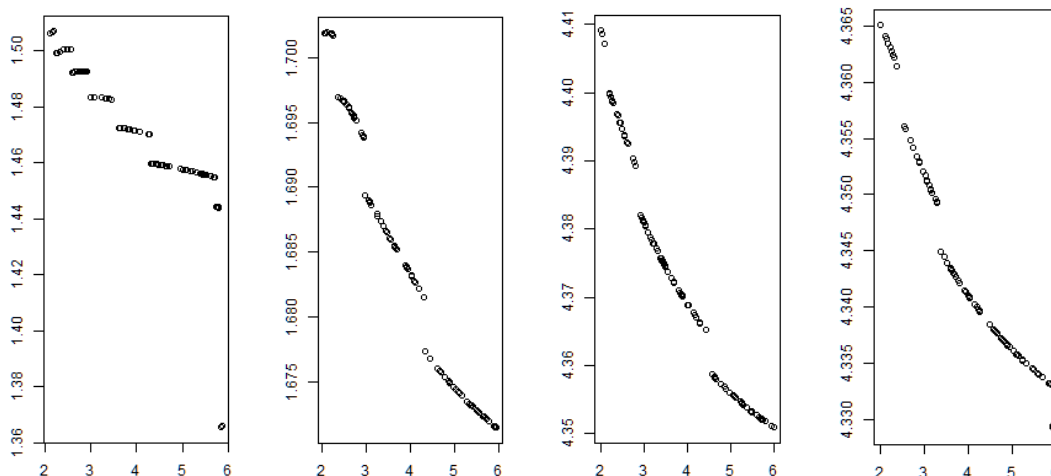


Fig A1.6. Effect of ethanol absorption rate from stomach ($k_{a_{stm}}$) on serum concentrations of EtG for: 4 units average man, 4 units average woman, 8 units average man, 8 units average woman (from left).

Ethanol renal clearance with median values of 20·BMI for men (4 units), 4·BMI (4 units women), 1·BMI (8 units men) and 0.1·BMI (8 units women) showed high impact on ethanol levels in the serum and slightly lower on EtS and EtG levels.

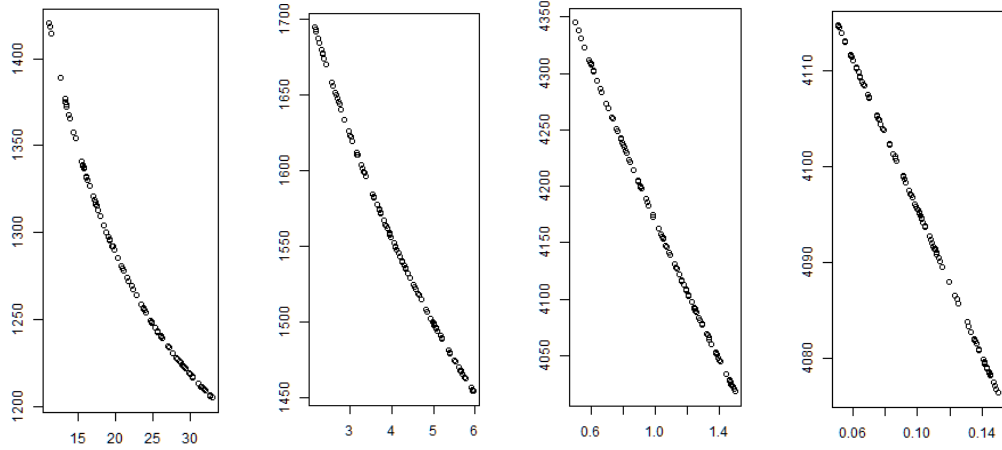


Fig A1.7. Effect of ethanol renal clearance on serum concentrations of ethanol for: 4 units average man, 4 units average woman, 8 units average man, 8 units average woman (from left).

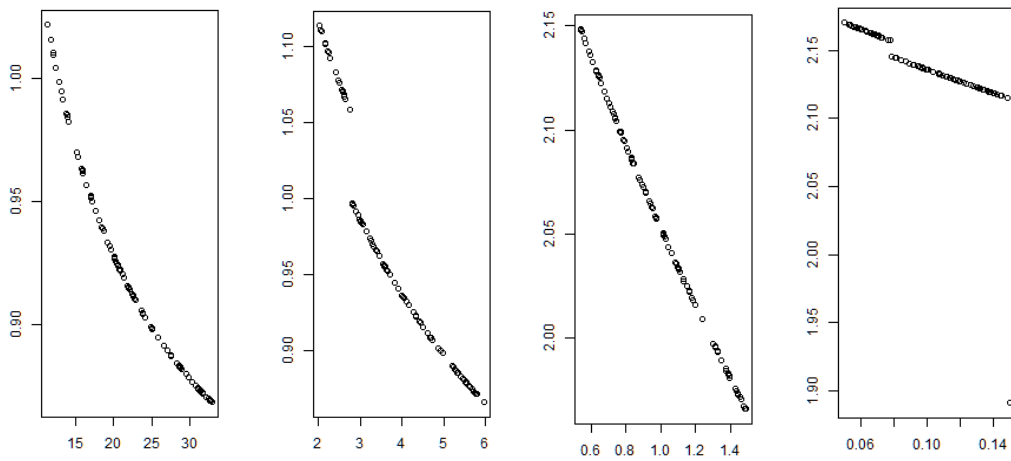


Fig A1.8. Effect of ethanol renal clearance (CLR_{Eth}) on serum concentrations of EtS for: 4 units average man, 4 units average woman, 8 units average man, 8 units average woman (from left).

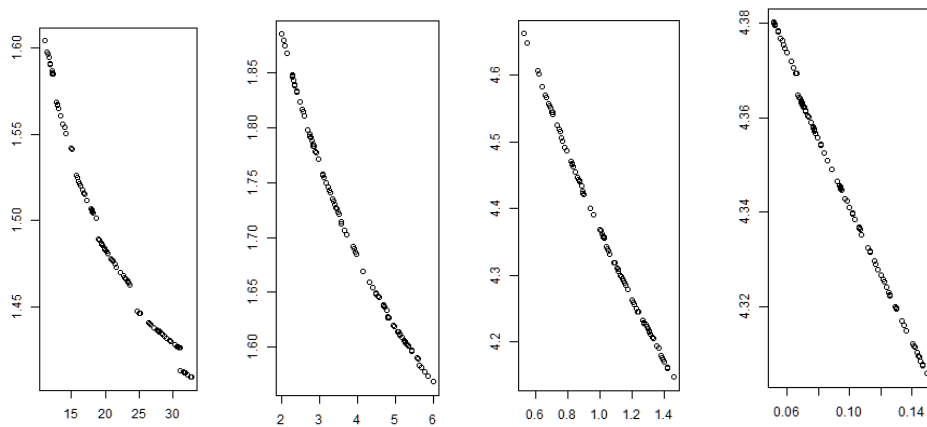


Fig A1.9. Effect of ethanol renal clearance from stomach (CLR_{Eth}) on serum concentrations of EtG for: 4 units average man, 4 units average woman, 8 units average man, 8 units average woman (from left).

Ethanol metabolism rate to acetaldehyde (V_{max}) with the average value of 10 BMI mg/h showed the highest changes in the resulting simulations for ethanol only. In case of metabolites, the results were not altered a lot.

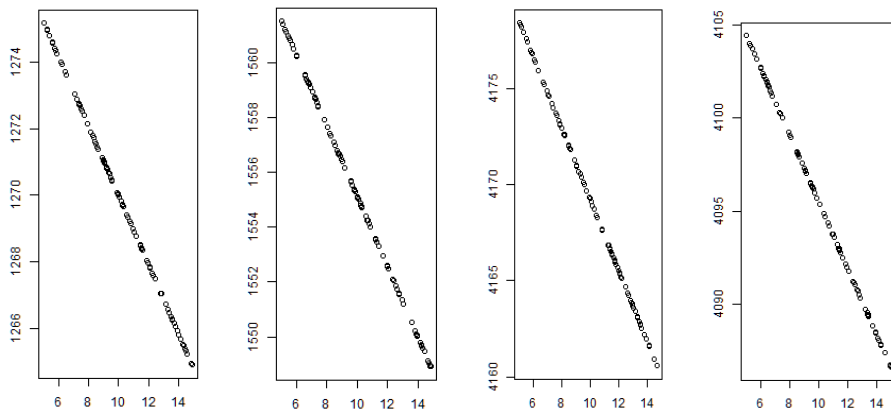


Fig A1.10. Effect of ethanol metabolism rate to acetaldehyde (V_{max}) on serum concentrations of ethanol for: 4 units average man, 4 units average woman, 8 units average man, 8 units average woman (from left).

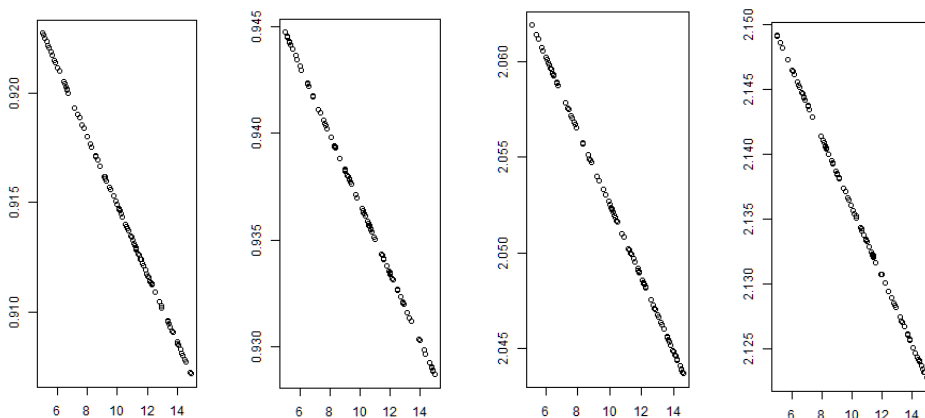


Fig A1.11. Effect of ethanol metabolism rate to acetaldehyde (V_{max}) on serum concentrations of EtS for: 4 units average man, 4 units average woman, 8 units average man, 8 units average woman (from left).

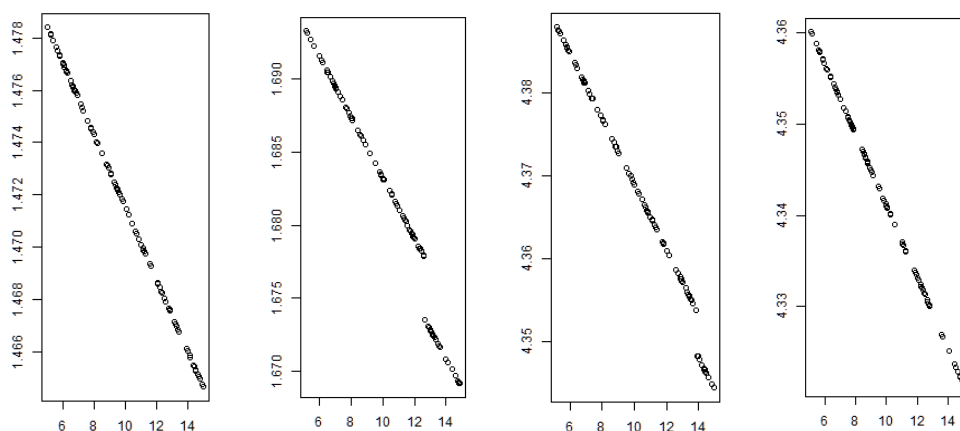


Fig A1.12. Effect of ethanol metabolism rate to acetaldehyde (V_{max}) on serum concentrations of EtG for: 4 units average man, 4 units average woman, 8 units average man, 8 units average woman (from left).

Formation rates of EtS and EtG produced the highest variation of simulated concentrations. Lower effect was observed in cases of their renal clearance values. What proves that using a population average value, instead of fitted individual rates, is sufficient.

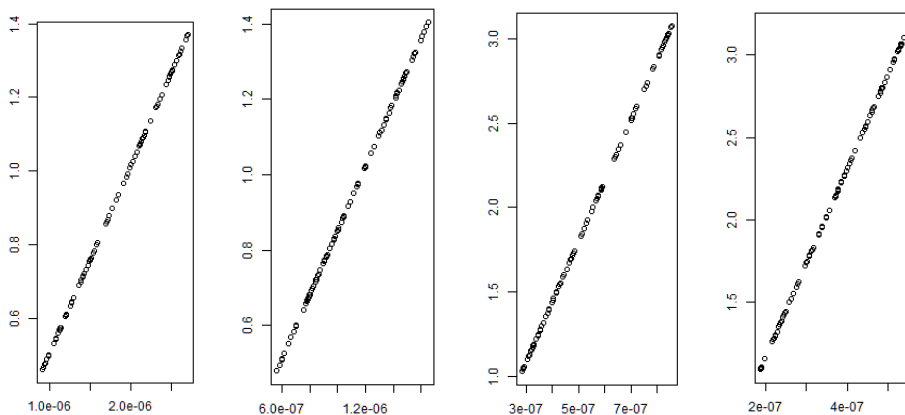


Fig A1.13. Effect of EtS formation rate (K_{formETS}) on serum concentrations of EtS for: 4 units average man, 4 units average woman, 8 units average man, 8 units average woman (from left).

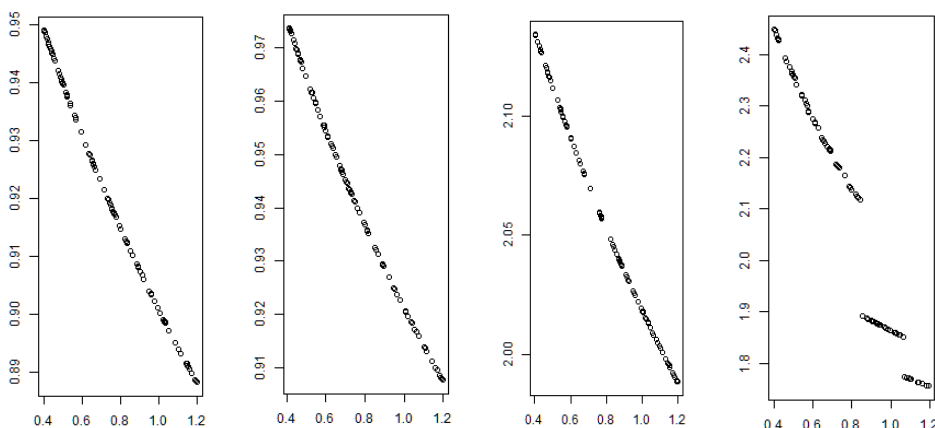


Fig A1.14. Effect of EtS renal clearance (CLR_{ETs}) on serum concentrations of EtS for: 4 units average man, 4 units average woman, 8 units average man, 8 units average woman (from left).

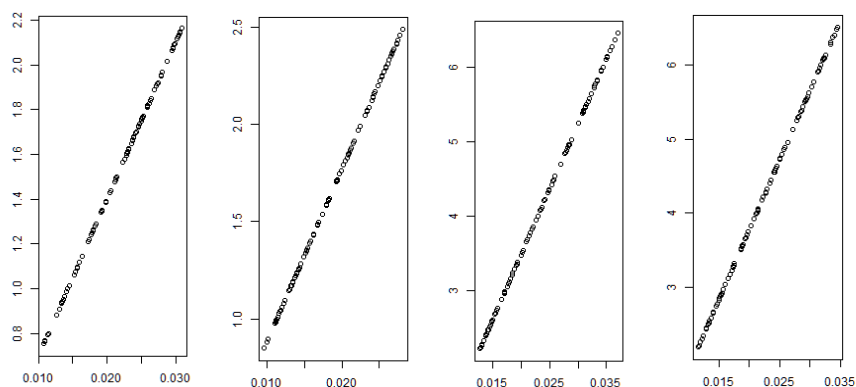


Fig A1.15. Effect of EtG formation rate ($K_{\text{form,ETG}}$) on serum concentrations of EtG for: 4 units average man, 4 units average woman, 8 units average man, 8 units average woman (from left).

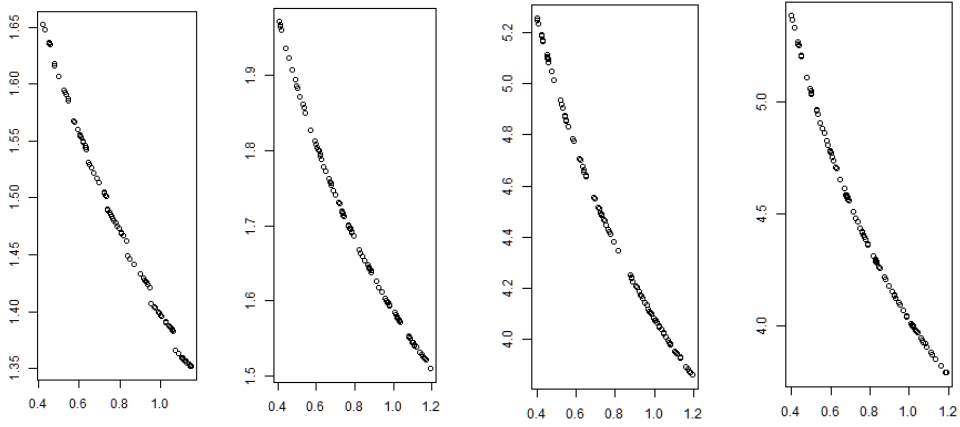


Fig A1.16. Effect of EtG renal clearance (CLR_{ETG}) on serum concentrations of EtG for: 4 units average man, 4 units average woman, 8 units average man, 8 units average woman (from left).